Magnesium Homeostasis in Plants

Siegfried Leher

University of East Anglia

A thesis submitted for the degree of Doctor of Philosophy

March 2022

This copy of the thesis has been supplied on condition that anyone who consults it is understood to recognize that its copyright rests with the author and that use of any information derived there from must be in accordance with current UK Copyright law. In addition, any quotation or extract must include full attribution.

This page is intentionally left blank

Blank pages are used throughout to allow legends to appear opposite display items in the paper copy of this document

Abstract

Magnesium (Mg^{2+}) is an essential nutrient for all life on earth. Mg^{2+} is required for the activity of a large number of enzymes, as well as for the structure of DNA, RNA, proteins and biological membranes. Mg^{2+} is also necessary for the activity of adenosine triphosphate (ATP) and is especially important for reactions producing and consuming this energy-currency. Despite the downstream symptoms of Mg^{2+}-deficiency (MgD) within plants being relatively well-known, knowledge about the initial symptoms of MgD, plant perception of MgD and regulatory mechanisms involved is lacking. This project therefore aims to elucidate the symptoms of and responses to MgD, using both forward and reverse genetic approaches.

A high-throughput method of inducing MgD was established and compared to methods used previously. In conjunction with the genetically-encoded, ratiometric sensors ATeam 1.03-nD/nA and pHusion, this method was used to show that levels of the Mg^{2+}-ATP-complex, as well as cytoplasmic and apoplastic pH, increase in leaves of *Arabidopsis* seedlings under MgD. An alternative model of the events occurring during MgD was generated. Additionally, the Mg^{2+}-sensitive FRET-sensor MARIO was functionally expressed in *A. thaliana*.

The MRS2-family makes up the most important family of Mg^{2+}-specific transport proteins in plants, but knowledge around their subcellular localisation and regulatory mechanisms is incomplete. Fluorescently-tagged expression constructs were used to provide additional data on the subcellular localisation and functional relevance of the family members MRS2-3 and MRS2-4.

RNA-sequencing on *A. thaliana* exposed to MgD was used to find potential MgD reporter genes. Transcriptional MgD reporter plants were generated and used to carry out a forward genetic screen with the aim of finding genes involved in the response to MgD. Putative Mg^{2+}-mutants were identified. Although mutant phenotypes could not be unambiguously attributed to individual mutations, lists of genetic variants potentially causative of mutant phenotypes are given.

Access Condition and Agreement

Each deposit in UEA Digital Repository is protected by copyright and other intellectual property rights, and duplication or sale of all or part of any of the Data Collections is not permitted, except that material may be duplicated by you for your research use or for educational purposes in electronic or print form. You must obtain permission from the copyright holder, usually the author, for any other use. Exceptions only apply where a deposit may be explicitly provided under a stated licence, such as a Creative Commons licence or Open Government licence.

Electronic or print copies may not be offered, whether for sale or otherwise to anyone, unless explicitly stated under a Creative Commons or Open Government license. Unauthorised reproduction, editing or reformatting for resale purposes is explicitly prohibited (except where approved by the copyright holder themselves) and UEA reserves the right to take immediate ‘take down’ action on behalf of the copyright and/or rights holder if this Access condition of the UEA Digital Repository is breached. Any material in this database has been supplied on the understanding that it is copyright material and that no quotation from the material may be published without proper acknowledgement.

“And then is heard no more. It is a tale

Told by an idiot, full of sound and fury,

Signifying nothing.”

- Macbeth

Macbeth by William Shakespeare

Table of Contents

Acknowledgements

I would like to extend my gratitude to my supervisory team, especially Dale Sanders and Tony Miller, for their help and support throughout the years. Even if I did not always appreciate your input properly or follow your advice, this would not have been possible without you. I am also grateful to Myriam Charpentier and Graham Moore, whose tough, but fair judgement as panel members helped keep me working hard and going in something resembling the right direction.

The Sanders/Miller lab has been exceptionally welcoming and supportive for the entire time I have been a part of it, and I deeply appreciate the help of Yi, Millie, Marco, Thomas and Josh at various stages. Also, Graham Chilvers from UEA Science Analytical Services, James Lipscombe, Saleha Bakht, Marco D'Ario, and many more collaborators and mentors have been indispensable.

I cannot thank the Gatsby Charitable foundation enough for the funding, training and mentoring that I have received ever since I first applied for a summer studentship way back when. Especially Jane Langdale, Ottoline Leyser and the rest of the Gatsby panel, David Hanke and Roxaana Clayton, and all the other members of the Gatsby network have provided me with much more than just academic support and expertise.

My thanks go out to my family, who continue to put up with me and want me around despite everything. My mother and father, who have worked tirelessly to make sure I can pursue my dreams. I still have not fully realized how lucky I am to have had the upbringing I did. To my brother, Viktor, who I am incredibly proud of. My grandparents, who are incredibly proud of me.

There are too many friends to acknowledge here, but every single one of them deserves it. Ned, Beth, Marco, Sam, Joanna, Basti, Jess, just to name a few. I could not have done it without them.

And finally, to my fiancée, Alex, AKA Luff Luff Trixiebelle, who has taught me more in a few short years than anyone ever has, or anyone ever will. More than anyone else, you made this possible. I did not think a relationship could be like this, especially not for me. In the good times and the bad, I never forget what you have given me, and continue to give me.

List of Figures

List of tables

List of common abbreviations

AA	antimycin A
AAA	AT2G18193
ADP	adenosine diphosphate
AE	agronomic effectiveness
AK	adenylate kinase
AMP	adenosine monophosphate
ANOVA	analysis of variance
ATP	adenosine triphosphate
BWA	Burrows-Wheeler aligner
Ca^{2+}	calcium ion
CBL	calcineurin B-like
cDNA	complementary DNA
CER	controlled environment room
CIPK	CBL-interacting protein kinase
CM-H2DCFDA	5-(and-6)-chloromethyl-2',7'-dichlorodihydrofluorescein diacetate acetyl ester
CNGC	cyclic nucleotide gated channel
DAG	days after germination
DCICA	dichloroisocyanuric acid
ddH_2O	distilled water
DEGs	differentially-expressed genes
dH_2O	deionized water
DHE	dihydroethidine
DNA	desoxyribonucleic acid
DTX3	DETOXIFICATION 3 (AT2G04050)
DTX4	DETOXIFICATION 4 (AT2G04070)
EDTA	ethylenediaminetetraacetic acid
EMS	ethyl methanesulfonate
EtOH	ethanol
FDR	false discovery rate

FDR2	FBOX/DUF295-RELATED 2
FPKM	fragments per kilobase per million reads
gDNA	genomic DNA
GFP	green fluorescent protein
GO	gene ontology
HeLa	Henrietta Lacks (cells)
HEPES	4-(2-hydroxyethyl)-1-piperazineethanesulfonic acid
HGA	high gel-strength agar
HM	medium adapted from Hermans *et. al.*, 2010a
HSD	(Tukey) honestly significant difference
ICP-MS	inductively coupled plasma - mass spectrometry
ICP-OES	inductively coupled plasma – optical emission spectrometry
indel	insertion / deletion
IPTG	Isopropyl ß-D-1-thiogalactopyranoside
K^+	potassium (ion)
K_d	dissociation constant
KEGG	Kyoto encyclopedia of genes and genomes
KO	knockout
LB	lysogeny broth
LUC	firefly luciferase
MATE	multidrug and toxic compound extrusion
Mg^{2+}	magnesium (ion)
MgADP	the magnesium-ADP complex
MgATP	the magnesium-ATP complex
MgD	magnesium deficiency
MGT	magnesium transporter
MHX	Mg^{2+}/H^+ exchanger
MRS2	mitochondrial RNA splicing of type II introns
MS	Murashige and Skoog (medium)
MTP	metal tolerance protein
N	nitrogen
Na^+	sodium (ion)

NASC	Nottingham *Arabidopsis* stock centre
NRT	no reverse transcriptase (control)
NTC	no template control
OD600	optical density at 600 nm
ORF	open reading frame
P	phosphorus
PCR	polymerase chain reaction
PER70	PEROXIDASE 70 (AT5G64110)
PM	plasma membrane
PMF	proton-motive force
Pi	inorganic phosphorus
qRT-PCR	(real-time) quantitative reverse transcription PCR
RCA	root cation channel
RCD1	RADICAL-INDUCED CELL DEATH 1
RFP	red fluorescent protein
RNA	ribonucleic acid
RNAseq	RNA sequencing
ROS	reactive oxygen species
SNV	single nucleotide variation
SOC	super optimal broth with catabolite repression
SRO3	SIMILAR TO RCD1 3
TAIR	the Arabidopsis information resource
TD	touchdown (PCR)
T-DNA	transfer DNA
TE	Tris-EDTA (buffer)
TKO	triple knockout
TkTp	transketolase targeting peptide
tris	tris(hydroxymethyl) aminomethane
WGS	whole-genome sequencing
WT	wild-type
X-Gal	5-Bromo-4-Chloro-3-Indolyl β-D-Galactopyranoside

This page is intentionally left blank

Blank pages are used throughout to allow legends to appear opposite display items in the paper copy of this document

Chapter 1: Introduction

1.1 The magnesium ion

1.1.1 Chemical properties of magnesium

Magnesium is a chemical element with an atomic number of 12, meaning that its nucleus contains twelve protons. Magnesium occurs on earth almost exclusively as one of its three stable isotopes; ^{24}Mg makes up 79% of Mg on earth, ^{25}Mg makes up 10%, and ^{26}Mg makes up 11%, giving magnesium an average atomic weight between 24.304 and 24.307 [1]. Magnesium, in its elemental form, has twelve electrons. This means that, according to the Aufbau principle, electron-shells 1s, 2s, 2p and 3s are filled in a neutral magnesium-atom, making magnesium an alkaline earth element. As such, magnesium has a relatively low electronegativity value of 1.31 on the Pauling scale [2], reflective of its tendency to shed its two "outermost" electrons, reaching a favourable energetic state in which its first two electron-shells are filled. Therefore, magnesium occurs almost exclusively as a divalent cation (Mg^{2+}) in nature, including in biological systems [3].

Mg^{2+} is set apart from other ions by its small ionic radius; among biologically-relevant cations, only Ni^{2+} and Mo^{4+} are smaller. Yet, Mg^{2+} has the largest hydrated radius of any cation. The water molecules in the hydrated shell of this ion are very tightly bound, as seen by the slow water exchange rate displayed by Mg^{2+}, orders of magnitude below that of Ca^{2+}, Na^{+} and K^{+} (**Table 1.1**) [3]. More accurately, Mg^{2+} obtains its first hydrated shell by forming a complex with six water-molecules, $Mg(H_2O)_6^{2+}$, which then becomes surrounded by a secondary hydrated shell of somewhat less tightly-bound water molecules. The first hydrated shell exhibits a sixfold, octahedral geometry, which is the coordination geometry almost universally adopted by Mg^{2+}-complexes, and exchange of water-molecules within this shell is comparatively slow [4, 5] (see **Table 1.1**).

Table 1.1 – Key properties of cations common in biological systems, compared

Ion	Na^+	K^+	Ca^{2+}	Mg^{2+}
Ionic radius (Å)[a]	0.95	1.38	0.99	0.65
Hydrated radius (Å)	2.75	2.32	2.95	4.76
Ionic Volume ($Å^3$)	3.6	11.0	4.1	1.2
Hydrated Volume ($Å^3$)	88.3	52.5	108	453
Coordination number	6	6-8	6-8	6
Water exchange rate[b] (s^{-1})	8×10^8	10^9	3×10^8	10^5

a – Ionic radii and volumes from Diebler *et al*. [6] and Eigen [7]. **b** – Solvent exchange rates from Diebler *et al*. [6]. Adapted from Maguire and Cowan [3].

1.1.2 Biological roles of magnesium

Mg^{2+} can interact with biological molecules in two distinct ways. Inner-sphere interactions occur when Mg^{2+} ions form complexes with a ligand directly, with the ligand displacing one of the six water-molecules of the inner shell surrounding Mg^{2+} in solution. Outer-sphere interactions occur when the magnesium hexahydrate complex contacts a ligand indirectly, via the water-molecules of the inner shell [8-10]. Inner-sphere interactions therefore represent the formation of a true complex between Mg^{2+} and the ligand of interest, whereas outer-sphere interactions are predominantly ionic in nature, with the $Mg(H_2O)_6^{2+}$-complex neutralising negative charges present on the other ligand. While most metal ions only participate in catalysis via inner-sphere interactions exclusively, both of these modes of interaction are utilized during Mg^{2+}-mediated catalysis; indeed, Mg^{2+}-ions are often supplied by the substrate during catalytic reactions, rather than being tightly bound by the enzyme [3, 11].

Mg^{2+} has a very low tendency to form complexes with proteins, compared to transition metals like copper, zinc or iron, according to the Irving-Williams series [12]. Many Mg^{2+}-dependent enzymes exhibit higher affinities for other metals, but the relatively high concentrations of free Mg^{2+} within living cells enable preferential binding to Mg^{2+} to take place in those cases [8]. Due to this abundance and mobility, Mg^{2+} is often found in ionic interactions.

In accordance with this, one of its most important roles in biological systems is to form outer-sphere interactions with nucleotides, such as ATP, interacting with the negatively charged phosphate-groups. In this capacity, Mg^{2+} acts as a Lewis acid, drawing electron density towards itself and facilitating hydrolysis of the bound nucleotide. Mg^{2+} therefore facilitates the splitting of phosphate-ester bonds, meaning that its role with regards to nucleoside triphosphates is not just that of a chelator, but also of a catalyst [3, 13]. Due to this, biological processes involving nucleic acids are inherently dependent on Mg^{2+}. Indeed, up to 50% of cytosolic Mg^{2+} is bound to ATP [3], and around 90% of all ATP and ADP is bound to Mg^{2+} at any point [14, 15].

The concentrations of ATP, ADP, AMP and (free) Mg^{2+} are intimately linked via the reaction catalysed by adenylate kinase (AK) [16]. **Figure 1.1** outlines the reaction catalysed by AK and associated ion-exchange processes. The ratio of magnesium-bound and free nucleotides is dependent on concentrations of free Mg^{2+}, or $[Mg^{2+}]$. ATP, or nucleotide triphosphates, have the highest tendency to bind Mg^{2+}, followed by nucleotide diphosphates like ADP and trailed by nucleotide monophosphates like AMP. At normal, physiological levels of $[Mg^{2+}]$, almost all ATP is bound to Mg^{2+}, about 70% of ADP is Mg^{2+}-bound, but almost all AMP is in its "free" form [16, 17]. Although MgATP generally represents the "active" form of ATP, and MgADP that of ADP, and rates of many enzymatic reactions respond to the MgATP/MgADP-ratio in practice, free ATP, ADP and AMP can represent allosteric modulators of enzymes, especially for kinase-type phosphotransferases, and sometimes also substrates in themselves [16, 17]. Since Ca^{2+} ions also show affinity for nucleotides, binding to nucleotides also links concentrations of $[Mg^{2+}]$ and free Ca^{2+} ($[Ca^{2+}]$), which means that changes in $[Mg^{2+}]$-levels will also influence $[Ca^{2+}]$-levels and Ca^{2+}-dependent enzymes, and vice versa [18]. Further, pH can influence the AK-reaction and shift its equilibrium, and is therefore also linked to concentrations of $[Mg^{2+}]$, $[Ca^{2+}]$, and nucleotides [16]. This relationship gives a basis for $[Mg^{2+}]$-levels to influence virtually all parts of cellular metabolism, and therefore the potential for Mg^{2+} to act as a cellular signal or a master regulator of metabolism [17]. Since AK exists in every living organism [19], this relationship likely exists across all life as well.

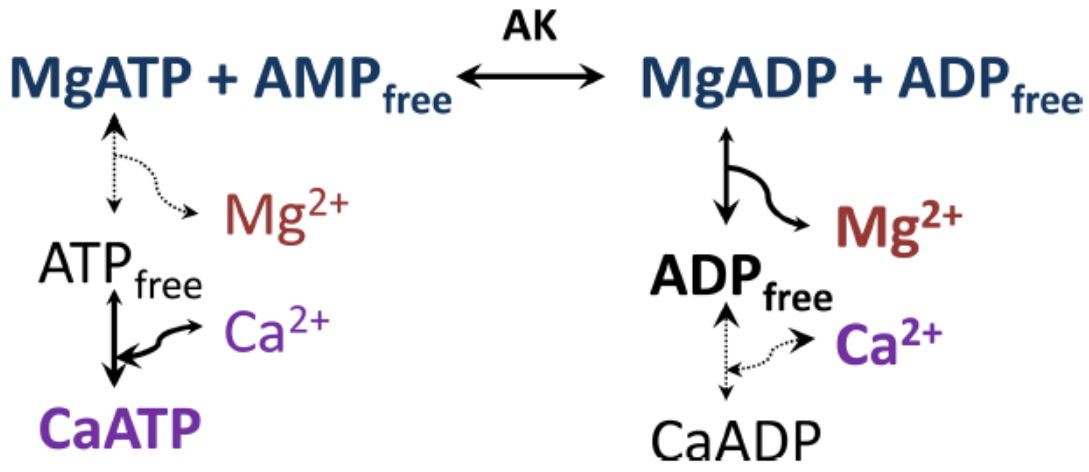

Figure 1.1 - The adenylate kinase (AK) reaction and ion balance.
AK catalyses the conversion of free AMP and MgATP to MgADP and free ADP. The Affinity of ADP for Mg^{2+} is lower than that of ATP, which means that Mg^{2+} is released when cellular energy is low, and conversely Mg^{2+} is required to maintain a high cellular energy-level. Ca^{2+} is also more tightly bound by ATP, which means that when this reaction is displaced to the right, Ca^{2+} is released as well. Adapted from Igamberdiev and Hill [18]

The rigid, clearly-defined coordination geometry adopted by Mg^{2+} makes it suitable for stabilizing the structure of RNA and DNA molecules, even when involved in outer-sphere interactions, as exemplified by its role in ribosome assembly [9] and maintenance of DNA structure [20]. Mg^{2+} is a necessary cofactor for most reactions involving DNA processing [20]. In fact, Mg^{2+} is the most common metal cofactor across known enzymatic reactions in general, and is commonly used in ligases, transferases, lyases and hydrolases [13, 21]. It is uncommon in oxidoreductases, since it cannot directly participate in these reactions due to its redox-stability. Mg^{2+} is often necessary to "lock" nucleotides and other ligands in active sites of enzymes. At times, the ability of Mg^{2+} to tightly bind water-molecules is instrumental in delivering catalytic water molecules to active sites [3, 10].

1.1.3 Magnesium in human nutrition

Mg^{2+} is the second most abundant cation in vertebrate cells, second only to K^+, and the most abundant divalent cation [22]. The biological roles of Mg^{2+}, as outlined in the previous section, are reflected in the clinical symptoms of Mg^{2+}-deficiency (MgD). MgD is associated with severe health problems, many of which can ultimately be attributed to disrupted energy metabolism. Among these are diseases of the cardiovascular system, such as cardiac arrhythmias, tachycardia, coronary artery disease and even heart failure and sudden cardiac death [23, 24]. This is not only due to the role of Mg^{2+} in correct muscle function and energy-supply to the heart [25, 26], but also due to the effects of MgD on levels of potassium and calcium [23, 24]. MgD can lead to the formation of calcium deposits in the kidneys and arteries [27], leading to other electrolyte abnormalities, enhanced lipid deposition in arteries, and promoting atherosclerosis and cardiac necrosis [28]. Indeed, appropriate serum Mg^{2+} levels have been associated with a 40% reduction in the risk of sudden cardiac death [29]. MgD is also associated with type type 2 diabetes mellitus. In this case, MgD represents a risk factor for this disease, and Mg^{2+} supplementation can alleviate symptoms [24, 29]. This is thought to be due to the insulin-sensitizing effects of Mg^{2+}, enhancing the insulin-dependent uptake of glucose [30], as well as anti-inflammatory effects of Mg^{2+}, mediated by a reduction of Ca^{2+}-uptake into adipocytes [31]. Other diseases associated with MgD in humans are hypertension [23], osteoporosis [24], migraines and headaches [24, 32]. Even mild, sub-clinical MgD has been suggested to contribute to these conditions in the long-term, despite the difficulties associated with diagnosis of MgD.

In humans, hypomagnesemia is sometimes thought to be present when total serum levels of the ion are below 0.7 mM [33], although this might not be the optimal way to estimate Mg^{2+}-levels. Most Mg^{2+} in humans and other animals is not present in the bloodstream, but is made up by intracellular Mg^{2+}, which is difficult to measure [23]. Intracellular Mg^{2+} and serum Mg^{2+} do not always correlate well, which makes it hard to relate Mg^{2+}-levels to disease outcomes [34].

In one study, the prevalence of hypomagnesemia in the general population was estimated at 2,5-15%, but the authors suggest this to be an underdiagnosis [33].

More modern ways to assess Mg^{2+} status of patients are available, such as magnesium loading tests, which assess the retention of a given dose of Mg^{2+}, but these are not yet routinely used [23, 24].

Nevertheless, the dietary requirements of this essential nutrient have been estimated. The recommended daily allowance for Mg^{2+} is 400-420 mg per day for adult men, and 310-320 mg per day for adult women over 30 years in the USA (source: National Institute of Health, NIH). In the United Kingdom, 300 mg are recommended for men, and 270 mg for women (source: National Health Service, NHS). Both of these recommendations might be too low to provide optimal health and longevity in practice, however, since ancestral diets have been estimated to have provided around 600 mg Mg^{2+} per day, and this is likely to be the level of intake humans are truly adapted to [35]. Even with these comparatively low intake recommendations, studies carried out across many countries have concluded that the recommended intake is not being met for a large percentage of the population [33, 36-38], prompting researchers to call for more routine tests of Mg^{2+}-status, measures to increase Mg^{2+}-intake across the population, and even classification of the problem as a health crisis [23, 24, 29].

Humans acquire most bioavailable dietary Mg^{2+} from plant-based foods [39]. There is strong evidence from the Broadbalk Experiment, the oldest continuous agricultural experiment in the world, that nutrient-contents of cereals have suffered since the Green Revolution and the drastic yield increases associated with it, even though soil content of nutrients has generally increased since then [40], which is referred to as the “dilution effect”. Selective breeding for increased yields and faster growth is thought to have led to reduced content of essential nutrients. The overall decrease in micronutrient concentration in wheat was determined to be between 20 and 30 percent, which is concerning considering a significant portion of the micronutrient intake of people is from cereals [40]. Other studies diagnose a similar decrease in wheat [41], and in fruits and vegetables [42].

Another review by Marles [43] asserts that no general decline in soil [micro]nutrient content can be said to have occurred over the last decades, with fertilisation practices generally being successful in restoring nutrient levels over time. While conceding that a certain decline in nutrient-levels of foods has occurred in new, high-yielding varieties of fruits and vegetables compared to older ones due to the dilution effect, this review makes the case that the new levels are still within the natural range of variation for the crops in question, and that a well-balanced, high-quality diet will still supply all the nutrients necessary [43]. However, this does not address the basic problem, which is that many people currently do not achieve the recommended intake of micronutrients. Changes in diets and in the varieties of crops grown could reduce the incidence of MgD in humans; however, there are limitations to this approach. Unwillingness to grow varieties with lower yield potential, or dietary habits, such as the tendency towards consumption of processed foods in the developed world, make it unlikely that these changes will be implemented successfully soon [29]. Additionally, it is difficult to say how far the dilution effect will influence nutrient-contents of future fast-growing, high-yielding, aesthetically pleasing or otherwise altered varieties of crops.

While supplementation with Mg^{2+} can increase the total dietary intake to acceptable levels and be beneficial for clinical outcomes, and should likely be adopted as widely as possible [32, 44-47], this approach relies on compliance by the population; not only do people have to be educated about their needs, supplements also have to be produced, then purchased and taken by each individual. Nutritional supplements vary widely in quality, may not contain the optimal form of the nutrient and not be properly bio-available, and there is therefore a risk of over-and underdosing. Trying to acquire optimal amounts of not just a few, but as many nutrients as possible through this approach can become increasingly cumbersome. As such, it would be more favourable to produce food that contains necessary levels of essential nutrients on its own. If even the more popular and affordable types of food were nutritionally more complete, human health would likely improve without a socioeconomic bias towards those with the means or time to come up with a highly optimized diet or supplement regime.

Increasing the Mg^{2+}-content of crop plants, especially cereals, could bring great benefits for human health and well-being. Therefore, it appears that crop biofortification efforts are necessary, or at least desirable, to decrease the incidence of hypomagnesaemia and other nutrient deficiencies. However, to be able to increase the nutrient content of crops, it is necessary to first understand how nutrient uptake and storage are achieved and regulated. Both the content of Mg^{2+} and its bioavailability should be increased without disrupting other biological processes in crops, and ideally without decreasing yields.

1.2 Magnesium in plants

1.2.1 Plant-specific functions of magnesium

An important role for Mg^{2+}, specifically in plants, is as the central ion of chlorophyll. While in leaves, up to 75% of cellular Mg^{2+} can be involved in protein synthesis directly or indirectly, roughly another 15-20% is associated with chlorophyll [48, 49], where it is chelated by a chlorin ring and bound tightly. Without the central Mg^{2+}-ion, light capture and subsequent photosynthesis are not possible. Mg^{2+} is also required for carbon fixation from CO_2 in plants. Ribulose-1,5-bisphosphate-carboxylase (RuBisCo) requires Mg^{2+} to bind to the enzyme before the substrate, ribulose-1,5-bisphosphate, can be effectively bound in the correct orientation [50, 51]. Phosphoenolpyruvate (PEP) carboxylase, present in C4 plants like maize, requires Mg^{2+} for a similar reason [52, 53]. Additionally, multiple enzymes further downstream in the Calvin Cycle require Mg^{2+} [54].

Mg^{2+} is also especially important in the export of sucrose from source tissues, *i.e.*, leaves, likely due to the problems associated with cellular energy levels under Mg^{2+} deficiency [55, 56] (see **Section 1.2.3**). **Figure 1.2** gives a summary of some of the cellular processes Mg^{2+} is involved in in plants.

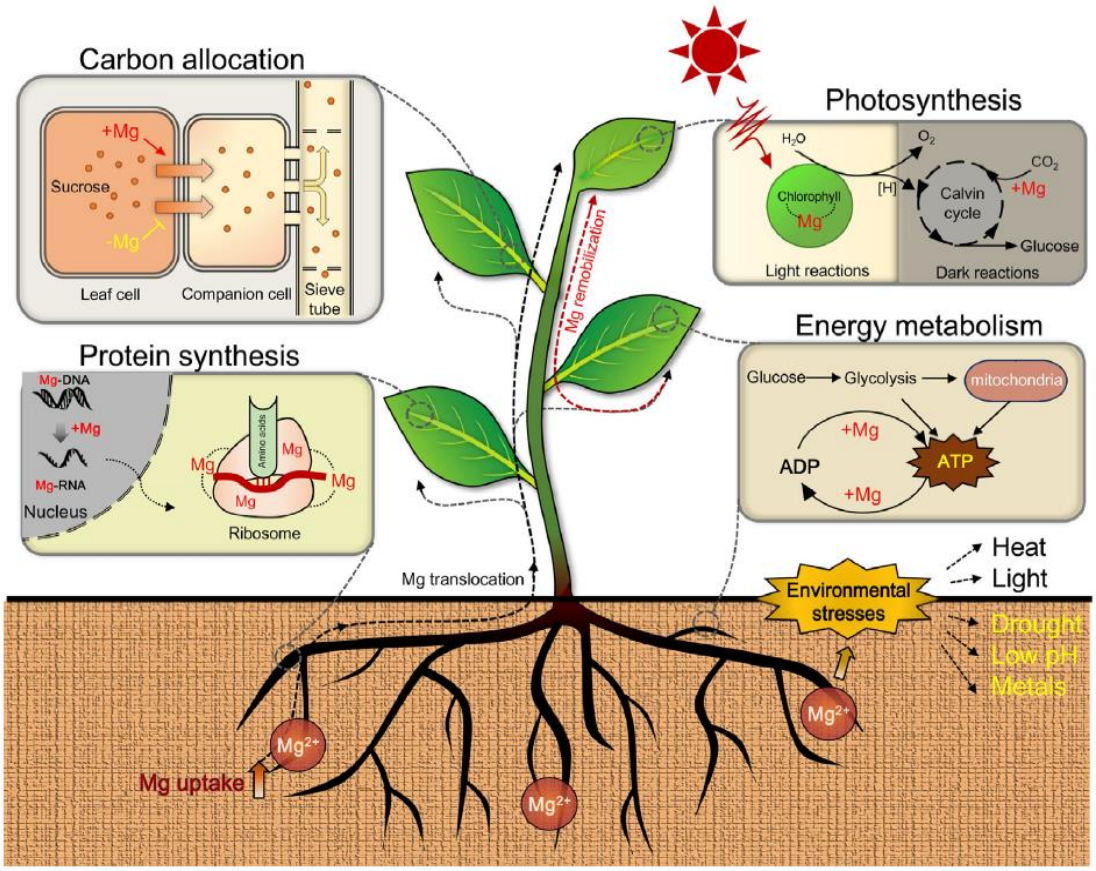

Figure 1.2 - Functions of magnesium in physiological processes in plants

Mg^{2+} is crucial for the energy-metabolism of all living cells, since it chelates and activates ATP and other nucleotides. This makes it especially important in glycolysis, oxidative phosphorylation, protein synthesis and associated processes. Mg^{2+} is also required for stabilisation of the structures of DNA, RNA and proteins. In plants, this ion is required for both the light and the dark reactions of photosynthesis, since it is the central ion of chlorophyll on the one hand, and required for the activity of RuBisCo, PEP carboxylase and other enzymes of the Calvin cycle on the other hand. Finally, Mg^{2+} is required for the export of photosynthetic metabolites from leaves.

Reprinted from Seminars in Cell and Developmental Biology, Vol. 74, February 2018, Chen *et al*. [57], “Functional dissection and transport mechanism of magnesium in plants”, 142-152, © 2018, with permission from Elsevier.

1.2.2 Soil chemistry of magnesium

Mg^{2+} is the eighth most common element in the earth's crust, making up about 2% of it, and is abundant in most soils [3]. However, although the ion is very mobile once in solution, most of this Mg^{2+} is firmly incorporated into the crystal lattice of minerals, and is not available for uptake by plants and other organisms [58]. The actual availability of Mg^{2+} depends on several factors: the content of the ion in the soil and the forms in which it is present, *i.e.*, the minerals making up the soil; the characteristics influencing release through weathering, such as grain size of soil contents and ambient temperature; the pH of the soil solution; the presence of other ions; and factors removing Mg^{2+} from the soil solution, such as uptake by organisms and leaching from the soil [58].

Mg^{2+}-containing minerals tend to weather into clay, and cation exchange sites present on clay particles can bind exchangeable Mg^{2+} relatively well. Therefore, clay-rich soils tend to be Mg^{2+}-sufficient, whereas sandy soils provide little Mg^{2+} and leach this ion easily, often providing insufficient quantities [59]. Coarse soils generally lead to lower exchangeable Mg^{2+}-levels, due to lower weathering rates and lower water retention [60]. As a result of the characteristics of the Mg^{2+}-ion outlined in **Section 1.1**, such as its small ionic radius and large hydrated shell, Mg^{2+} only binds weakly to negatively-charged soil particles and cell walls, which means that it can be leached from the soil easily by excess water [61].

Soil pH is especially important for available Mg^{2+}, since low pH increases weathering rates as well as improving the solubility of Mg^{2+}-ions directly. On the other hand, the saturation of ion binding-sites with protons and the presence of aluminium-ions (Al^{3+}) reduce the effective Mg^{2+}-availability at lower pH-values [58]. Al^{3+} is insoluble at high pH, since it tends to precipitate as a hydroxide, but under acidic conditions, presence of Al^{3+}-ions can lead to inhibition of important Mg^{2+}-transport systems [62-64]. Additionally, Al^{3+} can replace Mg^{2+} in active sites of enzymes due to its similar size, inactivating them, meaning that Al^{3+} and Mg^{2+} compete across multiple levels [65]. The optimal pH for Mg^{2+}-uptake therefore likely lies between 5.5 and 6.5 [66].

The presence of excessive amounts of other cations can be detrimental to Mg^{2+}-uptake, since Na^+, K^+, NH_4^+ and Ca^{2+} can all compete with Mg^{2+} for uptake by the plant [61, 67]. K^+ and/or NH_4^+ are sometimes applied in excess in agricultural systems, meaning that uneven fertilisation can lead to Mg^{2+}-deficiencies in crop plants [67]. Salinisation, leading to the presence of excess Na^+-ions in the soil, is a significant and growing problem [68]. It is caused both by natural processes, such as weathering of rocks and rainfall, and by irrigation, especially when carried out in an inefficient manner [69]. Increasing salinisation can indirectly reduce availability of Mg^{2+} in affected soils, reducing plant tolerance to light and heat [58]. Since hot climates with high light intensities are most in need of irrigation, these are most at risk from associated secondary salinisation [69], potentially affecting yields in these regions.

1.2.3 Importance of magnesium in agriculture

Exchangeable Mg^{2+}-levels in soil solutions around the globe are estimated to generally be between 125 µM and 8.5 mM [66]. Although this is generally considered sufficient for the growth of plants, including crop species, it has been suggested that the rate at which these levels are replenished are often not sufficient to support growth of high-yielding crops over long periods of time, requiring application of Mg^{2+} fertilizers [58, 67].

Mg^{2+} has been considered a "forgotten element in crop production" [49], and significant yield gains could be achieved simply by recognizing the importance of this ion and the fact that deficiencies are not always visible. This is exemplified by a meta-analysis by Wang *et al*. [70]. The analysis was carried out on 570 paired observations from 99 different studies on the impact of Mg^{2+} fertilisation on crop productivity. Mg^{2+} fertilisation was found to increase yield in almost all cases, across different crops, soil types, and fertilisation regimes. The mean increase in yield was 8.5%, with the highest effect on yield of fruits (12.5%), followed by grasses, tobacco, tubers, vegetables, cereals, oil crops, and tea (**Figure 1.3 A**).

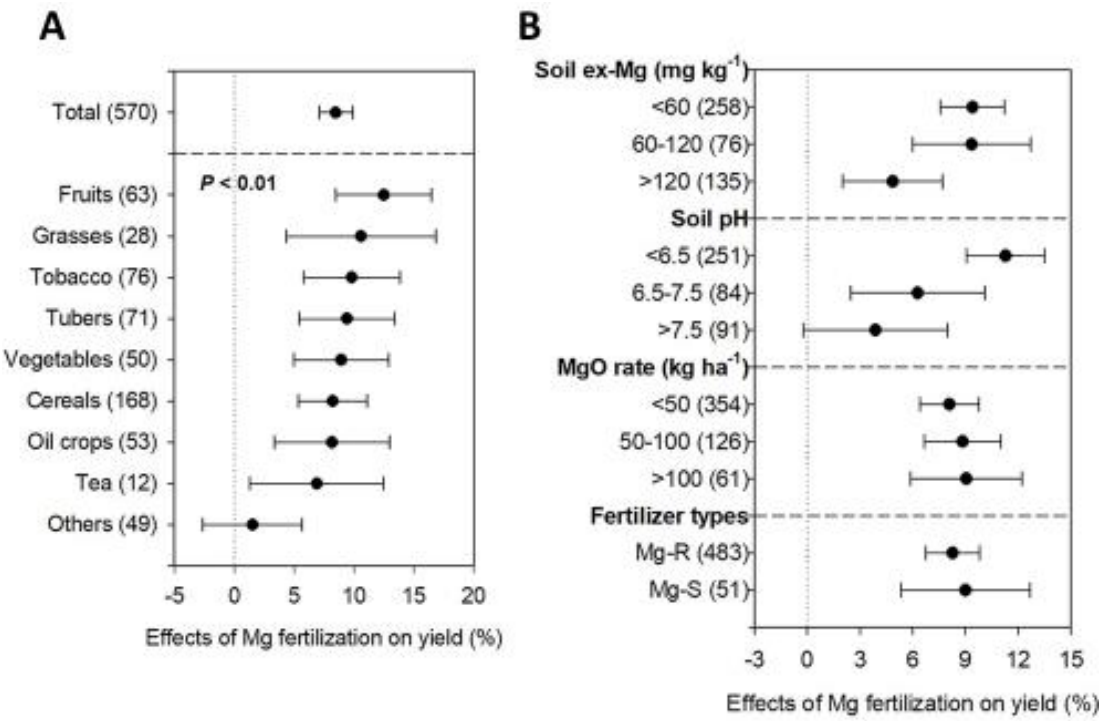

Figure 1.3 - Effect of Mg^{2+} fertilisation on yield for different crops and soils

A – Effects of Mg^{2+} fertilisation on different crops **B** – Effects on crops grown on different soils or under different fertilizer application regimes. Data points are given as mean values, with confidence intervals. Brackets next to each crop or condition give the number of observations used. Soil ex-Mg: Soil exchangeable magnesium; MgO rate: total application of MgO per soil area; Mg-R: rapidly released magnesium fertilizer types; Mg-S: slowly released magnesium fertilizer types. Adapted from Wang *et al*. [70].

The highest impact of Mg^{2+} fertilisation was achieved on soils of low Mg^{2+}-content or pH, as expected, and there was generally no further increase in yield when more than 100 $kg.ha^{-1}$ fertilizer was applied (**Figure 1.3 B**). The agronomic effectiveness (AE) of fertilizers is measured as the mass increase in yield per mass of fertilizer applied, in $kg.kg^{-1}$. In this study, the AE for Mg^{2+} fertilizers, on average, was found to be several times higher than for phosphorus, nitrogen or potassium fertilizers, with an average of 34.4 $kg.kg^{-1}$, and values as high as 73.7 $kg.kg^{-1}$ for vegetable crops. The results of this study have been validated since then [71, 72]. This study therefore comprehensively demonstrates the importance of Mg^{2+} within the agricultural setting and the value that can be generated when taking it into account.

Putting these findings into practice and tailoring Mg^{2+}-application to crop species, soil conditions, etc., potentially paired with improved systems for monitoring soil ion content and crop Mg^{2+} status, could significantly improve the productivity and sustainability of agriculture.

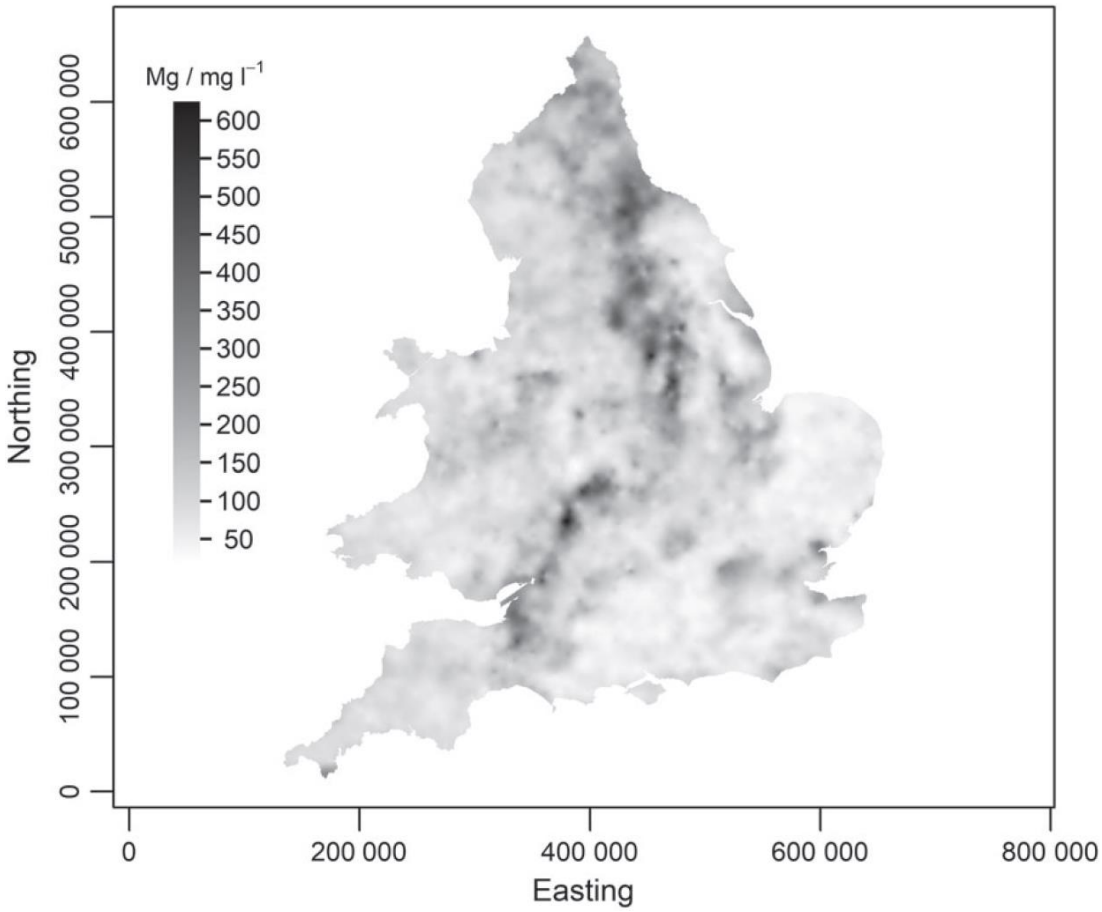

Figure 1.4 - Predicted concentrations of available Mg^{2+} in topsoils across England and Wales

Two datasets from national-scale soil sampling initiatives [73, 74] were combined to produce a statistical model of Mg^{2+}-concentrations across the country. Coordinates are relative to the origin of the British national grid, in metres. From Lark *et al*. [75].

While the previous study focuses strictly on input and output, Hauer-Jakli and Tränkner (2019) present a meta-analysis focused on reaching a consensus with respect to the Mg^{2+}-concentrations plant species require within their tissues, as well as with respect to the physiological consequences of MgD [76]. An analysis of the available literature showed that across studies, MgD significantly and consistently reduced both biomass accumulation and photosynthetic rate.

More importantly though, the available data was used to correlate growth of many different plant species with the internal Mg^{2+}-concentration. Concentrations of Mg^{2+} required for optimal plant growth and yield formation were estimated, and found to be between 0.1% and 0.2% of leaf dry weight for many important crop species, such as potato, wheat, barley and sorghum, but up to 0.35% for some species, such as sunflower or tomato. Critical concentrations for CO_2 assimilation were generally higher, indicating that the capability for CO_2 assimilation is not always the limiting factor for plant growth. These threshold concentrations were found to be remarkably similar across studies for most species. Once a reference concentration has been established for a species, therefore, it could be used to diagnose the Mg^{2+}-status across growth-stages and -conditions.

When choosing the right type of fertilizer, the above-mentioned factors should be considered, to provide crops with adequate levels of Mg^{2+} while causing minimal leaching of ions into the groundwater. To avoid waste and damage to the environment, further research into the design and production of tailored Mg^{2+} fertilizers is needed. Additionally, more efficient ways of determining site- and crop-specific requirements of this ion are needed to prescribe the ideal site-specific Mg^{2+}-supply plan [58, 67]. One site-specific map of soil Mg^{2+}-availability has been generated recently for England and Wales [75], based on two soil surveys: the representative soil sampling scheme [73] and the national soil inventory [74]. Sophisticated statistical methods make it possible to combine data from multiple soil sampling initiatives and generate a detailed map of predicted Mg^{2+}-availability within soils, including the probability of suboptimal Mg^{2+}-supply in any given location, which can be used to inform fertilizer use and/or choices of planted crops (**Figure 1.4**). With the advent of other techniques that are now being applied to the measurement of Mg^{2+}- and Ca^{2+}-concentrations in soils, such as gamma-ray spectrometry [77, 78], proximal soil sensing electromagnetic induction [77], apparent electrical conductivity measurements [79], and visible and near infrared spectroscopy [80], there is potential for true precision agriculture. Greater abundance of precise and accurate maps, combined with the advent of machine learning [81] could lead to refined and improved large-scale maps similar to that presented by Lark *et al*.

1.2.4 Magnesium deficiency in plants

Plants, including *A. thaliana*, maintain cellular Mg^{2+}-concentrations within a tight, specific range, and *Arabidopsis thaliana* is no exception. These concentrations vary between different cellular compartments, plant species, and cell types, and therefore any values reported only represent rough estimates. There must also be a distinction between free Mg^{2+}, i.e. [Mg^{2+}], and total Mg^{2+}, since [Mg^{2+}] usually only makes up about 5-10% of the total Mg^{2+} in a cell, with the rest bound to enzymes, nucleotides or other partners [3, 82]. Further, concentrations of Mg^{2+} and [Mg^{2+}] will vary dynamically in practice, especially in chloroplasts and mitochondria, where their concentrations depend on photosynthetic and general metabolic activity at the time [16, 83]. That being said, concentrations are lowest in the cytosol, at 0.2-0.4 mM [Mg^{2+}] [15, 61, 83], and somewhat higher in the mitochondria (0.2-0.5 mM [Mg^{2+}] [61], or 2-4 mM total Mg^{2+} [15]) and chloroplasts (1-5 mM [Mg^{2+}] in the stroma, 30-50 mM in the lumen [61, 84]), while metabolically-inactive Mg^{2+} is stored in the vacuole (5-80 mM total Mg^{2+}[61]). Many of the estimations of Mg^{2+}-concentrations have been carried out using calculations based on measurements of ATP- and ADP-concentrations [83, 85], although some have been obtained using fluorescent probes [84]. Many improvements on these values are conceivable, such as direct observations of Mg^{2+}, more dynamic *in vivo* measurements, observations across more species and conditions, *etc*.

To achieve and maintain Mg^{2+}-concentrations, plants generally require about 1.5-3.5 g Mg^{2+} per kg fresh weight for optimal growth [66, 76]. When plants become Mg^{2+}-deficient, young mature leaves are affected first, which sets apart MgD from other nutrient deficiencies. The first physiological process that seems to be affected is the export of sugar metabolites from source tissues, which manifests as accumulation of soluble sugars and starch in leaves. This has been observed consistently across multiple species, such as *Arabidopsis* [86, 87], sugar beet [56], *V. faba* (broad bean) [88], and rice [89]. The upstream causes of this have not been proven conclusively; however, several hypotheses have been put forward.

It has been proposed that structural damage to phloem tissues could be the cause; that reduced sink strength could impact export of sugar metabolites; or that phloem loading is impaired under MgD [90].

According to the third hypothesis, impairment of sucrose export is caused by reduced effectiveness of H^+/sucrose symporters involved in apoplastic phloem loading [90]. These transporters are responsible for the import of sucrose into the companion cells of sieve elements in many plant species, and they rely on proton-motive force (PMF) to accomplish this [91]. This PMF is generated in large part by the PM H^+ ATPase [92], which requires MgATP to function. Under MgD-conditions, it stands to reason that [Mg^{2+}] in the cytoplasm would be reduced, and therefore also MgATP-concentrations, which would lead to partial membrane depolarization, therefore reducing the capacity to export sucrose into the phloem [90]. If a strong PMF is required for proper sucrose export, even a comparatively small change in the pH-differential could lead to a large impairment in sucrose export. **Figure 1.5** illustrates this process for sugar beet, in which BvSUT1 is the H^+/sucrose symporter. Both *Vicia faba* and *Arabidopsis thaliana* rely on apoplastic phloem loading as their primary sucrose export mechanism as well, meaning that they are likely subject to the same mechanism. In *Arabidopsis*, AtSUC2 appears to be the primary H^+/sucrose symporter involved in phloem loading [93, 94], although other members of the SUC family also participate in this process [95].

Reduced phloem export currently seems to be the most probable cause for the sucrose accumulation observed, for multiple reasons. MgD led to greatly reduced concentrations of sucrose, as well as ions, in the phloem sap of *Vicia faba*, while sucrose concentrations in leaves were increased, indicating that export of metabolites, and not sink strength, is impaired [88]. In this case, sucrose export could also be restored within 12h of Mg^{2+} resupply; if damage to phloem tissues was the cause for reduced sucrose export, restoration would likely proceed less quickly. Additionally, expression of the BvSUT1 H^+/sucrose symporter could be shown to be increased in response to MgD in sugar beet [56].

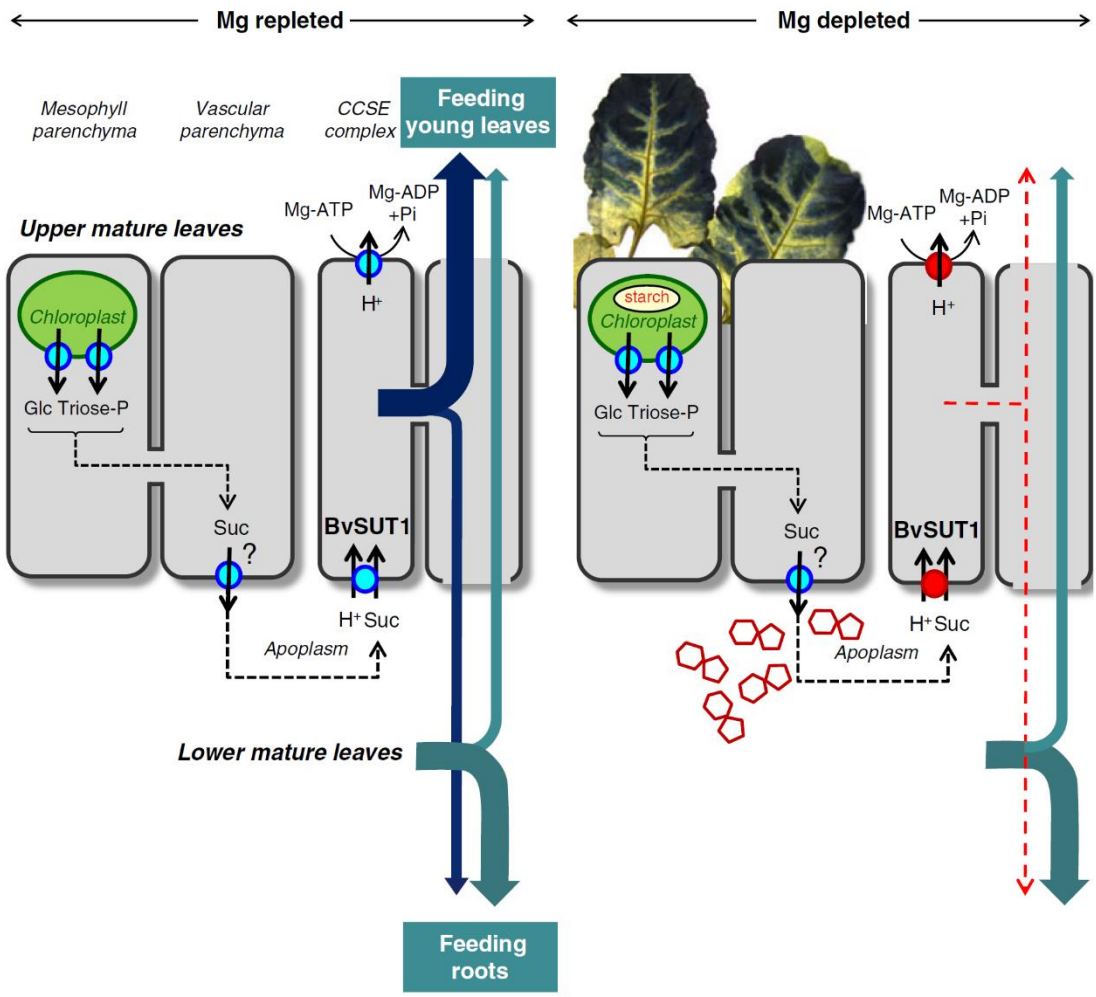

Figure 1.5 - The influence of MgD on phloem loading of sucrose [in sugar beet] The BvSUT1 transporter is responsible for phloem loading of sucrose in sugar beet, whereas AtSUC2 is responsible in *A. thaliana*. These transporters rely on the PMF generated by the PM H^+ ATPase, which in turn depends on MgATP-levels. Under MgD (right), MgATP-levels are reduced, therefore the PM proton gradient is reduced, which impairs sucrose import into companion cells and therefore export from source tissues. Reprinted by permission from Springer Nature: Springer *Plant and Soil* Verbruggen *et al.* [90], © Springer Nature Switzerland AG, 2013

Regardless of the reasons for impaired sucrose export from source tissues, this effect of MgD appears to be the cause of most of the other downstream effects observed. One of these is a reduction of chlorophyll concentrations under MgD [86, 96, 97]. Downregulation of expression of components of the photosynthetic machinery due to negative feedback–inhibition has been observed under MgD; specifically, *Cab2* (Chlorophyll a/b binding protein 2), shows reduced abundance under MgD [86, 87].

Accumulation of sucrose and other metabolites also leads to accumulation of reducing equivalents in the electron transport chain of photosynthesis itself [97]. Excess light energy then results in production of reactive oxygen species (ROS), damaging the photosynthetic apparatus further [49, 58]. This makes Mg^{2+}-starved plants sensitive to light, which is illustrated by high light intensities rapidly leading to chlorosis in leaves of low-Mg^{2+}-stressed plants, while low light produces this response much more slowly [98]. Another mechanism by which reduced chlorophyll abundance can occur is chlorophyll degradation associated with re-mobilisation of Mg^{2+}-ions; this has been shown to occur in rice, where expression of *OsSGR*, encoding a Mg^{2+} de-chelatase, responds specifically to MgD, although the response can be enhanced by the presence of ROS [96]. The associated chlorophyll degradation reduces the amount of ROS generated under MgD and makes Mg^{2+} available for other metabolic functions. Nutrient relocation under MgD has also been demonstrated in *Arabidopsis*, although the molecular players involved are unclear [87]. Therefore, chlorophyll becomes degraded under MgD, although it is not certain how much of this is due to mechanisms inducing Mg^{2+}-recovery and relocalisation, and how much due to photodamage to the molecule [99]. Since degradation of chlorophyll in plants with disturbed Mg^{2+}-homeostasis is dependent on the levels of light experienced by the plants, at least some of the degradation is the result of photodamage [100], and the example from rice shows that at least some species are capable of actively degrading chlorophyll and remobilizing Mg^{2+}.

In summary, it can be said that impaired sucrose export is the most obvious and universal symptom of MgD, and the earliest symptom that has been confirmed and characterized properly. Other symptoms, such as ROS evolution and reduced chlorophyll abundance, occur further downstream, and most likely as a direct result of impaired sucrose export. With the help of publications documenting the emergence of symptoms of MgD over time [56, 86, 87, 97], we can therefore create a simplified diagram illustrating the effects of MgD on plants (**Figure 1.6**).

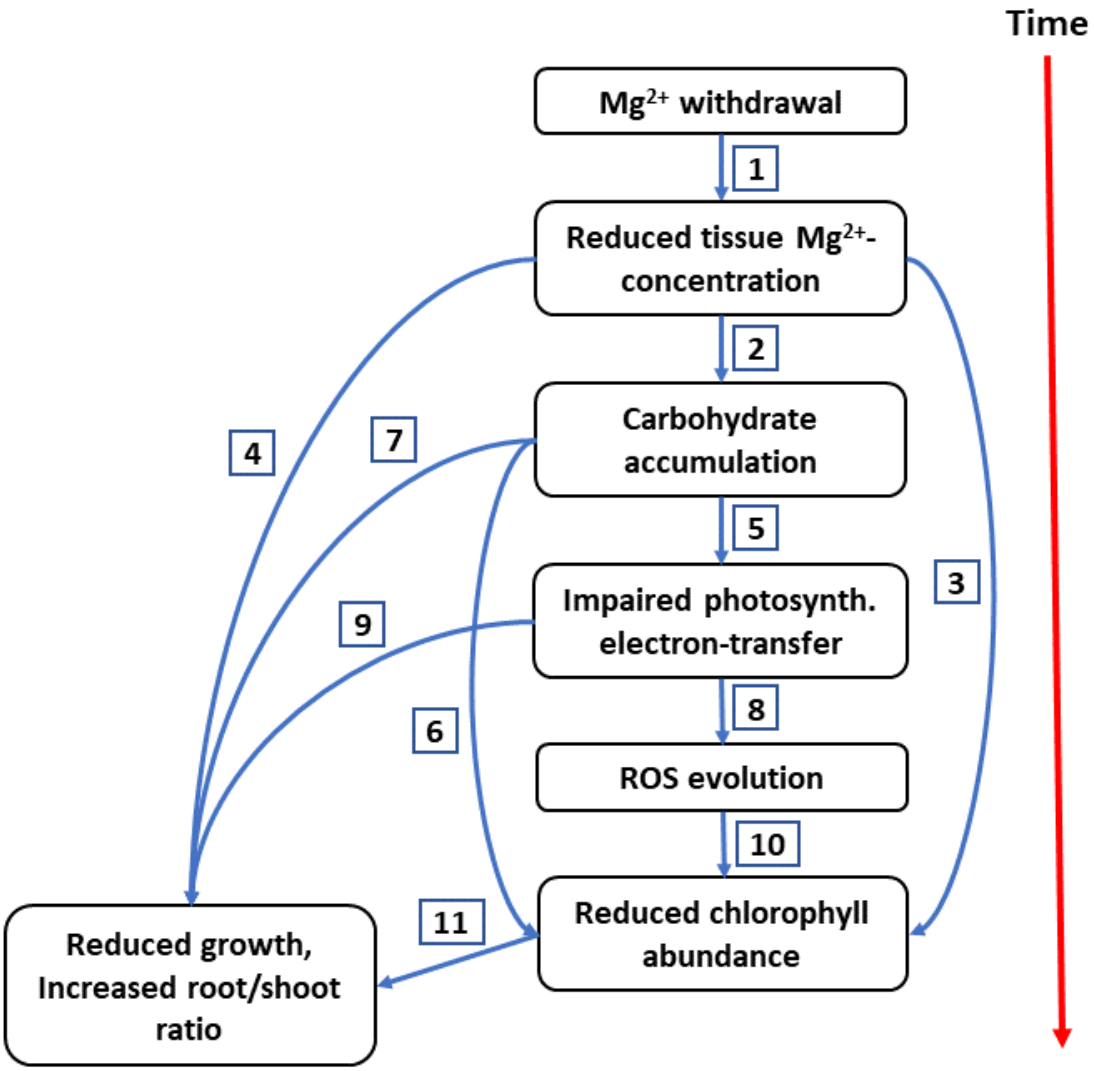

Figure 1.6 - Physiological symptoms of MgD, ordered by time of emergence

Results from multiple, similar studies were combined to obtain a more complete and robust picture [56, 86, 87, 97]. In all cases, plants were grown hydroponically under Mg^{2+}-replete conditions; at day 0, nutrient solution was exchanged for Mg^{2+}-free medium, and symptoms were observed. The red arrow on the right-hand side indicates time after withdrawal; symptoms further down occur later in time. Blue arrows indicate a confirmed or hypothesized causal connection between symptoms. **1** - Reduced uptake of Mg^{2+} from the medium. **2** - Impaired sucrose export from source tissues. **3** - Mg^{2+} remobilization by chlorophyll degradation. **4** - Various metabolic impairments and/or growth adaptations. **5** - Accumulation of reducing equivalents due to feedback-inhibition. **6** - Transcriptional feedback-inhibition of chlorophyll synthesis. **7** - Reduced sucrose supply to sink tissues. **8** - Excess light energy absorbed by photosystems. **9** - Reduced carbon fixation. **10** - ROS-mediated damage to chlorophyll. **11** - Reduced carbon fixation.

1.2.5 Mg^{2+}-sensing in plants

Changes in the *Arabidopsis* transcriptome in response to low Mg^{2+} have been described [101-105], and some of these changes take place as soon as several hours after onset of low-Mg^{2+} exposure [101]. Regardless, virtually nothing is known about how plants perceive low Mg^{2+}, and what signalling-processes are initiated in response. Transcriptional marker genes that react specifically to MgD have not been robustly identified so far, although attempts have been made [105].

The development of root hairs can be influenced by low Mg^{2+}-availability [106]. It appears that ROS and Ca^{2+}-signals lead to increased number and length of root hairs under low Mg^{2+}, whereas toxic levels of magnesium cause reduced root hair development. Ethylene and Nitrous Oxide (NO) act upstream of auxin to regulate increased root hair development under low Mg^{2+} [107]. Even in this case, though, the upstream sensing- and signalling-factors are unknown, and it is not certain whether the response is directly caused by low abundance of Mg^{2+} and not mediated via its antagonistic relationship with Ca^{2+}, the concentration of which can influence the effect of Mg^{2+}-supply on root hair development [106]. There are also changes in root system architecture in response to MgD [108], but even less is known about the mechanism behind this adaptation.

Some of the best candidates for potential Mg^{2+}-sensing proteins are EF-hand motif containing proteins. This motif forms a helix-loop-helix structure with the ability to bind a single, divalent cation; in *Arabidopsis*, up to 250 proteins containing this motif have been identified [109]. EF-hand proteins are usually considered Ca^{2+}-binding, and often Ca^{2+}-sensing, proteins, and many of them have been functionally characterized, confirming this function. However, at least some EF-hand proteins are also able to bind other divalent cations, specifically Zn^{2+}, Cu^{2+}, and also Mg^{2+} [110]. Even though the affinity of these proteins for Ca^{2+} is far greater than Mg^{2+}, the concentration of Mg^{2+} is about three orders of magnitude greater than that of Ca^{2+} under normal conditions, and it is estimated that for many EF-hand proteins, a portion of the binding-sites are occupied by Mg^{2+} in the resting state.

The conformation of EF-hands in their Mg^{2+}-bound form is thought to be different than their Ca^{2+}-bound form; Grabarek *et al*. therefore propose that Mg^{2+} stabilizes the "off" state of EF-hand proteins, and that MgD might cause excessive activation of the associated signalling processes [110]. While this is consistent with the antagonistic effect of Ca^{2+} and Mg^{2+}, the different structure creates an opportunity for the Mg^{2+}-bound forms of these proteins to initiate signalling-processes of their own in theory, and there is certainly a possibility for EF-hand motifs which primarily bind and sense Mg^{2+} to exist. Calmodulin-like 36, an EF-hand protein from *A. thaliana*, is thought to have two sites capable of binding Ca^{2+} or Mg^{2+}, both of which can stabilize the folded state [111].

Calcineurin B-like (CBL) proteins represent a subfamily of EF-hand proteins unique to plants; their primary functions are to sense Ca^{2+} and interact with and regulate CBL-interacting protein kinases (CIPKs) [112]. Tang *et al*. identified two CBLs, CBL2 and -3, which are important in plant tolerance to high Mg^{2+} concentrations. *cbl2 cbl3* mutants accumulate less Mg^{2+} in roots and shoots, accumulate less Ca^{2+} in shoots, and exhibit reduced growth under high Mg^{2+} or high Ca^{2+}. It was determined that CBL2 and CBL3 regulate Mg^{2+} sequestration into vacuoles [113]. While it is not certain whether this mechanism is mediated by Ca^{2+}-sensing or Mg^{2+}-sensing by CBL2 and -3, it nevertheless establishes a role for EF-hand proteins in the regulation of Mg^{2+}-homeostasis in plants, while once again highlighting the antagonistic relationship between Ca^{2+} and Mg^{2+}. Another set of candidates for Mg^{2+}-sensing and -signalling proteins is found among Mg^{2+}-transporters, as will be outlined in subsequent sections.

1.3 Magnesium transport

1.3.1 Magnesium uptake in plants

Movement of Mg^{2+} from the soil solution to plant roots mostly proceeds via mass flow, e.g., the transpiration stream moving ions with it, and via diffusion. Uptake of Mg^{2+} at the root cell plasma membrane is passive, ions moving from solutions of higher concentration to those of lower concentration driven by the electrochemical gradient. While ions can move into the root via the apoplastic pathway at first, they are eventually taken up into cells, proceeding via the symplastic pathway, to bypass the cell wall Casparian Strip. For Mg^{2+}, initial uptake into roots generally seems to take place in the direction of the electrochemical gradient, through channels embedded in the plasma membrane [57, 61]. Mathematically, uptake via diffusion can be modelled using the Nernst equation to estimate the reversal potential across the plasma membrane:

$$E_{Mg^{2+}} = \frac{R \times T}{z \times F} \times \ln \frac{Mg^{2+}_{out}}{Mg^{2+}_{in}}$$

E_{Mg2+} is the Nernst potential (e.g., the equilibrium- or reversal potential), across the plasma membrane, R is the universal gas constant, T is the temperature in Kelvin, z is the charge of the ion, and F is the Faraday constant. We can set T = 298.15 K, *i.e.*, 25°C, for the sake of the calculation. Further, R = 8.314 $J.mol^{-1}$, z = 2 for Mg^{2+}, and F = 96,485.333 $C.mol^{-1}$. We can further assume that only free Mg^{2+} can participate in the establishment of this potential, so using the typical cytosolic concentrations of 0.2-0.4 mM described earlier for Mg^{2+}_{in}, as well as the typical concentrations of Mg^{2+} in soil solutions, 0.125-8.5 mM for Mg^{2+}_{out}, the calculated reversal potentials range from -14.9 mV (0.125 mM out, 0.4 mM in) to 48.1 mV (8.5 mM out, 0.2 mM in). Cations will tend to move passively into a cell as long as the actual membrane potential is greater than the reversal potential for the ion, and since the membrane potential of plant cells is usually below -100 mV, Mg^{2+}should indeed move into the cell passively under this range of conditions. Even assuming exchangeable free Mg^{2+} to be lower than the total Mg^{2+} in soil solution, as well as competition from other ions (see **Section 1.2.1**), Mg^{2+} will likely move into root cells readily in most cases.

Whether this movement and the ability of the soil to replenish Mg^{2+} in soil solution is sufficient to enable optimal plant growth is still questionable, however, and is likely not always the case.

Knowledge of Mg^{2+}-transport from root to shoot is limited, especially compared to what is known about transport of other ions, such as iron and zinc [114]. To reach the shoot, ions must first enter the symplastic pathway to bypass the Casparian strip, before being loaded into the xylem-stream, generally against the prevailing electrochemical gradient. This seems to hold true for Mg^{2+} [61]. In rice, Tanoi *et al*. identified a saturable and a linear component of the process of Mg^{2+}-loading into the xylem stream, which likely equates to one or more "high-affinity" transport system(s), such as ion carriers, making up most of the transport at low concentrations, and one or more "low-affinity" transport system(s), such as ion channels, which are primarily active at high concentrations [115]. Both of these processes could be inhibited by the uncoupling agent dinitrophenol, which inhibits energy-consuming processes. Both of these components are dependent on cellular energy-charge, therefore, likely the membrane potential across the plasma membrane.

Once Mg^{2+} has been loaded into the xylem, it is transported shootward via the transpiration stream, then it must be unloaded in order to reach shoot tissues. Ions then move to various plant organs in the shoot. Often, plants have to compensate for varying transpiration rates of different organs and match the ion demands in each organ. For example, young leaves and reproductive organs have low transpiration rates, but a high demand for ions [66]. Plants therefore must have mechanisms for redistribution of ions between different organs, which must involve regulation of ion-transporters. The phloem-stream generally moves from source organs in the shoots to sink organs, carrying sugars and other metabolites, but also ions. Mg^{2+} is a phloem-mobile element and as such the phloem is important in its transport and redistribution as well [48].

1.3.2 Known magnesium transporters

The uptake of Mg^{2+} into plants, and the distribution between plant tissues, must take place via transport proteins. Transporter regulation is very likely to be a target for the Mg^{2+}-sensing and -signalling network, or potentially a starting-point, if they are themselves regulated directly by Mg^{2+}. Understanding the mechanisms of action and regulation of Mg^{2+}-transport systems could therefore represent a crucial step in unravelling this network. Several proteins or protein-families with the ability to transport Mg^{2+} have been identified so far, although their importance in Mg^{2+}-transport *in vivo* is often unclear.

The first Mg^{2+} transport-system from plants to be cloned and functionally characterized was the Mg^{2+}/H^{+}-exchanger MHX [116]. This protein is expressed in roots and shoots, and localizes to the tonoplast, where it exchanges protons with Mg^{2+}, Zn^{2+} and Fe^{2+} [114, 116]. Since it is strongly expressed in vascular tissues of shoots and roots, this protein might be involved in indirectly controlling xylem loading or retrieval of these ions [116]. Transgenic tobacco plants overexpressing this transporter are sensitive to elevated levels of Zn^{2+}, Cd^{2+} and Mg^{2+} in the growth medium, although the shoot concentrations of these ions remain unchanged [61, 116]. AtMHX is nevertheless strongly expressed in Mg^{2+}-hyperaccumulators like *A. halleri*, indicating a possible role in vacuolar sequestration of Mg^{2+} [61].

Since Mg^{2+}-uptake into roots is thought to be mainly passive, a significant amount could occur through non-selective channels such as the root cation channel *rca*, located in the plasma membrane of root cells and permeable to many different types of cations [114]. Another non-selective transporter which might be involved in Mg^{2+}-homeostasis is cyclic nucleotide-gated channel 10 (CNGC10). This channel transports K^{+}, Ca^{2+} and Mg^{2+} [117, 118], and is expressed in the root stele and the mesophyll parenchyma, the cell-type accumulating the highest vacuolar concentration of Mg^{2+} [61, 119]. *Arabidopsis* RNAi-lines for CNGC10 showed reduced root influx and shoot levels of Mg^{2+} and Ca^{2+}, implying this protein in root uptake and long-distance transport of these ions [117].

More recently, metal tolerance protein 10 (MTP10) has been implicated in long-distance transport of Mg^{2+}, with *mtp10* mutants being sensitive to high Mg^{2+}-concentrations and their growth being restored by concomitantly increased Ca^{2+}-supply [120]. The phenotype is notably similar to that of the *cbl2 cbl3* double mutant described by Tang *et al*. [113], and indeed, quantitative real-time polymerase chain reaction (qRT-PCR) analysis carried out by Ge *et al*. revealed that the expression of *CBL2*, *CBL3*, and several of the *CIPK*s they were found to interact with (*CIPK9*, *-23* and *-26*) was altered in the *mtp10* mutant under normal Mg^{2+}-supply, high Mg^{2+}, or both. Interestingly, the expression of other Mg^{2+}-transporters, namely *MRS2-1*, *MRS2-2*, *MRS2-4*, *MRS2-11*, and *MHX*, was altered as well. MTP10 was also found to interact with CIPK7 and -26 in yeast two-hybrid and bimolecular fluorescence complementation assays [120]. The authors did not test interaction with other CIPKs, which means it is possible that this transporter indeed interacts with CIPK3, -9, -23 and/or -26 *in vivo* and therefore represents the target of the regulation of Mg^{2+}-homeostasis by CBL2 and CBL3, which could represent the beginning of an emerging Mg^{2+}-homeostasis network.

The most well-described family of Mg^{2+}-transporters in plants, however, is the MRS2-family [57, 114], which will be described in the subsequent sections.

1.3.3 The CorA/MRS2/MGT-superfamily of magnesium transporters

The first member of this family was identified after screening a cDNA library for genes restoring the ability of a yeast *alr1 alr2* – mutant to grow on media containing 4 mM Mg^{2+}, with the rest of the family identified via sequence similarity [121].

Plant MRS2-family proteins are members of the CorA/MRS2/Alr superfamily, also termed 2-TM-GxN-type proteins for their two transmembrane helices and the conserved GxN-motif (most commonly GMN) present in all family members [122]. This superfamily includes CorA from prokaryotes; Mrs2p, as well as Alr1p and -2p from yeast, MRS2s from plants, and various other members [122]. Despite their low sequence similarity, the members of the superfamily can complement phenotypes caused by each other's absence even over wide phylogenetic distances, implying a degree of functional conservation [62, 121].

The CorA protein, named for its identification during a cobalt resistance screen, is present in roughly 50% of all the prokaryote genomes sequenced so far, and is thought to usually represent the most important Mg^{2+}-uptake system where it is present [122].

Members of the CorA family usually transport Mg^{2+} and Co^{2+}, sometimes with higher affinity for Co^{2+}, but other members of the superfamily have been found to transport other ions, such as Zn^{2+} [123]. The structure of CorA was the first to be determined [124-126], and it has become a model for the entire superfamily. The protein was found in the plasma membrane as a homopentamer, with two alpha-helices crossing the membrane per subunit. The first of the two helices in the sequence, termed TM1, mainly forms the pore, which is about 55 Å long, and between TM1 and TM2 lies a short "extracellular loop", with a conserved GxN-motif close to the beginning of the sequence [127]. This extracellular loop, especially the GxN motif, which is conserved across the entire superfamily, is heavily implied in establishing specificity and "concentrating" ions around the pore entrance [123]. When this motif is mutated, transport capability of the protein is abolished [127]. It appears that the extracellular loops of the subunits come together to form a "selectivity filter", allowing access only for the appropriate ion(s), making use of the ionic radius and hydration chemistry of the target ion(s) to establish selectivity [123]. Somewhat further down the pore lies a "hydrophobic gate" formed by specific residues along TM1, which prevents access when the channel is closed [123]. **Figure 1.7** shows the structure of the CorA-protein, with the selectivity filter and the hydrophobic gate visualized in **C** and **D**.

The CorA-molecule also possesses intracellular regulatory subunits. When the structure of CorA was first determined, it was noted that electron densities between specific residues pointed towards Mg^{2+}- or Co^{2+}-ions being chelated by these residues, between the individual subunits of the complex. It was speculated that the complex becomes locked in a closed state upon binding Mg^{2+} (or possibly Co^{2+}), with the channel opening when intracellular concentrations of the ion(s) are too low [124-126].

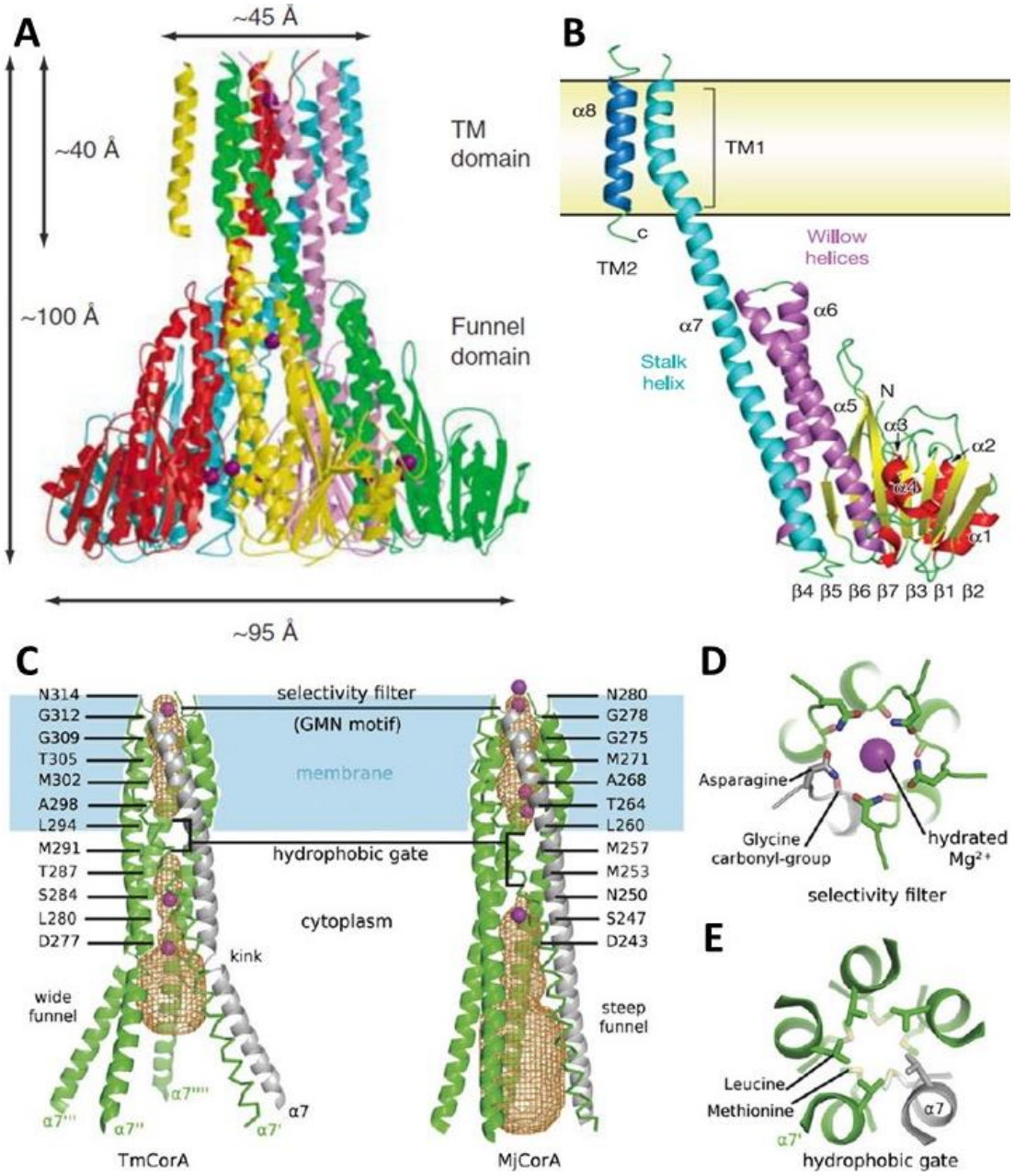
A
~45 Å
~40 Å
~100 Å
~95 Å
TM domain
Funnel domain
B
α8
TM1
c
TM2
Willow helices
α6
α7
Stalk helix
α5
N
α3
α2
α4
α1
β4 β5 β6 β7 β3 β1 β2
C
N314
G312
G309
T305
M302
A298
L294
M291
T287
S284
L280
D277
selectivity filter
(GMN motif)
membrane
hydrophobic gate
cytoplasm
kink
wide funnel
α7'''
α7''
α7''''
α7'
α7
TmCorA
N280
G278
G275
M271
A268
T264
L260
M257
M253
N250
S247
D243
steep funnel
MjCorA
D
Asparagine
Glycine carbonyl-group
hydrated Mg2+
selectivity filter
E
Leucine
Methionine
α7
α7'
hydrophobic gate

Figure 1.7 - Structure of the bacterial CorA channel and function of the individual parts

A – Structure of the homopentameric native *Thermotoga maritima* CorA-channel (TmCorA), with the dimensions of the complex and the individual domains shown. Adapted from Payandeh *et al*. [124]. **B –** Structure of one monomer of the TmCorA complex, with the secondary structural elements numbered. Parts in yellow and red represents the intracellular regulatory domain. Adapted from Lunin *et al*. [125]. **C –** Arrangement of the helices making up the pore of the CorA-complex (e.g. TM1) in TmCorA and *Methanococcus jannaschii* CorA (MjCorA), with the dimensions of the pore outlined (yellow net), and important residues along the pore marked in the structure, as well as the GMN motif. **D –** Model of the selectivity filter formed by the GMN motifs within the extracellular loop of CorA. **E –** Model of the hydrophobic gate within the pore of CorA. **C, D** and **E –** From Payandeh *et al*. [123]. Purple spheres represent Mg^{2+}-ions at their potential binding-sites within the molecule.

After initial difficulties in crystallising the channel in the Mg^{2+}-free state, high-quality cryo-electron microscopy images of both open and closed states could be obtained. It was confirmed that the Mg^{2+}-free state represents a less rigid, asymmetric state, instead of the fivefold rotationally symmetric closed state. CorA is therefore subject to an interesting regulatory mechanism, which seems to prevent intracellular Mg^{2+}-concentrations from increasing above required concentrations without the need for additional regulatory proteins [128]. The channel has now been increasingly well-characterized [129], and this gating-mechanism is well-established [130]. Indeed, the conformational change the Mg^{2+}-sensing domain of CorA undergoes upon binding Mg^{2+} has been used to create the Mg^{2+}-sensitive Förster resonance energy transfer (FRET) sensor MARIO [131].

Mrs2p is one out of two Mg^{2+}-channels present in the inner mitochondrial membrane of yeast, with the other being Lpe10p. Mrs2p was named for the RNA-splicing defects with respect to type II introns in mitochondria observed in mutants, which was later identified to be due to Mg^{2+}-deficiency within mitochondria in mrs2Δ mutants. Both proteins, as well the plasma-membrane Mg^{2+}-channels Alr1p and -2p from yeast, are homologues of CorA, and members of the CorA/MRS2/Alr superfamily [122]. Unlike CorA, Mrs2p was not found to transport Co^{2+}, but rather to be selective for Mg^{2+}, with some Ni^{2+}-transport capability and potent transport inhibition by cobalt hexammine (III) [132, 133]. Even though the sequence of Mrs2p only bears low similarity to CorA, determination of the protein structure revealed major similarities between the two proteins [134] (**Figure 1.8**). The regulatory domain was found to adopt a somewhat different fold, but the Mg^{2+}-binding/sensing site is present. It is made up by Asp97 and Glu270 in the sequence of MRS2p, which are equivalent to Asp89 and Asp253 in the sequence of TmCorA (**Figure 1.8 B**). The hydrophobic gate is made up of Met309 and Leu313, and the GMN-motif is present in the equivalent position [134]. Additionally, single-channel patch-clamp experiments could show that Mrs2p is a high-conductance Mg^{2+}-channel like CorA [132]. The transport activity of this protein is also regulated by intracellular Mg^{2+}-concentrations, with the open probability of the channel dropping drastically at internal Mg^{2+}-concentrations of 1 mM compared to 0 mM.

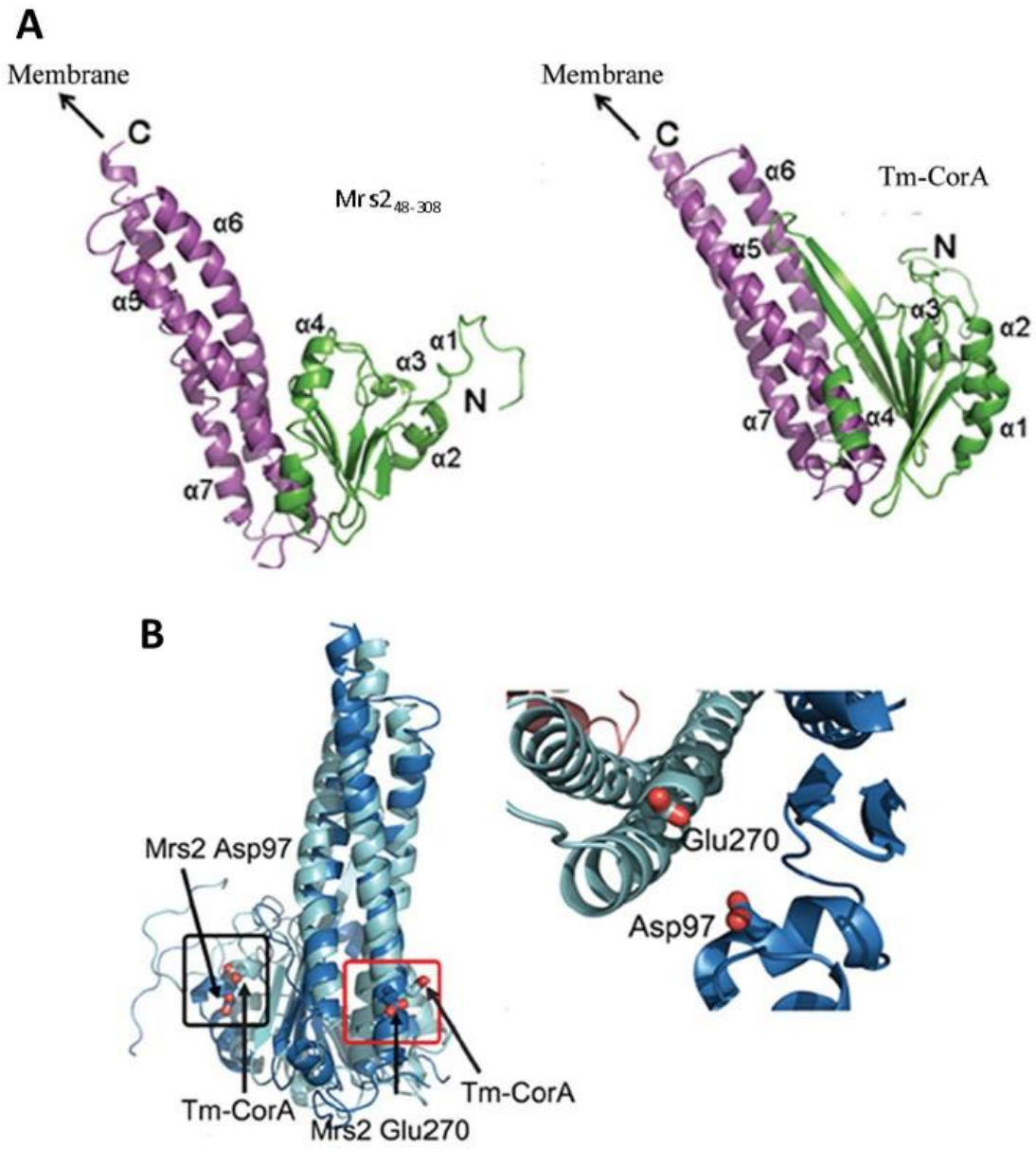

Figure 1.8 -Comparison between CorA-homologues from bacteria and yeast.

A – Comparison between the structures of *Thermotoga maritima* CorA (Tm-CorA, right) and the N-terminal fragment of Mrs2p ($Mrs2p_{48-308}$, left). **B** – Left: Superposition of the structures of TmCorA (cyan) and MRS2p (blue), with the Mg^{2+}-binding residues highlighted. Right: The putative Mg^{2+}-binding pocket in Mrs2p, with the regulatory domains from two different subunits, highlighting the way the Mg^{2+}-ion is bound between two subunits. Adapted from Khan *et al*. [134]

1.3.4 MRS2/MGT magnesium transporters in *A. thaliana*

The plant MRS2-family was discovered independently by Li *et al*. [121] and Schock *et al*. [135]. Due to this, two different nomenclatures were adopted, with members being characterized as MRS2-1 to MRS2-11 [135], but also as MGT1 to MGT10 (MGT for magnesium transporter) [121]. **Table 1.2** gives their names in both systems, as well as the genomic locus, for each family member. Since then, members of the MRS2 family have been functionally characterized in *Arabidopsis* [119, 136-140], and, more recently, in maize [141-143], rice [144-147], *B. napus* [148], banana [149], pear [150], the *Malvaceae* family [151], and *Saccharum* [152], among others.

Table 1.2 - The MRS2 family of Mg^{2+}-transporters in *A.thaliana*

MRS2 name	MGT name	genomic locus	subgroup / clade	subcellular localisation
MRS2-1	MGT2	AT1G16010	I / B	Tonoplast [119]
MRS2-2	MGT9	AT5G64560	III / E	PM [153]
MRS2-3	MGT4	AT3G19640	I / C	ER [154]
MRS2-4	MGT6	AT3G58970	II / D	Chloroplasts [155] / PM [138, 153] / ER [103]
MRS2-5	MGT3	AT2G03620	I / B	Tonoplast [119]
MRS2-6	MGT5	AT4G28580	II / D	Mitochondria [156] / PM [153]
MRS2-7	MGT7	AT5G09690	III / E	ER [136]
MRS2-8	MGT8	AT5G09720	III / E	Unclear
MRS2-9	-	AT5G09710	-	-
MRS2-10	MGT1	AT1G80900	I / B	PM [119, 121]
MRS2-11	MGT10	AT5G22830	IV / A	Chloroplast [139, 157]

Name of each MRS2 family member present in *A. thaliana*, equivalent MGT name, and genomic locus are given, as well as data on membership in subgroups based on Lie *et al*. [121] and Gebert *et al*. [136] and putative subcellular localisation of each member.

In the Columbia (Col-0) accession of *A. thaliana*, only nine members of the MRS2 family are functional. AtMRS2-8 contains a naturally-occurring frame-shift mutation in Col-0, but is functional in Landsberg erecta (Ler-0). AtMRS2-9 lacks the GMN motif and is thought to be non-functional in both Col-0 and Ler-0 [136]. Besides these variations, AtMRS2-7, MRS2-8 and MRS2-9 show large degrees of sequence similarity, and they are part of the same gene cluster, pointing to a recent gene duplication. Since different members of this subset are functional in different *A. thaliana* accessions, they potentially represent an interesting target for studies of ecotype variation.

All functional MRS2s from Col-0 have been shown to complement the yeast *mrs2*-mutant to various degrees [135, 136]. For individual members of the family, Mg^{2+} transport capability could be confirmed in yeast [121, 138, 157], as well as *Salmonella* mutants [140, 156] and more recently in proteoliposomes [63, 158, 159]. The transporters in question were found to also transport Ni^{2+}, although with reduced affinity; in fact, their ability to transport Mg^{2+} was first shown by observing inhibition of $^{63}Ni^{2+}$-tracer uptake by added Mg^{2+} [121, 138, 140]. They were not found to transport any metals tested in these assays aside from Mg^{2+} at their physiologically-relevant concentrations. AtMRS2s are therefore likely Mg^{2+}- specific transporters in their natural state, although some members were later found to be permeable to Al^{3+} [63]. Based on their transport activity and the ability to function in reconstituted proteoliposomes, AtMRS2s are most likely Mg^{2+}-channels, passively transporting Mg^{2+} across biological membranes, although some of their homologues from prokaryotes have been reported to be proton-metal symporters [129]. AtMRS2 Mg^{2+}-transport is generally strongly inhibited by Al^{3+}, which has a similar ionic radius to Mg^{2+} and therefore competes for uptake [65, 160]. Both proteoliposomes and *E. coli* TM2 Mg^{2+}-uptake mutants were recently used to demonstrate that MRS2-1 and MRS2-10 show large differences in terms of aluminium-sensitivity, despite their high sequence identity of around 88% [63]. MRS2-1 is not permeable to Al^{3+}, unlike MRS2-10, and its Mg^{2+} transport activity is only inhibited by very high concentrations of Al^{3+}, whereas MRS2-10 is highly sensitive to this ion, showing that sequence similarity is not always indicative of transport activity, and additional experiments may be required to assess Al^{3+}-sensitivity of other family members.

Arabidopsis MRS2s can be divided into four subgroups, labelled I to IV [121], or five clades, labelled A to E [136], based on sequence homology (**Table 1.2**). The only difference between the two classifications is that in the latter, MRS2-3 is in its own group, easily justified by it being the only member lacking introns in its gene model. Additionally, MRS2-1, -5, and -10 appear to be functionally redundant [137], supporting their membership in the same, distinct group, whereas MRS2-3 knockout causes severe fertility phenotypes [154].

MRS2s were found to be expressed in various tissues and developmental stages [136]. The individual members also appear to localize to different subcellular membranes [103, 119, 136, 138, 139, 153, 154, 156, 157] (**Table 1.2**), presumably controlling the Mg^{2+}-concentrations in different subcellular compartments. Every major subcellular compartment is represented in the list, with several family members being attributed to multiple membranes by different authors, and membership in different phylogenetic clades not correlating with localisation to a specific compartment / membrane.

The concrete physiological functions exhibited by *Arabidopsis* MRS2s are diverse. Many MRS2 family members are crucial for normal fertility, specifically for pollen development, with knockout of MRS2-2 [140], MRS2-3 [154] and MRS2-6 [156], members of three different clades, all causing pollen defects and therefore partial or complete male sterility. All of these transporters were found to be expressed in the male reproductive tissues, either at different stages of development or within different substructures [136, 153, 161], indicating that they are most likely responsible for translocation of Mg^{2+} into pollen and associated tissues (**Figure 1.9**). Interestingly, not only increased Mg^{2+} supply can restore fertility in *mrs2-6* mutants [153], but also slower growth, either due to a short-day growth regime, or even due to additionally knockout of MRS2-4 [161], indicating that import of Mg^{2+} is slowed, but not abolished in these mutants.

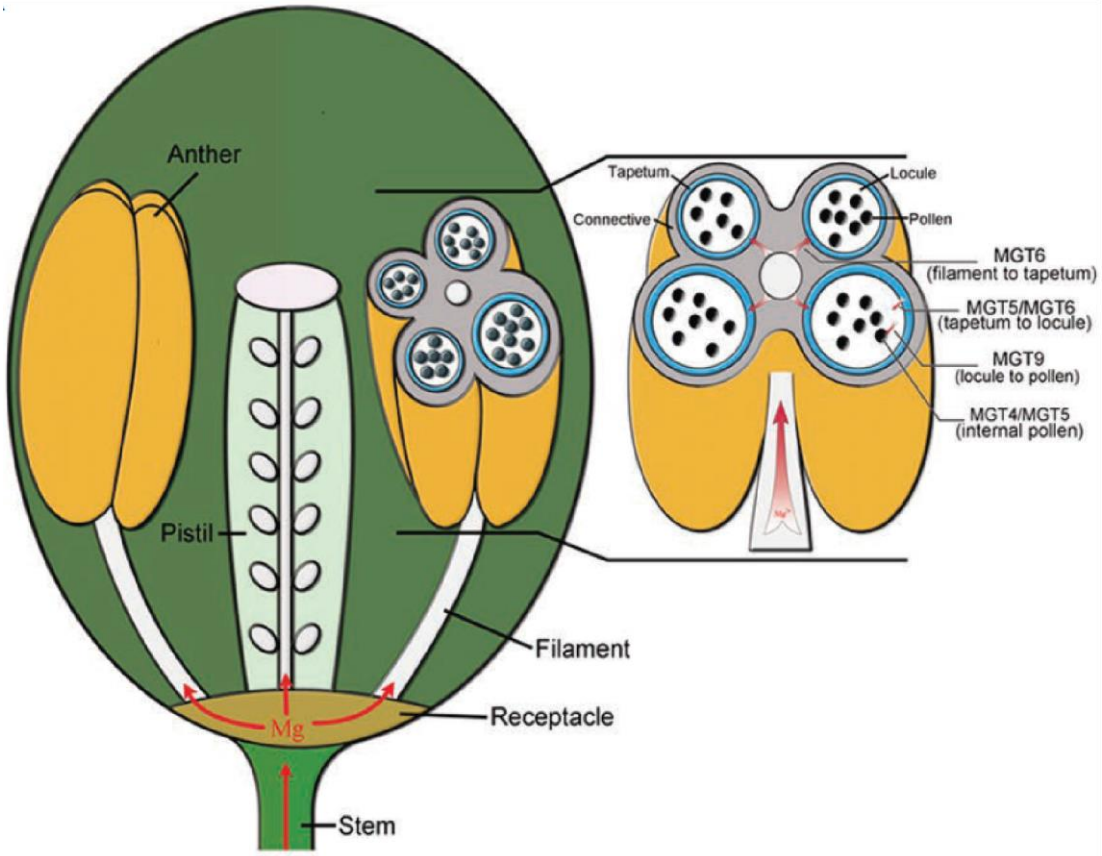

Figure 1.9 - MRS2-mediated Mg^{2+}-transport to pollen.

Model of Mg^{2+}-translocation from filament to pollen within *Arabidopsis* male reproductive tissues, mediated by MRS2 family transporters; based on spatial and temporal expression data, as well as phenotypes observed for *mrs2* knockout mutants. Adapted from Xu *et al.* [161]

MRS2-1 and MRS2-5 appear to be important for sequestration of Mg^{2+} into vacuoles of leaf mesophyll cells of *Arabidopsis* [119]. Although the transcript abundance of MRS2s generally does not change with varying Mg^{2+}-supply [102], transcript abundance was correlated with leaf Mg^{2+} concentrations across 23 *Arabidopsis* ecotypes, and both proteins were targeted to the tonoplast membrane [119]. MRS2-10, the third member of clade B, appears to be localized to the plasma membrane [119, 121] of various cell types throughout development [136], potentially having changed its localisation comparatively recently in evolutionary history [137].

Although single knockouts of clade B MRS2s do not cause appreciable macroscopic phenotypes, multiple knockouts lead to sensitivity to low Mg^{2+}-concentrations, implying importance of clade B MRS2s in Mg^{2+}-uptake and -transport, as well as functional redundancy [137]. These plants were also found to be sensitive to Cd^{2+}-toxicity, highlighting the interplay between Mg^{2+} and Cd^{2+} [162].

Two further MRS2 family members appear to be involved in Mg^{2+}-uptake and translocation from root to shoot: MRS2-4 and MRS2-7. Knockout of MRS2-7, a clade E MRS2, was shown to cause sensitivity to low concentrations of Mg^{2+} during early attempts to characterize the family and was found to be localized within the endoplasmic reticulum (ER) [136]. This family member appears to exhibit a complex expression pattern. Mao *et al*., [163] characterize the gene as a low-affinity Mg^{2+}-transporter and identify two splice isoforms, only one of which was found to transport Mg^{2+}. These results were recently strengthened further, when a mutant arising from a forward genetic screen for seedlings with impaired Mg^{2+}-homeostasis was found to harbour a mutation in SMU1, a splice factor [164]. Although the splicing process was found to be independent of Mg^{2+}-concentrations, these findings highlight the possibility for post-transcriptional regulation of Mg^{2+}-transport processes. Currently, the gene model of MRS2-7 registered on TAIR (www.arabidopsis.org) contains 10 introns and 13 splice isoforms.

MRS2-4 is the most well-characterized member of the MRS2 family in *A. thaliana*. MRS2-4 is a member of clade D, like MRS2-6, but while MRS2-6 expression appears to be restricted to male reproductive tissues, the expression of MRS2-4 is far less restricted, and symptoms caused by knockout of this gene are far more universal. *mrs2-4* plants were originally found to be sensitive to both low concentrations of Mg^{2+}, and to exhibit lower internal Mg^{2+}-concentrations, as demonstrated using RNAi lines. This indicates that MRS2-4 could be responsible for Mg^{2+}-uptake in *Arabidopsis* roots, especially under low external concentrations, which is consistent with its putative role as a high-affinity Mg^{2+}-uptake system [138]. This study also assigned a plasma membrane localisation to this protein, as demonstrated via a GFP fusion construct, expressed in mesophyll protoplasts. Before this, Gebert *et al*. assigned a chloroplast localisation to MRS2-4 [136], after a study of chloroplast membrane proteins by Froehlich *et al*., [155].

Oda *et al*. [103] identified an *mrs2-4* mutant from a forward genetic screen for plants impaired in Mg^{2+}-homeostasis, which was determined to be sensitive to high and low Mg^{2+}-concentrations. Further, the transcriptomic profile of *mrs2-4* plants at Mg^{2+}-replete conditions was similar to that of wild-type (WT) plants experiencing MgD. The authors determined GFP-fused MRS2-4 to be localized to the ER.

Newer research, in addition to confirming earlier findings, has further elucidated a dual role for this channel in roots and shoots [165]. *mrs2-4* plants were shown to contain less Mg^{2+} under both high and low Mg^{2+}-concentrations. During grafting-experiments, when *mrs2-4* roots were grafted with WT shoots, roots exhibited lower Mg^{2+}-concentrations than WT roots under low external Mg^{2+}. Additionally, *mrs2-4* shoots grafted onto WT roots exhibited reduced Mg^{2+}-levels under high external Mg^{2+}, indicating that this transporter could fulfil an additional role in long-distance Mg^{2+}-transport through the xylem, either in xylem loading or unloading. *mrs2-4* shoots with WT roots generally exhibited stronger phenotypes than *mrs2-4* roots with WT shoots, implying this transporter's roles in shoot tissues are as crucial as in root tissues, if not more so. Mg^{2+}-sequestration, which appears to occur mostly in vacuoles of leaf mesophyll cells in *Arabidopsis* [119], likely becomes impaired in absence of MRS2-4, resulting in increased sensitivity to Mg^{2+} toxicity. Finally, both in the study by Yan *et al*. and by Oda *et al*., *mrs2-4 mrs2-7* double mutants were generated and found to exhibit more severe symptoms than either single mutant, with impaired growth even under Mg^{2+}-replete conditions [103, 165]. Both transporters therefore seem to mediate a significant portion of *Arabidopsis* Mg^{2+}-uptake individually, possibly acting synergistically or interacting in some way. Work by Ogura *et al*. further solidified MRS2-4 and MRS2-7 as important mediators of Mg^{2+}-uptake in *Arabidopsis* roots. When *A. thaliana* were grown on low Mg^{2+}-concentrations for 24 hours and then transferred to replete Mg^{2+}, rates of Mg^{2+}-uptake were initially high, but dropped as soon as 5 minutes after transfer [166]. In *mrs2-4* and *mrs2-7* mutants, the initially high rate of uptake was not observed, with low Mg^{2+}-conditioned *mrs2-4* and *mrs2-7* plants taking up Mg^{2+} at similar rates to WT or mutant plants without low Mg^{2+} adaptation. Therefore, MRS2-4 and MRS2-7 are both crucial for Mg^{2+}-uptake when concentrations are low, and it appears that this uptake can be regulated across very short spans of time.

In summary, the MRS2 family is responsible for much of the Mg^{2+} transport in *A. thaliana*, with individual members specialized to act in different organs, subcellular membranes, and concentration-ranges.

1.3.5 Plant MRS2s as Mg^{2+}-gated Mg^{2+}-channels

Since both the prokaryotic and yeast homologues of plant MRS2s appear to be regulated by external Mg^{2+}-concentrations, it would not be particularly surprising if this regulatory mechanism was found in the members of the superfamily from plants as well. Indeed, despite the sequence identity between the AtMRS2s and yeast Mrs2p being around 20% (source: www.uniport.org/blast), and that between CorAs and AtMRS2s being even lower, the predicted structure of AtMRS2s is very similar to that of CorA (and Mrs2p) [167] (**Figure 1.10 A**). The hydrophobic and negatively-charged residues along the pore, which are likely essential for ion-conduction and specificity, seem to be especially conserved, together with the GMN-motif and several others [167]. Schmitz *et al*. state that the residues responsible for ion-sensing and closing of the pore in CorA are not conserved in AtMRS2s, after performing sequence alignments between CorA and AtMRS2s [167]. However, this might be an oversight. Alignment of the sequence of Mrs2p, instead of CorA, to AtMRS2-4 reveals that that the residues hypothesized to participate in Mg^{2+}-sensing in Mrs2p, Asp97 and Glu270 [134] (**Figure 1.8 B**), are present in MRS2-4. They can also be seen in other plant homologues, and several residues around them are identical or highly conserved (**Figure 1.10 C**). Those residues forming the hydrophobic gate appear to be conserved as well, although M309 in Mrs2p is replaced by an isoleucine residue (I368) in AtMRS2-4. Therefore, contrary to the results from Schmitz *et al*., it appears likely that at least some of the plant MRS2-channels are subject to the same regulatory mechanism as other members of the superfamily. It stands to reason that a regulatory mechanism must exist, given that there should be a strong electrochemical force driving Mg^{2+} into plant cells under most conditions (see **Section 1.3.1**), especially at the root-soil interface, which would suggest that plasma membrane Mg^{2+}-channels would have to remain closed, or otherwise inactive, some of the time.

The results from Ogura *et al*. [166] also point towards a gating mechanism in plant MRS2s, since Mg^{2+}-transport mediated by MRS2-4 and MRS2-7 was seen to be completely suppressed within 5 minutes of exposure to Mg^{2+}-replete conditions. Although it is possible that this reduction in uptake is due to partial saturation of the intracellular space with Mg^{2+}, and therefore equilibration of concentrations inside and outside the root, the fact that the portion of total Mg^{2+}-uptake showing this rapid change was entirely dependent on MRS2-4 and MRS2-7 implies that these channels represent a significant amount of total Mg^{2+}-uptake by the root within the first five minutes, then almost none after that. This pattern would be consistent with the action of a Mg^{2+}-gated Mg^{2+}-channel, with few other kinds of regulation able to explain a change in conductance of this magnitude and on this timescale.

Another interesting feature of AtMRS2s is the presence of additional structural elements not found in their homologues from unicellular organisms. The plant family of these channels possesses a large insertion between the sixth and seventh α-helix in the protein structure, termed the "α6b-helix" (**Figure 1.10 B & C**), and others around helices four and five. These insertions have variable lengths and sequences in the different AtMRS2s, and they occur before and after the "willow helices" characteristic of this superfamily, and likely crucial for the opening and closing of the channel [167]. In one experiment, generation of insertions and deletions within helices five and seven in yeast Mrs2p led to protein variants with an impaired ability to close at high Mg^{2+}-levels [132]. Since different cellular compartments exhibit different concentrations of Mg^{2+}, it would be tempting to assume that the insertions in the plant homologues produce channels closing at different concentrations, establishing and maintaining variable concentrations in this way. Other functions for these structures cannot be excluded, of course, including roles in protein-protein interactions. The anomalous α6b-helix and the α4-α5 linker region in plant MRS2s, absent in their homologues, might play a role in signalling processes not required in single-celled organisms, opening the possibility for another low- Mg^{2+} signalling network based on protein-protein interactions. As such, plant MRS2-transporters represent one of the best targets for further research efforts in the field, and their functional characterisation from multiple perspectives should receive focussed attention.

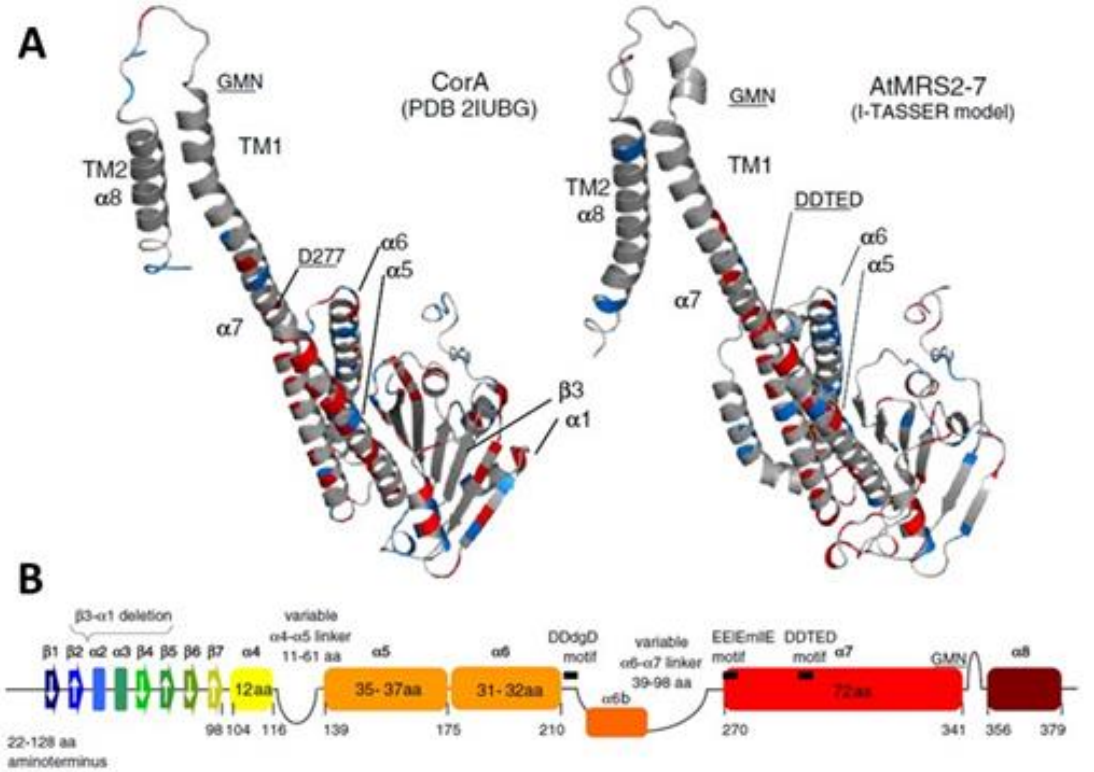


```
Q01926 MRS2_YEAST        84   KWSFLTEHSLFPRDLRKIDNSSIDIIPTIMCKPNCIVINLLHIKALIERDKVYVFDTTNP
                              K + +   S+  RDLR I          I+ +   IV+NL  IKA++  ++V + D   P
Q93ZD7 MRS24_ARATH       81   KSTIIKRASVPARDLRRILGPVFSHSSNILAREKAIVVNLEVIKAIVTAEEVLLLDPLRP
                                                D97
Q01926 MRS2_YEAST        144  SAAAKLSVLMYDL------ESKLSSTKN--------------NSQFYEHRALESIFINVM
                                 +  L             E+ L ++ N              +   +E + LE     V
Q93ZD7 MRS24_ARATH       140  EVLPFVERLKQQFPQRNGNENALQASANVQSPLDPEAAEGLQSELPFEFQVLEIALEVVC

Q01926 MRS2_YEAST        184  SALETDFKLHSQICIQILNDLENEVNRLKLRHLLIKSKDLTLFYQKTLLIRDLLDELLEN
                              S ++            +L++L   V+   L ++     +LT    +   +RD L+ LL++
Q93ZD7 MRS24_ARATH       200  SFVDKSVAALETEAWPVLDELTKNVSTENLEYVRSLKSNLTRLLARVQKVRDELEHLLDD

Q01926 MRS2_YEAST        244  DDDLANMYLTVK----------------------------------------KSPKD
                              ++D+A++YLT K                                          + +D
Q93ZD7 MRS24_ARATH       260  NEDMADLYLTRKWIQNQQTEAILAGTASNSIALPAHNTSNLHRLTSNRSASMVTSNTEED
                                                large insertion, α6b helix
Q01926 MRS2_YEAST        261  NFSDLEMLIETYYTQCDEYVQQSESLIQDIKSTEEIVNIILDANRNSLMLLELKVTIYTL
                              +  DLEML+E Y+ Q D    +  ++ + I  TE+ VNI LD  RN L+ L+L +TI +
Q93ZD7 MRS24_ARATH       320  DVEDLEMLLEAYFMQLDGMRNKILTVREYIDDTEDYVNIQLDNQRNELIQLQLTLTIASF
                                   E270                                    M309 & L313,
Q01926 MRS2_YEAST        321  GFTVASVLPAFYGMNL                            hydrophobic gate
                                   ++L + +GMN+
Q93ZD7 MRS24_ARATH       380  AIAAETLLASLFGMNI
                                   GMN-motif
```

Figure 1.10 - Comparison of the structure and sequence of A. thaliana MRS2s with their homologues

A – The structure of the TmCorA-monomer compared to the predicted structure of the AtMRS2-7 monomer. Conserved basic side-chains are highlighted in blue, and conserved acidic side-chains in red. Secondary structure elements and sequence motifs are highlighted. **B –** Sequence elements in AtMRS2-4 compared to CorA. Variations are highlighted as curved lines or with curly brackets, including the "α6b-helix"-insertion in AtMRS2s. **A & B –** Adapted from Schmitz et al., 2013 [167]. **C -** Sequence alignment of ScMRS2 and AtMRS2-4, from a BLAST-search on www.uniprot.org/blast. Conserved sequence elements are highlighted, as well as the large "α6b-helix" insertion.

1.4 Genetically-encoded ratiometric sensors with potential uses in research on Mg^{2+}-homeostasis

1.4.1 Methods for tracking Mg^{2+}-concentrations within cells and tissues

A significant obstacle for further research into Mg^{2+}-homeostasis in plants is the difficulty of measuring internal Mg^{2+}-concentrations with suitable resolution. The standard method for measuring Mg^{2+}-concentrations within plant tissues is inductively coupled plasma – optical emission spectrometry (ICP-OES) or – mass spectrometry (ICP-MS); however, this method cannot usually achieve resolutions beyond the organ-level, *i.e.*, root vs. shoot or leaf vs. stem. To resolve ion distribution between tissues, or between individual cells, higher-resolution techniques are needed, such as synchrotron X-Ray fluorescence [168], X-ray microanalysis [119], or indirect measurement via nuclear magnetic resonance spectroscopy for the phosphorus in nucleotides (^{31}P-NMR) [169]. These techniques are expensive, time-consuming, and not always available, however, as they require specialist equipment. Another major drawback is the fact that the number of observations is limited due to the destructive nature of these techniques, which means that each sample can only be analysed once, which makes it difficult to follow biological processes.

Another approach for determining cellular and sub-cellular Mg^{2+}-concentrations is the use of fluorescent chemosensors, development of which has progressed at a rapid rate within the last years. Liu *et al*. list a vast number of such compounds that have become available [169]. SBL-3, developed by Yu *et al*., stands out as a probe that has been developed for, *Arabidopsis*, although sub-cellular resolutions have not been achieved yet [170]. Ion-sensitive dyes, however, still have significant drawbacks. Samples must be stained with the dye in question before imaging can take place, which may expose samples to unnatural conditions and alter tissue physiology before measurements can be taken. Samples will usually be completely permeated by the dye, which makes it difficult to isolate signals from individual tissues or cell types during the experiment. Similarly, it is difficult to direct dyes to individual subcellular compartments to achieve sub-cellular resolution, although ways have been found [171].

Förster resonance energy transfer (FRET) is based on the ability of energy transfer to take place between a donor fluorophore and an acceptor fluorophore by nonradiative dipole-dipole coupling. This energy transfer can only occur if the donor emission spectrum overlaps with the acceptor absorption spectrum, and if the two molecules are sufficiently close together in space, with the likelihood of transfer decaying with the sixth power of distance [172]. This essentially enables small differences in the distance between fluorophores to be measured by exciting the donor fluorophore and measuring the emission from the donor and acceptor fluorophore; the ratio between the two intensities will change depending on the inter-fluorophore distance. Therefore, if the distance between fluorophores is dependent on another factor, then that factor can be measured by proxy. Since measurements are ratiometric, expression-levels and most kinds of artefacts do not influence measurements, as long as appropriate controls and corrections are used. FRET sensors for use in biological systems are generally based on two fluorescent proteins, most often a form of cyan fluorescent protein (CFP) as the donor fluorophore and yellow fluorescent protein (YFP) as the acceptor fluorophore, which are linked by a protein known to change its conformation upon binding a ligand of interest. These FRET-sensors based on proteins can be genetically-encoded, which means that different promoters and targeting sequences can be used to elicit specific expression in different cell types and sub-cellular compartments. Additionally, measurements are non-destructive and can be carried out continuously, allowing biological processes to be followed in real time at high resolution [173]. FRET sensors have been used in plants for more than 20 years [174, 175], and have been used to elucidate various biological processes, but FRET sensors with the ability to sense Mg^{2+} have only become available comparatively recently, and have not seen widespread application [176].

The MagFRET series of sensors have been developed based on the high-affinity Mg^{2+}-binding domain of human centrin 3; various mutations in the protein sequence have allowed the creation of sensors with a range of affinities for Mg^{2+}, enabling measurements of a large range of Mg^{2+}-concentrations in theory [177]. MagFRET has been used to study the effects of lactate application on metabolism in animal cells recently [178], but has not been applied within plants to date.

More recently, another novel FRET sensor capable of reporting changes in intracellular Mg^{2+}-concentrations has been developed; MARIO is based on the Mg^{2+}-binding domain from the CorA Mg^{2+}-channel from *E. coli*, which has been truncated and some point mutations introduced into the sequence. It shows a higher affinity for Ca^{2+} than Mg^{2+}, but since intracellular calcium-concentrations are orders of magnitude below those of magnesium, it reports specifically on magnesium at physiological ion-concentrations [131]. It has initially been used in human cells to discover a transient rise in free magnesium within the cytosol during mitotic chromosome-condensation, the first measurement of Mg^{2+}-concentrations in live cells by genetically-encoded biosensors [179], and has been used in *Drosophila* since then [180].

MARIO and/or MagFRET can likely be functionally expressed in plant cells and be used to report on changes in Mg^{2+}-concentrations under different conditions or between different cells in real time, which could greatly simplify the study of Mg^{2+}-homeostasis.

1.4.2 Genetically-encoded, ratiometric sensors have the potential to elucidate the symptoms of MgD

As outlined in **Section 1.2.4**, the early symptoms of MgD are not properly understood. Both the reduction in MgATP-levels and PM pH-differentials are currently only hypothetical, and modern tools are needed to investigate them with sufficient accuracy and resolution.

ATeam, a series of FRET-sensors reporting on MgATP-concentrations, is based on the ε subunit of *Bacillus subtilis* ATP synthase, fused to monomeric super-enhanced cyan fluorescent protein (mseCFP) and circularly-permuted monomeric venus, a yellow fluorescent protein (YFP) variant [181]. One of the derivatives of ATeam, ATeam1.03-nD/nA, which shows a K_d of 0.74 mM for MgATP, has been used to report on ATP-levels in *A. thaliana*, revealing differences in cytoplasmic ATP-concentrations within young seedlings [182], and giving insights into chloroplastic ATP dynamics [183]. Since this sensor has already been used within *Arabidopsis*, it should be possible to use it to investigate changes in MgATP-levels under MgD.

The reduction in the PMF thought to cause the impaired sucrose export observed under MgD (see **Section 1.2.4**) can likely be investigated using genetically-encoded, ratiometric sensors as well. Many genetically-encoded pH sensors have been developed, and have been used to gain insight into biological processes. Some FRET-based sensors exist among them, but most commonly, these sensors make use of the ability of some GFP derivatives to change their absorbance and emission spectrum based on their protonation state. These mutated fluorescent proteins can reversibly transition between a neutral and an anionic form of the central chromophore. During this, their fluorescence, measured as emission at one specific wavelength range, will change according to external pH. Therefore, many GFP variants can be used as intensiometric pH sensors [184]. One such protein is ecliptic pHluorin, a GFP mutant that loses fluorescence at lower pH values, being completely non-fluorescent at its "normal" excitation and emission wavelengths at pH 6 or lower [185]. Intensiometric sensors, however, can only be used to determine changes or differences in pH; since the observed intensity is based on protein expression, photobleaching, autofluorescence and absorption of emitted light by surrounding tissues, among other things. These problems can be mostly eliminated by creating a ratiometric sensor. Ratiometric pHluorin was constructed by introducing further mutations into the protein, causing excitation intensity at 395 nm to increase at higher pH, and excitation intensity at 475 nm to decrease [184]. A ratiometric sensor can also be created by fusing a second, pH-insensitive fluorophore with a different excitation and/or emission maximum to the pH-sensitive fluorophore; pHusion was created by fusing the pH-sensitive eGFP to the pH-insensitive mRFP [186]. Ratiometric pHluorin has been used to estimate pH gradients across the plasma membrane of *Arabidopsis* roots [187]. It is therefore likely that significant changes to the membrane potential caused by MgD could be tested using ratiometric pH sensors.

1.5 Objectives

1.5.1 Aims of this project

The importance of Mg^{2+} in both human and animal nutrition and agriculture is becoming more and more clear. Unfortunately, there are knowledge gaps with respect to Mg^{2+}-sensing and -signalling, Mg^{2+}-transport and its regulation, and the effects of MgD that need to be addressed. Knowledge about these processes is ultimately necessary to advance efforts in biofortification, yield improvement through improved crop- and soil-management, as well as crop improvement through selective breeding and/or transgenic approaches.

The three most viable options available for gaining novel insight into Mg^{2+}-homeostasis in plants are as follows: Bioinformatic methods could reveal patterns in gene expression leading to identification of the missing factors [188]. Non-specific, high-throughput methods such as forwards genetic screens could reveal the missing factors [103, 164]. Work on the function and regulation of Mg^{2+}-transporters could reveal interaction-partners either regulating or being regulated by them [120].

The aim of this project is to address each of these options to some degree. The project aims to first establish a firm basis for further research on the symptoms of MgD by establishing a robust, well-defined, high-throughput pipeline for induction of MgD in *A. thaliana*. This method is then utilized to carry out a forward genetic screen for genes involved in or responding to MgD. Further, the physiological role and subcellular localisation of several MRS2 Mg^{2+}-transporters in *Arabidopsis* are investigated.

1.5.2 Overview of thesis contents

Chapter 3: An investigation of the physiological consequences of magnesium-deficiency in A. thaliana

A literature search for available, published transcriptomic datasets including data on *Arabidopsis thaliana* exposed to MgD was carried out. These datasets were compared to find putative MgD reporter genes. Then, to determine whether MgD could be induced in *A. thaliana* by growing plants on low-Mg^{2+} media for two weeks, the expression of putative MgD marker genes was compared between *A. thaliana* seedlings transferred to low-Mg^{2+} media and those grown on low Mg^{2+} continuously. Growth of plants on different concentrations of Mg^{2+} was characterized, and physiological symptoms of MgD were determined for plants grown on continuous low Mg^{2+}. Symptoms were compared to those reported in the literature, and a relationship between medium Mg^{2+}-concentrations and observed symptoms was established.

Additionally, the early, hypothesized symptoms of MgD were investigated using genetically-encoded, ratiometric sensors. The MARIO FRET-sensor was cloned and transgenic *A. thaliana* expressing the sensor generated. The MgATP FRET-sensor ATeam, as well as the ratiometric pH-sensor pHusion, were used to investigate changes in cytosolic MgATP-concentrations and cytosolic and apoplastic pH under MgD, respectively. The results generated were compared to the model of events taking place under MgD described in **Figure 1.5** and **Figure 1.6**.

Chapter 4: The localisation and physiological role of MRS2 magnesium transporters in A. thaliana

SALK T-DNA insertion lines carrying T-DNA insertions in all MRS2s functional in *A. thaliana* ecotype Col-0 were obtained, and presence of T-DNA insertions within each was confirmed by PCR. Visual growth phenotypes and fertility phenotypes were established for each line used. To investigate sub-cellular localisation and tissue distribution of select MRS2 family members, *mrs2* mutant lines found to exhibit suitable phenotypes were transformed with expression constructs containing the respective MRS2 sequence, fused to GFP. Expression of the transgene and complementation of mutant phenotypes was tested for each line. Then, confocal laser-scanning microscopy was used to investigate the sub-cellular localisation of the GFP-tagged MRS2 in each of the transgenic lines found to express the transgene.

Chapter 5: A forward genetic screen for factors involved in magnesium homeostasis

To carry out a luciferase (LUC) reporter-based forward genetic screen for genes involved in Mg^{2+}-homeostasis, RNA-sequencing was carried out using RNA from *A. thaliana* seedlings grown on media containing different concentrations of Mg^{2+}. Lists of up- and downregulated transcripts were compared to previously-published transcriptomic datasets including data on gene expression under MgD.

Candidate genes with the potential to be robustly and specifically upregulated under MgD were chosen, and their promoters were cloned from Col-0 genomic DNA (gDNA) before being fused to the *LUC* open reading frame (ORF). Candidates that were cloned successfully were transformed into *A. thaliana*. Reporter expression was tested for plants grown on different Mg^{2+}-concentrations, and under several other stress conditions.

Seeds of *LUC* reporter plants were mutagenized using ethyl methanesulphonate (EMS) to generate a mutagenized screening population. M_2 seedlings were screened for loss of reporter expression and increased reporter expression. Candidates found to exhibit altered reporter expression were carried forward. Identification of causative mutations in each mutant line was carried out according to the MutMap/LumiMap pipeline [189, 190].

1.5.3 Contributions to thesis

All experiments were carried out by me, Siegfried Leher (S.L.), except for cloning of the MARIO construct for *Arabidopsis* expression, which was carried out by Tantawat Nardwattanawong (T.N.), who was a year-in-industry student at John Innes Centre (JIC, Norwich, UK) at the time. ICP-OES analysis was performed by technical staff at University of East Anglia (Norwich, UK). All contributions by collaborators with respect to plant material, DNA primers and data analysis are acknowledged fully and appropriately in **Chapter 2** of this thesis.

Chapter 2: Materials and Methods

All chemicals were purchased from Sigma-Aldrich® (subsidiary of Merck KGaA©, Germany), unless otherwise stated. Where chemicals were purchased from Sigma-Aldrich, only catalogue numbers are given.

Data analysis was carried out in RStudio (v. 2021.09.1), based on R (v. 4.1.2), and all Graphs were produced in RStudio using the ggplot2 package, unless otherwise stated. Figures were assembled in Adobe illustrator v. 25.3.2.

All DNA Primers were purchased from Eurofins Genomics GmbH (Ebersberg, Germany).

2.1 Plant maintenance and growth media

2.1.1 *Arabidopsis* lines used in this work

Table 2.1 describes the individual *A. thaliana* lines used in this work, including where each line was obtained from and any publications describing initial creation and/or use of the respective line. All *Arabidopsis* lines used were in the Columbia-0 (Col-0) background.

2.1.2 Growth conditions for *Arabidopsis* on agar plates

Seeds were surface-sterilized in 1.5 mL Eppendorf tubes by adding 1.4 mL of a solution of 62.5% (v/v) EtOH, 37.5% (v/v) dH_2O, and 7.5 $mg.mL^{-1}$ dichloroisocyanuric acid (DCICA) (35915-50G), and shaking for 15 min at 150 rpm. Following this, seeds were immersed in 1 mL 70% (v/v) EtOH twice, for one minute each time, then washed three times with ddH_2O. Seeds were then suspended in 1 mL ddH_2O and stratified for at least 48 h at 4°C before use. Seeds were placed on agar plates containing an appropriate medium, then sealed using micropore tape (R&L Slaughter Ltd., Basildon, England), before being placed in a controlled environment room (CER).

Temperature in the CER was maintained at approximately 22°C, with a photoperiod of 16 h light (≈100 $\mu mol.m^{-2}s^{-1}$) and 8 h dark. Plants were used at different stages of growth, as stated. In each case, the age is given as days after germination (DAG), assuming two days between plating of seeds and germination (*i.e.*, the day seeds are plated is -2 DAG).

Table 2.1 – *Arabidopsis* lines used in this work.

Line	Mutation in [a]	Construct [b]	Source [c]	Reference
Col-0	-	-	C.S.	-
SALK_006797C / *mrs2-1*	AT1G16010 / MRS2-1/MGT2	-	NASC	[191]
SALK_080443 / *mrs2-3* 1	AT3G19640 / MRS2-3/MGT4	-	NASC	[191]
SALK_201976C / *mrs2-3* 2	AT3G19640 / MRS2-3/MGT4	-	NASC	[191]
SALK_203866C / *mrs2-4* 1	AT3G58970 / MRS2-4/MGT6	-	NASC	[191]
SALK_145997 / *mrs2-4* 2	AT3G58970 / MRS2-4/MGT6	-	NASC	[191]
SALK_105475C / *mrs2-5*	AT2G03620 / MRS2-5/MGT3	-	NASC	[191]
SALK_127086C / *mrs2-7*	AT5G09690 / MRS2-7/MGT7	-	NASC	[191]
SALK_006528C / *mrs2-10* 1	AT1G80900 / MRS2-10/MGT1	-	NASC	[191]
SALK_100361C / *mrs2-10* 2	AT1G80900 / MRS2-10/MGT1	-	NASC	[191]
***mrs2-1 mrs2-5 mrs2-10* 2 / TKO**	MRS2-1, MRS2-5, MRS2-10	-	V.K.	[137]
***mrs2-3* 1 + 5-1**	AT3G19640 / MRS2-3/MGT4	*pMRS2-3:: MRS2-3::eGFP*	S.L.	-
***mrs2-3* 1 + 6-4**	AT3G19640 / MRS2-3/MGT4	*pMRS2-3:: MRS2-3::eGFP*	S.L.	-
***mrs2-3* 2 + 1-4**	AT3G19640 / MRS2-3/MGT4	*pMRS2-3:: MRS2-3::eGFP*	S.L.	-
***mrs2-4* 1 + 3-4**	AT3G58970 / MRS2-4/MGT6	*pMRS2-4:: MRS2-4::GFP*	S.L.	-
***mrs2-4* 2 + 3-4**	AT3G58970 / MRS2-4/MGT6	*pMRS2-4:: MRS2-4::GFP*	S.L.	-
cATeam 1.1	-	*p35S::ATeam 1.03-nD/nA*	M.S.	[182]

Line	Mutation in[a]	*Construct*[b]	Source[c]	Reference
cpATeam 1.1	-	*p35S::TkTp:: ATeam1.03-nD/nA*	M.S.	[182]
cPhusion	-	*p35S:: mRFP1–eGFP*	J.J.	[186]
aPhusion	-	*p35S::chit:: mRFP1–eGFP*	J.J.	[186]
***mrs2-4* 1 + cpMARIO**	AT3G58970 / MRS2-4/MGT6	*p35S::Ω:: 6xHis::RbcS::MARIO*	T.N.	-
pAAA::LUC	-	*pAT2G18193::LUC*	S.L.	-
pPER70::LUC	-	*pPER70::LUC*	S.L.	-
pDTX3::LUC	-	*pDTX3::LUC*	S.L.	-
SALK_082081C / *mrs2-2*	AT5G64560 / MRS2-2/MGT9	-	NASC	[191]
SALK_037061C / *mrs2-6*	AT4G28580 / MRS2-6/MGT5	-	NASC	[191]
SALK_028422C / *mrs2-11*	AT5G22830 / MRS2-11/MGT10	-	NASC	[191]

[a] – *Arabidopsis* gene identifier, as well as gene name of any genes mutated in the line in question. [b] – Transgenic construct present in the line in question, if any. [c] – Source of each individual line; "S.L." denotes lines that were generated during the project, SALK lines were purchased from the Nottingham Arabidopsis Stock Centre (NASC, Nottingham, UK), other names indicate gifts from other researchers. C.S.: Camilla Stanton (JIC, Norwich); V.K.: Volker Knoop (Universität Bonn, Germany); T.N.: Tantawat Nardwattanawong (JIC, Norwich); M.S.: Markus Schwarzländer (Universität Münster, Germany); J.J.: Joshua Joyce (JIC, Norwich).

2.1.3 Media used for plant growth

The standard growth medium used in this work was similar to that used by Hermans *et al*. [101, 102], adapted for use on agar plates by adding 1% (w/v) agar and 0.5% (w/v) sucrose, henceforth referred to as Hermans-medium, (HM). Where necessary, the Mg^{2+}-concentration in plates used for experiments was decreased by reducing the amount of $MgSO_4$ added to the medium, to achieve the theoretical concentration specified, while adding an amount of Na_2SO_4 equal to the amount of $MgSO_4$ left out to keep the concentration of SO_4^{2-} and the osmotic potential consistent. Where the Mg^{2+}-concentration was increased above 1000 µM, the amount of Mg^{2+} exceeding 1000 µM was added as $MgCl_2$. For specific experiments, other changes were made to this medium to induce deficiency or excess conditions for various nutrients. **Table 2.2** gives the composition of HM, along with all changes made over the course of the experimental work.

For selection of transformants during the establishment of transgenic lines, as well as for some microscopy experiments, 0.25x Murashige and Skoog (MS) medium was used (M0221.0050, Duchefa Biochemie, Haarlem, Netherlands) [192].

Experiments using HM were carried out using chelator-washed agar (see **Section 2.1.3**), unless otherwise specified. Most experiments were carried out using 100 mm square petri dishes (R & L Slaughter Ltd.), but in some cases, 120 mm square petri dishes were used (Scientific Laboratory Supplies Ltd., Nottingham, UK), as a result of a temporary supply shortage affecting availability of 100 mm square petri dishes.

Table 2.2 – Media used throughout this work

Compound	Concentration added to medium [µM]				
	Standard	Low PO_4^{3-}	High Ca^{2+}	Salt Stress	Low K^+
$Ca(NO_3)_2$	1000				
$MgSO_4$	1000				
K_2SO_4	880				0
KH_2PO_4	250	10			2.5
FeNa(EDTA)	20				
NaCl	2000			58,000	
H_3BO_3	10				
$ZnSO_4$	1				
$CuSO_4$	0.1				
$MnSO_4$	1				
$(NH_4)_6Mo_7O_{24}$	0.01				
Sucrose	0.50%				
Na_2SO_4	0				880
$CaCl_2$	0		24,000		
NaH_2PO_4	0				247.5
KCl	0	240			

Composition of the standard growth medium used throughout this work (Adapted from Hermans *et al*., 2010a [101]), as well as changes made to induce various stress conditions. Empty cells in columns denote amounts being unchanged from the standard medium.

2.1.4 Preparation of chelator-washed agar

For most experiments, including those aiming to induce nutrient deficiencies, agar was purified using an EDTA-washing procedure adapted from [193], removing metal ions contained in standard agar preparations. In a 2 L Erlenmeyer flask, 50 g Type A agar (A4550-500G) were washed three times for 5 h with 1 L of a 50 mM EDTA-solution (VWR International, Radnor, U.S.A.), pH 7.5, while stirring on a magnetic stirrer. Agar was then washed six times with dH_2O for 1.5 h each time, with stirring. Between each and after the final wash, agar was filtered using Miracloth (Merck Millipore Ltd., Watford, UK). The agar was then partially dried at room temperature for at least one day, before being used to make media.

To confirm the effectiveness of this procedure, ion concentrations within the plates produced were measured. Agar plates made with washed Type A agar, unwashed Type A agar, high gel-strength agar (HGA agar, A9799-500G), as well as nutrient solutions without agar were submitted to inductively coupled plasma – optical emission spectrometry (ICP-OES) analysis (**Section 2.5.1**). The results are shown in **Figure 2.1** and summarized in **Table 2.3**. Raw values are shown in **Appendix B**, **Table S2.1**.

As can be seen from **Figure 2.1** and **Table 2.3**, concentrations of sodium, calcium and phosphorus in plates made with washed agar appear similar to nutrient-solutions without any added agar, as does the concentration of Mg^{2+} at low concentrations of added Mg^{2+}, indicating near-complete removal of ions during the wash-procedure. At higher added Mg^{2+}-concentrations, apparent concentrations in plates made with washed agar are lower than in pure nutrient solutions as a result of water remaining in the agar from the wash-procedure and diluting the medium, as can be seen from the slightly shallower slope in **Figure 2.1 A**. Besides introducing large amounts of sodium and phosphorus, although not calcium, use of unwashed agar shifts the added Mg^{2+}/measured Mg^{2+} - curve upwards, by introducing around 30 µM Mg^{2+}, as calculated from the ordinate intercept of the linear regression curve in **Figure 2.1 A** and shown in **Table 2.3**. Although there are significant differences between theoretical/added Mg^{2+} and apparent/measured Mg^{2+}, for ease of use, added Mg^{2+} is used when describing experiments going forward.

This page is intentionally left blank

Blank pages are used throughout to allow legends to appear opposite display items in the paper copy of this document

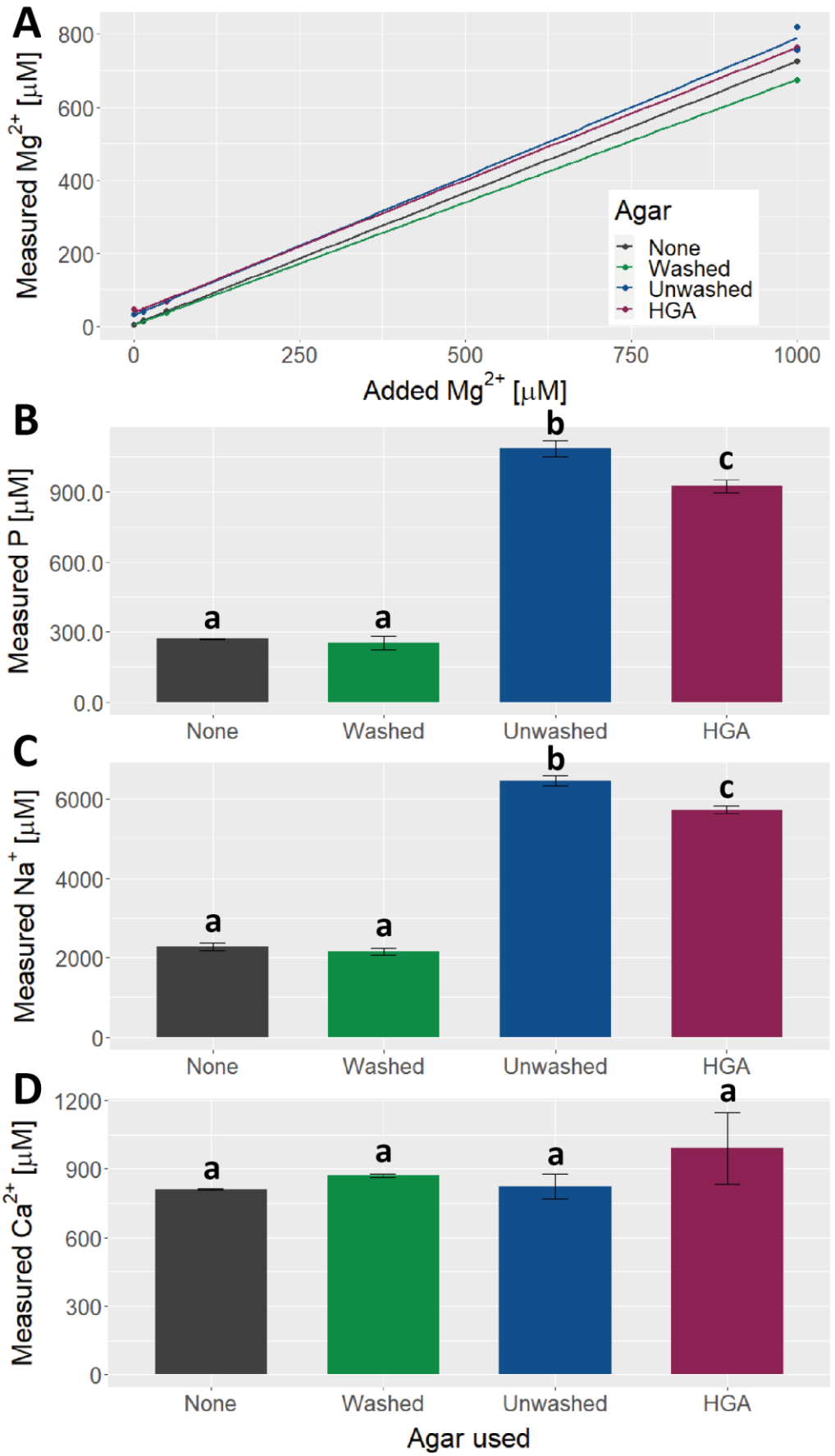
A
Measured Mg2+ [µM]
800
600
400
200
0
0
250
500
750
1000
Added Mg2+ [µM]
Agar
None
Washed
Unwashed
HGA
B
Measured P [µM]
900.0
600.0
300.0
0.0
a
a
b
c
None
Washed
Unwashed
HGA
C
Measured Na+ [µM]
6000
4000
2000
0
a
a
b
c
None
Washed
Unwashed
HGA
D
Measured Ca2+ [µM]
1200
900
600
300
0
a
a
a
a
None
Washed
Unwashed
HGA
Agar used

Figure 2.1 – Effective concentrations of ions in nutrient solutions and agar plates made using different types of agar.

A – Relationship between theoretical, added Mg^{2+}-concentration and measured Mg^{2+}-concentration in plates made with different types of agar. Four to five ICP-OES measurements per agar type were made, at different theoretical Mg^{2+}-concentrations, for each set. Trendlines represent best-fit first-order linear regression lines for each type of agar. **B, C, D** – Concentrations of other ions across plates made with different types of agar. Measurements from A were combined into one set for each type; error bars represent standard error. **Washed**: Type A agar, subjected to an EDTA-washing procedure. **HGA**: High gel-strength agar. **Unwashed**: Type A agar, used unaltered. **None**: Nutrient solutions made without added agar.

Table 2.3 – Relationship between theoretical and apparent Mg-concentrations in media using different forms of Agar.

Type of agar	Residual Mg^{2+} [µM][a]	Slope [$\mu M.\mu M^{-1}$][b]	R^2 [ ]	p-value [ ]
None	4.82 ± 0.291	0.721 ± 0.000580	1.000	6.48×10^{-7}
Washed	3.46 ± 0.778	0.672 ± 0.00155	1.000	5.35×10^{-6}
Unwashed	30.5 ± 15.0	0.758 ± 0.0237	0.9971	6.67×10^{-5}
HGA	37.2 ± 4.85	0.726 ± 0.00968	0.9996	1.78×10^{-4}

Values shown give characteristics of the linear regression lines from **Figure. 2.1 A**. The apparent Mg^{2+}-concentration for a given type of agar and concentration of added Mg^{2+} can be calculated as y = **a** + **b** * x; where y is the apparent Mg^{2+}-concentration; **a**, the y-intercept, is the residual amount of Mg^{2+} in the medium from contaminations in the agar, water and stock solutions; x is the theoretical concentration of Mg^{2+} added via stock solutions; and b is the "slope", *i.e.*, the conversion factor between theoretical, (added) and apparent (measured) Mg^{2+}-concentration for each type of agar. **Washed:** Type A agar, subjected to the EDTA-washing procedure. **HGA:** High gel-strength agar. **Unwashed:** Type A agar, unaltered. **None:** Nutrient solutions made without added agar.

2.1.5 Growth conditions for *Arabidopsis* on soil

For collection of seeds and DNA-samples from leaves, plants were grown on "John Innes F2 Starter + Grit", consisting of 90% (w/w) peat, 10% (w/w) grit, 4 $kg.m^{-3}$ dolomitic limestone and 1.2 $kg.m^{-3}$ Osmocote Start fertilizer (ICL Specialty Fertilizers, Ipswich, UK). Sensitive plants, such as EMS mutants, were grown on "Levington F2 Starter" with added insecticide, consisting of 100% peat and 0.28 $g.L^{-1}$ Exemptor® chloronicotinyl insecticide (Bayer CropScience Ltd., St. Louis, USA). Plants were grown in 24-cell trays of pots, with each pot measuring 5 x 5 x 5 cm, in a long day CER maintained at approximately 22°C with a photoperiod of 16 h light (90 $\mu mol.m^{-2}s^{-1}$) and 8 h dark.

2.2 *Arabidopsis* growth phenotyping

2.2.1 Determination of shoot weights

Arabidopsis seedlings were grown vertically on 100 mm square agar plates containing HM with different concentrations of Mg^{2+} until 14 DAG. At this point, shoots were separated from roots using forceps, and shoots were gently blotted dry twice between two sheets of absorbent paper. Shoots were then weighed on an analytical laboratory balance (Mettler AE 240, Mettler-Toledo Ltd., Leicester, UK) to an accuracy of 0.1 mg.

For the experiment in **Figure 3.5** and **3.6**, **Chapter 3** as well as **Figure 4.3** and **4.4, Chapter 4**, seedlings were grown on HM, using washed agar. Individual seedlings were weighed, before calculating the average shoot weight for each concentration and genotype; 260 Col-0 seedlings, 207 *mrs2-4* 1 seedlings and 223 *mrs2-7* seedlings, respectively, were analysed, distributed across three independent biological replicates. For the experiment in **Figure 4.5**, seedlings were grown on HM using unwashed agar. Seedlings were weighed individually, before calculating the average shoot weight for each concentration and genotype. Between 48 and 77 seedlings per independent replicate and genotype were analysed, for each of seven genotypes (Col-0, *mrs2-3* 1, *mrs2-3* 2, *mrs2-4* 1, *mrs2-10* 1, *mrs2-10* 2, TKO).

For the experiments in **Figure 4.7**, seedlings were grown on HM using unwashed agar. In this case, all seedlings from one plate were weighed together and the average shoot weight for each plate calculated, then the total number of plates was used to calculate the average shoot weight across plates. three to six plates were analysed per genotype, concentration and replicate, containing three to six seedlings each. The first experiment contained six genotypes (Col-0, *mrs2-3* 1, *mrs2-3* 2, *mrs2-3* 1 + 5-1, *mrs2-3* 1 + 6-4, *mrs2-3* 2 + 1-4), and the second experiment contained five genotypes (Col-0, *mrs2-4* 1, *mrs2-4* 2, *mrs2-4* 1 + 3-4, *mrs2-4* 2 + 3-4). Both experiments were carried out over three independent biological replicates.

In all cases, significant differences between mean values across genotypes and Mg^{2+}-concentrations were determined using two-way analysis of variance (ANOVA) with Tukey honestly significant difference (HSD) test.

2.2.2 Root measurements

Arabidopsis seedlings were grown vertically on 100 mm square agar plates containing HM with different concentrations of Mg^{2+}, until 10 DAG. At this point, plates were scanned using an Epson Perfection V550 Photo scanner (Epson, Suwa, Japan), with a scan definition of 300 dpi. Images were analysed in ImageJ (National Institutes of Health, USA) v.2.1.0. The number of lateral roots per plant was counted visually, and the length of main roots was measured using the NeuronJ© plugin (Erik Meijering), v. 1.4.3. Root measurements were taken for the experiment in **Figures 3.5** and **3.6**, **Chapter 3** and the experiment in **Figures 4.3** and **4.4, Chapter 4**, with numbers of seedlings and replicates, as well as genotypes used as described in **Section 2.2.1**.

For main root length, significant differences across genotypes and Mg^{2+}-concentrations were determined using two-way ANOVA and Tukey HSD test. For numbers of lateral roots, a Kruskal-Wallis test [194], followed by a Dunn test [195] for multiple comparisons were used.

2.3 DNA methods

2.3.1 DNA Extraction

Samples of leaves from plants grown on soil according to **Section 2.1.5**, or of whole plants grown on agar plates according to **Section 2.1.2**, not exceeding 300 mg fresh weight, were taken, transferred to 2 mL Eppendorf tubes, frozen in liquid nitrogen and initially stored at -70°C. Before DNA extraction, samples were homogenized using a TissueLyser LT (Qiagen GmbH, Hilden, Germany), pre-cooled with liquid nitrogen. Samples were shaken at 50 Hz for one minute, twice, after adding one stainless steel ball bearing (3 mm, M31G100, Simply Bearings Ltd., UK) to each tube. Homogenized samples were then "vortexed" with 400 µL extraction buffer, consisting of 5 M urea, 0.3 M NaCl, 20 mM EDTA, 0.05 M tris (tris(hydroxymethyl) aminomethane) (B2005, Melford Laboratories Ltd., Chelsworth, UK), 2%(w/v) sodium lauryl sarcosinate (L9159-50G), 0.5% (w/v) sodium dodecyl sulphate (L4390-100G), 5% (w/v) phenol (P4557-400ML), and incubated for 5 min at room temperature. Then, 400 µL of a 25 : 24 : 1 mixture of phenol, choroform and isoamylalcohol, prepared from phenol and chloroform : isoamylalcohol 24 : 1 (C0549-1PT) was added. Samples were centrifuged for 20 min at 10,000 g, before transferring the aqueous phase (500 µL) to new 1.5 mL Eppendorf tubes, adding 400 µL isopropanol and centrifuging for another 20 min at 10,000 g, producing a DNA pellet. Remaining isopropanol was discarded and the pellet washed twice with 500 µL 70% (v/v) EtOH, then the pellet was left to dry and DNA dissolved in 50 µL ddH_2O or low TE buffer (10 mM tris, 0.1 mM EDTA), pH 7.5. DNA quality and concentration were determined using a Nanodrop™ One Microvolume UV-Vis Spectrophotometer (Thermo-Fisher Scientific Inc., Waltham, U.S.A.).

2.3.2 Genotyping by PCR

Genotyping of plants was carried out by polymerase chain reaction (PCR) using GoTaq® DNA Polymerase (Promega Co., Madison, USA). Each reaction contained 2 mM $MgCl_2$, 0.2 mM of all DNA trinucleotides, 0.8 µM of each primer used, green GoTaq® buffer to a concentration of 1x, and 100-500 ng template genomic DNA (gDNA). 0.15 µL polymerase were added for 25 µL reactions, and 0.3 µL polymerase for 50 µL reactions. PCR was carried out in a Mastercycler® pro thermocycler (Eppendorf, Hamburg, Germany). Reactions were carried out as Touchdown (TD) PCR. Conditions were as follows: 95°C for 2 min; followed by five cycles of 95°C for 20 s, 60°C, decreasing by 1°C with each cycle, for 20 s, and 72°C for 2 min; followed by 30 cycles of 95°C for 20 s, 54°C for 20 s, 72°C for 2 min; and a final step of 72°C for 5 min.

Most genotyping PCRs were carried out as "three-primer PCRs"; three primers were added to each reaction mixture, giving PCR products of different sizes depending on whether the line in question contained the transfer DNA (T-DNA) insertion or construct in question or not, or both products in the case of plants heterozygous for T-DNA insertions. **Table 2.4** gives the primers that were used for genotyping. LBb1.3-Ext was used in all reactions for genotyping SALK T-DNA insertion lines, in addition to the primers given for the respective line. Lines containing GFP-tagged insertions were genotyped once using the same primers as for the respective SALK line, and once with the primers given for the line in addition to the "GFP Rev. 2" primer (**Table 2.4**). Lines containing MARIO and ATeam constructs were genotyped together, including Col-0 plants as negative control, using the same primers, since both constructs contain sequences encoding both YFP and CFP. Constructs present in each line were distinguished via the sizes of the produced PCR-products.

Table 2.4 – Primers used for DNA genotyping in this work.

Mutant line /Transgene	Primer name	Sequence (5' to 3')
All SALK lines	LBb1.3-Ext.	ATTTTGCCGATTTCGGAACCAC
TKO (*mrs2-1*)	006797_LP	AGAGCAGGCTTGTAGCACTGAC
	006797_RP	CCATCTGAATGCACCTGGCTG
mrs2-2	006797_LP_X	AGAGCAGGCTTGTAGCACTGAC
	006797_RP	CCATCTGAATGCACCTGGCTG
***mrs2-3* 1 & 2**	080443_LP	GCATCTCTCAAAGACTGACGTG
	080443_RP	GATTCATTTGGACTGTGATTGGAGG
***mrs2-4* 1 & 2**	203866C_LP	CATGCAACTGGATGGAATGCG
	145997_RP	CAAGTGGCACATGGTTTGTAAGAGAG
TKO (*mrs2-5*)	105475_LP	CGCCTTCAATCAAACCACAACCT
	105475_RP	TGCTCAGAGTGTTATCAACAACGAC
mrs2-6	037061_LP	GCTAGCCCGTGTACAAAAGG
	037061_RP	GCCGTTGAAGATTTGGTTGG
mrs2-7	90559_LP	ACTTTTTCTGATTCCAACTGGG
	90559_RP	TGAGGGGTACCATCTTCTTCAC
***mrs2-10* 1**	006528C_LP	AAACTTGGTGGTGAGAGGAAAC
	006528C_RP	GCAGGATCGTCTTTCAAATACC
***mrs2-10* 2 & TKO**	100361C_LP	GCGGTTTAATCACCTGCAACTC
	100361C_RP	TGTCTTCACAGAGGCATGAGT
mrs2-11	028042_LP	AATGTTTCGCCAAGTCTCCG
	028042_RP	GGCCAAACCAACCTCTAGTTC
ATeam* and *MARIO	MARIO seq1	AGAGCGCCTCGTCGTAC
	MARIO_seq3	GTGACCACCCTGACCTGG
	MARIO_seq4	GTAGCCCAGGGTGGTCAC
Both GFP Constructs	GFP Rev. 2	ATTTTGCCGATTTCGGAACCAC

Mutant line/transgene – Mutant line(s) or transgenic construct(s) the primers given were used with.

This page is intentionally left blank

Blank pages are used throughout to allow legends to appear opposite display items in the paper copy of this document

2.3.3 DNA Sequencing

DNA sequencing was carried out using the LightRun tube service offered by Eurofins Genomics GmbH. Primers used for DNA sequencing are listed in **Table 2.5**.

Table 2.5 – Primers used for DNA sequencing in this work.

Insertion/Construct	Primer name	Sequence (5' to 3')
All SALK line insertions	LBb1.3-ext	ATTTTGCCGATTTCGGAACCAC
***mrs2-1* & TKO**	006797_LP	AGAGCAGGCTTGTAGCACTGAC
***mrs2-3* 1**	080443_LP	GCATCTCTCAAAGACTGACGTG
	080443_RP	GATTCATTTGGACTGTGATTGGAGG
***mrs2-3* 2**	201976_LP	TGTCGCATTGCCACAAATCT
	201976_RP	CGACATGTTTCTCTCACCGAAG
***mrs2-4* 1**	203866C_LP	CATGCAACTGGATGGAATGCG
***mrs2-4* 2**	145997_LP	CGCTTGCTAGCTCGTGTACAAAAG
	145997_RP	CAAGTGGCACATGGTTTGTAAGAGAG
***mrs2-10* 1**	006528_LP	AAACTTGGTGGTGAGAGGAAAC
	006528_RP	GCAGGATCGTCTTTCAAATACC
***mrs2-10* 2 & TKO**	100361C_LP	GCGGTTTAATCACCTGCAACTC
TKO	105475_RP	TGCTCAGAGTGTTATCAACAACGAC
	006797_LP	AGAGCAGGCTTGTAGCACTGAC
	006797_RP	CCATCTGAATGCACCTGGCTG
All Gateway Constructs	pDONR F	AACGCTAGCATGGATCTC
	pDONR R	AGCTGGATGGCAAATAATG
pAAA::LUC	pAAA 1	GCCTGAACGAACAACATAC
	pAAA 2	GAGCATCTTTATTGGTAAGC
pPER70::LUC	pPER70 1	GAGTTGGATCAGAAACCG
	pPER70 2	GTATTTTCATACTCCCTCTG
	pPER70 3	CCTAAACTAGTCAGGATGG
	pPER70 4	CGTCCCGTTACAACATC
pDTX3::LUC	pMATE 1	AATTGGTAACTCGATAGCG
	pMATE 2	AGTATTAAAGGTTCACCCG
	pMATE 3	TGCTCTTTAAGGCACTAAG
Luciferase Constructs	QLUC R	CGATAAATAACGCGCCCA
L0 GoldenGate fragments	T7	TAATACGACTCACTATAGGG
	SP6	ATTTAGGTGACACTATAG

Insertion/Construct	Primer name	Sequence (5’ to 3’)
pMRS2-4:: MRS2-4::eGFP	M13 fwd.	GTAAAACGACGGCCAGT
	M13 rev.	ACAGGAAACAGCTATGACC
	MRS2-4 (TK) 1	CTCTGTGCTGTGAATCGG
	MRS2-4(TK) 2	CTACGTTTTGTTTCCAACC
	MRS2-4 1	TGGGCTTATCTAGTTGGG
	MRS2-4 2	GCTAGGCTGTGGATGAG
	MRS2-4 3	ACTAAGAATGTCAGCACTG
	MRS2-4 4	TACCATGTCCATTGTATAGC
	MRS2-4 5	AGAACGGCATCAAGGTG
pMRS2-3::MRS2-3::eGFP	MRS2-3 1	CCAATATGAGTTCGTCAGG
	MRS2-3 2	CATTCCTCAGCTGCTCG
	MRS2-3 3	GTCTCCTTTTGTTTGTGC
	MRS2-3 4	GCTGGTTGCAATAACTGG
	MRS2-3 5	GCAGATCGATGGTATACTG
	MRS2-3 6	TGACCACCCTGACCTAC

Insertion/Construct – T-DNA insertion flanking region or DNA construct sequenced using the respective primers. Primers “pDONR F”, “pDONR R” and “QLUC R” were provided by Camilla Stanton; Primers “T7” and “SP6” were provided by Marco D‘ario (both John Innes Centre, Norwich).

2.3.4 Whole-genome sequencing

Whole-genome sequencing (WGS) was carried out using the short-read non-human WGS service by GENEWIZ Germany GmbH (Leipzig, Germany).

Samples consisted of genomic DNA from 21 – 36 individual seedlings from segregating F_2 populations (see **Section 5.2.5**, **Chapter 5**), selected for increased luciferase expression according to **Section 2.7.2**. Selected seedlings were pooled, producing nine samples derived from mutant lines and one control, consisting of 20 seedlings of the unaltered parent line *pAAA::LUC*. Then, DNA was extracted from the samples according to **Section 2.3.1**. DNA quantity was assessed using a Qubit™ Fluorometer (Thermo Fisher Scientific), before submitting the samples for analysis.

Sequencing was carried out using an Illumina platform with a 2x 150 bp paired-end setup. The raw sequencing data were processed by Genewiz, removing adapter sequences using the Trimmomatic v0.36 package [196], then reads were aligned to the TAIR10 reference genome for Col-0 using the Burrows-Wheeler aligner (BWA) [197]. SNPs and indels were detected using the SamTools [198] and VarScan [199] packages, then pairwise comparisons between each sample and the control were carried out.

2.4 RNA methods and Real-Time PCR

2.4.1 RNA extraction

Arabidopsis seedlings were grown on 100 mm square Agar plates according to **Section 2.1.2**, then shoots were separated from roots using forceps, sampling shoots and/or roots. Up to 100 mg fresh weight were transferred into 2 mL RNAse and DNAse – free Eppendorf tubes for each sample, pooling parts from multiple seedlings. Samples were then flash-frozen in liquid nitrogen and stored at -70°C until use. Before RNA extraction, samples were homogenized using a TissueLyser LT (Qiagen GmbH), pre-cooled with liquid nitrogen. Samples were shaken twice at 50 Hz for one minute after adding a single stainless steel ball bearing (3 mm, M31G100, Simply Bearings Ltd., UK) to each tube. RNA-extraction was carried out using the RNEasy® Plant Mini Kit (Qiagen GmbH), according to the manufacturer's instructions. The optional on-column DNAse-digestion step using the RNAse-free DNAse set (Qiagen GmbH) described in the RNEasy mini handbook was carried out at the relevant point in the procedure. RNA quality and concentration were determined using a Nanodrop™ One Microvolume UV-Vis Spectrophotometer (Thermo-Fisher Scientific Inc.).

2.4.2 cDNA synthesis

cDNA synthesis was carried out in 20 µL reactions using the GoScript™ Reverse Transcription System (Promega) according to the manufacturer's instructions, using oligo$(dT)_{15}$ primer, with approximately 500 µg total RNA per reaction and a final concentration of 2.5 mM $MgCl_2$. Reactions were carried out in a Mastercycler® pro thermocycler (Eppendorf). A "no template control" (NTC) and a "no reverse transcriptase" (NRT) control reaction were included as negative controls. cDNA was diluted 1:10 to give a final volume of 200 µL and stored at -20°C.

2.4.3 Quantitative reverse transcription PCR

Real-time quantitative reverse transcription PCR (qRT-PCR) was carried out as 10 µL reactions in Lightcycler® 480 384-well plates (Roche Diagnostics, Burgess Hill, UK), using diluted cDNAs and SYBR® Green Jumpstart™ *Taq* ReadyMix™ (S4438). Each 10 µL reaction contained 5 µL SYBR Green, 0.5 µL of each primer at a concentration of 10 µM, 1 µL ddH_2O and 3 µL cDNA, prepared according to **Section 2.4.2**. Primers used in qRT-PCR analysis are shown in **Table 2.6**.

All primer-pairs used for qRT-PCR were validated by testing the primer efficiency before use. To do this, cDNA from samples to be used with the primer pair was mixed in equal parts, before creating four serial tenfold dilutions (1 : 10, 1 : 100, 1 : 1000, 1 : 10 000). 20 µL qRT-PCRs were set up for each primer-pair with each dilution of cDNA-mix, including undiluted cDNA-mix, according to the protocol above, in a 96-well plate (Scientific Laboratory Supplies Ltd.), in triplicate, giving fifteen reactions per primer, over five dilutions of cDNA. Primers for the same experiment were tested together on the same 96-well plate, if possible, together with three replicates of both NTC and NRT negative controls. Reactions were then carried out in a Bio-Rad CFX96 real-time PCR detection system (Bio-Rad Laboratories, Inc., Hercules, USA). The PCR program used was as follows: 94°C for 2 min; followed by 40 cycles of 94°C for 20 s, 59°C for 20 s, 72°C for 20 s, and a plate-read step; 30 s at 50°C, then a melt-curve from 65°C to 95°C, at 0.5°C intervals. Primer efficiency was evaluated by taking the arithmetic mean of C_t values given by the thermocycler for each set of technical replicates, excluding up to one obvious outlier per set of three replicates, then plotting the mean C_t values against the decadic logarithm of the quantity of cDNA (undiluted cDNA = 1.0). The primer efficiency (in %) was calculated as:

$$Efficiency\ (\%) = \left(10^{-\frac{1}{S}} - 1\right) * 100$$

where S is the slope of the plot. Primers with efficiencies between 90 % and 110 % were used for subsequent qRT-PCR experiments, whereas primers with efficiencies outside of this range were rejected.

When setting up qRT-PCR reactions, all solutions except cDNA were pre-mixed in screw-cap tubes, as "Primer-mixes", containing appropriate amounts of primers, ddH_2O, and SYBR Green, for all reactions using one set of primers at one time. Required amounts of cDNA were dispensed into wells of a fully skirted 96-well qPCR plate (Scientific Laboratory Supplies Ltd.). Both these solutions were then supplied to a Biomek NXP Span-8 automated liquid handling system (Beckman Coulter Life Sciences, Indianapolis, USA), automatically dispensing 7 µL "Primer-mix" and 3 µL cDNA into the required wells of the 384-well plate. qRT-PCR reactions were then carried out in a LightCycler® 480 System (Roche diagnostics); the protocol used was the same as for the primer-efficiency tests (see above).

Each reaction was carried out in triplicate (technical replicates), and each plate contained samples from three independent biological replicates. All reactions pertaining to one experiment were carried out on the same plate, and each experiment included two reference transcripts, *ACTIN2/AT3G18780* and *EF1α/AT1G07940*, as well as NTC and NRT negative controls. The PCR protocol used was the same as for primer efficiency reactions (see above).

When analysing the data, the mean C_t value out of two or three technical replicates (up to one obvious outlier was excluded from three original technical replicates) was calculated, then the expression for each biological replicate, relative to *ACTIN2* (E_{rel}) was calculated as:

$$E_{rel} = 2^{-(C_t(Candidate) - C_t(ACTIN2))}$$

The arithmetic mean and standard error of relative expression values between biological replicates for each sample was calculated, then mean and standard error for each gene were normalized to the relative expression of the respective gene at the control concentration or in the control genotype ($\Delta\Delta C_t$). Significant differences across measurements were determined using two-way ANOVA, followed by Tukey HSD test.

Table 2.6 – Primers used for qRT-PCR in this work.

Gene Name	Primer name	Sequence (5' to 3')
ACT2/AT3G18780	Actin2 F	GATGAGGCAGGTCCAGGAATC
	Actin2 R	GTTTGTCACACACAAGTGCATC
EF1a/AT1G07940	EF1a F	TGGTTGTTTGTGTTACCGCTTCG
	EF1a R	CACCTCCGATCAAGAACCCAATTC
AAA/AT2G18193	AAA_Tr_F	TGCTGAAGTGAGAGATAGGGAAGC
	AAA_Tr_R	TCCCTGATAGAGTCACCTTTCCC
PER70/AT5G64110	PER70_Tr_F	CACGTGACTTCGTCCATTTGGC
	PER70_Tr_R	AGAAATTCGGCCATCGAGTCTCC
DTX3/AT2G04050	MATE_Tr_F	ATGTGAGGTACTCCAGCTCCTG
	MATE_Tr_R	ATAGCCACCATTCTAGGCAAACC
MRS2-3/AT3G19640	MRS2-3_Tr_F	CCGTCTCCTTCACTATTTGCATTTCTTTC
	MRS2-3_Tr_R	AAGCAAGAAGGAAACTATGCAATTTGCTC
MRS2-4/AT3G58970	MRS2-4_Tr_F	CGCAGAGACATTGTTGGCCAGC
	MRS2-4_Tr_R	GAGCCTAGCAGCTTCTTCCACC
19650/AT3G19650	19650_F	TCATGAGACCACCAAAGCAGCTC
	19650_R	ACTTCTCCACGATCCTCTCACAG
LUC [a]	luc_Tr_F_2	GATGTACACGTTCGTCACATCTCATC
	luc_Tr_R_2	CAGTGCAATTGTCTTGTCCCTATCG
PPR/AT2G20720	PPR F	CTTCTCTCACGCTCTCCAGGTATC
	PPR R	ACACCACCAACTTTAGCAGCCAAG
ACA1/AT1G27770	ACA1 F	ATCAGCCTGCCTCACTGGAAAC
	ACA1 R	TTCATCAGGTCGTCCTGTGGTG
DTX4/AT2G04070	MEP F	GTCTTCTGTCAAGCAGTTCTTCCG
	MEP R	TAGCCACCATTCTAGGCAAAGC

Gene Name – Designated name and/or and gene identifier of genes transcript levels of which were quantified using the respective primers. [a] – the firefly luciferase transcript, from the *LUC* transgene.

2.5 Biochemical and histochemical assays

2.5.1 Agar-equilibration and ICP-OES

To determine concentrations of ions within agar plates, plates in question were cut into pieces measuring about 0.5 cm x 2 cm, using a scalpel. Segments were transferred into 15 ml falcon-tubes, pre-weighed (w_1) on an analytical laboratory balance (Mettler AE 240, Mettler-Toledo Ltd.). Tubes were weighed again (w_2), then ddH_2O was added to each tube to a total volume of about 15 mL, and tubes were weighed a third time (w_3). Nutrient solutions without agar, prepared separately, were sampled at the same time to serve as controls. Both the tubes with agar segments and water and the tubes with nutrient solutions were stored at 4°C for at least three days to allow ion-concentrations to equilibrate between agar and water, then the supernatant was separated from the agar-pieces in the sample tubes by centrifugation, followed by decanting.

All samples were submitted for ICP-OES analysis to the University of East Anglia's Science Analytical Facility, and analysed for concentrations of magnesium, potassium, sodium, calcium, and phosphorus. For samples from agar plates, concentrations within agar plates were calculated as follows:

$$c_{app} = c_M * \frac{w_2 - w_1}{w_3 - w_1}$$

With c_{app} being the apparent ion-concentration within the agar plates in question and c_M being the concentration measured in the sample during ICP-OES.

For Mg^{2+}-concentrations across different types of agar, a linear model relating added to measured Mg^{2+}-concentrations was created for each agar, and a two-way ANOVA was used to establish significant differences between agars. For concentrations of other ions, measurements across different Mg^{2+}-concentrations for each type of agar were combined, mean values and standard errors calculated, then significant differences between them established using two-way ANOVAs and Tukey HSD tests.

2.5.2 Starch staining using Lugol's solution

To visualize accumulation of starch in leaves of *A. thaliana* at different Mg^{2+}-concentrations, a protocol adapted from Feike *et al.*, 2016 [200] was used. Seedlings grown on agar plates according to **Section 2.1.2**, using washed agar, were harvested at the end of the dark period, *i.e.*, 06:00. For seedlings grown on agar plates containing sucrose, this was carried out at 14 DAG, whereas for seedlings grown on plates without sucrose, the time-point chosen was 17 DAG. Four to six seedlings from each Mg^{2+}-concentration were chosen at random, shoots were separated from roots using forceps, then shoots were immersed in around 12 mL 80% (v/v) EtOH in falcon tubes and incubated at 80°C for 2 h to remove chlorophyll. De-stained shoots were washed three times in ddH_2O for 5 min on a rotary shaker, shaking at 30 rpm, then immersed in Lugol's solution (L6146-1L) for at least 6 h with shaking to visualize Starch within rosettes. Shoots were then washed three times in ddH_2O for 5 min again, before individual shoots were transferred to a sheet of paper, arranged such that each leaf was unfurled and visible, and blotted dry with absorbent paper. Images of each rosette were taken using a ZEISS Axio Zoom.V16 stereo fluorescence microscope (Carl Zeiss AG, Jena, Germany), using the bright-field (colour) setting, a Plan-NEOFLUAR Z 1x objective and an Axiocam 512 colour camera (Carl Zeiss AG), generating three-channel images.

To quantify differences in starch accumulation at different Mg^{2+}-concentrations, three independent replicates were carried out for each experiment, with four to five seedlings imaged per Mg^{2+}-concentration and replicate. Images obtained as specified above were imported into ImageJ v. 2.1.0. For each seedling, leaves were numbered according to the order of emergence, from one to eight, then the outline of each leaf was traced and the average colour intensity on the red channel over the area of the leaf determined using the "measure" function. A generalized linear model of the relationship between colour intensity and Mg^{2+}-concentration, grouped by leaf number, was generated. A two-way ANOVA was used to determine significant differences within the model.

2.5.3 ROS imaging using fluorescent ROS-sensitive probes

To visualize ROS accumulation in leaves of seedlings grown at different Mg^{2+}-concentrations, a protocol adapted from Peng *et al.* [96] was used. Seedlings grown on agar plates according to **Section 2.1.2**, using washed agar, until 14 DAG, were harvested around the middle of the light period, *i.e.*, 14:00. Seedlings, chosen at random, were removed from plates and immersed in a solution of either 10 µM 5-(and-6)-chloromethyl-2',7'-dichlorodihydrofluorescein diacetate acetyl ester (CM-H_2DCFDA), or 40 µM dihydroethidine (DHE) (both Thermo-Fisher Scientific) in 50 mM phosphate buffer, pH 7.4. Seedlings were incubated in the staining solution for 30 min at room temperature, then de-stained by washing three times in phosphate buffer for 1-3 min with shaking. Leaves 4, 5 and/or 6 were removed from the washed seedlings and placed on a microscope slide, immersed in phosphate buffer, then images were taken on a Zeiss LSM 780 confocal laser-scanning microscope (Carl Zeiss AG), using an EC Plan-Neofluar 20x objective with a numerical aperture (NA) of 0.5. Excitation wavelength was 488 nm and emission at 517-540 nm for CM-H_2DCFDA. Excitation at 514 nm and emission at 520-580 nm for DHE. A chlorophyll channel was included in both cases, with emission recorded at 660-700 nm. Other settings were as described in **Section 2.6.3**. Unstained leaves were used as negative control, whereas leaves from seedlings sprayed with a solution of 20 µM Antimycin A (A8674-25MG) in 0.1% (v/v) Tween® 20 (P9416-50ML) 2 h before harvesting were used as a positive control.

To quantify differences in ROS accumulation across seedlings grown at different Mg^{2+}-concentrations, three replicates of the above experiment were carried out, with four to five images per Mg^{2+}-concentration (and control) and replicate. Images were imported into ImageJ v. 2.1.0. For each image, chlorophyll fluorescence was used to judge the area that was sufficiently in focus, then that area was traced and the average intensity on the channel used for the respective dye was measured. Mean and standard error for average fluorescence across samples were calculated for each sample type, then significant differences between fluorescence after growth on 1000 µM Mg^{2+} and all other sample types were determined using two-way ANOVA followed by Tukey HSD test.

2.5.4 Chlorophyll quantification

To determine concentrations of chlorophyll in *Arabidopsis* shoots, seedlings grown on agar plates according to **Section 2.1.2** until 14 DAG were harvested, separating shoots from roots using forceps. Shoots were gently blotted dry between two sheets of absorbent paper, twice, then weighed on an analytical laboratory balance (Mettler AE 240, Mettler-Toledo Ltd.) to an accuracy of 0.1 mg (m_1). 20-50 mg fresh weight per sample, from shoots chosen at random, were transferred to a 2 mL Eppendorf tube and flash-frozen in liquid nitrogen. Samples were homogenized using a TissueLyser LT (Qiagen GmbH), pre-cooled with liquid nitrogen, after adding a 3 mm stainless steel ball bearing (Simply Bearings Ltd.) to each tube, then exactly 2 mL methanol was dispensed into each sample tube, and samples were incubated at 30°C for 30 min while shaking at 300 rpm. Samples were centrifuged at 10 000 rpm for 1 min, then put on ice, protected from light, until measurements were taken. Absorbance of each sample was measured on an MBA 2000 spectrophotometer (Perkin-Elmer, Waltham, U.S.A.) at 650 nm (A_{650}) and 665 nm (A_{665}). Concentration of chlorophyll within the samples (Chl) in µg.mg^{-1} was calculated as follows:

$$Chl = \frac{(A_{650} * 22.5 + A_{665} * 4) * 2}{m_1}$$

Two or three samples were analysed per condition and replicate, over three independent replicates, with seedlings grown on plates containing 60 mM NaCl acting as positive control. To determine significant differences between conditions, paired Student's T-tests were carried out.

2.5.5 Quantitative and ratiometric ATP-assay

ATP-levels within leaf samples, and ATP/ADP ratios within the same, were determined using the ATP/ADP ratio assay kit from Sigma-Aldrich (MAK135-1KIT). *Arabidopsis* seedlings (Col-0) were grown on agar plates containing HM with different concentrations of Mg^{2+} according to **Section 2.1.2**, using washed agar, either until 14 DAG on plates containing sucrose, or until 17 DAG on plates without sucrose.

Leaves 4,5 and/or 6 were removed from randomly chosen seedlings using forceps, then blotted dry between two sheets of absorbent paper, twice.

Leaves were weighed on an analytical laboratory balance (Mettler AE 240, Mettler-Toledo Ltd.) to an accuracy of 0.1 mg, and 10-50 mg leaf material per sample were transferred into 2 mL Eppendorf tubes and flash-frozen in liquid nitrogen. Samples were homogenized using a TissueLyser LT (Qiagen GmbH), pre-cooled with liquid nitrogen, after adding a 3 mm stainless steel ball bearing (Simply Bearings Ltd.) to each tube, then 100 µL 0.5x assay buffer (included in the kit, diluted with ddH_2O) were added to each sample. Samples were shaken, then centrifuged at 10,000 g for 2 min to clarify the extracts. Extracts were used in the assay according to the manufacturer's instructions. A white, fully skirted 96-well plate (Nunc™ F96 MicroWell™, Thermo-Fisher Scientific) was used to conduct the assay, and a CLARIOStar® plate reader (BMG Labtech, Ortenberg, Germany) was used to take the required measurements.

ATP/ADP – ratios for each sample were calculated as described in the MAK135 assay kit user manual. Mean values and standard error were calculated for each combination of plant part (leaves and roots) and Mg^{2+}-concentration, then two-way ANOVAs, followed by Tukey HSD test, were used to determine significant differences between different Mg^{2+}-concentrations for each plant part. To quantify ATP-concentrations in addition to obtaining the ATP/ADP ratio for the samples tested while accounting for background absorbance, a calibration-curve of luminescence versus ATP-concentration was generated via standard addition. One sample was chosen, and solutions of ATP (A7699-1G) were added to achieve final concentrations of 200 nM, 40 nM, and 8 nM added ATP. During data analysis, a linear regression line constructed from these standards and the unaltered sample allowed calculation of ATP-concentrations within the samples analysed. ATP- and ADP-concentrations determined during the assay were converted to concentrations within the initial samples, then mean values and standard error were calculated for each combination of plant part (leaves and roots) and Mg^{2+}-concentration. Two-way ANOVAs, followed by Tukey HSD test, were used to determine significant differences between different Mg^{2+}-concentrations for each plant part.

2.6 Microscopy and light-based methods

2.6.1 Luciferase imaging on agar plates

To quantify expression of luciferase in *Arabidopsis* seedlings across different genotypes or nutrient conditions, seedlings were grown on agar plates of HM using washed agar according to **Section 2.1.2**. Either 20 seedlings were placed on each plate when 100 mm square agar plates were used, or 32 seedlings per plate on 120 mm square plates, in two evenly spaced rows of seedlings. Around mid-day on the final day of the growth period, plates were removed from the growth room, and seedlings were sprayed with a solution of 1 mM luciferin (Carbosynth Ltd., UK) and 10 mM $MgCl_2$, while still on the plates, taking care to achieve complete coverage of shoot tissues. Plates were incubated for 10 min in the dark, then images were taken using a NightOwl II LB 983 *in vivo* imaging system (Berthold Technologies GmbH & Co KG, Germany).

To acquire the luminescence image, an exposure time of 30 s was used, with a peak emission wavelength of 560 nm, x-binning and y-binning of 1, with cosmic suppression and background suppression enabled. The photo the luminescence image was overlayed on was acquired with an exposure time of 0.1 s and 10% illumination intensity.

2.6.2 Fluorescence microscopy

For several experiments, fluorescence microscopy was used to detect expression of fluorescent proteins within transgenic lines of *A. thaliana*. An Axio Zoom.V16 stereo fluorescence microscope (Carl Zeiss AG) was used for this purpose, with light provided by an X-Cite XYLIS Broad Spectrum LED Illumination System (Excelitas Technologies Corp., Mississauga, Canada), and light filters included with the microscope used to set appropriate wavelengths for fluorophores imaged. For eGFP, an excitation wavelength of 488 nm and an emission wavelength of 509 nm were used; for CFP, excitation and emission wavelengths of 434 and 474 nm were used; for YFP, 514 and 526 nm.

Images were taken using an ORCA-Flash4.0 V3 Digital CMOS camera (Hanamatsu Photonics K.K., Hanamatsu, Japan). Generally, seedlings were grown on agar plates according to **Section 2.1.2** and left on plates during the imaging process, but in some cases, leaves from plants grown on soil according to **Section 2.1.5** were used.

2.6.3 Confocal microscopy

All confocal microscopy was carried out on a Zeiss LSM 780 confocal laser-scanning microscope (Carl Zeiss AG). The acquisition software used was ZEN 2012 SP5 (Black); excitation light was provided by a 25 mW Argon Ion laser (excitation lines: 458 nm, 488 nm, 514 nm). A pinhole size of 1 AU was used for all experiments, a pixel dwell time of 1.6 µs, and 4-line averaging for all images representing experimental output. A 32-channel GaAsP PMT array and transmitted light PMT were used as detectors.

Confocal microscopy was used to attempt to establish the subcellular localisation of MRS2-3-GFP and MRS2-4-GFP in transgenic lines expressing the respective constructs, and therefore the localisation of the respective protein. For this purpose, seedlings of *mrs2-4* 1 + 3-4 were primarily used, and the plasma membrane (PM) stain FM™4-64 ((N-(3-Triethylammoniumpropyl)-4-(6-(4-(Diethylamino) Phenyl) Hexatri-enyl) Pyridinium Dibromide), Thermo-Fisher Scientific) was used to visualize the PM of seedlings used in experiments. Seedlings to be imaged were immersed in a solution of 0.7 µg.mL^{-1} FM4-64 for 15 min while being kept on ice, then washed three times in HM liquid medium containing 50 µM Mg^{2+}.

Images in **Figure 4.11 A** were obtained using an EC Plan-Neofluar 20x air objective with an NA of 0.5; images in **Figure 4.11 B** were obtained using a C-Apochromat 40x water immersion objective with NA of 1.2. In this case, a Z-Stack was taken, with a voxel size of 5 nm (x/y) and 63 nm (z), 36 slices tall, sufficient for deconvolution analysis. A corresponding image of a slide of 250 nm Tetraspeck™ microspheres in ProLong™ Diamond antifade mountant (both Thermo-Fisher Scientific) was taken, to enable chromatic aberration to be corrected by channel alignment. An excitation wavelength of 488 nm was used, and emission was detected at 515-525 nm for GFP (900 V gain) and at 600-650 nm for FM™4-64 (250 V gain).

Deconvolution analysis and channel alignment were carried out in Huygens essential v.19.10 (Scientific Volume Imaging, Hilversum, Netherlands). For deconvolution, a CMLE algorithm was used, with 30 iterations. Channel intensities were adjusted manually.

Images in **Figure 4.12** and **Figure 4.13** were obtained using a C-Apochromat 40x water immersion objective with NA 1.2. In this case, original images were obtained as lambda-stacks, with 9.6 nm per slice. Individual images were obtained of Col-0 seedlings, (background autofluorescence only), as well as Col-0 seedlings stained with FM™4-64 (FM4-64 only) and unstained *mrs2-4* 1 + 3-4 (GFP only). Spectra for each of these fluorophores were saved. Images shown are the result of lambda-stacks of *mrs2-4* 1 + 3-4 seedlings, stained with FM4-64, subjected to the linear unmixing algorithm included with the ZEN black software, resolving lambda-stacks into multi-channel images with one channel for FM™4-64, GFP, autofluorescence and residuals. channel intensities were adjusted manually.

2.6.4 Plate-reader – based ratiometric assays

Plate-reader – based assays on *Arabidopsis* leaves were adapted from De Col *et al.* [182]. Seedlings were grown on agar plates containing different concentrations of Mg^{2+}, according to **Section 2.1.2**, either until 14 DAG on plates containing sucrose, or until 17 DAG on plates without sucrose. For leaf measurements, leaves 4, 5 and/or 6 were removed from randomly chosen seedlings using forceps, then floated on 300 µL liquid HM of the same Mg^{2+}-concentration the seedlings were grown on, in wells of a clear flat-bottom 96-well plate (Greiner CELLSTAR® 96 well, M0812). Between one and three leaves were placed per well, depending on leaf size, to keep total leaf area per well consistent. For root measurements, entire root systems from one or two seedlings were submerged in 300 µL liquid HM in wells of the same plate. Measurements were taken using a CLARIOStar® plate reader (BMG Labtech), at a focal height of 12 mm, with the internal temperature kept at 25°C. Wavelength and gain settings for fluorophores used are given in **Table 2.7**.

Measurements for all fluorophores used in the assay were carried out in sequence, for all wells in the plate each time. All sample readings were subjected to background correction, subtracting the average fluorescence intensity measured from four wells with leaves or roots of Col-0 seedlings grown under the same conditions as the sample seedlings.

To analyse the data, background-corrected emission values for each fluorophore and well were retrieved, then the YFP/CFP – ratio was calculated as the output of the experiment for ATeam, and the GFP/RFP – ratio for both pHusion lines. Three independent biological replicates of the experiment were carried out, with four technical replicates per concentration, reporter line, plant part and replicate. All measurements for each biological replicate were carried out on the same plate. Mean values of fluorescence ratios for each concentration and part were calculated, then mixed-effect linear models were generated for the relationship of fluorescence ratio to Mg^{2+}-concentration and plant part for each reporter. Two-way ANOVAs were applied within each model to determine significant differences between Mg^{2+}-concentrations. Additionally, apparent pH-gradients between cytoplasm and apoplast were calculated by subtracting fluorescence ratios of aPHusion from fluorescence ratios of cPHusion.

Table 2.7 – Settings for detection of fluorescence intensities for all fluorophores used in plate-reader experiments.

Fluorophore	Excitation [nm]	Emission [nm]	Gain setting []
CFP	435 ± 10	483 ± 9	1600
YFP [a]	435 ± 10	539 ± 7	1600
GFP	480 ± 8	525 ± 13	1600
RFP	558 ± 8	615 ± 8	2500

CFP and YFP readings were used to determine FRET ratios for ATeam samples. GFP and RFP readings were used to determine GFP/RFP ratios for pHusion samples. [a] – to obtain the YFP reading, the excitation wavelength for CFP was used, therefore the output is the YFP fluorescence generated through FRET only.

Before carrying out the assay, the experimental approach was validated by determining the strength of the signal for each fluorophore, compared to the background signal. Additionally, since transfer of samples to the 96-well plate was time-consuming and had to be carried out under ambient light conditions, it was determined whether (further) incubation of finished plates changed the readings observed. Finally, although only fully-grown true leaves were considered for the assay (leaves 3 through 6), it was not clear whether different leaves would give different values in the assay.

To address all these issues, an experiment was carried out comparing FRET ratios observed for leaves 3 or 4 and 5 or 6, from seedlings grown on 15 and 50 µM Mg^{2+}, for both cATeam and cpATeam. Readings were taken immediately after the 96-well plate was set up, as well as every 30 minutes during the next two hours of incubation. Results are summarized in **Appendix A**, **Figure S2.1**. Readings observed for cpATeam were similar to background readings, indicating that this line was not suitable for use in this assay. For cATeam, observed signals for both shoots and roots were sufficiently strong. FRET ratios observed for leaves 3 or 4 and leaves 5 or 6 were similar; accordingly, no differentiation was made between leaves 3 through 6 in subsequent experiments. Readings did not change during additional incubation time, indicating that time required to set up the experiment likely did not pose a problem and additional incubation was not detrimental to the experiment.

To determine functionality of the MARIO Mg^{2+}-FRET-sensor, expressed in *A. thaliana*, in principle, a "crushed leaf assay", adapted from **Figure S3** and **Method S8** in Wagner *et al.*, [201], was carried out. Leaves from 5-week-old *A. thaliana*, both Col-0 and *mrs2-4* 1 + *cpMARIO*, grown on soil according to **Section 2.1.5**, were collected, placed in pre-weighed 2 mL Eppendorf tubes, then tubes were weighed again and flash-frozen in liquid nitrogen. Weighing was carried out on an analytical laboratory balance (Mettler AE 240, Mettler-Toledo Ltd.) to an accuracy of 0.1 mg. Samples were homogenized using a TissueLyser LT (Qiagen GmbH), pre-cooled with liquid nitrogen, after adding a 3 mm stainless steel ball bearing (Simply Bearings Ltd.) to each tube, then 500 µL extraction buffer per 100 mg plant material were added, tubes shaken vigorously, and extracts clarified by centrifugation at 10 000 g for 4 min.

Extraction buffer contained 10 mM 4-(2-hydroxyethyl)-1-piperazineethanesulphonic acid (HEPES, H3375-500G), 100 mM NaCl, 1 mM EDTA, set to pH 7.5. 30 µL of this cleared cell extract were then added to 220 µL Assay buffer (100 mM HEPES, 100 mM NaCl, 1 mM EDTA, pH 7.5) in wells of a clear, flat-bottom 96-well plate (Greiner CELLSTAR® 96 well, M0812). 50 µL of solutions containing various concentrations of $MgCl_2$ were then added to the wells of the plate, to achieve final concentrations of $MgCl_2$ of 0, 1, 5, 10, 25, 50 and 100 mM, then emission values for the CFP and YFP settings from **Table 2.7** were measured using a CLARIOStar® plate reader, at a focal height of 11.5 mm, internal temperature 25°C. All readings from *mrs2-4* 1 + *cpMARIO* wells were background-corrected by subtracting the equivalent reading from wells with Col-0 leaf extract; all readings were carried out as three technical replicates. Average fluorescence ratios (YFP/CFP) and standard errors were calculated for each Mg^{2+}-concentration, then values were plotted in a scatterplot.

2.7 Generation of transgenic *A. thaliana*

2.7.1 PCR amplification of DNA fragments for cloning

DNA fragments for cloning were obtained from PCR reactions using Q5® High-Fidelity DNA Polymerase (New England Biolabs Inc., Ipswich, U.S.A.). Each 50 µL PCR reaction contained 10 µL Q5® reaction buffer, 1 mM additional $MgCl_2$ (3 mM total Mg^{2+}), 0.2 mM of each DNA trinucleotide, 0.8 µM of each primer, 10 µL Q5® High GC enhancer, 0.5 µL Q5® DNA polymerase, template DNA, and ddH_2O to a final volume of 50 µL. Where gDNA or cDNA was used as a template, about 100 ng DNA were added; when using plasmid DNA, 10-50 ng were added. PCRs were carried out in a Mastercycler® pro thermocycler (Eppendorf). Reactions were run as TD-PCRs. The PCR program used was as follows: 2 min at 98°C; followed by five cycles of 98°C for 15 s, 68°C, decreasing by 1°C each cycle, for 25 s, 72°C for 2 min; followed by 30 cycles of 98°C for 15 s, 62°C for 25 s, 72°C for 2 min; ending with a final amplification at 72°C for 2 min. The entire PCR reaction was then loaded into one well of a 1% (w/v) agarose gel (A20080, Melford Laboratories Ltd., UK) with 5 $\mu g.mL^{-1}$ Ethidium bromide (E1510-10ML). Sizes of DNA bands were verified, then the correctly sized band for each reaction was excized and DNA extracted using the QIAquick gel extraction kit (Qiagen), according to the manufacturer's specifications. Concentration and purity of extracted DNA was measured using a Nanodrop™ One Microvolume UV-Vis Spectrophotometer (Thermo-Fisher Scientific).

2.7.2 Golden Gate assembly

Golden-Gate assembly was used to produce the GFP-tagged *MRS2* constructs and the MARIO plant expression constructs used in this work.

To generate *MRS2* constructs, necessary DNA fragments were amplified from genomic DNA extracted from Col-0 seedlings according to **Section 2.3.1**, using the PCR protocol described in **Section 2.7.1**. Primers used and fragments amplified are listed in **Table 2.8**.

After gel extraction, purified DNA-fragments were ligated into the pGEM® vector using the pGEM® T easy vector system kit (A1360, Promega) according to the manufacturer's instructions, resulting in "level 0" modules for Golden Gate assembly. Before use with the kit, DNA fragments were subjected to an "A-tailing" procedure, adding a single A overhang to both ends of the fragment. Roughly 200 ng of the DNA fragment were added to a 10 µL reaction containing 1 µL GoTaq® buffer, 0.1 µL GoTaq® DNA polymerase, and 0.5 mM dATP.

1 µL of the finished reaction-mixture after ligation into pGEM was used to transform *E. coli* and recover plasmid DNA according to **Section 2.7.4**. Resulting DNA was subjected to restriction-digestion according to **Section 2.7.5**, and plasmids passing this step were sequenced according to **Section 2.3.3**. Fragments giving the expected sequence were used in the Golden Gate DNA assembly protocol to create "level 1" constructs for *Arabidopsis* expression. *pMRS2-3::MRS2-3::GFP* was assembled from *pMRS2-3, MRS2-3 F1, MRS2-3 F2, eGFP* and *tMRS2-3*; *pMRS2-4::MRS2-4::GFP* was assembled from *pMRS2-4, MRS2-4, eGFP* and *tMRS2-4*; *pMRS2-10::MRS2-10::GFP* was assembled from *pMRS2-10, MRS2-10 F1, MRS2-10 F2, eGFP* and *tMRS2-10* (see **Table 2.8**). The *eGFP* fragment, in the pGEM® vector, with GGTG and AAGC overhangs, was generously provided by Marco D'Ario (John Innes Centre, Norwich). All constructs were assembled into the pICSL86900OD vector backbone. Each expression vector was assembled in a 15 µL reaction containing 100 ng of all required modules, 1.5 µL 10x bovine serum albumin (New England Biolabs), 1 µL BsaI-HFv2 enzyme (New England Biolabs), 1 µL T4 DNA ligase (Thermo-Fisher Scientific), and ddH_2O to a final volume of 15 µL. The reactions were carried out in a Mastercycler® pro thermocycler (Eppendorf). The protocol was as follows: 35 cycles of 37°C for 3 min and 16°C for 4 min; then one step of 50°C for 5 min and 80°C for 5 min. 1 µL of each reaction-mixture was used to transform *E. coli* and plasmid DNA recovered according to S**ection 2.7.4**. Purified plasmids were subjected to restriction digestion according to **Section 2.7.5**, and those showing the correct pattern of bands were used to transform *A. tumefaciens* according to **Section 2.7.6**.

Table 2.8 – Level 0 modules created during Golden Gate cloning *of MRS2::GFP constructs*, and primers used to amplify them from genomic DNA.

Fragment	Primer name	Sequence	Product size [bp]
pMRS2-3	p2-3 F	X A **GGAG** CCTGATCACAATCATCAAACCAAGGC	1125
	p2-3 R	X A **CATT** CGCTTATGATTGTTGTGATCAGAGAGAG	
MRS2-3 F1	2-3 F	X T **AATG** AGAGGAGCTAGACCCGATG	400
	2-3 F1 R	X A **AGGG** TGAAACCGAAGGATCCTTG	
MRS2-3 F2	2-3 F2 F	X A **CCCT** TTATTGATGAG	1770
	2-3 R	X T **CACC** TTCAAGAAGGCGCTTGTACTTGC	
tMRS2-3	t2-3 F	X A **GCTT** GTCGACCAACAACATATTGGGAGAG	452
	t2-3 R	X A **AGCG** CGCCTCGTCGACATGTTTCTCTC	
pMRS2-4	p2-4 F	X A **GGAG** GCTTGTGATTGCATTTCTCGGG	1528
	p2-4 R	X T **CATG** GATTCCAGCCACGAAACAA	
MRS2-4	2-4 F	X T **CATG** GGGAAGGGCCCCTTATC	1499
	2-4 R	X T **CACC** TGAGCCTAGCAGCTTCTTCCAC	
tMRS2-4	t2-4 F	X A **GCTT** CTCCCTCTCTCTTACAAACCATGTG	839
	t2-4 R	X A **AGCG** CTAATTGGAAGAAAGTTCTCGATCTAC	
pMRS2-10	p2-10 F	X A **GGAG** CGCACGTTGTTGTCACCTATACTC	807
	p2-10 R	X A **CATT** GTTGCCAATCTCCAGATACTACAAAAC	
MRS2-10 F1	2-10 F	X T **AATG** TCTGAACTCAAAGAGCGTTTGC	163
	2-10 F1 R	X C **TTCT** TGAGGCCCAAAACATCAACTC	
MRS2-10 F2	2-10 F2 F	X A **AGAA** GCGTGGAC	1456
	2-10 R	X T **CACC** CAGAGGCATGAGTCTTCTACGTTTG	
tMRS2-10	t2-10 F	X A **GCTT** AGACATAACTACCCTGACACGTAGAC	403
	t2-10 R	X A **AGCG** CCACTTGGATGGAGACTCTAGTCAAC	

X = GT GGTCTC, two bases to serve as a spacer and the BsaI restriction enzyme recognition site, present on every primer to allow Golden Gate assembly to proceed. Bases in bold represent the 4-base overhang which enables ligation during Golden Gate assembly.

Table 2.9 – Level 0 modules created during Golden Gate cloning of MARIO expression vectors and primers used to amplify the required DNA fragments.

Fragment	Primer name	Sequence	Product size [bp]
MARIO F1	Mario F	GT GAAGAC GGCTCAAAT **GAGCTCGGATCCCATGGTGAGCAAGG**	
	M F1 R	GT GAAGAC AA **GCCGATGC TTCGATATCTTCCAGTTCCGGGCGGGTTGC**	
MARIO F2	M F2 F	GT GAAGAC GGCGGCACG **TTTCTTTGA AGATGACGACGGCCTGCATGATCACTCC**	
	Mario R	GT GAAGAC GGCTCGAAGC **GGATATCTGCAGAATTCTTACTCGATG**	

Work carried out by Tantawat Nardwattanawong in cooperation with Mark Youles. Underlined parts of sequences represent the BpiI recognition sequence, parts in bold represent sequences aligning to template DNA.

Table 2.10 – Additional level 0 modules used during Golden Gate cloning of MARIO expression vectors.

Module name	Fragment identity	Overhangs (5' / 3')
pICH41373	CaMV 35S promoter	GGAG/TACT
pAGM1479	TMV Ω enhancer, 6x His tag	TACT/AAGT
pAGM5331	TMV Ω enhancer, SV40 NLS	TACT/AAGT
pAGM5355	TMV Ω enhancer, RbcS chloroplast targeting signal	TACT/AAGT
pICH41414	35S terminator	GCTT/CGCT

All modules were obtained from TSL Synbio, courtesy of Mark Youles.

The *MARIO* constructs for *Arabidopsis* expression were generated by Tantawat Nardwattanawong in collaboration with Mark Youles (The Sainsbury Laboratory, Norwich, UK). The *MARIO* sequence was obtained as the *MARIO*/pcDNA3 plasmid, purchased from addgene (www.addgene.org), and the required DNA fragments were amplified by PCR using the primers listed in **Table 2.9**. Fragments were initially ligated into the pUAP1 plasmid via a Golden Gate assembly, using the same protocol as above, but using the BpiI restriction enzyme (New England Biolabs), creating level 0 modules. After *E. coli* transformation, plasmid purification, restriction digestion and DNA sequencing, level 0 modules were used in Golden Gate assembly reactions with BsaI, carried out as described above, to create level 1 *Arabidopsis* expression vectors.

Additional level 0 modules were obtained from TSL Synbio, and therefore represent gifts from Mark Youles. These are listed in **Table 2.10**. Each reaction contained pICSL86900OD, pICH41373, *MARIO F1, MARIO F2*, and pICH41414. One reaction was carried out with pAGM1479, pAGM5331, and pAGM5355 each, creating expression vectors targeting the protein to the cytoplasm, nucleus and chloroplasts, respectively. 1 µL of each reaction-mixture was used to transform *E. coli* and plasmid DNA recovered according to **Section 2.7.4**. Purified plasmids were subjected to restriction digestion according to **Section 2.7.5**, and those showing the correct pattern of bands were used to transform *A. tumefaciens* according to **Section 2.6.6**.

2.7.3 Gateway™-cloning

To generate MgD-responsive reporter plants used in **Chapter 5**, promoter-regions of putative MgD-responsive genes, identified after RNA-sequencing (see **Section 2.8** and **Section 5.2.1, Chapter 5**) were cloned and used to generate expression-cassettes in which the respective promoter was fused to the firefly luciferase open reading frame (ORF).

Promoter regions of three chosen candidate genes were amplified by PCR according to **Section 2.7.1** from Col-0 genomic DNA extracted according to **Section 2.3.1**. Primers used for each promoter are listed in **Table 2.11**.

Promoter fragments successfully extracted in the previous step were integrated into the pDONR207 entry vector by using BP Clonase II enzyme mix (11789100, Thermo Fisher Scientific) according to the manufacturer's instructions. 1 µL of the finished reaction-mixture was used to transform *E. coli* according to **Section 2.7.4**. For each promoter fragment, four different colonies of *E. coli* thus transformed were selected for plasmid extraction. Resulting DNA was subjected to restriction-digestion according to **Section 2.7.5**, and plasmids "passing" this step were sequenced according to **Section 2.3.3**.

One entry vector construct giving the expected sequence per promoter fragment was ligated into the pGW_LUC destination vector in an LR reaction using LR Clonase II enzyme mix (11791020, Thermo Fisher Scientific) according to the manufacturer's specifications. 1 µL of the finished reaction-mixture was used to transform *E. coli* according to **Section 2.7.4**. Four colonies per construct were subjected to restriction-digestion and DNA sequencing as in the previous step. Plasmids showing the expected sequence were used to transform *A. tumefaciens* according to **Section 2.7.6**.

Table 2.11 – Primers used during Gateway-cloning of putative Mg^{2+}-responsive promoters

Fragment	Primer name	Sequence	Product size [bp]
pAAA	pAAA-F	**attB1-**TCTGGTATCAAAGTTTGGTCCTTTTCC	1416
	pAAA-R	**attB2-**GTGTCGGCTGAAGTAAAAAATTTCCG	
pPER70	pPER70-F	**attB1-**TCGTGAAAATTCTCTGGTCTAACTGCC	3061
	pPER70-R	**attB2-**GGGTTTCTTCTTAGTTTTTAACCAAATGGTG	
pDTX3	pDTX3-F	**attB1-**TCCCAGATATGGAGGAATGATGATGATG	2754
	pDTX3-R	**attB2-**GTGTTGTCCTTCCTAATGTTGAAAGC	

attB1 = GGGGACAAGTTTGTACAAAAAAGCAGGCT

attB2 = GGGGACCACTTTGTACAAGAAAGCTGGGT

2.7.4 Transformation of *Escherichia coli* and plasmid purification

Transformation of plasmids into *E. coli* was achieved by heat shock treatment. Stellar™ competent cells (TaKaRa Bio Inc., Kusatsu, Japan) were used, in aliquots of 25 µL. 1 to 2 µL reaction-mixture from golden-gate or gateway cloning (**Sections 2.7.1** and **2.7.2**, respectively) were added to 25 µL Stellar™ cells, in a 1.5 mL Eppendorf tube, kept on ice. The mixture was kept on ice for another 20 min, then heat-shocked at 42°C for 60 s, followed by another 2 min on ice. Then, 250 µL liquid super optimal broth with catabolite repression (SOC) medium was added, and cells incubated at 37°C for 1 h.

The mixture was streaked out onto round agar plates of lysogeny broth (LB) medium, containing the appropriate antibiotic, as specified in **Table 2.12** (bacterial resistance), as well as 200 µg.mL^{-1} X-Gal (5-Bromo-4-Chloro-3-Indolyl β-D-Galactopyranoside, Thermo-Fisher Scientific) and 1mM IPTG (Isopropyl ß-D-1-thiogalactopyranoside, Thermo-Fisher Scientific) to enable blue-white screening. For each transformation, one plate was streaked with 200 µL cell suspension, and one plate was streaked with 50 µL of the same; with each set of transformations, a positive control with the pUC19 plasmid, and a negative control with ddH_2O were included. Plates were incubated at 37°C overnight, then four single, white colonies were picked from either plate using a sterile toothpick, and used to inoculate 10 mL aliquots of LB medium, which were incubated at 37°C overnight once again, before being subjected to plasmid extraction using the QIAprep® Spin Miniprep Kit (Qiagen).

2.7.5 Restriction digestion

For restriction digestion, a combination of BsaI-HFv2, BpiI, BamHI, HindIII, and/or Eco321 (latter three Anza™, Thermo-Fisher Scientific) restriction enzymes was used, depending on the plasmid in question. Enzymes were chosen such that the reaction, for the correct plasmid, would produce three to seven DNA fragments of different sizes, each longer than 200 bp. Each reaction was carried out as a 20 µL reaction, using either 2 µL Anza buffer (10x) or 2 µL CutSmart Buffer (10x), 1 µg plasmid DNA, 20 U of the restriction enzyme(s) in question, and ddH_2O to a final volume of 20 µL. Each reaction was incubated at 37°C for 1 h, before the entire reaction was loaded into a 1% (w/v) agarose-gel (Melford Laboratories) with 5 µg.mL^{-1} ethidium bromide (E1510-10ML), separated by electrophoresis, and bands visualized.

Table 2.12 – Antibiotics used during selection of transformants

Plasmid backbone	Bacterial resistance / working concentration	Plant resistance / working concentration
pGEM®	Ampicillin (Amp^R) 100 $\mu g.mL^{-1}$	-
pDONR207	Gentamycin (Gm^R) 20 $\mu g.mL^{-1}$	-
pUAP1	Chloramphenicol (Cm^R) 50 $\mu g.mL^{-1}$	-
pGW_LUC	Kanamycin (Kan^R) 50 $\mu g.mL^{-1}$	BASTA® (BlpR) 20 $\mu g.mL^{-1}$
pICSL86900OD	Kanamycin (Kan^R) 50 $\mu g.mL^{-1}$	Kanamycin (Kan^R) 50 $\mu g.mL^{-1}$

Antibiotics for both bacteria and plants are given, by plasmid backbone used, including working concentrations.

2.7.6 Electroporation of *Agrobacterium tumefaciens* (*A. tumefaciens*)

A. tumefaciens used in the course of this project were of strain AGL1, carrying the pSOUP helper plasmid. One aliquot was initially received as a gift from Mark Smedley (John Innes Centre, Norwich); subsequent aliquots were produced as follows:

A 10 mL aliquot of LB medium containing 50 $\mu g.mL^{-1}$ rifampicin and 10 $\mu g.mL^{-1}$ gentamycin was inoculated with *A. tumefaciens* AGL1 (pSOUP) and incubated at 28°C for 48 h. 5 mL of this culture were used to inoculate 500 mL of LB containing 50 $\mu g.mL^{-1}$ rifampicin and 10 $\mu g.mL^{-1}$ gentamycin, which was incubated at 28°C with shaking until the optical density at 600 nm (OD_{600}) reached 0.5 – 1. The entire culture was then centrifuged at 4000 g for 15 min at 4°C, before re-suspending the cells in 500 mL of an ice-cold solution of 1 mM HEPES in dH_2O, pH 7.0. Centrifugation was repeated, followed by resuspension in 250 mL HEPES buffer and another similar centrifugation-step. Next, cells were resuspended in 200 mL 10% (v/v) glycerol, centrifuged again, then resuspended in 1.5 mL 10 % (v/v) glycerol. This suspension was divided into 40 µL aliquots and flash-frozen in liquid nitrogen, then stored at -70°C until use.

Transformation of expression vectors into *A. tumefaciens* was achieved via electroporation. 40 µL aliquots of *Agrobacterium* from the above protocol were mixed with 5 – 100 ng of purified plasmid DNA from **Section 2.7.4**, chilled on ice for 5 min, before being transferred into 0.1 cm electroporation cuvettes (1652083, BioRad). Electroporation was carried out using a Gene Pulser™ electroporation system (Biorad) with the following conditions: 25 µF, 2.4 kV, 200 Ω. 1 mL of SOC medium was added immediately afterwards; the mixture was then incubated with shaking for 2 h (250 rpm) at 28°C. 200 µL and 50 µL of the cell suspension, respectively, were then spread onto two LB agar plates containing 50 $\mu g.mL^{-1}$ rifampicin, 100 $\mu g.mL^{-1}$ carbenicillin, 10 $\mu g.mL^{-1}$ gentamycin, and the antibiotic suitable for selection for the vector backbone used in the transformed construct (see **Table 2.12**). Plates were then incubated for 2 d at 28°C, before single colonies were selected for use in *A. thaliana* transformation according to **Section 2.7.7**.

2.7.7 Floral dipping of *A. thaliana* and T1 transformant selection

Transformation of *Arabidopsis* was carried out via the floral dip method [202]. *A. thaliana* to be transformed were grown on soil according to **Section 2.1.5** until bolt formation. The primary bolt was cut back, followed by growth for another five to seven days, to encourage secondary bolt formation. Three days before transformation, a 10 mL aliquot of LB medium containing 50 $\mu g.mL^{-1}$ rifampicin, 100 $\mu g.mL^{-1}$ carbenicillin, 10 $\mu g.mL^{-1}$ gentamycin, and the antibiotic according to **Table 2.12**, was inoculated with *A. tumefaciens* containing the desired expression vector (**Section 2.7.6**), incubated for two days at 28°C with shaking, then used to inoculate 500 mL of LB medium containing the same antibiotics. This culture was incubated overnight at 28°C with shaking, until the OD_{600} was between 0.8 and 1.2. Then, cells were pelleted by centrifugation at 3000 g for 20 min, before being resuspended in 400 mL of a solution of 500 $\mu L.L^{-1}$ Silwet L-77 (306302161, Fisher Scientific) and 5% (m/v) sucrose in ddH_2O. All siliques already formed on the chosen *Arabidopsis* plants were removed, then aerial parts of the plants were submerged in the *Agrobacterium* cell suspension for 2-3 min with gentle agitation.

Plants were then placed in autoclave bags and kept in the dark overnight, before being transferred back to the CER under standard growth conditions until seeds were ready to collect. Seeds successfully transformed with the chosen DNA construct were then selected according to **Section 2.7.8** below.

2.7.8 Selection of homozygous transformant lines

To distinguish successfully transformed individuals expressing the DNA construct in question from untransformed individuals, seeds of *A. thaliana* from **Section 2.3.7** (T_1 seeds) were surface-sterilized in 1.5 mL Eppendorf tubes by adding 1.4 mL of a solution of 62.5% (v/v) EtOH, 37.5% (v/v) dH_2O, and 7.5 $mg.mL^{-1}$ DCICA and shaking for 20 min at 250 rpm. Following this, seeds were immersed in 1 mL 100% EtOH three more times for one minute each time, then seeds were transferred onto sterile filter paper and left to dry for 20 min. Then, seeds were sprinkled onto 100 mm square plates of 0.25x MS medium containing the appropriate antibiotic to select for the construct used to transform the plants in the previous step, according to the cloning vector used (see **Table 2.12**). Roughly 1000 seeds were applied per plate. Plates were sealed and placed in a CER maintained according to **Section 2.1.2**. After at least seven days of growth (7 DAG), seedlings growing notably better than surrounding individuals were transferred to soil, grown to maturity, allowed to self-fertilize, and seeds collected from each individual plant. No fewer than 20 plants were selected for each construct transformed at this stage.

Seeds from T_1 individuals, e.g., T_2 seeds, were sterilized according to **Section 2.1.2** and placed onto 100 mm square agar plates of 0.25x MS medium again, generally in two rows of ten seeds. Seeds were placed on plates containing the same antibiotic as in the previous step, as well as antibiotic-free plates, in parallel. Then, seedlings were counted for both resistance to the respective antibiotic, as well as expression of the respective construct (luciferase expression according to **Section 2.6.1**, or fluorescent protein expression according to **Section 2.6.2**). Numbers for both resistance and transgene expression were subjected to a chi-squared test against an expected ratio 75% of plants resistant and expressing the transgene, respectively.

Only “lines” (batches of seeds from one individual) consistent with this pattern were carried forward, with several individuals put to soil and allowed to self-fertilize in each case. At least five lines per construct transformed were carried forward at this stage.

T_3 seeds were subjected to the same process as T_2 seeds, however, in this case, only lines showing 100% antibiotic resistance and transgene expression were selected and carried forward, *i.e.*, lines homozygous for the transgene.

2.7.9 Crossing of *Arabidopsis*

Plants to be crossed were grown on soil according to **Section 2.1.5**, until buds and flowers were both present on plants of both genotypes to be crossed. Then, for the genotype chosen to be the female part of the cross, two buds per stalk were selected, with at least three stalks included for each cross to be made. Any siliques present on the selected stalk, as well as any fully developed flowers and surplus buds were removed, leaving only the chosen buds. Chosen stalks were marked using a small bit of micropore tape and care was taken to keep them from coming into contact with remaining flowers on the same plant going forward. Then, using forceps with sharp, pointed tips, buds were teased apart, and petals, sepals and stamens were removed, leaving only female reproductive tissues. Once completed, fully developed flowers without visibly emerging, fertilized siliques were removed from the plant(s) chosen to be the male part of the cross, and their stamens were brought into contact with female reproductive tissues on chosen, dissected buds. Three to five flowers from the male counterpart in the cross were brushed against each dissected bud of the female counterpart, with one flower being used to pollinate multiple buds.

Once siliques developed from dissected and fertilized buds, these seeds were collected separately from other seeds from the same plant.

2.8 EMS mutagenesis and mutant screening

2.8.1 EMS mutagenesis

Seeds from multiple individuals of a homozygous luciferase reporter-line (*pAAA::LUC* 2-4-X), previously tested for retention of luciferase expression and BASTA resistance, were pooled together, making up approximately 0.5 mL of seeds. Seeds were transferred to a 50 mL Falcon tube, then soaked in 20 mL 0.1% (w/v) KCl solution overnight. The solution was decanted and replaced with 20 mL 0.1 M phosphate buffer, pH 7. Using a syringe and needle, a volume of EMS (Sigma-Aldrich, Cat. No. M0880-1G) sufficient to reach a concentration of 65 mM was then added. The tube was sealed with parafilm, then gently rocked for 6 h at room temperature. After this, the seeds were washed twice with 20 mL 0.1 M sodium thiosulphate (72049-250G), then twice with distilled water. Then, the seeds, now considered M_1 seeds, were transferred onto filter paper and left to dry, after which they were sprinkled thinly onto a total of 20 1L soil trays.

2.8.2 Growth of M_1 plants and pooling

Over the course of their growth, trays were thinned out three times, each time removing excess seedlings from the trays until individuals were no longer touching, to allow for uninhibited growth. removed seedlings were discarded, and remaining plants were allowed to grow to maturity and self-fertilize. At this stage, seeds were collected for roughly ten individuals at a time, as “pools” of seeds (M2 seeds). A total of 50 pools were generated.

2.8.3 Estimation of seed viability and frequency of mutations

M_2 seeds from pools 1-16 from the previous section were mixed in roughly equal proportions, then they were sterilized, plated and grown according to **Section 2.1.2**. Seeds were placed on agar plates in 3 evenly-spaced rows of 23 seeds each, for 69 seeds per plate. A total of 2070 M_2 seeds and 276 seeds of *pAAA::LUC* 2-4 ("parent line") were used. At 10 DAG, seedlings that failed to germinate and number of seedlings exhibiting white or pale-green coloration ("albino mutants") were counted. Germination rate and frequency of albino mutants were determined for both M_2 seeds and *pAAA::LUC* 2-4 seeds.

2.9 RNA-sequencing

2.9.1 Sample preparation for RNA-sequencing

Samples of RNA submitted for RNA-sequencing (RNAseq) were obtained by growing *A. thaliana* on agar plates containing HM made with washed agar and containing different concentrations of Mg^{2+} (15, 50, 150, 250 and 1000 µM added Mg^{2+}) according to **Section 2.1.2**, until 14 DAG. Shoots of plants were sampled and RNA-extractions carried out according to **Section 2.4.1**. Three biological replicates of the experiment were carried out, resulting in 15 samples of RNA, three per concentration tested. Immediately after RNA-extraction, the obtained RNA was split into two aliquots, with one being flash-frozen and stored at -70°C immediately. In addition to Nanodrop™ analysis, the aliquot left behind was tested for RNA concentration using a Qubit™ Fluorometer and the Qubit™ RNA high sensitivity kit (Thermo Fisher Scientific); integrity of the RNA was tested using a 2100 Bioanalyzer system with the RNA 6000 Nano kit (Agilent Technologies Inc., Santa Clara, U.S.A.).

2.9.2 RNA-sequencing and initial data analysis

RNA-sequencing was carried out by Novogene Co., Ltd. (Beijing, China), using their whole transcriptome sequencing service. Quality control was carried out on samples upon receipt, via Nanodrop™ and agarose gel electrophoresis, followed by mRNA enrichment using oligo(dT) beads. cDNA synthesis was carried out using random DNA hexamers and reverse transcriptase. After first-strand synthesis, the second strand was generated by nick-translation using a custom second-strand synthesis buffer (Illumina) with dNTPs, RNase H and *E. coli* polymerase I. DNA purification, terminal repair, A-tailing, ligation of sequencing adapters, size selection and PCR enrichment was used to generate the final sequencing library. Library concentration was quantified using a Qubit 2.0 fluorometer before checking insert size on a 2100 Bioanalyzer and quantifying to greater accuracy by qRT-PCR (library activity >2 nM). Sequencing was carried out on an Illumina platform, with a 2x 150 bp paired-end setup. Error rate for each base was assessed, GC and AT content calculated, reads were filtered to remove adapter sequences or uncertain reads.

Raw reads were then aligned to the TAIR10 reference genome using the TopHat v2.0.12 package. HTSeq v0.6.1 was used to calculate expression levels of genes, as FPKM values (fragments per kilobase per million reads). Gene expression levels across the genome at different conditions were assessed using FPKM distribution plots and violin plots, and correlation between samples was assessed using Person's correlation coefficient. DESeq v1.10.1 software [203] was used to assess differential gene expression across Mg^{2+}-concentrations, generating fold-changes in expression and p-values for each transcript in the analysis. Volcano-plots were generated to assess differentially expressed genes (DEGs), then DEGs were subjected to hierarchical clustering by expression-profile. Gene ontology (GO) analysis [204] was carried out using the GOSeq package [205], release 2.12, and bar charts for enriched GO terms in each sample were generated. Kyoto encyclopedia of genes and genomes (KEGG) analysis was carried out using KOBAS v2.0 [206].

Wherever applicable, false discovery rate (FDR) p-value cut-offs of $p < 0.05$ were used.

2.10 Bioinformatic methods

2.10.1 Comparing existing MgD transcriptomic data

A literature search was carried out for existing, published transcriptomic data sets containing expression data from *A. thaliana* exposed to MgD conditions. Five different data sets were found ([101], [102], [103], [104], [105]), and data downloaded. These data sets were obtained using different conditions and methods, as summarized in **Table 3.1**.

Gene lists including expression for all genes were first trimmed to include only genes with differential expression. For data from Kamiya *et al.* [105], a list of differential expression values was given for all transcriptomes tested. Since no FDR p-values were given, transcripts with expression increased more than five-fold at low Mg^{2+} were included in the analysis (1165 transcripts). For Niu *et al.* [104] Expression levels (FPKM values) for all transcripts in the genome were given, for multiple combinations of conditions and two samples each. Expression-values for "ambient CO_2, control Mg^{2+}, shoots" and "ambient CO_2, low Mg^{2+}, shoots" were included in the analysis. The arithmetic mean between the two samples given for each condition was calculated, then transcripts for which expression was not detected at low Mg^{2+} (0.0 FPKM) were excluded from the analysis. Fold-change in expression was calculated by dividing the expression under control Mg^{2+} by expression under low Mg^{2+}. Since no FDR p-values were available, all transcripts showing more than five-fold increase in expression were included in the analysis (3626 transcripts). For Hermans *et al.*, 2010 ([101], [102]), **Table S3**, provided with the supplementary data in both cases, included data on differentially-expressed genes in young mature leaves. Since stringent selection-criteria with FDR < 0.001 were already applied, all transcript showing more than a two-fold increase in expression in young mature leaves at any of the time-points tested, but reduced expression at none of the time-points tested, were included in the analysis (3618 transcripts for long-term MgD, 329 transcripts for short-term MgD). For data from Oda *et al.* [103], the list "Wild type (Ctrl vs. -)" included only genes differentially expressed in Col-0 plants at low Mg^{2+} (q-value < 0.05).

10 genes showed reduced expression under MgD and were excluded; otherwise, the list was used as given (389 transcripts). All five lists of genes were imported into RStudio, creating a data frame encompassing all five gene lists. A custom script was created in collaboration with Marco Fioratti (John Innes Centre, Norwich), allowing comparison of a "query" list of gene identifiers to the data frame and determination of any transcriptomic data sets each member of the query was present in. Venn-Diagrams were created using the ggVennDiagram package [207]; colours were assigned manually after export of the created figures using Inkscape V. 1.1.

2.10.2 Additional analysis of WGS data and discovery of causal mutations

The comparison files received from Genewiz contained a large amount of false-positives due to low coverage of the control genome (*pAAA::LUC*). Raw data were therefore re-analysed with assistance from Burkhard Steuernagel at the JIC bioinformatics platform. Sequence data from samples was individually mapped to the TAIR10 Col-0 reference genome, downloaded from ftp.arabidopsis.org. Mapping was performed with BWA, v.0.7.17-r1188 [197].
Mapping was sorted and converted to mpileup format using SamTools v.1.10 [198]. Mapping and sorting were performed using default parameters. Conversion to mpileup format was done using parameters -B and -Q 0.

A custom program implemented in Java was used to find single nucleotide variations (SNVs) that could have originated from the mutant screen or from the back-crossing procedure. SNVs present in the control were considered noise and discarded from further analysis. Positions in the genome with an SNV in more than two mutants were also considered noise, since a random mutation occurring in two independent mutants is highly unlikely (except for MgMt-2 and MgMt-3, as well as MgMt-9 and MgMt-10, respectively, which were from the same pools of M_2 seeds). Each observed SNV was, in addition to its allele frequency in the sample, enriched with information on its presence within the exon of a gene or in a promotor region, *i.e.*, within 3 kb of a gene start codon. For each mutant, an output table was generated to support manual inspection using IGV.

Lists of variants and their frequencies within the sequenced DNA were obtained. These lists were validated manually. Mutations occurring at a frequency below 90% in the sequenced DNA, as well as those predicted to lie within introns, intergenic regions (not within 3 kb of a transcriptional start site), or within or close to genes annotated as “transposable element gene” only, were excluded from the analysis. Remaining variants were considered potentially causative, and for these, the amino acid change the respective mutation would cause was determined. Functional information on genes that were likely to be affected by the mutation was obtained from the *Arabidopsis* information resource (TAIR, https://www.arabidopsis.org/), the Uniprot database (https://www.uniprot.org/), as well as any associated publications.

2.10.3 Construction of a phylogenetic tree for the BCS1-clade of AAA ATPases in *A. thaliana*

The phylogenetic tree was constructed using the MEGA software, version 10.1.7, according to the method outlined by Hall [208]. The sequences used were chosen manually, including all BCS1-clade AAA ATPases with “reviewed” protein sequences in the UniprotKB Database (https://www.uniprot.org/uniprot/), as well as AtFtsH2/VAR2 (At2g30950) and AtAPP1 (At5g53540), which were included as an outgroup. One sequence, from AT3G45210, was excluded, since the sequence of this protein was identical to that of BCS1 itself, and the sequence registered for this locus identifier on TAIR was different, indicating that this entry is erroneous. The MUSCLE algorithm was used to align the sequences. The alignment was also checked using the GUIDANCE algorithm (guidance.tau.ac.il), which gave a GUIDANCE alignment score of 0.808.

The evolutionary history was inferred using the Neighbor-Joining method. The “JTT + G + F” model (Jones-Taylor-Thornton model including Frequency information, with rates among sites Gamma-distributed) was used to produce the tree. The evolutionary distances were computed using the Poisson correction method. All ambiguous positions were removed for each sequence pair (pairwise deletion option). 500 bootstrapping iterations of the algorithm were run. Once the tree was calculated, it was rooted on the branch leading to AtFtsH2 and APP1.

Chapter 3: An Investigation of the Physiological Consequences of Magnesium-Deficiency in *A. thaliana*

3.1 Introduction

3.1.1 Important gaps in the magnesium homeostasis network

As outlined in the Introduction (**Chapter 1**, **Section 1.2.5**), knowledge pertaining to Mg^{2+}-sensing, and the regulation of Mg^{2+}-homeostasis is extremely limited. Although some candidates, such as EF-hand proteins and MRS2 Mg^{2+}-transporters, have emerged, reliable MgD marker genes have proven to be exceedingly elusive [105, 188]. It is possible that Mg^{2+} is sensed indirectly; for example, Mg^{2+} can influence transcription to regulate gene expression, as has been demonstrated in prokaryotes [209-211], but in any case, a mechanism must exist to explain the often rapid and large-scale transcriptional and physiological changes observed under MgD. Mg^{2+}-transporters are likely subject to regulatory mechanisms as well, either being regulated by upstream factors or participating in Mg^{2+}-sensing and -signalling themselves (see **Chapter 1**, **Section 1.3**). This work therefore aims to gain further insight into the processes governing uptake and distribution of Mg^{2+}.

3.1.2 Forward genetic screens can reveal members of nutrient homeostasis networks in *A. thaliana*

The presence of other yet undiscovered Mg^{2+}-sensing proteins and specific marker genes cannot be excluded. As such, large-scale, broad approaches might yet reveal one or more of the central elements of Mg^{2+}-homeostasis. Forward genetic screens represent one such method.

In a forward genetic screen, a parent population is treated with a mutagen, which produces mutations distributed across the genome at random. The parent population is then self-fertilized (in the case of a polyploid organism), leading to a screening population in which both dominant and recessive mutations can be revealed by testing offspring for alterations in a phenotype or characteristic of interest.

As such, a forward genetic screen can reveal a gene associated with a process with little prior knowledge about the process and without introducing bias, if the screen is properly set up and carried out. Forward genetic screens have successfully revealed members of nutrient homeostasis networks with respect to other ions in the past, including potassium (K^+) [212], nitrogen (N) [213] and iron (Fe) [214, 215].

Although a forward genetic screen for Mg^{2+}-related genes in plants has been carried out before and has produced interesting results, the mutants identified by this screen and characterized so far have been shown to be an *mrs2-4* mutant [103] and a mutant in *smu1*, a gene which encodes a splicing factor required for correct splicing of MRS2-7 [164]. This screen was carried out on a growth medium low in Mg^{2+} while also containing excess Ca^{2+} to mitigate the problem of introducing Mg^{2+}-levels sufficient for plant growth with the agar used to solidify the medium, and candidate mutants were identified by visual inspection [103]. This screen revealed genes that are important for growth under these conditions and upstream factors necessary for their correct expression, but since the SMU1-mediated splicing of MRS2-7 appears to be independent of exogenous Mg^{2+}-levels [164], it failed to reveal true regulatory factors. Similarly, forward genetic screens for altered ion-accumulation in *A. thaliana* [216, 217] and *Brassica rapa* [218] have led to the identification of mutants with altered Mg^{2+}-concentrations; in both of these cases, the identified mutants are defective in formation of the Casparian strip, the endodermal diffusion barrier normally responsible for preventing the flow of water and solutes into the stele of the root of vascular plants. While these results have great implications for research on Casparian strip formation and could aid biofortification efforts [218], they have not [yet] revealed Mg^{2+}-sensing or -signalling factors.

The main difference between the forward genetic screens outlined in the previous paragraph and those that have successfully identified members of other mineral nutrient homeostasis networks is the use of a transcriptional reporter. In a reporter-based screen, the mutagenized population contains a transgene consisting of a promoter which is known to regulate expression according to the condition of interest, which is fused to the coding sequence (CDS) of an easily-detectable reporter, such as a fluorescent protein or firefly luciferase (LUC).

During screening of the mutagenized population, plants with altered reporter expression, either unexpectedly high or low, are selected. Mutated plants that do not show the differential expression of the reporter may contain a defect in a part of the signalling-mechanism normally regulating expression, or be unable to establish normal homeostasis due to a mutation in a crucial component, such as an ion transporter.

Since a reporter-based screen does not rely on mutants showing visual or physiological changes, it is more likely to reveal mutations causing relatively subtle changes. Additionally, if the promoter has been chosen properly, *i.e.*, if it is part of a signalling network, mutations in upstream regulatory factors can be identified through their effects on reporter expression. As such, a screen utilising a transcriptional reporter will be more effective at identifying Mg^{2+}-sensing or -signalling factors, as well as having the potential to reveal transporters and other factors influencing Mg^{2+}-homeostasis which have not been identified so far.

3.1.3 Prerequisites for carrying out a reporter-based forward genetic screen

Several decisions must be made before setting up a forward genetic screen using a transcriptional reporter, particularly the choice of the reporter gene, *i.e.*, the promoter to be used for the reporter construct, and the choice of screening conditions.

It is necessary to find a candidate gene showing differential regulation under the conditions in question relative to control conditions; in this case when plants experience MgD compared to Mg^{2+}-replete conditions. The differential regulation must be as specific to these conditions as possible, since otherwise the screen could identify genes regulating a pleiotropic response. For example, Mg^{2+}-deficiency leads to production of ROS (see **Chapter 1**, **Section 1.2.4**), and while it is possible that ROS are one of the prime factors eliciting and modulating low-Mg^{2+}-responses, it is also possible that the responses are mostly independent of one another. In this case, the screen could primarily identify components of the ROS-signalling pathway. This makes it necessary to evaluate potential candidate genes carefully.

Although there are several transcriptomic datasets of good quality obtained from plants exposed to MgD [101-105], the search for genes with MgD-specific upregulation has been unsuccessful [105]. To find a suitable candidate for the reporter, it was therefore necessary to generate additional data by carrying out RNAseq on *Arabidopsis* grown under the specific conditions used for the screen. These RNAseq data can be compared to previously-generated, published data to further confirm the findings. A good candidate gene should be part of a universal MgD-response, *i.e.*, it should be upregulated whenever plants experience MgD; it should therefore be present in sets of genes upregulated under MgD even if the exact conditions used to obtain these sets were different. Then, the expression of the reporter gene or construct needs to be evaluated under various different stress conditions to ensure the specificity of the response.

To carry out a forward genetic screen, it is necessary to grow large numbers of plants, which means that the use of younger and smaller plants is favourable. However, the symptoms of MgD in *Arabidopsis* have previously been elucidated and defined primarily in mature plants, usually five weeks old at the start of experiments [86, 101, 102, 162]. Additionally, these plants were grown hydroponically and MgD was induced by exchanging the nutrient solution for one without added Mg^{2+}, termed "Mg^{2+} withdrawal"; systems such as this are not suitable for large-scale screening. Withdrawal of Mg^{2+} from the medium is not feasible during a large-scale screen utilising younger plants, especially since chelating agents specific for Mg^{2+}-ions are not available. It was found necessary to grow plants used for screening on medium containing one specific concentration of Mg^{2+}. A screen for loss of reporter expression, specifically, would have to be carried out on a concentration suitable for inducing the symptoms of MgD without excessive effects on plant growth. Additionally, on a Mg^{2+}-concentration barely sufficient for plant growth, even small disruptions would lead to increased reporter expression; a screen for induction of reporter expression in these conditions could therefore identify factors subtly influencing Mg^{2+}-homeostasis that could not be found so far. Both of these concentrations will have to be determined first however, which necessitates an investigation of the physiological symptoms of MgD in *A. thaliana*.

To define the symptoms experienced by younger plants grown on agar plates containing one specific Mg^{2+}-concentration, symptoms should be confirmed with methods similar to those used in the past. Then, new methods can be used to investigate parts of the response that have only been hypothesized. This work lays the foundation for the forward genetic screen, but also for further progress in elucidating the symptoms of MgD in plants.

3.1.4 Knowledge gaps regarding the symptoms of MgD in *A. thaliana*

The physiological consequences of MgD have been well documented [56, 86, 96, 97, 162, 219-221] (see **Chapter 1**, **Section 1.2.4**). **Figure 3.1** shows a model for the series of symptoms of MgD experienced over time, assuming that the inhibition of sucrose export from source leaves is caused by reduction in sucrose/H^+-symporter activity, as well as the assays used to establish them. However, not every step in this "pathway" has been experimentally confirmed to a satisfactory degree, and individual steps await clarification. Additionally, until recently [87], symptoms had been established in mature plants, and they have been investigated almost exclusively in plants exposed to Mg^{2+} withdrawal.

Growth assays are featured in almost every study involving MgD, and while they are easy to carry out, they give no information on the molecular processes taking place to cause the reduction in growth or change in biomass allocation. Nevertheless, establishing the point at which plant growth suffers represents an important step in defining the effects of any stress condition.

Starch accumulation is usually measured using iodine staining, as well as photometric assays measuring sugar content [56, 86, 97]. Together, this provides spatial and quantitative information, making this a well-established part of the response.

The increase in ROS concentrations, and resulting increase in activities of antioxidant enzymes, is usually determined photometrically as well [96, 221, 222], and the results are mostly consistent across the literature [76], but these assays are carried out on homogenized tissues. Recently, fluorescent ROS-sensitive probes have been used to good effect [96], but more data on the nature and distribution of ROS could be valuable.

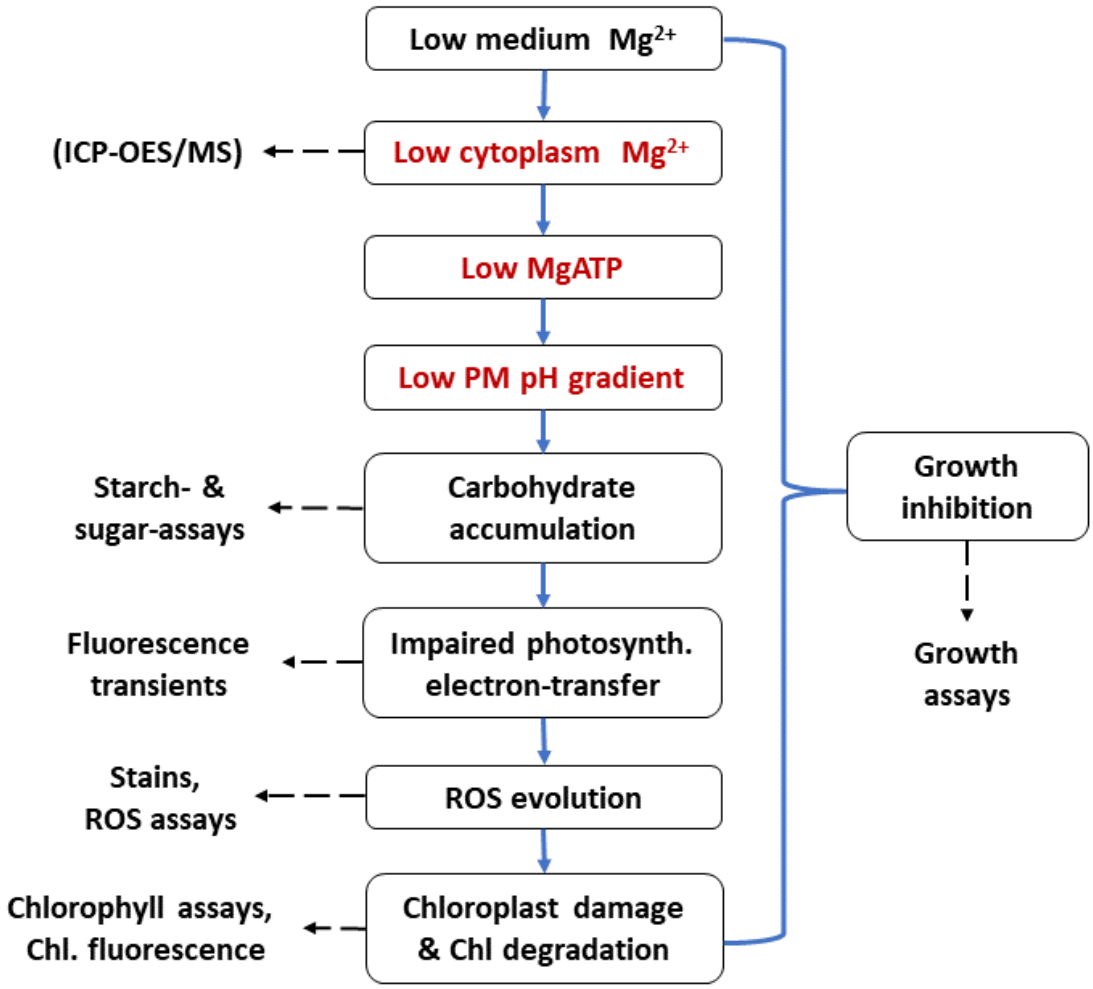

Figure 3.1 - Physiological symptoms of MgD, in "causal" order, along with assays used to test for each.

Starting with "Low medium Mg^{2+}" at the top, each box indicates one symptom, each of which is thought to cause the next one in the sequence, as indicated by the blue, solid arrows. Black, interrupted arrows indicate assays used to confirm or measure each of the disturbances. Red text indicates symptoms that have not been tested or confirmed yet. Brackets around "ICP-OES" indicate that this assay is not suited to confirming this symptom.

Spectrophotometric chlorophyll assays are commonly performed and simple to carry out, and show reduced chlorophyll content in Mg^{2+}-deficient leaves [86, 96, 97, 219]. Chlorophyll-content can also be determined by measuring chlorophyll fluorescence, which has been used as well [96, 97, 100, 221]. More importantly though, more sophisticated measurements can be used to gain deeper insights into the disruptions to photosynthesis. Photosynthetic electron-transport can be examined by measuring fluorescence transients of the photosystems; this method has determined impairments of photosynthetic electron-flow during MgD independently of the abundance of chlorophyll. This impairment is likely to precede reductions in chlorophyll abundance in time during MgD. This kind of study is technically complex, however, and seems to have been carried out for MgD only once [97]. More recently, this type of technique has been used to elucidate the exact effects of phosphate-deficiency on the electron transport chain [223]. The results from these two studies appear very similar, and could indicate that MgD and phosphate deficiency share their primary molecular "target": ATP synthase and the electron transport chain. However, more evidence is needed to support this hypothesis.

ICP-OES or ICP-MS are often used to confirm a reduction in Mg^{2+}-abundance in plant tissues exposed to MgD [86, 96, 97, 221]. However, Mg^{2+}-pools within organelles are much larger than the cytoplasmic pool [61], and this technique lacks the ability to distinguish between the two. There are no data on [Mg^{2+}] within the cytosol or specific organelles under MgD. Assessing the concentration of MgATP, thought to be a crucial step in the occurrence of the symptoms of MgD, is even more difficult, and data are similarly lacking. Therefore, while the downstream symptoms of MgD are well-characterized, the initial steps thought to cause these symptoms are not sufficiently understood, and new tools are needed in order to improve this situation.

To test the model of MgD from **Figure 3.1**, it is necessary to ascertain whether cytoplasmic Mg^{2+}, and subsequently cytoplasmic MgATP, is reduced to a significant degree in leaf cells before the onset of other symptoms. It would be necessary to create a time-course of intracellular concentrations of these metabolites, or to define their concentrations over a range of external Mg^{2+}-concentrations. A plethora of dyes are available which can report on Mg^{2+}-concentrations [169], but it is difficult to introduce them into cells in physiologically-relevant states, as well as to control their subcellular localisations, and there are no such dyes for MgATP. As outlined in **Chapter 1**, **Section 1.4**, genetically encoded, ratiometric sensors for Mg^{2+} and MgATP likely offer the best chance for the proper characterisation of the first steps of the MgD causal chain, since they can offer the necessary specificity for subcellular compartments, as well as enable a sufficient number of observations to be made to achieve the sample size and/or temporal resolution required. Similarly, the hypothesized reduction in the PM pH differential can be investigated using ratiometric pH sensors present on both sides of the PM.

3.1.5 Aims of this chapter

The aim of the experiments described in this chapter was to first establish a protocol for reliably inducing variable levels of MgD in *A. thaliana* seedlings grown on agar plates by varying the concentration of Mg^{2+} added to the medium, then to use this protocol to advance knowledge of the "early" symptoms of MgD. **Sections 3.2.1** and **3.2.2** of this chapter lay the foundation for the reporter-based, forward genetic screen described in **Chapter 5** by establishing said protocol and confirming that the symptoms of MgD induced are similar to those previously described. **Section 3.2.3** describes the generation of an *Arabidopsis* line expressing the Mg^{2+}-responsive FRET-sensor MARIO, as well as *in vitro* validation of MARIO function. Results of evaluation of cytoplasmic MgATP-levels, as well as cytoplasmic and apoplastic pH using the genetically-encoded ratiometric sensors ATeam and pHusion are described in **Section 3.2.4**.

3.2 Results

3.2.1 Expression of putative MgD marker genes can be induced by continuous growth on low Mg^{2+}

The most efficient way to establish the possibility of inducing MgD in *Arabidopsis* seedlings grown on low Mg^{2+} continuously, as opposed to transfer to low Mg^{2+}, was to compare the expression of genes known to show increased expression under MgD. Since there are no known specific and sensitive reporter genes for MgD, a literature search for transcriptomic datasets including data from plants exposed to low Mg^{2+} was carried out. This search returned five datasets associated with recent publications. The conditions used to grow the plants in question and to induce MgD in each of these studies varied widely, as shown in **Table 3.1**.

Table 3.1 – Existing *A. thaliana* transcriptomic data sets including data on gene expression under MgD used over the course of this project

Reference	Conditions	Mg^{2+}-stress	Age [DAG]	Method	Name
Hermans *et al.*, 2010b [102]	Hydroponic	Withdrawal (7 d)	42	Microarray	A
Kamiya *et al.* [105]	Hydroponic	Continuous (15 µM)	14	Microarray	B
Niu *et al.* [104]	Hydroponic	Withdrawal (7 d)	42	RNAseq	C
Oda *et al.* [103]	Agar plates	Continuous (0 µM[a])	14	RNAseq	D
Hermans *et al., 2010a* [101]	Hydroponic	Withdrawal (4-28 h)	35/36	Microarray	E

Conditions – Conditions used to grow the plants in question. **Mg^{2+}-stress** – Type of Mg^{2+}-stress applied to plants, either continuous growth on low Mg^{2+} or withdrawal of Mg^{2+} from the medium at a certain point. **Age** – Age at which plants were harvested before transcriptome data were obtained. **Method** – Method by which transcriptome data was obtained. **[a]** – Plants were grown on agar plates containing 1.5% (w/v) purified agar; effective Mg^{2+}-concentration was therefore greater than 0 µM.

Lists of differentially expressed genes (DEGs) associated with each of the publications in **Table 3.1** were downloaded and trimmed to include only genes expression of which was significantly induced by MgD (either adjusted p-value < 0.05 or > 5-fold increase in expression where p-values were not available (see **Chapter 2**, **Section 2.10.1**). This gave lists of 3618 genes (Hermans *et al.*, 2010a, **A** in **Table 3.1**); 1165 genes (Kamiya *et al.*, **B**); 3626 genes (Niu *et al.*, **C**); 389 genes (Oda *et al.*, **D**); and 329 genes (Hermans *et al*., 2010b, **E**), respectively. To determine genes likely to be useful as MgD reporters, these lists were combined, and genes appearing in multiple lists were determined. Of the 6398 individual genes appearing in at least one of the lists generated, 4435 genes (69.3%) were present in one of the datasets only, 1349 genes (21.1%) were present in two sets, 476 genes (7.4%) were present in three sets, 127 genes (2.0%) were present in four sets, and 11 genes (0.2%) were present in all five of the transcriptomic datasets compared. **Table 3.2** gives the 11 genes present in all five of the datasets.

From the available descriptions and functional annotations of the genes appearing in **Table 3.2**, it appears that a significant portion of these genes are either general stress-responsive or involved in the response to ROS-stress, one of the downstream symptoms of MgD (entries # 1, 4, 5 and 18). Two are thought to respond to or bind Ca^{2+} (# 6 and 10), and two appear to be involved in responses to biotic stress (# 4 and 10). Of special interest are three poorly annotated genes, two putative P-loop NTPases and one EF-hand protein (# 6, 7 and 9). Entries # 6 and 7 appear to be primarily expressed in senescing leaves, but # 9 seems to be expressed in most tissues, according to the Klepikova atlas [224]. Nevertheless, none of these genes were deemed sufficiently likely to respond specifically to MgD to be used as candidate MgD reporter genes, since even entry # 9 is known to respond to many biotic stresses, as well as cold and UV-B exposure according to the *Arabidopsis* eFP browser [225]. Therefore, the search was broadened to include genes present in fewer than five of the examined datasets.

Table 3.2 – Genes upregulated in all MgD transcriptomic datasets analysed.

#	Locus Identifier	Gene Description	Gene Symbol
1	***AT1G13340***	Regulator of Vps4 activity in the MVB pathway protein.	IST1-LIKE 6 (ISTL6)
2	***AT1G15520***	PM ABC transporter, involved in ABA transport and resistance to lead.	ATP-BINDING CASS. G40 (ABCG40)
3	***AT1G21240***	Encodes a wall-associated kinase. The mRNA is cell-to-cell mobile.	WALL ASSOCIATED KINASE 3 (WAK3)
4	***AT2G29350***	Senescence associated, resistance to fungal pathogens. Induced by ROS.	SENESCENCE-ASS. GENE 13 (SAG13)
5	***AT2G29460***	Tau class of glutathione S transferases. Role in degradation of H_2O_2 to H_2O.	GSH S-TRANSF. TAU 4 (GSTU4)
6	***AT3G01830***	Calcium-binding EF-hand family protein.	-
7	***AT3G28580***	P-loop containing nucleoside triphosphate hydrolases superfamily.	-
8	***AT4G39670***	Member of the glycolipid transfer protein superfamily.	PHOSPHOLIPASE-LIKE PROTEIN (GLTP)
9	***AT5G17760***	P-loop containing nucleoside triphosphate hydrolases superfamily.	-
10	***AT5G26920***	Calmodulin binding is dependent on Ca^{2+}. Inducible by bacterial pathogens	CAM-BINDING PR. 60-LIKE G (CBP60G)
11	***AT5G62480***	Encodes glutathione transferase belonging to the tau class of GSTs.	GSH S-TRANSF. TAU 9 (GSTU9)

Genes upregulated by MgD treatments from each of the datasets given in **Table 3.1** were combined and number of occurrences for each gene was determined. 18 genes occurred in all of the datasets and are given here, together with gene description and primary gene symbols as obtained from TAIR (www.arabidopsis.org).

To visualize the overlap between the transcriptomic datasets from **Table 3.1**, a Venn-diagram was created from the first four gene lists, shown in **Figure 3.2**. The short-term dataset (**E**) was excluded to keep the diagram simple, since it is the smallest and least relevant to the methodology of a mutant screen. In this analysis, 84 genes appear in all four included datasets. List **C**, the largest, contains many unique genes (2047), likely including many false-positives, whereas for the smallest list, that of Oda *et al.*, around 25% of the total number of genes are present in all the other lists as well, despite being the only experiment carried out on agar plates rather than in hydroponic culture.

When choosing putative MgD marker genes for qPCR analysis, not only occurrence in multiple transcriptomic datasets was considered, but also absolute expression, fold upregulation, putative functions and whether the respective candidate had been used previously. **Table 3.3** shows all transcripts used in the analysis, including reference transcripts. *ACT2* and *EF1a* were used as references according to Czechowski *et al.* [226]. *MRS2-4* was included in the analysis to confirm whether the transcript level changes under MgD condition, since recent results indicate this might be the case [138], contrary to previous results [101, 102]. *PPR/AT2G20720* was included after noticing an abundance of pentatricopeptide repeat family proteins in the transcriptomic data, as well as due to its strong increase in expression in many of the datasets (63-fold in Hermans *et al.*, 2010b/**A**). *DTX4/AT2G04070* was included due to its implied function during chlorophyll degradation, strong upregulation, and similarity to *DTX3* highlighted in Kamiya *et al.*/**B**.

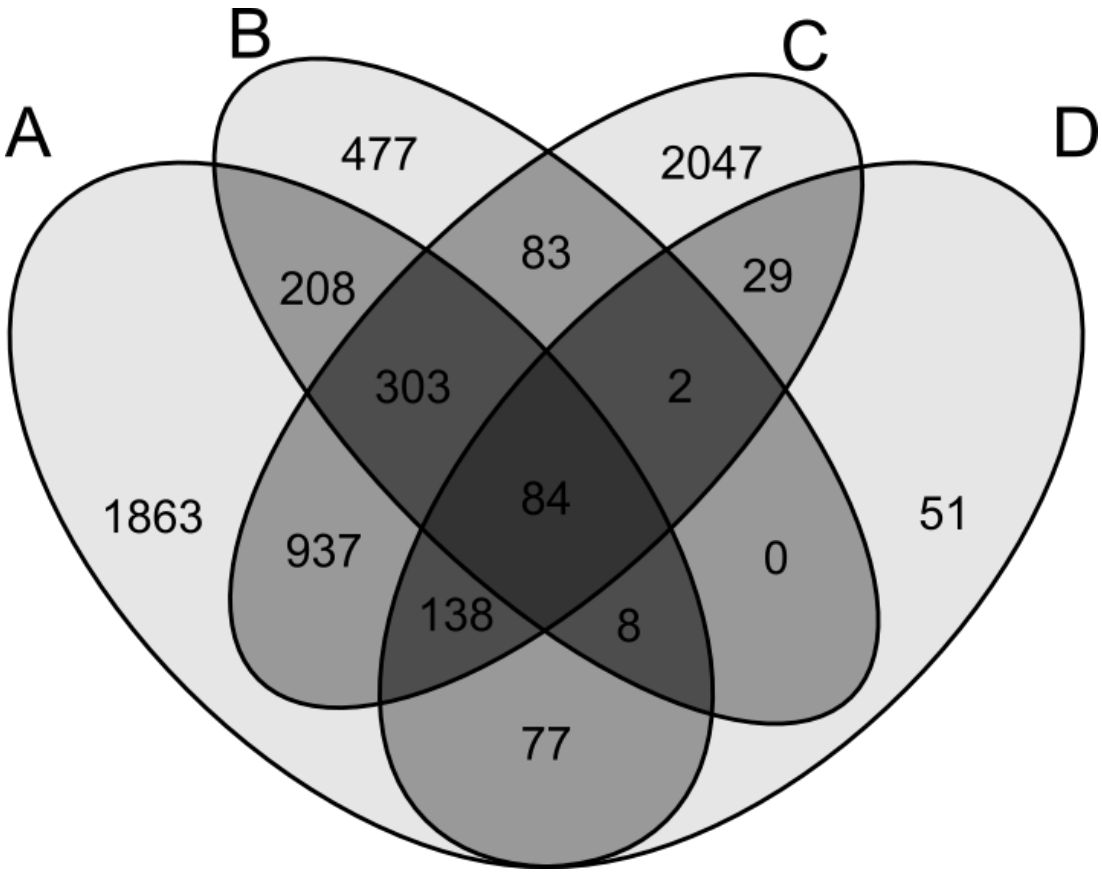

Figure 3.2 – Venn-diagram giving overlap between four of the transcriptomic datasets described in Table 3.1

Each ellipse denotes one dataset from **Table 3.1**, according to letters from the "Name" column. Hermans *et al.*, 2010a [101] (E) was excluded since it was the only "short-term" dataset, and to keep the diagram easy to view. Shading of each area correspond to number of datasets overlapping to give the set of genes represented by the area, with darker areas containing genes represented in more datasets. Numbers give the number of genes in the subset.

Table 3.3 – Transcripts included in qRT-PCR analysis

Gene symbol	Locus identifier	Gene Description	Datasets [a]
ACT2	***AT3G18780***	Encodes a constitutively expressed actin	0
EF1a	***AT1G07940***	GTP binding Elongation factor Tu family protein	2
MRS2-4 / MGT6	***AT3G58970***	Transmembrane magnesium transporter	0
PPR	***AT2G20720***	Pentatricopeptide repeat (PPR) superfamily protein	4
ACA1	***AT1G27770***	Encodes a chloroplast envelope Ca^{2+}-ATPase	3
DTX4	***AT2G04070***	Xenobiotic detoxification by transmembrane export	4

qRT-PCR analysis was carried out to detect effects of MgD on a transcriptional level in Arabidopsis exposed to low Mg^{2+}. *ACT2* and *EF1a* were used as reference transcripts. Gene descriptions were obtained from TAIR. **a** – Number of transcriptomic datasets from **Table 3.1** in which expression of the respective transcript is upregulated.

To compare the effects of MgD induced by transfer to low Mg^{2+} to those induced by continuous growth on low Mg^{2+} in *Arabidopsis* seedlings, two different experiments were carried out; in both case, agar used to solidify the plates was subjected to an EDTA-wash procedure, removing contaminating ions and ensuring that MgD could be induced (see **Section 2.1.4**).

For the transfer-experiment, Col-0 seedlings were grown on agar plates containing Hermans-medium (HM, see **Chapter 2**, **Section 2.1.3**) supplemented with sufficient Mg^{2+} (1000 µM) until 14 DAG, then transferred to Mg^{2+}-replete plates (control), plates containing HM with 0 µM Mg^{2+} (-Mg) or HM containing 60 mM NaCl (+NaCl). The salt-stress condition was included to test whether genes in the assay were generally stress-responsive. Seedlings were harvested three days and seven days post-transfer, then expression of the genes in **Table 3.3** was quantified in both roots and shoots via qRT-PCR. **Figure S3.1** gives results of the experiment for roots, and **Figure 3.3** those for shoots.

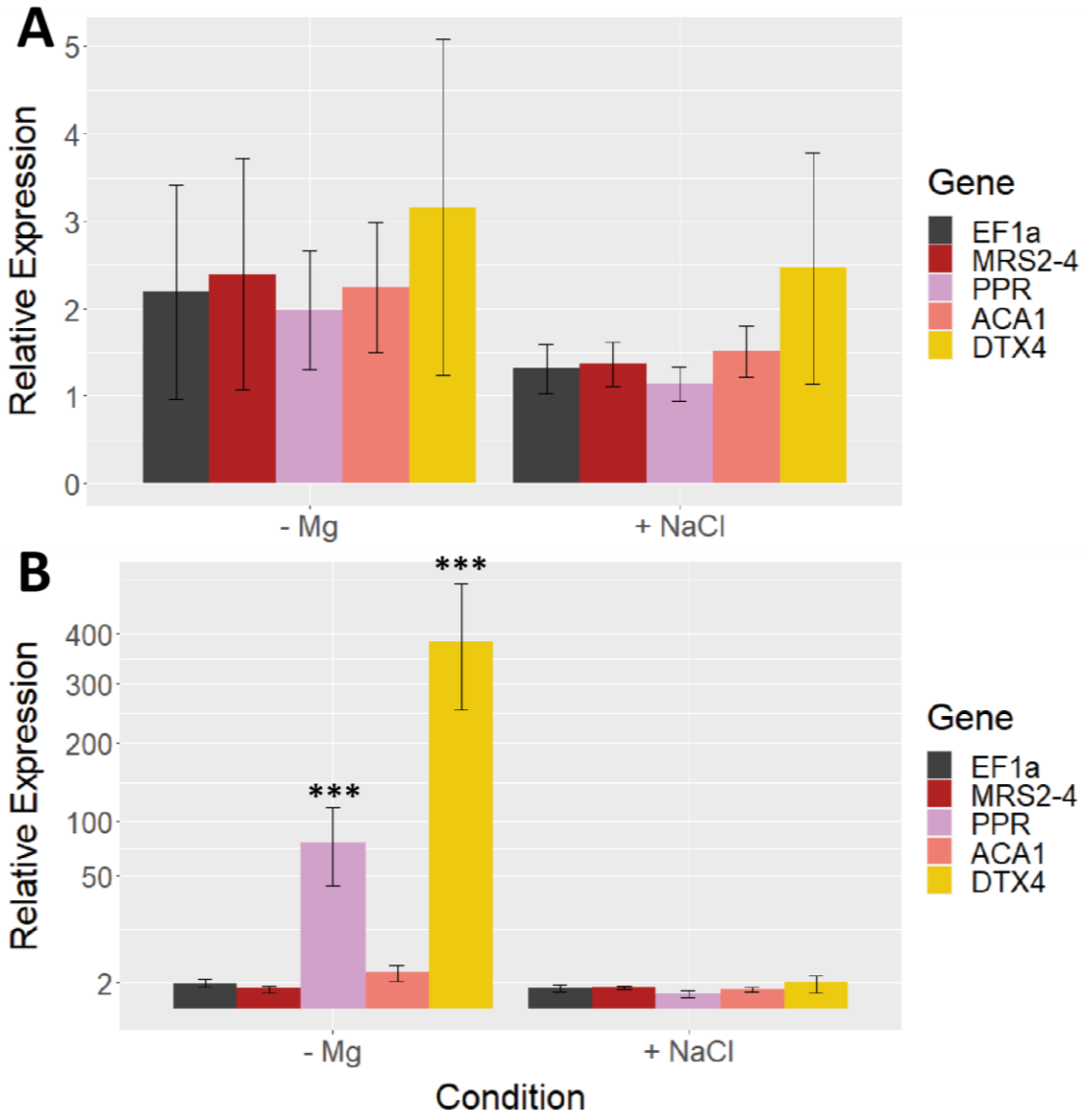

Figure 3.3 – Relative expression of candidate MgD-responsive genes in shoots of seedlings after transfer to low Mg^{2+} or excess NaCl.

Col-0 seedlings were grown on Mg^{2+}-replete plates until 14 DAG, then transferred to plates without added Mg^{2+} (- Mg), with 60 mM NaCl (+ NaCl) or 1000 µM Mg^{2+}. Gene expression in shoots of seedlings after 3 days (**A**) and 7 days (**B**) was determined by qRT-PCR. Expression levels for all transcripts were normalized to expression of ACTIN2 and expression of the respective transcripts at 1000 µM according to the $\Delta\Delta C_T$ method. The dimensions of the Y-Axis in **B** are scaled to match the square root of the associated values. Columns represent mean values (± SEM) from three independent experiments, each carried out as three technical replicates. Symbols above error bars denote significant differences between expression on 1000 µM Mg^{2+} and the respective condition, as determined by a two-way ANOVA followed by Tukey HSD post-hoc test (▪ - $p < 0.1$; * - $p < 0.05$; ** - $p < 0.01$; *** - $p < 0.001$).

For the experiment on continuously low Mg^{2+}, seedlings were grown on plates of washed Agar containing 0, 15, 50, 150, 250 or 1000 µM Mg^{2+} until 14 DAG, then gene expression was tested in shoots only. Seedlings from 0 µM Mg^{2+} could not be included in the analysis since seedlings were extremely stunted at this concentration and not enough biomass was available to extract RNA. Results for all other concentrations are summarized in **Figure 3.4**.

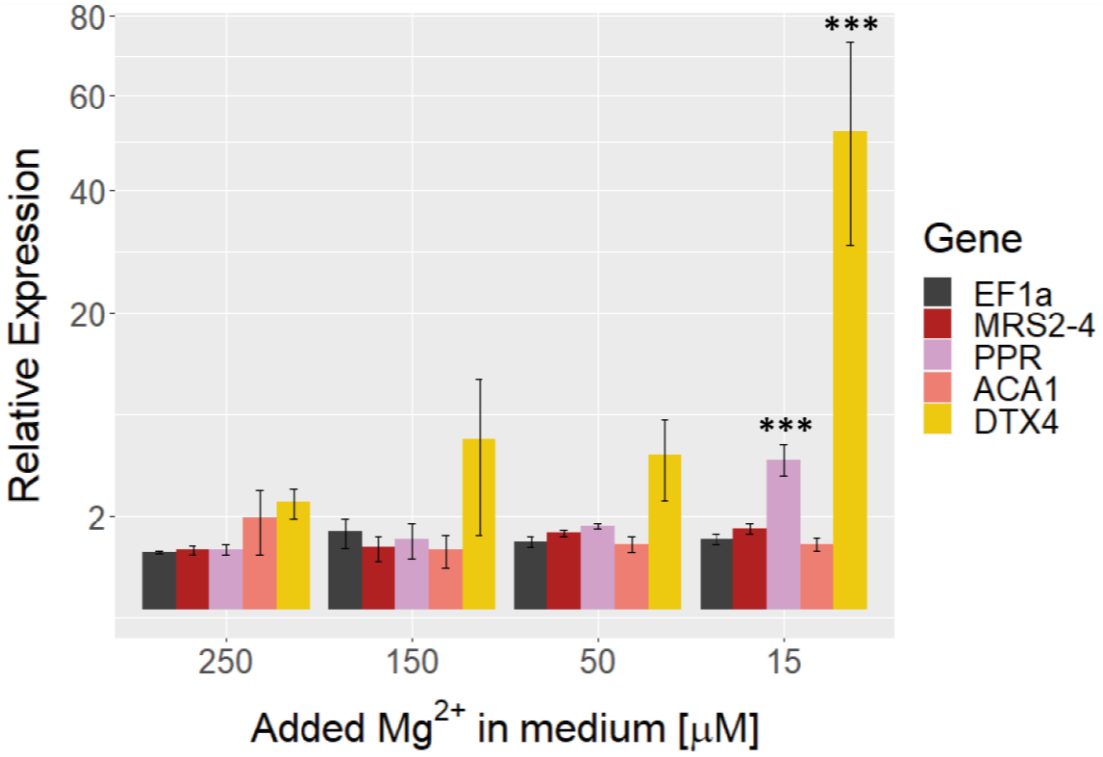

Figure 3.4 - Relative expression of candidate MgD-responsive genes in shoots of seedlings after growth on different concentrations of Mg^{2+}.

Col-0 seedlings were grown on agar plates containing different amounts of Mg^{2+} until 14 DAG. Gene expression for candidate genes from **Table 3.3** was determined by qRT-PCR. Expression levels for all transcripts were normalized to expression of *ACTIN2* and expression of the respective transcripts at 1000 µM according to the $\Delta\Delta C_T$ method. The dimensions of the Y-Axis are scaled to match the square root of the associated values. Columns represent mean values (± SEM) from three independent experiments, each carried out as three technical replicates. Symbols above error bars denote significant differences between expression on 1000 µM Mg^{2+} and the respective concentration, as determined by a two-way ANOVA followed by Tukey HSD post-hoc test (▪ - $p < 0.1$; * - $p < 0.05$; ** - $p < 0.01$; *** - $p < 0.001$).

In both experiments, expression of the two reference transcripts did not vary relative to each other at any of the conditions, indicating that they represented suitable references. Expression of *MRS2-4* or *ACA1* did not change significantly in either of the conditions tested; however, expression of both *PPR* and *DTX4* was significantly increased both after transfer to low-Mg^{2+} media or after growth on plates with 15 µM added Mg^{2+}. The two treatments therefore seemed to cause similar effects. Although the magnitude of the increase in expression observed for *DTX4* and *PPR* in shoots was greater after transfer to low-Mg^{2+} media, the variation in expression was smaller for the continuous experiment.

3.2.2 Continuous, moderate Mg^{2+}-deficiency elicits previously established symptoms of MgD

The physiological symptoms experienced by plants grown on individual Mg^{2+}-concentrations continuously were tested and compared to those reported previously and outlined in **Section 3.1.4.**

First, growth of seedlings on different concentrations of Mg^{2+} was tested. Col-0 seedlings were grown on agar plates containing washed agar and Mg^{2+}-concentrations of 1000, 250, 150, 50, 15 and 0 µM until 14 DAG, then average shoot weight was quantified for each concentration. Additionally, main root length and number of lateral roots per plant were determined at 10 DAG. Results are shown in **Figure 3.5**. Both shoot weight and main root length increased significantly at lower, but sufficient Mg^{2+}-concentrations (**Figure 3.5 A** & **B**). At 15 µM Mg^{2+}, the number of lateral roots was significantly lower than at 1000 µM Mg^{2+} (**Figure 3.5 C**) and the shoot weight was slightly decreased. At 0 µM Mg^{2+}, induction of lateral roots was nearly completely abolished and shoot weight never exceeded 1 mg, but main root length was not significantly reduced. To quantify the reduction of lateral root numbers at lower Mg^{2+} the number of lateral roots per plant was divided by the length of the main root for each concentration, giving the number of lateral roots per mm main root (**Figure 3.6**). This revealed a consistent trend, with lateral roots per mm decreasing with decreasing medium Mg^{2+}, despite seedlings showing higher shoot weights and main root lengths at the intermediate concentrations tested.

This page is intentionally left blank

Blank pages are used throughout to allow legends to appear opposite display items in the paper copy of this document

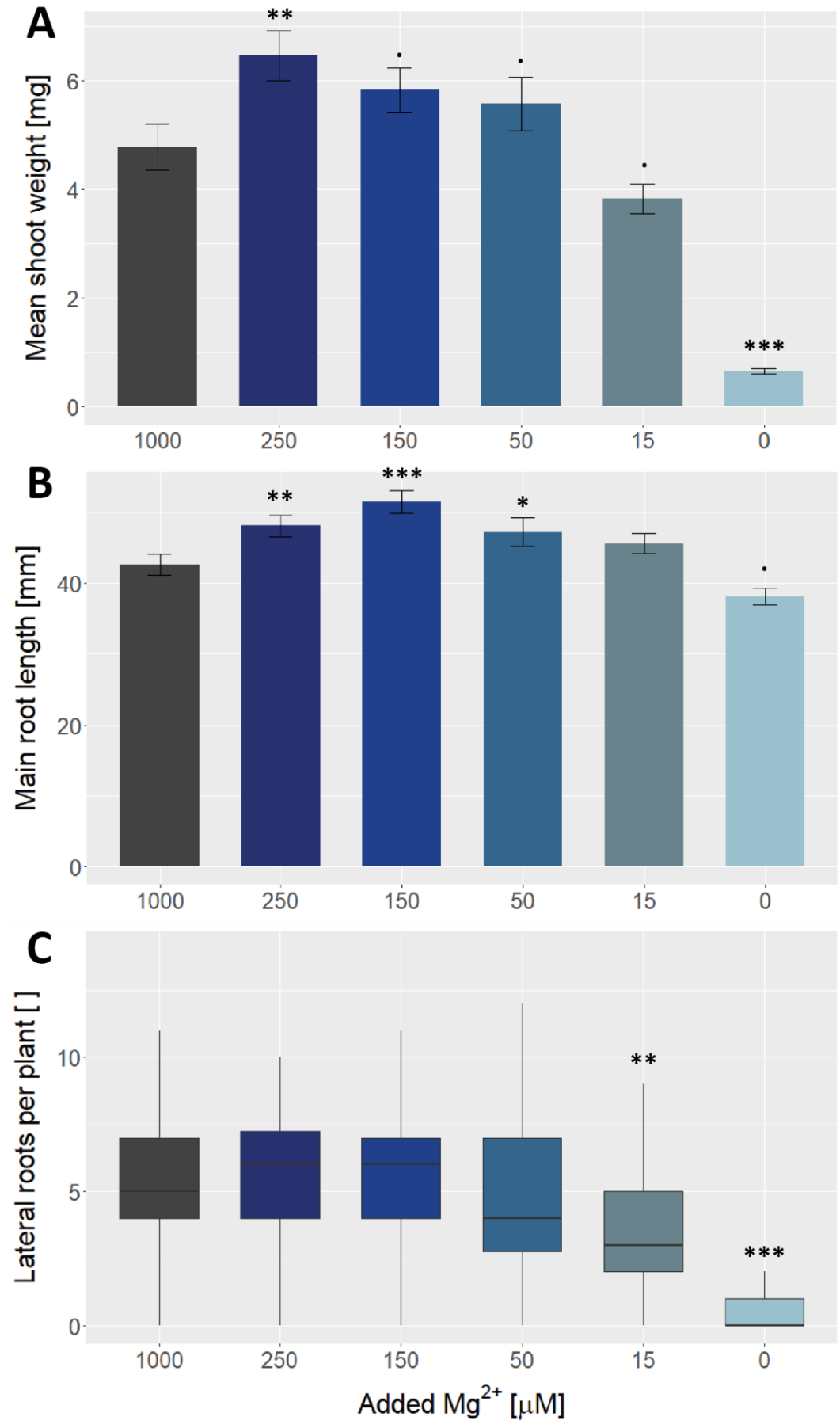
A
Mean shoot weight [mg]
0
2
4
6
**
***
1000
250
150
50
15
0
B
Main root length [mm]
0
20
40
**
***
*
1000
250
150
50
15
0
C
Lateral roots per plant [ ]
0
5
10
**
***
1000
250
150
50
15
0
Added Mg2+ [µM]

Figure 3.5 – Growth of *A. thaliana* seedlings on different Mg^{2+}-concentrations. Seedlings of Col-0 were grown on agar plates containing HM made with washed agar, with different concentrations of added Mg^{2+}, until 14 DAG; various characteristics of the seedlings were determined. **A** – Mean shoot fresh weights of seedlings at 14 DAG. **B** – Main root length of seedlings at 10 DAG. **C** – Boxplot of numbers of lateral roots per plant at 10 DAG. Columns in **A** and **B** represent mean values (± SEM); Significant differences were determined using a two-way ANOVA followed by Tukey HSD post-hoc test. Boxes in **C** represent first and third quartile, while the median is shown as a horizontal line. Significant differences between conditions in **C** were determined by a Dunn test, followed by a Kruskal-Wallis test. All data are from three independent replicates. Symbols above data for each condition denote significant differences between values observed on 1000 µM Mg^{2+} and the respective concentration (▪ - $p < 0.1$; * - $p < 0.05$; ** - $p < 0.01$; *** - $p < 0.001$).

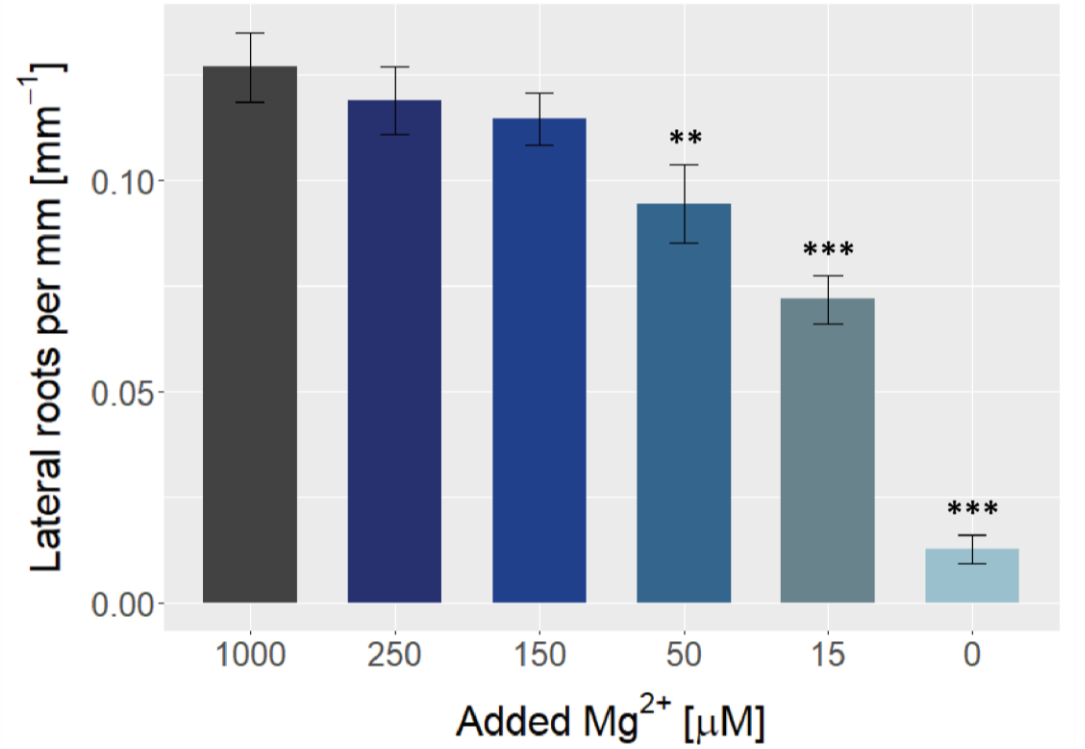

Figure 3.6 – Lateral roots per mm main root length for *A. thaliana* grown on different Mg^{2+}-concentrations.

Seedlings of Col-0 were grown on agar plates containing HM made with washed agar, with different concentrations of added Mg^{2+}. At 10 DAG, length of the main root and number of lateral roots for each seedling were determined. The number of lateral roots was divided by the length of the main root, and values plotted grouped by concentration. Columns represent mean values (± SEM) from three independent biological replicates. Significant differences between conditions were determined by two-way ANOVA followed by Tukey HSD. Symbols above error bars denote significant differences between values observed on 1000 µM Mg^{2+} and the respective concentration (▪ - $p < 0.1$; * - $p < 0.05$; ** - $p < 0.01$; *** - $p < 0.001$).

The next symptom tested was starch accumulation in leaves of plants exposed to MgD. Seedlings were grown on plates containing different Mg^{2+}-concentrations until 14 DAG, as before. Since no significant overall growth impairment could be seen at concentrations above 50 µM Mg^{2+}, and 0 µM caused stunted growth to the point of preventing seedlings from being used in experiments, concentrations of 1000, 50, 15 and 7.5 µM added Mg^{2+} were chosen for this experiment. At 14 DAG, seedlings were harvested at the end of the dark period. Under normal conditions, little starch is present in leaves at this time, having been consumed during the dark period. Starch present in shoots was visualized by staining with Lugol's solution; representative images of stained seedlings are shown in **Figure 3.7 A**. Additionally, starch levels were quantified by numbering leaves in order of emergence (as shown in **Figure 3.7 A**) and measuring the average colour intensity over the entire area of each leaf of the stained plants on the red channel of the three-channel images taken (**Figure 3.7 B**). The red channel was chosen because blue coloration reduces the detected intensity of red light the most.

As can be seen from both the images and graphs, increased starch-accumulation is not detectable at 50 µM Mg^{2+} or above, but can be seen for the two lowest concentrations. At 15 µM Mg^{2+}, starch accumulation is significant in leaves 1 through 5, the oldest leaves. At 7.5 µM Mg^{2+}, significant staining can be seen in leaves 1 through 7, which most likely equates to all fully-expanded leaves, *i.e.*, all true source tissues.

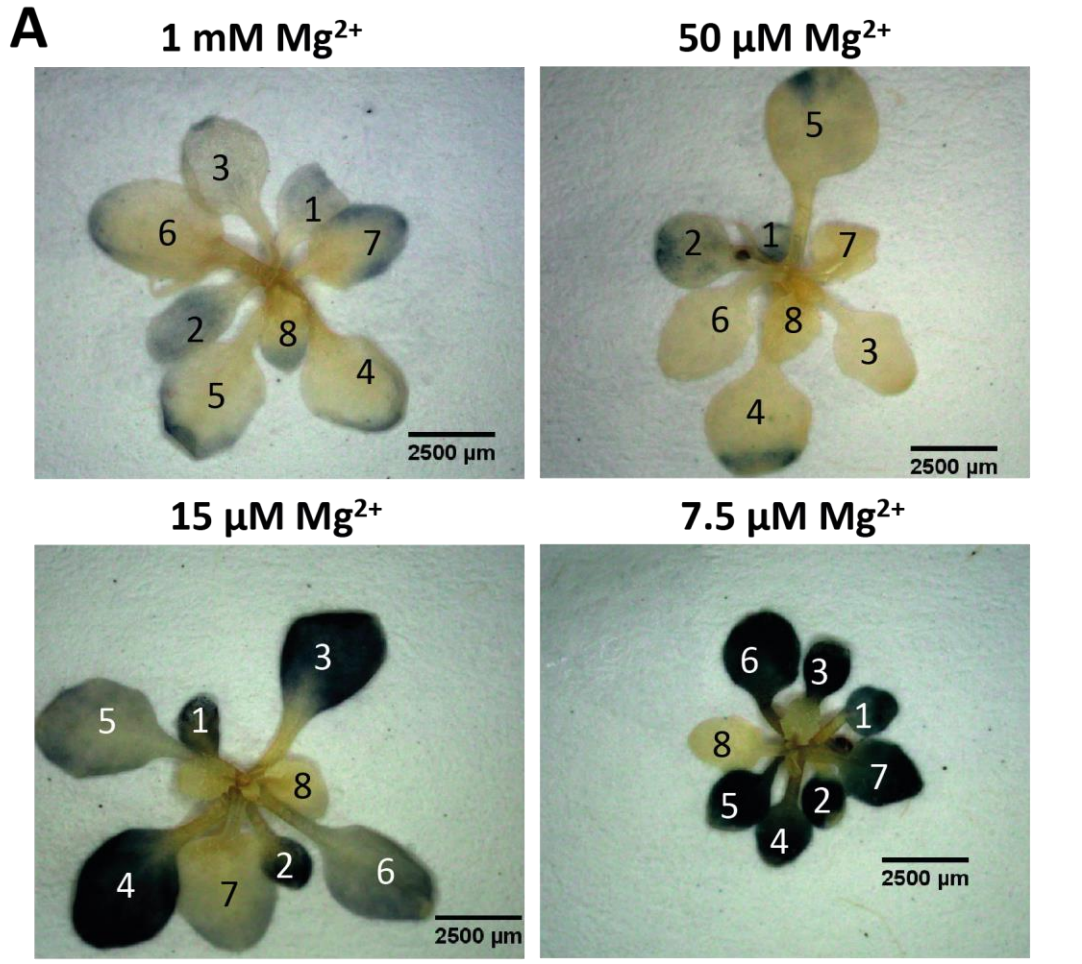
A
1 mM Mg2+
50 µM Mg2+
15 µM Mg2+
7.5 µM Mg2+
2500 µm
B
Colour intensity
9000
6000
3000
1
2
3
4
5
6
7
8
Leaf No.
Mg2+ [µM]
1000
50
15
7.5

Figure 3.7 - Starch staining of plants grown on different Mg^{2+}-concentrations. *A. thaliana* (Col-0) seedlings were grown on agar plates containing HM made with washed agar, with different concentrations of added Mg^{2+}, until 14 DAG, before being subjected to a starch staining protocol using Lugol's solution. **A** – Representative image of a stained seedling from each concentration tested. Leaves are numbered according to order of emergence. **B** – Images of seedlings were analysed by measuring the average colour intensity over the area of each leaf on the red channel of the image. Mean and confidence intervals for each leaf are displayed, from a mixed-effect linear model generated using the data. Data are from three independent replicates of 3-4 plants per concentration. Lower values indicate darker areas.

To confirm the presence of increased levels of reactive oxygen species (ROS) in leaves of *A. thaliana* under MgD, seedlings grown in the same way as for detection of starch accumulation were treated with two different ROS-sensitive probes: CM-H_2DCFDA, a general ROS-sensitive probe, and DHE, a superoxide-specific probe. These cell-permeable dyes exhibit increased fluorescence upon encountering either any ROS species or superoxide (O_2^-), respectively. In both cases, shoots were immersed in a solution containing the respective dye, then images of representative areas of stained leaves were taken on a confocal laser-scanning microscope. Average fluorescence intensity across the in-focus area of the image was measured and analysed. Unstained seedlings were used as negative control, and seedlings exposed to the ROS-stress inducing chemical Antimycin A (AA) were used as positive control. Results are summarized in **Figure 3.8**. For both CM-H_2DCFDA (**Figure 3.8 A**) and DHE (**B**), significant differences in measured fluorescence intensity relative to 1000 µM Mg^{2+}, and therefore ROS accumulation, could be seen for seedlings grown on 7.5 µM Mg^{2+}, as well as for the positive control. Results show a higher statistical significance, bigger difference in fluorescence intensity, and greater similarity to the positive control for DHE, suggesting that superoxide is the primary ROS species present in seedlings exposed to MgD.

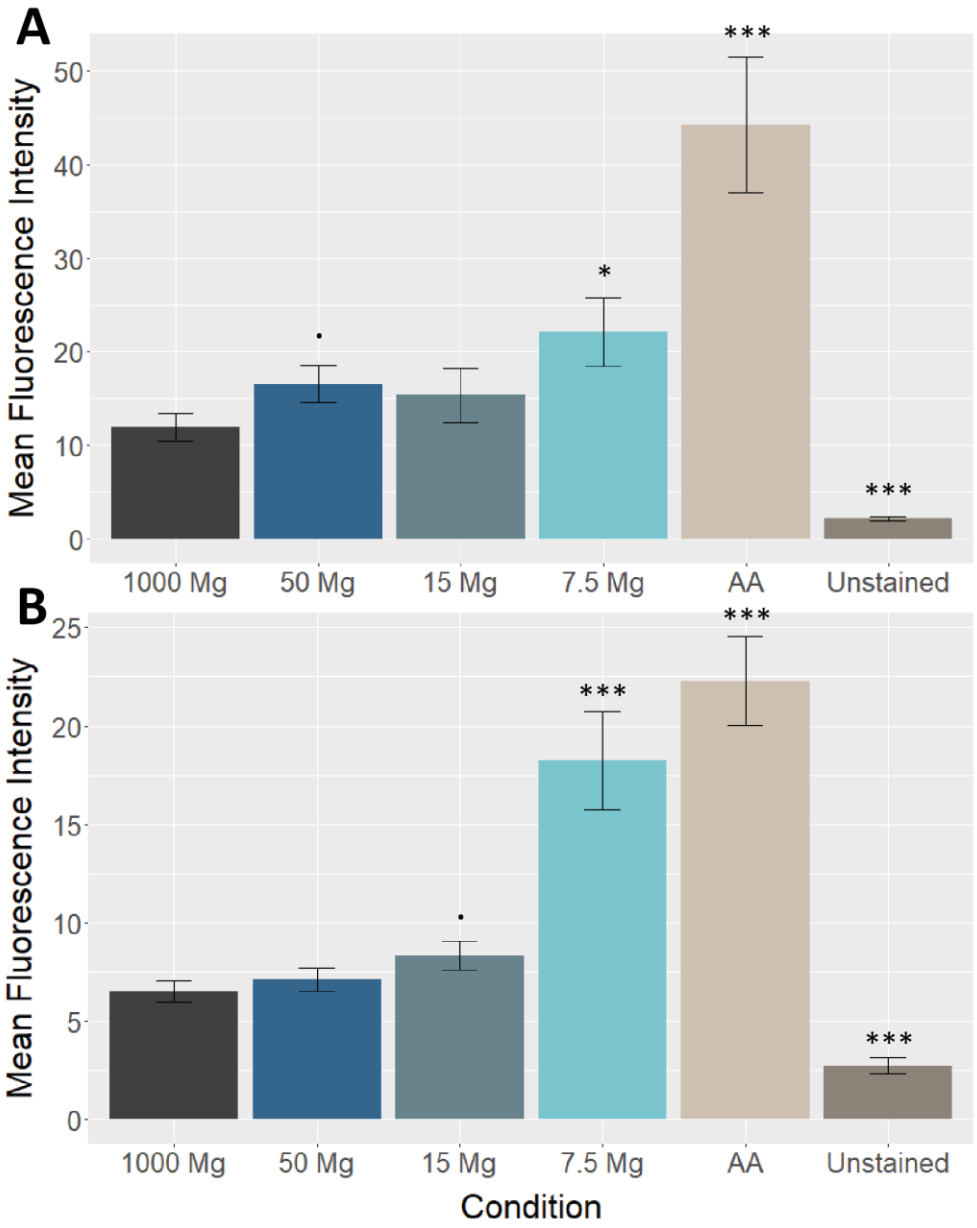

Figure 3.8 – ROS levels in plants grown on different Mg^{2+}-concentrations.
A. thaliana (Col-0) seedlings were grown on agar plates containing HM made with washed agar, with different concentrations of added Mg^{2+} (X-Axis, concentrations in µM), until 14 DAG, before being stained with the fluorescent ROS-sensitive probes CM-H_2DCFDA (**A**) or DHE (**B**). Fluorescence intensities were recorded; columns represent mean values (± SEM) from three independent replicates of 4-5 leaves per replicate and concentration. **AA** – Seedlings were sprayed with a solution containing 20 µM Antimycin A (**AA**) before being stained, for use as a positive control. Significant differences between conditions were determined by two-way ANOVA followed by Tukey HSD. Symbols above error bars denote significant differences between values observed on 1000 µM Mg^{2+} and the respective condition (▪ - $p < 0.1$; * - $p < 0.05$; ** - $p < 0.01$; *** - $p < 0.001$).

Finally, to confirm the reduction in chlorophyll concentrations reported previously for plants exposed to MgD, seedlings grown as before were harvested and subjected to a chlorophyll extraction protocol. Concentrations of chlorophyll in resulting solutions were measured by spectrophotometry, and concentrations in fresh leaf tissue calculated for seedlings from each of the Mg^{2+}-concentrations used. Seedlings exposed to salt stress were used as a positive control. Results are shown in **Figure 3.9**. A significant reduction in chlorophyll concentrations can be seen for seedlings grown on 7.5 µM Mg^{2+}, as well as those under salt stress (60 mM NaCl).

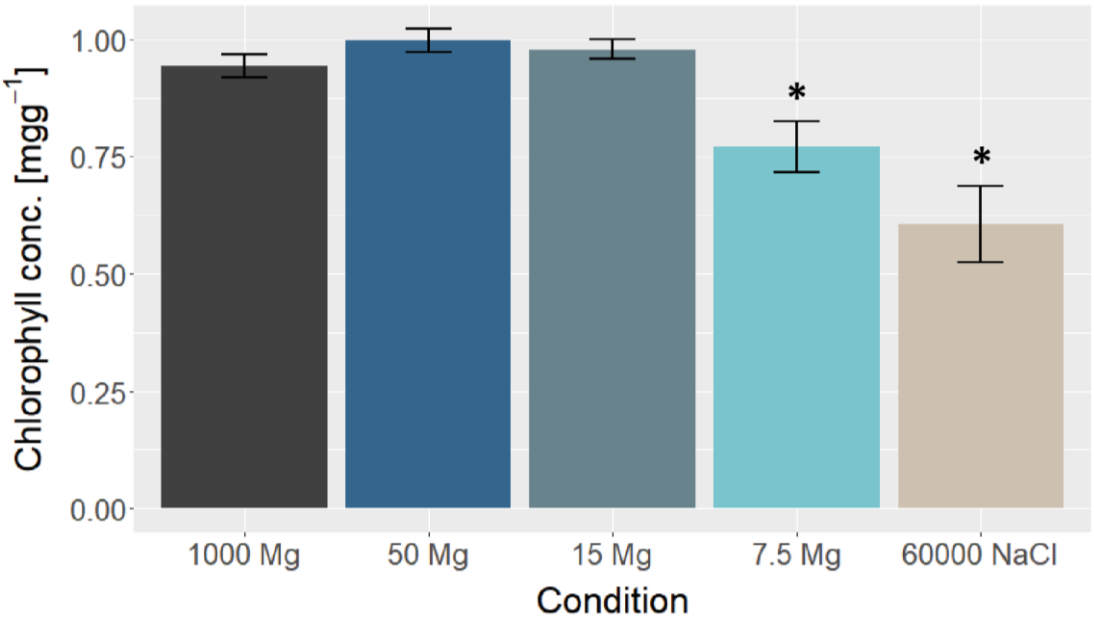

Figure 3.9 – Chlorophyll levels in plants from different Mg^{2+}-concentrations. *A. thaliana* (Col-0) seedlings were grown on agar plates containing HM made with washed agar, with different concentrations of added Mg^{2+} (X-Axis, concentrations in µM), until 14 DAG, before chlorophyll was extracted from shoots and quantified by spectrophotometry. Plants grown on 60 mM NaCl were included as a positive control. Columns represent mean values (± SEM) from three independent replicates. Significant differences between conditions were determined by two-way ANOVA followed by Tukey HSD. Symbols above error bars denote significant differences between values observed on 1000 µM Mg^{2+} and the respective condition (▪ - $p < 0.1$; * - $p < 0.05$; ** - $p < 0.01$; *** - $p < 0.001$).

3.2.3 MARIO can be functionally expressed in *A. thaliana* and used to report on Mg^{2+}-concentrations

To confirm the reductions of [Mg^{2+}] in plants grown on low-Mg^{2+} media reported in the literature, as well as to investigate spatial and temporal dynamics of [Mg^{2+}], the Mg^{2+}-sensitive FRET sensor MARIO had to be expressed in *A. thaliana*. A plasmid containing the *MARIO* CDS was obtained and used to create several genetic constructs, designed to induce strong MARIO expression and target the protein to different subcellular compartments: the cytoplasm, chloroplasts, and nucleus, respectively, as outlined in **Figure 3.10** (work performed by T.N.). Next, Col-0, *mrs2-4* 1 and *mrs2-4* 2 plants were transformed with each of the constructs via floral dip. After transformant selection, expression of the reporter within transformants was tested via fluorescence microscopy, but expression could only be detected in one transformant out of 108 individuals tested (see **Table 3.4**), an instance of *mrs2-4* 1 + *cpMARIO* (chloroplastically-targeted MARIO). MARIO expression in this line was detected in both cotyledons and true leaves, and within roots to a lesser degree. However, transgene expression was inconsistent (**Figure 3.11**). Although small foci of fluorescence indicate correct chloroplast targeting in some areas, larger fluorescent areas show that expression in this individual is not always restricted to plastids, indicating mis-targeting of the protein. Genotyping of six different transformants by PCR showed that all individuals tested contained the *MARIO* CDS, indicating that while the transgene was present in these lines, MARIO protein was not being expressed. Growth of *mrs2-4* 1 + *cpMARIO* on soil appeared similar to the parent line, *mrs2-4* 1, although rosette size may be slightly reduced (**Figure S3.2**).

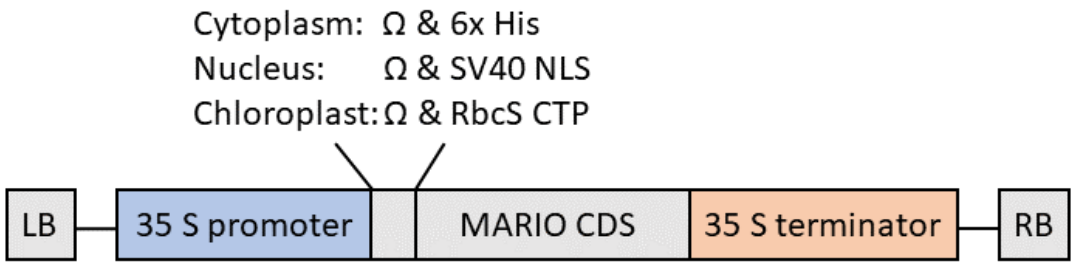

Figure 3.10 – Structure of *MARIO* constructs used to transform *A. thaliana*
To obtain each of the constructs used, one of the sequences given was inserted between the cauliflower mosaic virus (CaMV) 35S promoter and the *MARIO* CDS, giving different (theoretical) subcellular localizations. Experiment conceived by S.L. and carried out by T.N. **Ω** – Tobacco mosaic virus omega enhancer. **6x His** – A tag sequence consisting of 6 Histidine bases, amenable to purification by affinity chromatography. **SV40 NLS** – Nuclear localisation signal (NLS) from simian vacuolating virus 40 (SV40). **RbcS CTP** – Rice Rubisco small subunit (RbcS) chloroplast targeting peptide (CTP). **LB** – *A. tumefaciens* left border (LB) sequence. **RB** – *A. tumefaciens* right border (RB) sequence.

Table 3.4 - Number of transformants tested for MARIO expression for each background transformed and targeting sequence used.

Background	Target	Individuals tested (Number showing expression)
Col-0	Cytoplasm (*cyMARIO*)	22 (0)
	Chloroplast (*cpMARIO*)	9 (0)
	Nucleus (*nMARIO*)	19 (0)
***mrs2-4* 1**	Cytoplasm (*cyMARIO*)	8 (0)
	Chloroplast (*cpMARIO*)	4 (1)
	Nucleus (*nMARIO*)	19 (0)
***mrs2-4* 2**	Cytoplasm (*cyMARIO*)	10 (0)
	Chloroplast (*cpMARIO*)	2 (0)
	Nucleus (*nMARIO*)	15(0)
All	All	108 (1)

A. thaliana of the Col-0, *mrs2-4* 1 and *mrs2-4* 2 backgrounds were transformed with MARIO expression constructs designed to direct the protein to the cytoplasm (cyMARIO), chloroplast (cpMARIO) and nucleus (nMARIO). Transformants were selected on agar plates containing Kanamycin, put to soil, then protein expression was tested by fluorescence microscopy. Only one transformant (*mrs2-4* 1 + *cpMARIO* 1) was found to express the protein.

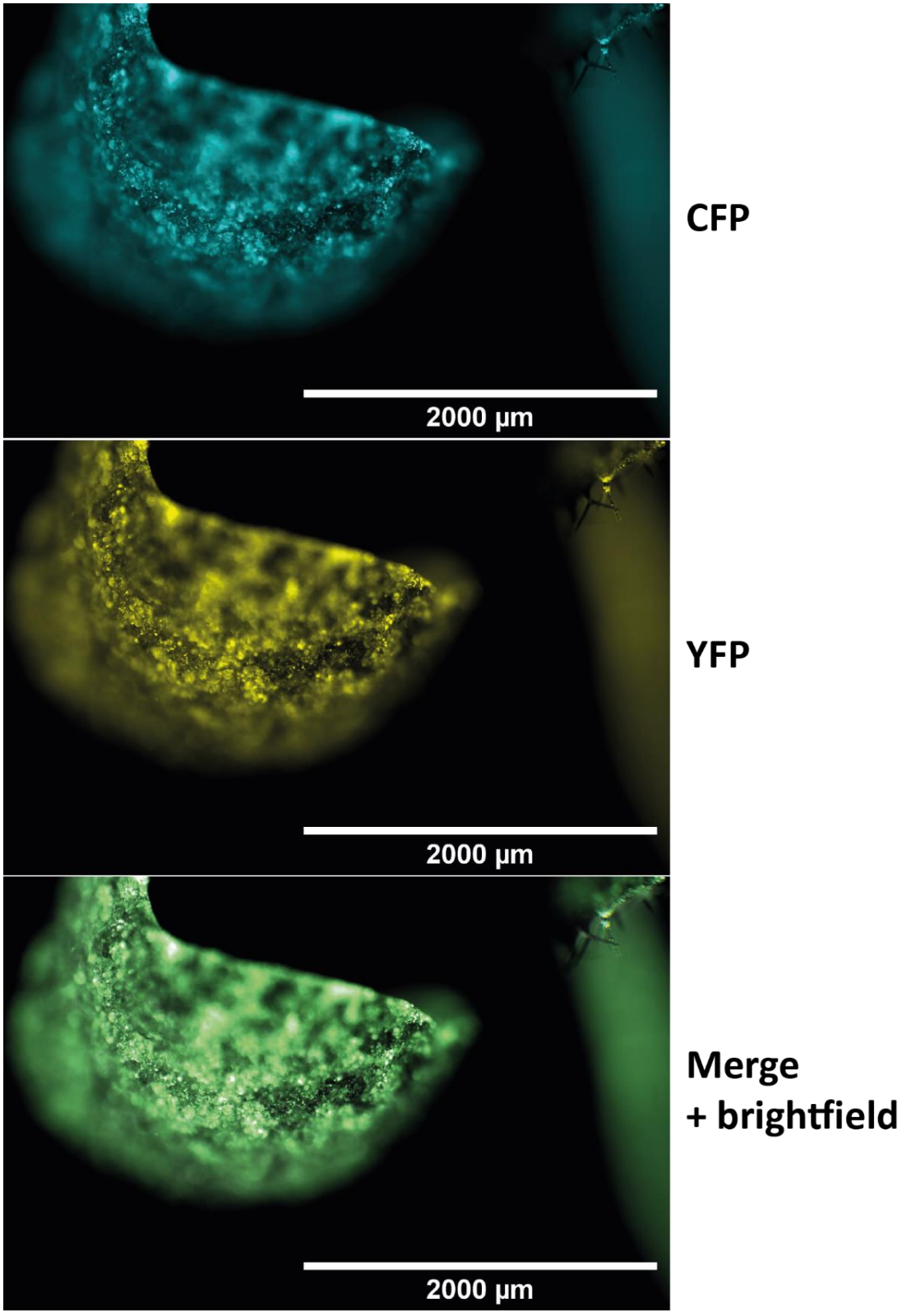

Figure 3.11 – MARIO expression in *mrs2-4* 1 + cpMARIO

MARIO expression was detected in cotyledons via fluorescence microscopy. CFP expression was detected using an excitation wavelength of 434 nm and emission wavelength of 474 nm. For YFP, 514 and 526 nm were used, respectively. Each image was acquired separately, in sequence, before being merged in ImageJ.

Because only a single transformant line expressing MARIO was available, which was in a mutant background and showing inconsistent reporter expression, no *in vivo* experiments were possible. However, it was possible to validate functionality of the reporter, as expressed in *A. thaliana*, in a proof-of-concept experiment adapted from Wagner *et al.* [201]. Leaves of two individual mrs2-4 1 + *cpMARIO* plants were therefore harvested and protein-extracts prepared. After addition of different concentrations of $MgCl_2$ to clarified protein extracts, FRET ratios exhibited by the extracts were measured; results are summarized in **Figure 3.12**. A clear correlation between added Mg^{2+} and FRET ratio could be seen, indicating that the reporter is functioning correctly. although there are noticeable differences between the two biological replicates, especially for the raw FRET values (YFP/CFP ratio, **Figure 3.12 A**), these differences are much smaller when normalized values are used (ΔR/R0, **B**). Variation between technical replicates for the same individual/extract was small.

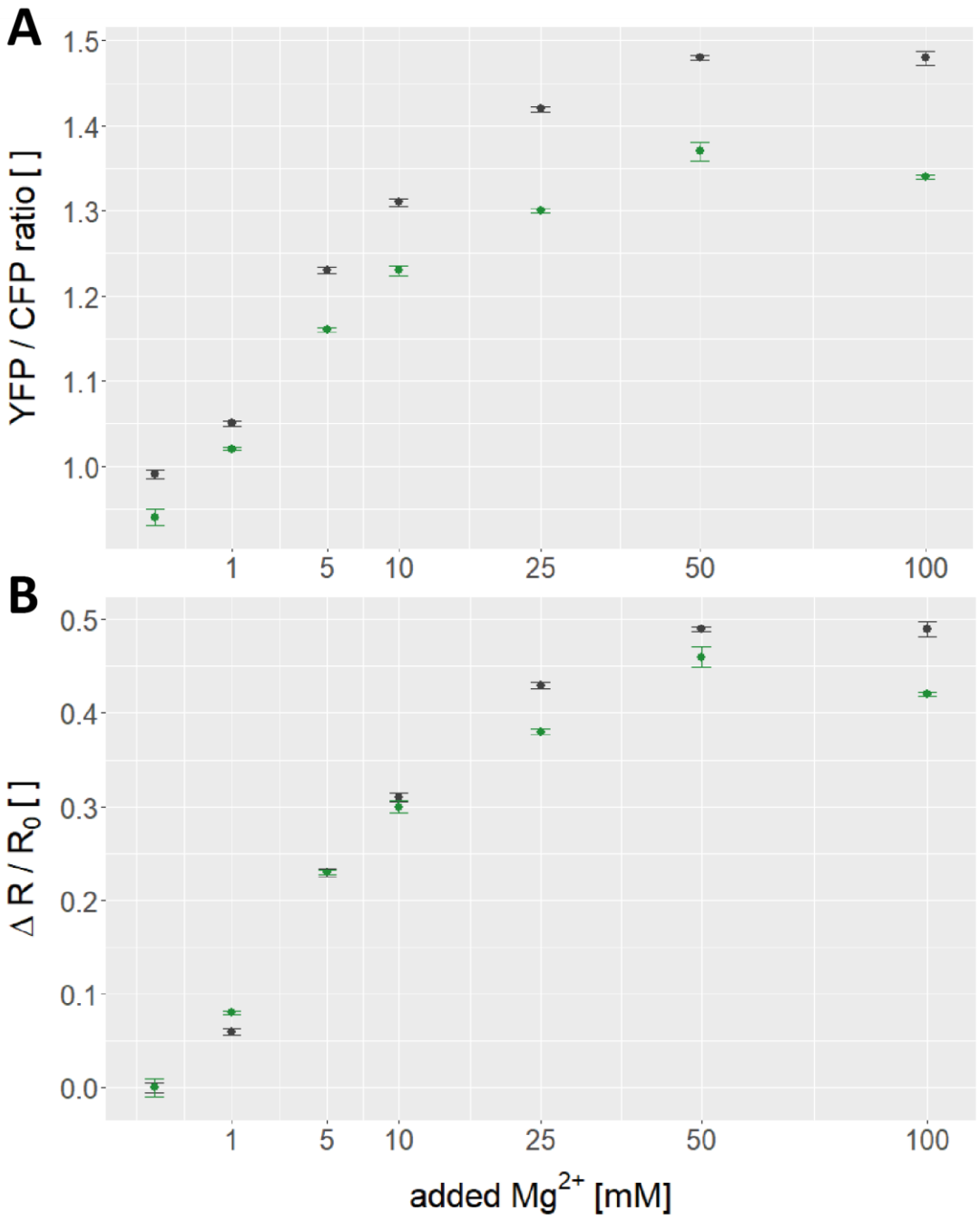

Figure 3.12 – FRET ratio exhibited by MARIO at different Mg^{2+}-concentrations. **A** – FRET ratios recorded for each concentration. **B** – FRET ratios, normalized to the ratio observed at 0 mM added Mg^{2+} ($\Delta R / R_0$). True leaves from *A. thaliana* expressing the MARIO FRET sensor were ground and whole-leaf extracts prepared. After adding various concentrations of $MgCl_2$ to the extracts, FRET ratios (YFP/CFP emission after excitation of CFP) for each Mg^{2+}-concentration were measured. Data-points represent mean values (± SEM) from three technical replicates carried out on protein extracts from two different individual plants (black and green data points). The X-Axis has been scaled to match the square root of the associated values.

3.2.4 Mg^{2+}-deficiency may lead to altered ATP-levels and pH in *A. thaliana*

To measure changes in $MgATP^{2-}$-levels in plants exposed to MgD, *A. thaliana* expressing the $MgATP^{2-}$-sensitive FRET sensor ATeam1.03-nD/nA in the cytoplasm and chloroplasts, referred to as cATeam and cpATeam, respectively, described in De Col *et al.* [182], were obtained, courtesy of the Schwarzländer lab at Universität Münster, Germany. Additionally, to measure changes in intracellular and extracellular pH under MgD, *A. thaliana* expressing the pHusion pH-sensor in the cytoplasm and apoplasm, termed cpHusion and apHusion, respectively [186], were received courtesy of Joshua Joyce at John Innes Centre. cATeam, cpHusion and apHusion plants, but not cpATeam plants, showed sufficiently strong fluorescence signals to be used in a plate-reader based assay reporting on cytoplasmic $MgATP^{2-}$-concentration, cytoplasmic and apoplastic pH simultaneously (see **Chapter 2**, **Section 2.6.4**).

Seedlings of cATeam, cpHusion and apHusion, as well as Col-0, were grown on agar plates containing either 1000, 50 or 15 µM Mg^{2+}, as before. At 14 DAG, randomly chosen leaves and roots were excised and placed in the wells of a 96-well plate. Emission values for CFP and YFP after CFP excitation (ATeam FRET response), as well as GFP and RFP after excitation of the respective fluorophore (pHusion) were measured. All emission values were corrected against the background of Col-0 leaves or roots from plants grown under the same conditions and excited in the same way. YFP/CFP ratios (ATeam) and GFP/RFP ratios (pHusion) were then calculated, and ratios compared between plants grown on different Mg^{2+}-concentrations. Results are summarized in **Figure 3.13**.

The apparent MgATP-concentration in leaves of plants grown at 15 µM Mg^{2+}, as reported by cATeam, was significantly higher than for plants grown at 1000 µM Mg^{2+} (**Figure 3.13 A**). This represented a genuine FRET response, with average YFP fluorescence across samples higher and CFP fluorescence lower at 15 µM Mg^{2+}. The apparent cytoplasmic pH was significantly higher at 15 µM Mg^{2+}, in both leaves and roots (**B**), while the leaf apoplastic pH, but not the root apoplastic pH, was increased relative to control (**C**).

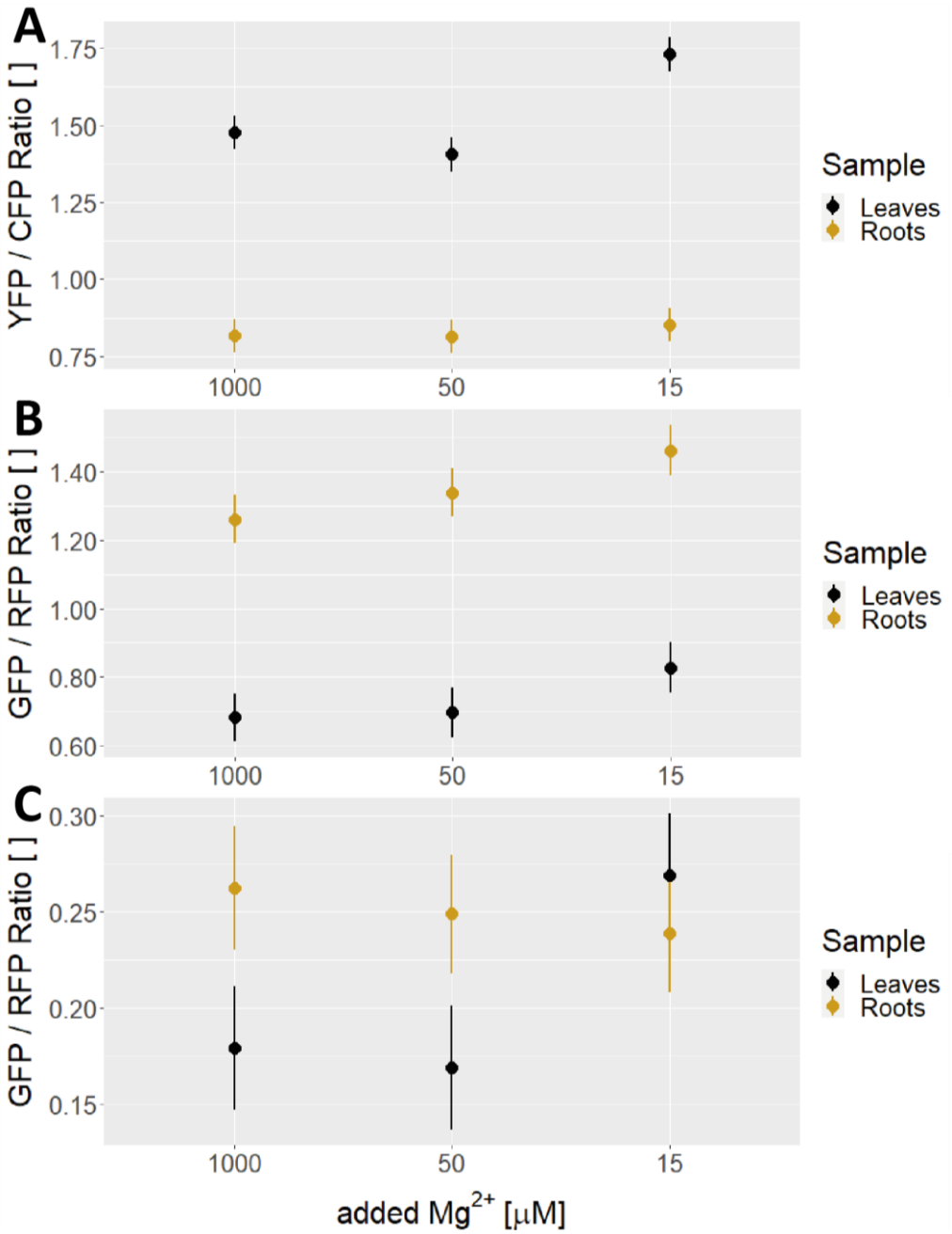

Figure 3.13 - Results of the plate-reader assay including ATeam and pHusion

A – FRET ratios (YFP/CFP after CFP excitation) for ATeam at different Mg^{2+}-concentrations. **B** – GFP/RFP ratios recorded for cpHusion. **C** – GFP/RFP ratios for apHusion. Seedlings of Col-0, cATeam, cpHusion and apHusion were grown on agar plates containing HM with different concentrations of added Mg^{2+}, with 0.5% (w/v) sucrose, until 14 DAG, before leaves and roots were transferred to the wells of a 96-well plate, filled with liquid HM. Emission values were recorded according to **Chapter 2, Section 2.6.4**, then emission ratios were calculated. A mixed-effect linear model was generated for the emission-ratio over different concentrations and plant parts. Data points represent mean values and confidence intervals for each concentration, from three independent replicates, with three technical replicates each.

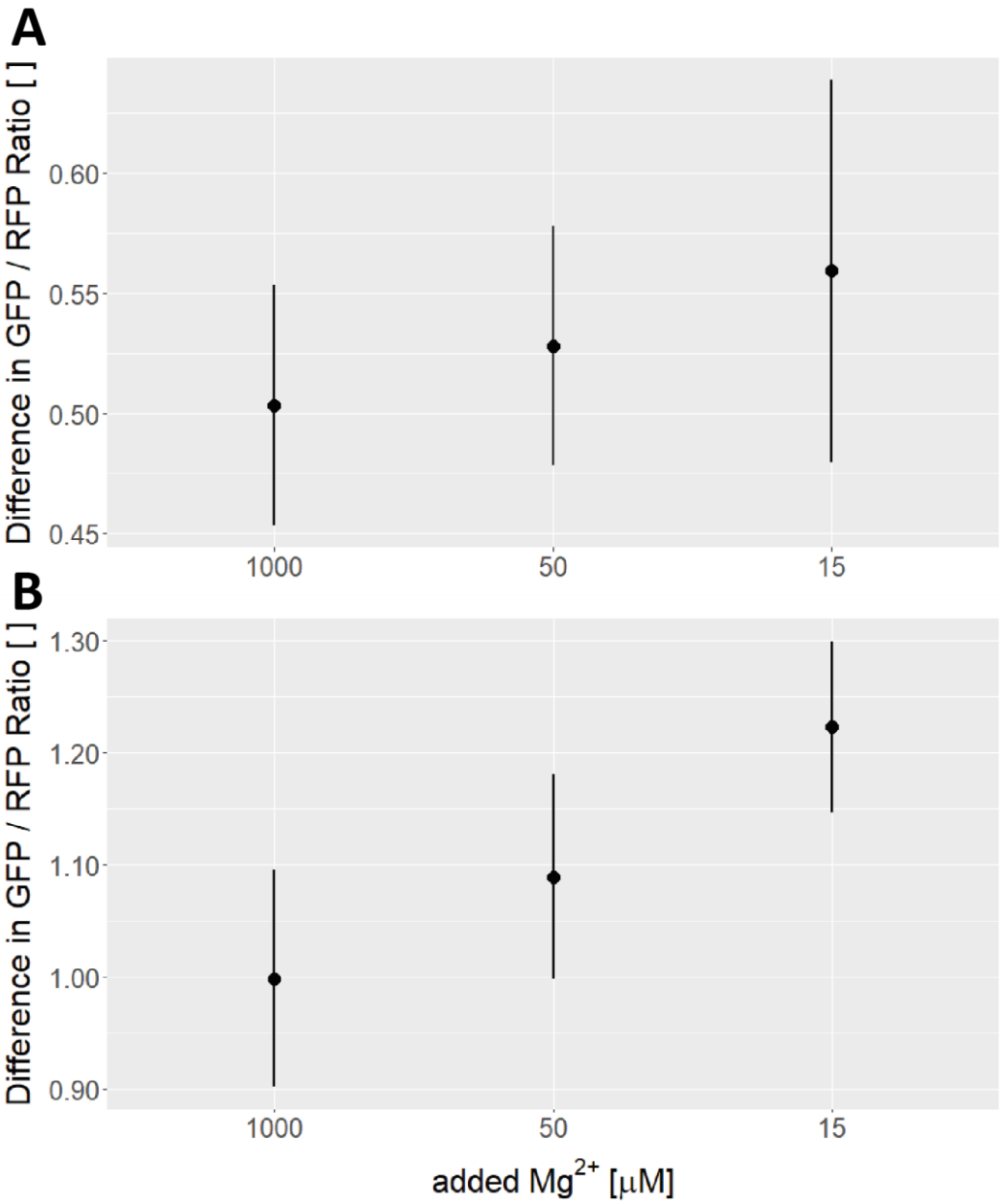

Figure 3.14 – Apparent pH differential across the PM

A – apparent pH differential within leaves. **B** – Apparent pH differential within roots. Seedlings of Col-0, cATeam, cpHusion and apHusion were grown on agar plates containing HM with different concentrations of added Mg^{2+}, until 14 DAG, before leaves and roots were transferred to the wells of a 96-well plate, filled with liquid HM. Emission values were recorded according to **Chapter 2, Section 2.6.4**, then emission ratios were calculated. For each concentration, GFP/RFP ratios recorded for apHusion were subtracted from those recorded for cpHusion, to obtain the apparent pH differential across the PM. A mixed-effect linear model was generated for the differential of emission-ratio over different concentrations. Data points represent mean values and confidence intervals for each concentration, from three independent replicates, with three technical replicates each.

To determine whether the pH differential across the PM changes under MgD, apparent pH (GFP/RFP ratio) recorded for apHusion was subtracted from the value recorded for cpHusion at the same Mg^{2+}-concentration, giving the apparent pH differential across the PM. Results are shown in **Figure 3.14**. No significant difference for different concentrations could be seen in leaves (**Figure 3.14 A**) since apparent pH in both the cytoplasm and apoplasm was higher under MgD (**Figure 3.13 B** & **C**). Within roots however, a significant increase in the pH-differential was seen (**Figure 3.14 B**). Cytoplasmic pH was significantly higher and apoplastic pH was lower.

Since these results contradicted the model of how impaired sucrose export may arise under MgD (see **Chapter 1**, **Section 1.2.4**), additional scrutiny was applied to the way plants were grown for experiment. Previously, all media used for plant growth contained 0.5% (w/v) sucrose, standard practice in *A. thaliana* culture on solid media. However, since supplying sucrose to the roots may interfere with the impaired sucrose export from source tissues occurring as a result of MgD, it was rationalized that some of the previous experiments would have to be repeated without added sucrose. The starch staining experiment summarized in **Figure 3.7** was carried out on Col-0 seedlings grown on agar plates with HM containing no sucrose, with Mg^{2+}-concentrations of 1000, 50, 40 and 15 µM. Growth time was adjusted to 17 DAG to account for the fact that plant growth is slower without added sucrose. Two biological replicates of the staining-procedure were carried out; results are shown in **Figure S3.3**. Results were similar to those from the assay carried out on plants grown on media with sucrose, with seedlings grown on 15 µM Mg^{2+} showing noticeable staining across all but the youngest, developing leaves, while seedlings from other concentrations showed little to no staining.

Next, the plate-reader experiment with cATeam, cpHusion and apHusion was repeated for plants grown without sucrose, until 17 DAG. Once again, leaves and shoots of seedlings grown on media containing 1000, 50 and 15 µM Mg^{2+} were excised and placed in the wells of a 96-well plate, before emission ratios were measured and compared. Results are summarized in **Figure 3.15** and **Figure 3.16**. The apparent MgATP-concentration reported by ATeam was again significantly higher for seedlings grown on 15 µM Mg^{2+} than for those grown on 1000 µM Mg^{2+}, while apparent cytoplasmic pH increased more noticeably, both at 50 and 15 µM Mg^{2+}.

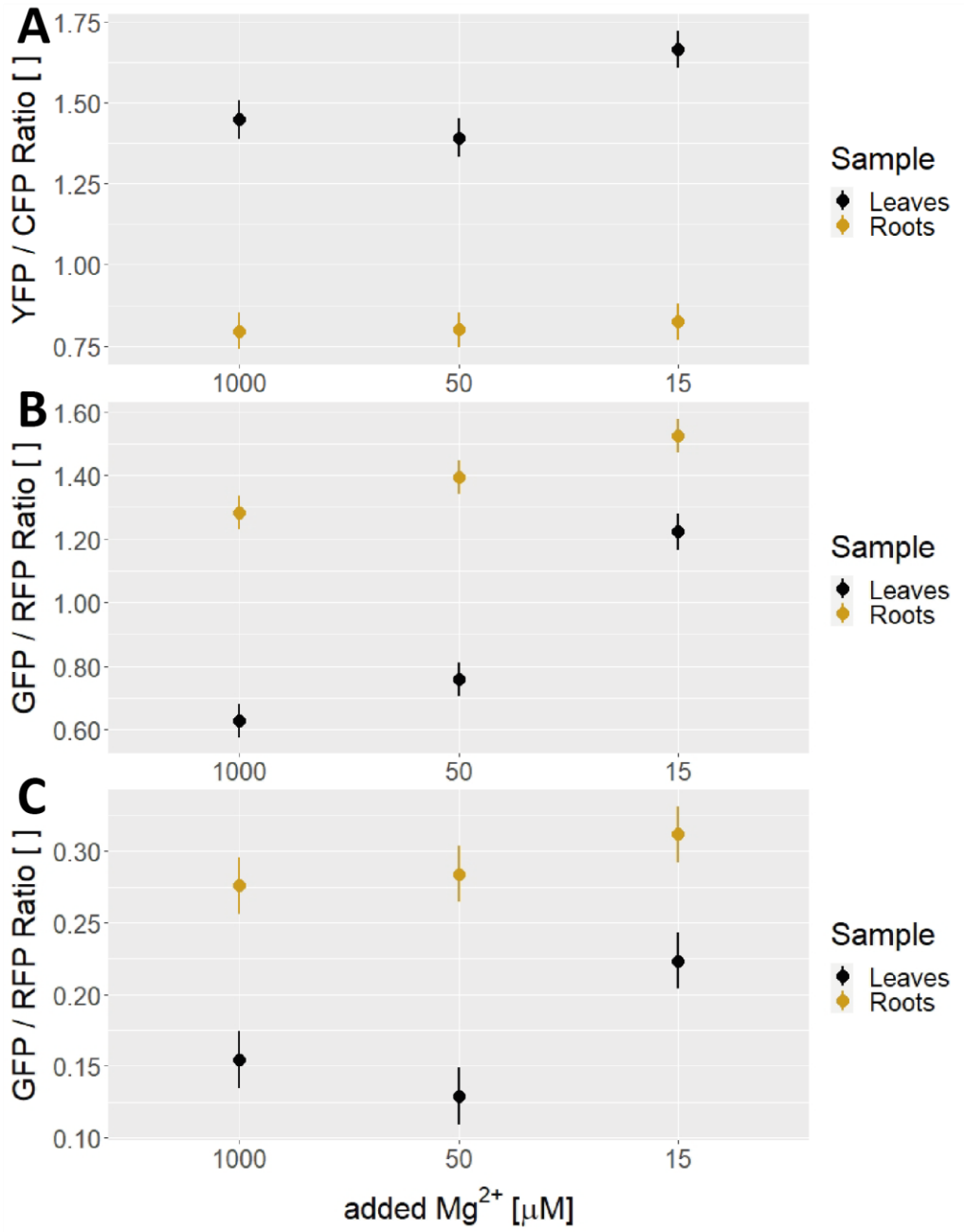

Figure 3.15 - Plate-reader assay results for plants grown without sucrose

A – FRET ratios (YFP/CFP after CFP excitation) for ATeam, at different Mg^{2+}-concentrations. **B** – GFP/RFP ratios recorded for cpHusion. **C** – GFP/RFP ratios recorded for apHusion. Seedlings of Col-0, cATeam, cpHusion and apHusion were grown on agar plates with different concentrations of added Mg^{2+}, without added sucrose, until 17 DAG, before leaves and roots were separated and transferred to the wells of a 96-well plate, filled with liquid HM of the same composition. Emission values were recorded, then emission ratios were calculated. A mixed-effect linear model was generated for the emission-ratio over different concentrations and plant parts. Data points represent mean values and confidence intervals for each concentration, from three independent replicates, with three technical replicates each.

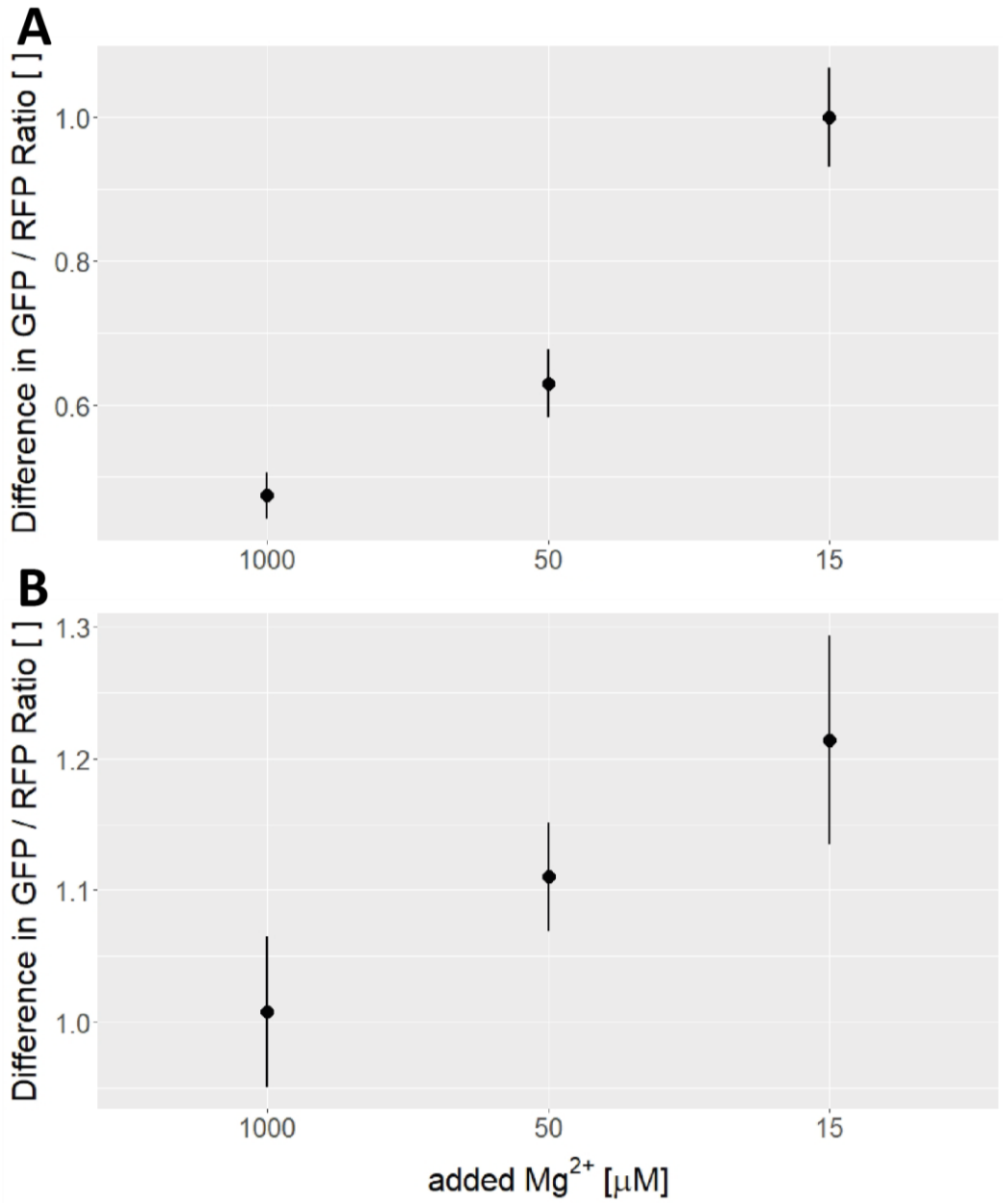

Figure 3.16 - Apparent pH differential across the PM

A – apparent pH differentials within leaves. **B** – Apparent pH differentials within roots. Seedlings of Col-0, cATeam, cpHusion and apHusion were grown on agar plates with different concentrations of added Mg^{2+}, without added sucrose, until 17 DAG, before leaves and roots were separated and transferred to the wells of a 96-well plate, filled with liquid HM of the same composition. Emission values were recorded. For each concentration, GFP/RFP ratios recorded for apHusion were subtracted from those recorded for cpHusion, to obtain the apparent pH differential across the PM. A mixed-effect linear model was generated for the difference of emission-ratio over different concentrations. Data points represent mean values and confidence intervals for each concentration, from three independent replicates, with three technical replicates each.

Apparent apoplastic pH was significantly higher in leaves and roots grown on 15 µM Mg^{2+} without sucrose (**Figure 3.15 C**). This is the only qualitative difference observed between the experiments with and without sucrose; for plants grown with sucrose, a non-significant slight decrease in root apoplastic pH was observed (**Figure 3.13 C**).

Although both the apparent cytoplasmic and apoplastic pH increased during the sucrose-free experiment, a significant increase in the apparent pH-differential across the PM was seen for both the leaves and roots (**Figure 3.16**), while for the experiment with sucrose, only the root pH-differential was increased significantly, although an upwards trend could be seen in leaves (**Figure 3.14**).

Finally, since ratiometric sensors rarely allow determination of absolute concentrations of metabolites, and since ATeam specifically has been shown to be sensitive to changes in pH [182], it was deemed necessary to validate the results of the plate-reader assays with an independent experiment. Samples of leaves and roots from seedlings grown together with those used for the plate-reader experiment had been taken, and these samples were used in a bioluminescent ATP-assay based on firefly luciferase. Cell extracts were prepared for one sample per biological replicate of the plate-reader experiment, both with and without sucrose, and subjected to intensiometric determination of ATP-concentrations within the original tissue (**Figure 3.17 A**) and ratiometric determination of ATP/ADP-ratios within the samples (**Figure 3.17 B**). Both for plants grown on media with and without sucrose, a significant increase in absolute ATP-concentration could be seen on 15 µM Mg^{2+}. Additionally, ATP/ADP ratios were significantly increased on 50 and 15 µM Mg^{2+} without sucrose, while a noticeable, but non-significant increase was observed at those Mg^{2+}-concentrations with sucrose. Although this assay reports on different parameters than the plate reader assay (MgATP versus ATP or ATP/ADP ratio) and more replicates should be performed, these results nevertheless confirm those obtained from the plate-reader assay.

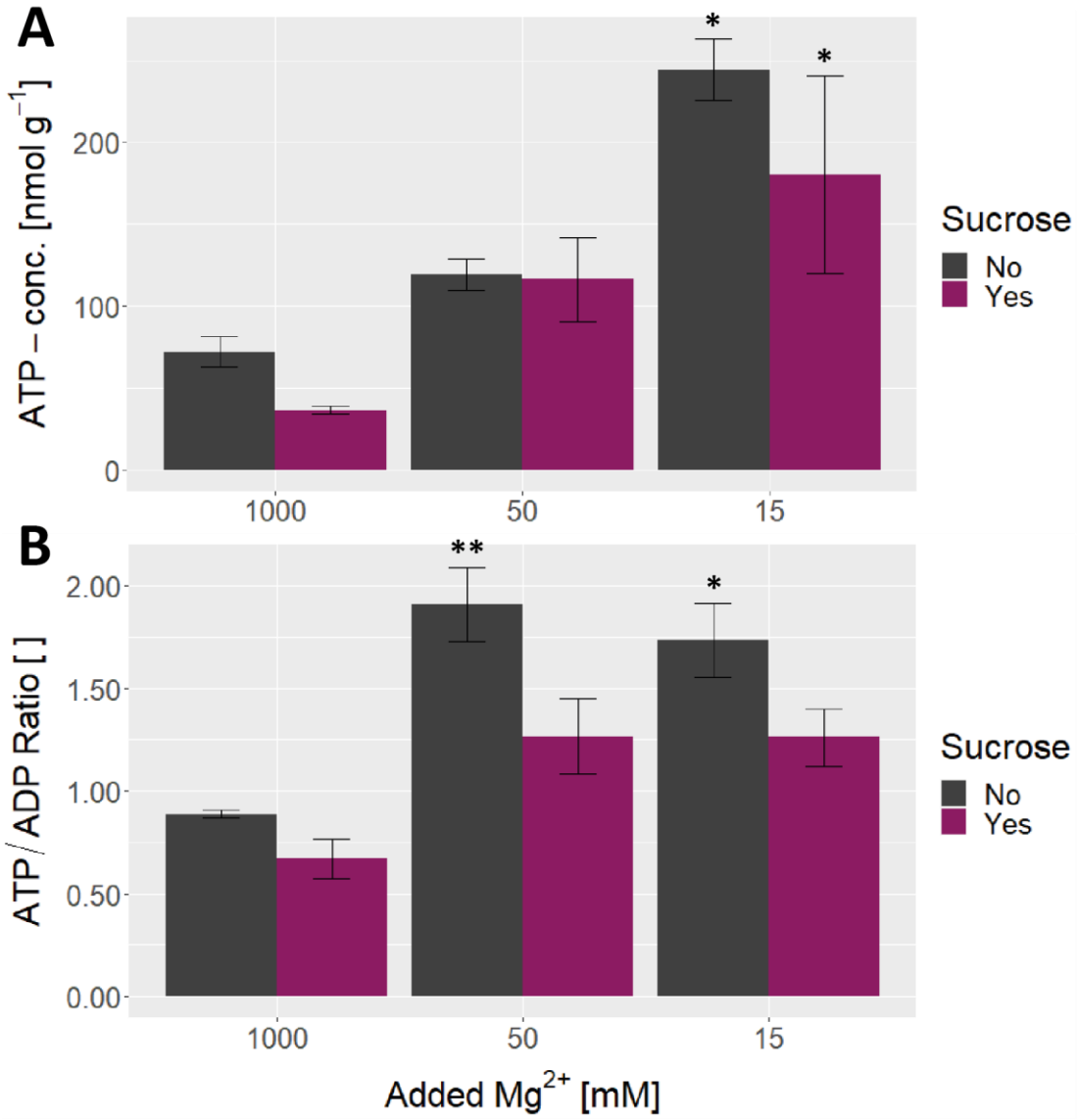

Figure 3.17 – Results of an ATP-Assay carried out on leaves

Samples of leaves from *A. thaliana* grown for plate-reader assays were taken before the plate-reader assays were carried out. Leaf samples were flash-frozen and later used to carry out a luciferase-based, bioluminescent ATP-assay. **A** – ATP-concentrations in leaves, calculated from luminescence intensities after constructing a calibration curve using standard addition. **B** – ATP/ADP ratios in leaves. Columns represent mean values (± SEM) from three independent biological replicates. Significant differences were determined two-way ANOVA followed by Tukey HSD. Symbols above error bars denote significant differences between values observed on 1000 µM Mg^{2+} and the respective condition (▪ - $p < 0.1$; * - $p < 0.05$; ** - $p < 0.01$; *** - $p < 0.001$).

3.3 Discussion

3.3.1 Symptoms of MgD appear to be consistent across method and age

The results shown here demonstrate that the symptoms of MgD observed previously within mature *Arabidopsis* transferred to Mg^{2+}-free medium in hydroponic culture apply to two-week-old seedlings grown continuously on agar plates containing low-Mg^{2+} medium. It also appears that increasing the severity of MgD by adding less Mg^{2+} to media has the same effect as longer withdrawal times, *i.e.*, more severe MgD produces symptoms further down in the "pathway" (**Figure 3.1**) regardless of the method used. As outlined in **Figure 3.1** and **Chapter 1**, **Section 1.2.4**, previous data from time-course experiments suggests that starch accumulation occurs first (after whole-tissue Mg^{2+}-concentrations drops), followed by reduced growth, ROS evolution, and reduced chlorophyll abundance [90]. In accordance with this, starch accumulation was observed when seedlings were grown on 15 µM Mg^{2+} or lower (**Figure 3.7**), whereas increases in ROS abundance (**Figure 3.8**), reductions in chlorophyll abundance (**Figure 3.9**) and reductions in shoot weights (**Figure 3.5 A**) were only observed on 7.5 or 0 µM added Mg^{2+}, respectively. Additionally, although the number of transcripts tested was small, expression of the same transcripts was induced after transfer to low Mg^{2+} and after continuous growth on low (15 µM) Mg^{2+}, again indicating that the two methods produce similar results. The Venn-Diagram in **Figure 3.2** appears to indicate the same, since the level of overlap between datasets does not appear greater between datasets obtained using a similar method. The datasets from Hermans *et al*. [227] and Niu *et al*. [104], *i.e.*, the two datasets obtained after withdrawing Mg^{2+} from the medium later on, at over 3600 DEGs each, are far larger than those by Kamiya *et al*. [105] and Oda *et al*. [103], *i.e.*, the datasets obtained after growth on one Mg^{2+}-concentration continuously, which only contain 1165 and 389 genes, respectively. This could indicate that transfer to an almost completely Mg^{2+}-free medium causes greater effects on the transcriptome than continuous growth on a moderately low Mg^{2+}-concentration, but may also reflect the influence of age (14 DAG vs. 42 DAG at harvest). Since many of the genes in the two "transfer" datasets are unique to each, these genes may also reflect false-positives.

The two “continuous” datasets share little overlap besides the 84 genes shared between all four datasets, each sharing a relatively large, but separate, portion of their total number of genes with one or both of the two “withdrawal” sets (**Figure 3.2**).

It appears that continuous growth on agar plates containing moderately low Mg^{2+} represents a valid method for inducing MgD in *A. thaliana*. Going forward, 15 µM added Mg^{2+} will be used as a low-Mg^{2+} concentration that clearly elicits the characteristic, “early” symptoms of MgD while only having a minor effect on growth, which equates to the condition used to select for loss of reporter expression during the genetic screen At this concentration, starch accumulation is observed, but not ROS evolution or reduced chlorophyll abundance. In the same way, 50 µM added Mg^{2+} was selected as a “pre-MgD” condition, which does not yet elicit detrimental effects on plant growth or physiology, equating to the condition used to select for “prematurely” induced reporter expression during the screen.

3.3.2 The reduction of lateral root growth under low Mg^{2+} likely represents an environmental adaptation

Interestingly, the number of lateral roots per seedling was reduced significantly on 15 µM Mg^{2+} (**Figure 3.5 C**), when shoot weights were not yet significantly reduced. Upon calculating the number of lateral roots per main root length, a significant difference could be seen on 50 µM Mg^{2+} or below (**Figure 3.6**), making this the earliest physiological change observed in this series of experiments. In fact, the number of lateral roots per main root length determined in this experiment seems to follow an inverse correlation with the Mg^{2+}-concentration used even at higher concentrations, despite shoot fresh weights and main root lengths increasing between 1000 and 50 µM added Mg^{2+}. Since these Mg^{2+}-concentrations are obviously sufficient for *Arabidopsis* growth, this indicates a genuine adaptive response rather than a growth impairment.

The reduction of lateral root numbers in low external Mg^{2+}-concentrations has been observed previously in Col-0 by Cristescu *et al.* [228], and further characterized by Niu *et al.*, [229]. Xiao *et al.*, [108] investigated this response across *A. thaliana* ecotypes, and could confirm its presence across all accessions tested, although some show it less strongly. As outlined in **Chapter 1**, **Section 1.2.1**, Mg^{2+} is a soil-mobile element, and therefore likely does not usually form horizontal concentration-differences. At the same time, it is easily leached to deeper soil strata, which might explain the presence of such an adaptation. Therefore, while this is not a new finding, it nevertheless further confirms that the results of these experiments are in line with previous findings.

3.3.3 MARIO can significantly improve understanding of Mg^{2+}-homeostasis

As outlined previously, the inability to track concentrations of Mg^{2+}, and especially those of $[Mg^{2+}]$, across cells and tissues presents a significant obstacle to the advancement of knowledge regarding Mg^{2+}-homeostasis. The difficulties associated with distinguishing between the different Mg^{2+}-pools within cells are especially troublesome in this context, since a decrease in total cell or tissue Mg^{2+} could be entirely explained by a decrease in Mg^{2+}-stores, without any impact on cytosolic and organellar Mg^{2+}-pools involved in cellular functions. Genetically-encoded, ratiometric sensors, if properly expressed and calibrated, could solve this problem almost entirely.

No MARIO-expressing line suitable for *in vivo* experiments could be generated in this work. Only less than 1% of all transformants tested showed detectable levels of sensor expression, despite all individuals tested containing the *MARIO* CDS. All the *MARIO* constructs used the 35S promoter, which is known to be a “strong” promoter inducing high levels of expression, as well as the TMV Ω enhancer. Use of strong promoters is known to cause silencing of transgenes, especially when foreign sequences are introduced [230]. Further, the relatively bright fluorescence present across entire cells in *mrs2-4* 1 + *cpMARIO* (**Figure 3.11**) is likely caused by excessive expression of the protein, leading to accumulation in the endomembrane system or the cytoplasm, rather than exclusively within chloroplasts.

The fact that some cells do show expression in discrete individual foci, presumably representing chloroplasts, indicates that transgene expression is lower in these cells, enabling the protein to be localized correctly. It is therefore likely that the *MARIO* transgene was subject to post-transcriptional cis-inactivation, completely preventing expression at detectable levels in all but one individual, with the remaining one subject to partial silencing of the transgene. It should be possible to prevent this issue in the future by using "weaker" promoters, potentially plant-native promoter sequences. Additionally, the *MARIO* sequence, which was used in its unchanged form in this work, could be codon-optimized for *Arabidopsis* expression, reducing the risk of the CDS being recognized as foreign genetic material, and/or the post-transcriptional gene silencing-deficient *rdr6* line of *A. thaliana* [231] could be transformed instead of WT plants.

Maeshima *et al.* [131] report that MARIO, expressed in human-derived Henrietta Lacks (HeLa) cells shows an apparent K_d of 7.2 mM for Mg^{2+}, with a dynamic range of 153% observed for the YFP/CFP FRET ratio. The data shown in **Figure 3.12** indicate that under the conditions used here, the apparent K_d of the sensor for Mg^{2+} is 2-5 mM, with more data required to establish a more accurate value. Although this value only represents added Mg^{2+}, with some additional Mg^{2+} present from the initial leaf tissue used to prepare the cell extract, the plant material was diluted roughly 60-fold before the start of the experiment, and as such should only represent a negligible amount of Mg^{2+}. During the experiment, 10 mM EDTA was added to one of the samples, which further reduced the FRET ratio by 0.04 compared to 0 mM Mg^{2+} (data not shown), showing that the residual Mg^{2+} did have a small, but appreciable effect. It nevertheless appears that the K_d of MARIO, as expressed in *A. thaliana*, is lower than when expressed in HeLa cells. Including these data, the dynamic range of the sensor was estimated to be 50-55% under these conditions, which is only roughly 1/3 of the dynamic range measured by Maeshima *et al*. Both differences could have multiple explanations. It is possible that the mis-expression and mis-targeting of the sensor observed in *mrs2-4* 1 + *cpMARIO* (**Figure 3.11**) lead to a significant portion of the sensor being retained in the ER. Oxidising conditions in the ER can lead to the formation of sensor aggregates, which can restrict dynamic range and lead to altered apparent K_d [232].

Similar problems could be caused by the conditions present in plant cells compared to human cells, or by the buffer used in the experiment in this work. Regardless, the data here presented show that the sensor can be functionally expressed in *A. thaliana*. Calibration of the sensor should be repeated once the problems around mis-expression and gene silencing have been solved. According to the data in **Figure 3.12**, sub-millimolar Mg^{2+}-concentrations can be distinguished using MARIO, which should make it possible to measure changes in both cytoplasmic and organellar [Mg^{2+}] using this sensor in its current form in the future.

3.3.4 ATP-levels and PM pH-differentials appear to increase, not decrease, under MgD

The results generated here using ATeam indicate that cytoplasmic MgATP-levels are higher in plants grown under MgD, regardless of whether sucrose is added to the growth media. Further, results obtained using pHusion indicate that leaf cytoplasmic and apoplastic pH, and root cytoplasmic pH, are higher under MgD in both cases, whereas root apoplastic pH is higher under MgD only on sucrose-free media (**Figure 3.13** & **3.15**). The apparent pH differential across the PM, calculated from the pHusion GFP/RFP ratios recorded for the cytoplasm and the apoplast, is higher under MgD in roots of *Arabidopsis* grown on plates with sucrose, and higher in leaves and roots of those grown on plates without sucrose. Results obtained using genetically-encoded ratiometric sensors should always be treated with caution, however, since emission and absorption values can be influenced by an array of factors. In this case, the most obvious factor, specifically in leaves, is the contribution of leaf pigments to the changes in emission ratios recorded. Although all emission-values were subjected to background-corrections by subtracting emission values recorded for WT leaves and roots, these can only account for autofluorescence. Background correction of this nature cannot account for differential absorption of fluorescence emission from the two fluorophores used to calculate emission ratios, for example. **Figure 3.18** shows the absorption-spectrum of the most common pigments in leaves; the two forms of chlorophyll, chlorophyll a and b, as well as carotenoids, with the excitation and emission wavelengths used in the plate-reader experiment marked.

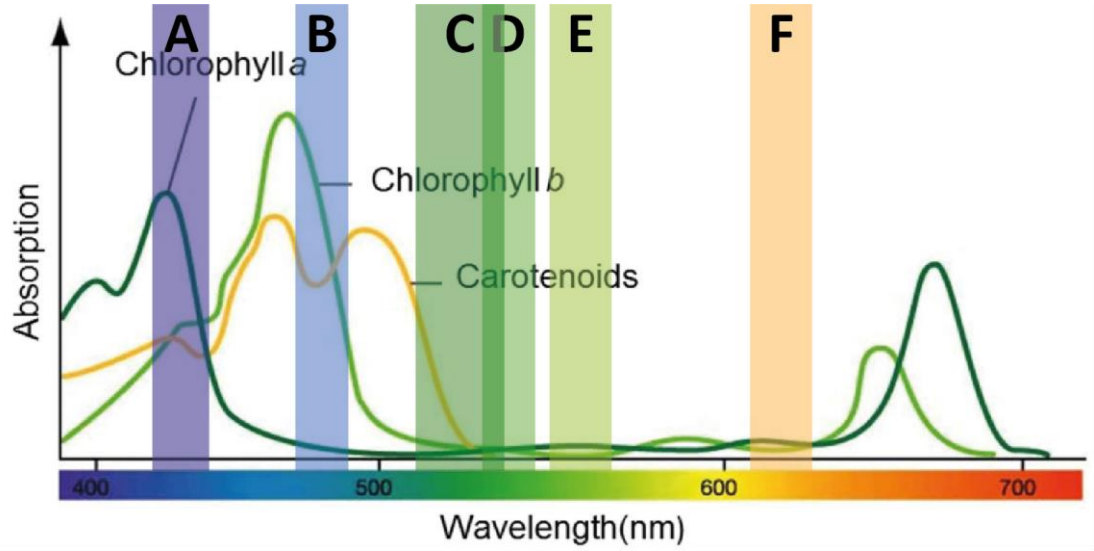

Figure 3.18 - Influence of common leaf pigments on data collected during the plate-reader assay. Spectra taken from Gouveia-Neto *et al.* [233]
Absorption spectra of chlorophyll a, chlorophyll b and carotenoids, compared to excitation and absorption wavelengths used in the plate-reader assay. Placements and thicknesses of the coloured columns over the spectra represent the actual ranges of wavelengths used according to the instrument settings. **A** - ATeam excitation. **B** - CFP fluorescence and GFP excitation. **C** - GFP emission. **D** - YFP emission. **E** - RFP excitation. **F** - RFP fluorescence.

During measurements of FRET ratios, only the donor fluorophore is excited, which then may pass the excitation energy on to the second fluorophore. For ATeam, only CFP is excited (**A** in **Figure 3.18**). Changes in leaf pigment levels would therefore not differentially affect excitation of CFP and YFP. However, while YFP fluorescence is outside the absorption-range for chlorophyll a and b, as well as for carotenoids (**D** in **Figure 3.18**), CFP fluorescence (**B**) overlaps with the largest peak of chlorophyll b absorption, as well as absorption from carotenoids. The GFP excitation band is in the same range, while GFP fluorescence (**C**) could be influenced by carotenoid levels as well, but not by chlorophyll levels. On the other hand, neither RFP excitation (**E**), nor RFP fluorescence (**F**) appears to overlap with significant absorption peaks for the pigments considered here. Going by this, an increase in the levels of chlorophyll b or carotenoids in the leaves tested could reduce the recorded CFP fluorescence intensity while having little influence on YFP fluorescence, and therefore conceivably lead to the increase in YFP/RFP ratio observed under MgD.

However, the same increase would lead to a reduction in the GFP/RFP ratio observed, since both wavelengths used to excite and emitted from GFP would be absorbed to a higher degree. Since both fluorescence ratios increase under MgD, it seems unlikely that a change in levels of these pigments could be responsible for the changes observed. Additionally, levels of chlorophyll were unchanged under these conditions (**Figure 3.9**), and decreased at 7.5 µM Mg^{2+}.

Another important consideration with respect to ATeam is pH itself. During development of the sensor for use in plants, *in vitro* experiments showed that this sensor appears to be pH-sensitive, with a large increase in YFP/CFP ratio observed between pH 7 and 7.5, although this increase could be due to the pH-dependence of the stability of the MgATP-complex itself [182]. Since an increase in apparent cytosolic pH was observed in leaves together with the increase in YFP/CFP-ratio, we cannot exclude the possibility that the increase in pH could be responsible for the increase in apparent MgATP-levels. However, in roots, an increase in cytosolic pH was observed while ATeam FRET ratios remained similar.

The results of the luciferase-based ATP-assay summarized in **Figure 3.17** lend further support to the findings from the plate-reader assay, even though this assay technically measures ATP-levels and ATP/ADP ratios rather than MgATP-levels. The reaction of firefly luciferase is dependent on MgATP as well in theory [234], but since sufficient amounts of Mg^{2+} are supplied with the assay buffer, only ATP-concentrations are measured in practice. Although the assay carried out here suffers from a lack of technical replicates for each sample, values obtained for ATP-levels in Mg^{2+}-replete seedlings are not too dissimilar to those expected or previously measured, although ATP/ADP-levels are somewhat low [235, 236]. Mean ATP-levels at 15 µM Mg^{2+} were approximately three-fold relative to 1000 µM Mg^{2+} for seedlings grown without sucrose, and around five-fold for seedlings grown with sucrose, which seems extremely high. While some of this increase can be explained by the increase in ATP/ADP ratios observed at these concentrations, a full explanation for this change would require either ATP/AMP-levels to be drastically increased under MgD as well, or the total nucleotide pool to be increased.

The measurement of PM pH-differential by subtracting GFP/RFP ratios recorded for apHusion from those recorded for cpHusion also suffers from several problems. First, this method relies on the emission ratios for these two reporters to be changing with pH on the same scale, and in a linear manner. Since both reporters are the same protein, these proteins are relatively stable and insensitive to external influences, and the reporting pH-range is relatively wide, this should not pose a significant problem in itself [186]. Nevertheless, the measurements carried out here would benefit greatly from calibration of the sensor, which could allow actual pH-values to be reported rather than "raw" fluorescence ratios. In this case, the feasibility of measured pH values under all conditions could be assessed, and the size of the PM pH-differential under different conditions could be determined, rather than just differences in it. Unfortunately, the time limitations of this project did not permit a full calibration. The apoplastic version of pHusion also suffers from additional problems; apHusion tends to be retained in the ER, especially within roots [186], which can lead to inaccurate results. Additionally, this protein could diffuse too far from the plasma membrane to be useful for reporting on the PM pH differential. Recently, both of these problems have been lessened through the development of membrane-anchored versions of apHusion [237] and ratiometric pHluorin [187]. Use of these new sensors could doubtless improve the accuracy of the results. Nevertheless, the changes in GFP/RFP ratios, and their differences, recorded here appear too substantial to be entirely attributed to inaccuracies and artifacts.

Therefore, despite the problems associated with the assays and tools used, the results obtained here suggest that there is a genuine increase in both cellular energy-charge and PM pH differential in leaves of *Arabidopsis* grown on low-Mg^{2+} media for two weeks.

3.3.5 An alternative model of sucrose accumulation under MgD

My results disagree with the model put forward in **Chapter 1**, **Section 1.2.4**, which assumes that both cytoplasmic MgATP-levels and PM pH-differentials decrease under MgD. This attractive hypothesis focusses on the role of the BvSUT1 H^+/sucrose symporter, which relies on proton-motive force across the PM to import sucrose into companion cells [90]. The results obtained here therefore initially seem difficult to explain; however, there is an additional family of sucrose transporters that is crucial for sucrose export in *A. thaliana*: the SWEET family. AtSWEET11 and AtSWEET12 are responsible for sucrose efflux from mesophyll cells into the apoplastic space, which precedes the import of sucrose back into phloem companion cells [95]. SWEET transporters were not well-described when the previous model of MgD was proposed; in the figure describing that model, sucrose efflux transporters are marked with a "?" [90] (see **Figure 1.5**). However, since then, knowledge about this family has grown considerably.

sweet11 sweet12 knockout mutants exhibit reduced root growth on media not supplied with sucrose, reduced carbon content in root exudates, as well as starch accumulation in the oldest leaves [238]. The pattern of starch accumulation exhibited by these mutants appears similar to that observed in seedlings exposed to MgD (**Figure 3.19**). SWEETs are considered sucrose channels, mediating passive efflux of sucrose into the apoplastic space [95, 239]. Experiments in heterologous systems show that they can mediate bidirectional sucrose transport, with little affinity for glucose [238]. Their activity can still be modulated and controlled, however, as phosphorylation has been shown to be able to increase their transport activity under drought stress [240]. It is therefore possible that inhibition of sucrose export through SWEET transporters, not sucrose import through SUC transporters, is the cause of the sucrose accumulation observed under MgD.

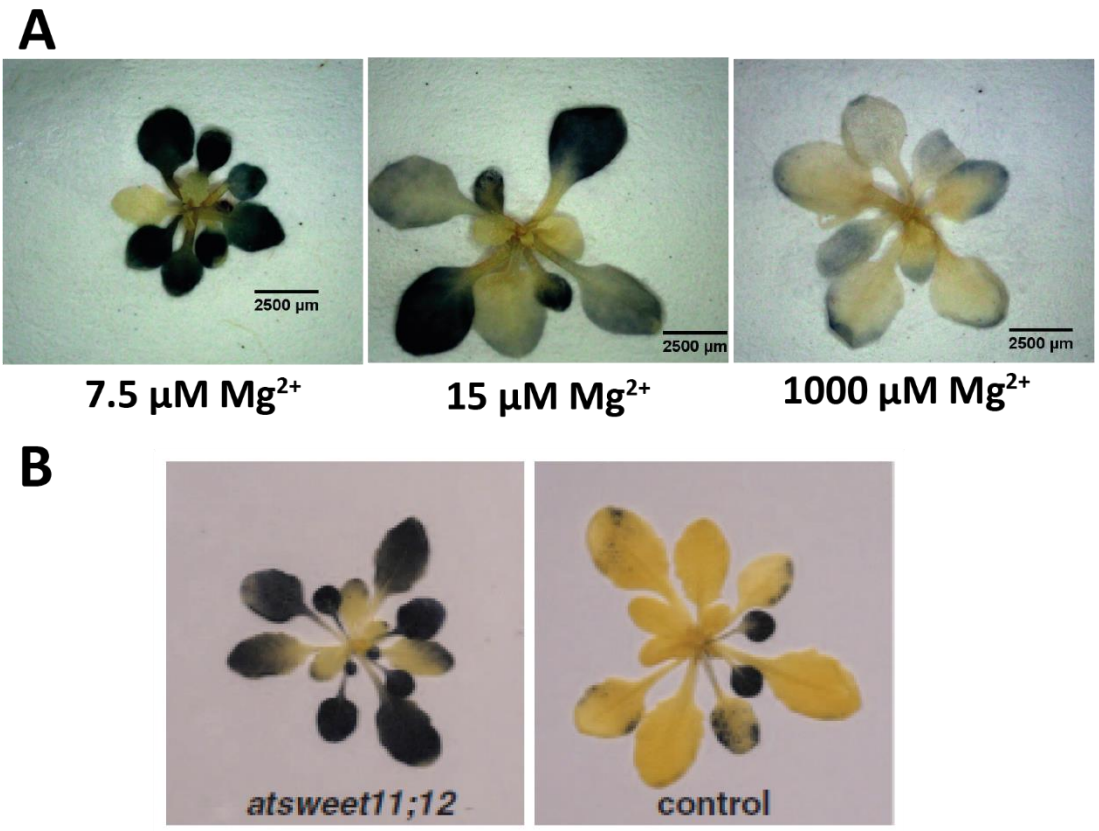

Figure 3.19 – Starch accumulation in seedlings grown under MgD is similar to *sweet11 sweet12* mutants

A – Starch accumulation in seedlings after two weeks of growth on agar plates containing media with different amounts of added Mg^{2+}, visualized by starch staining using Lugol's solution. **B** – Starch accumulation in leaves of *sweet11 sweet12* double mutants and WT plants after growth on soil for three and a half weeks, visualized by starch staining using Lugol's solution. From Chen *et al*. [238].

If this is the case, or sucrose transport is inhibited at a yet earlier step in the process, the transport of sucrose and H^+ through SUC H^+/sucrose symporters would be impossible, abolishing the associated membrane depolarization, and reducing the amount of MgATP consumed by the PM H^+ ATPase in re-building the proton-motive force. This could lead to accumulation of MgATP and increase in the PM pH-differential. Additionally, accumulating sucrose could prompt both accumulation of ATP, no longer consumed in the production of sugars, as well as excessive accumulation of starch, both due to the failure to export sucrose and the need to remove excess sugars from solution.

This alternative model of the causes of starch accumulation, outlined in **Figure 3.20**, can therefore explain the results observed here, although further work is required to test and refine this model further. Specifically, the mechanism by which the activity of SWEET transporters could be inhibited need to be elucidated.

Many experiments using currently-available methods could be used to test this new model. A time-course of ATP-levels, MgATP-levels and pH in leaves after Mg^{2+}-withdrawal, for example, carried out using the assays developed and used here, could provide additional evidence. Activity of SWEET transporters at different Mg^{2+}-levels could be tested *in vitro*, while protein abundance and presence of post-translational modifications of SWEET transporters could be tested in plants exposed to MgD. Additionally, the abundance of sucrose within the cytoplasm, compared to that within the apoplastic space, could be compared, potentially by using sucrose-sensitive FRET sensors, which are now available [241]. If the previous model is accurate, sucrose would be accumulated in the apoplast first, and in the cytoplasm of cells only as a consequence of this, while with this model, sucrose accumulation would take place in the cytoplasm, while apoplastic sucrose-concentrations would be decreased.

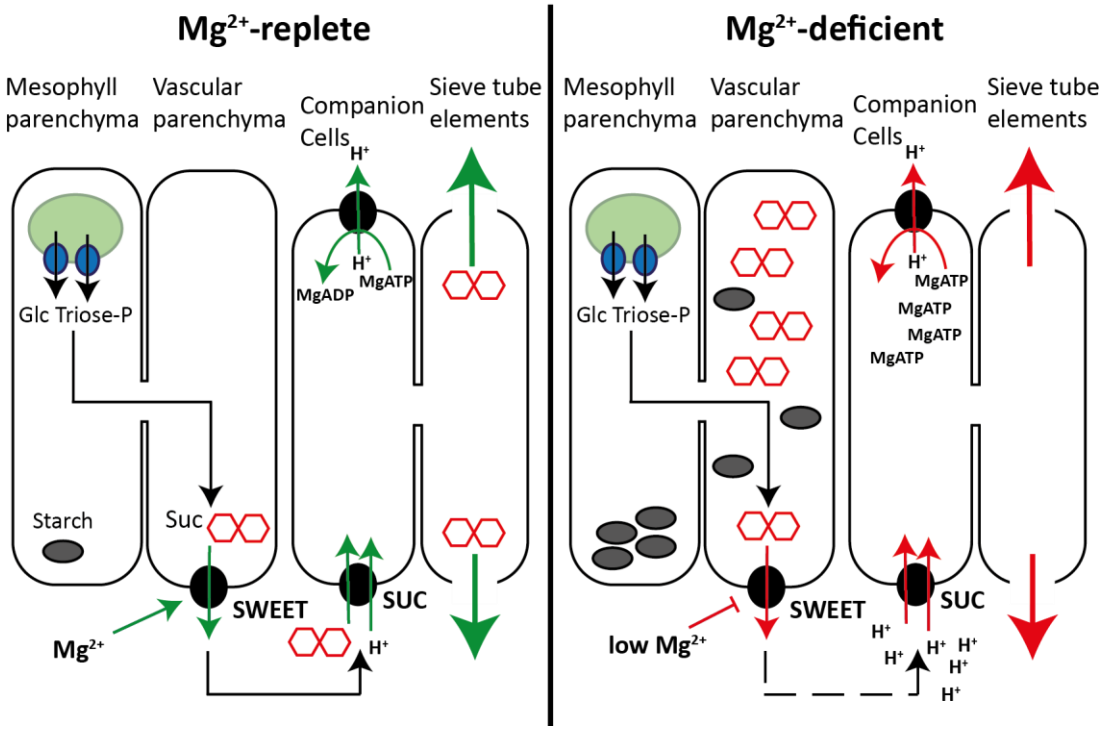

Figure 3.20 – An alternative model of the causes of sucrose accumulation in leaves of *Arabidopsis*

Under Mg^{2+}-replete conditions, sucrose is produced in leaves through the energy-consuming processes of the light and dark reactions of photosynthesis. Sucrose is transported through the mesophyll via the symplastic pathway, then exported into the apoplast through SWEET transporters in vascular parenchyma cells. Sucrose enters phloem companion cells via SUC H^+/sucrose symporters by using the PM pH-differential generated by the PM H^+ ATPase, among others, before being transported to sink tissues through the phloem. Under MgD, the activity of SWEET transporters is inhibited, which makes import of sucrose via SUC transporters impossible. This prevents the reduction of the PM proton-motive force by H^+/sucrose symport, which reduces the amount of MgATP consumed by the PM H^+ ATPase. Accumulation of sucrose in mesophyll and vascular parenchyma cells leads to accumulation of starch. Feedback-inhibition on further production of starch leads to the accumulation of energy currencies in cells in the form of ATP, among others. Green arrows in the above diagram represent processes functioning properly, while red arrows represent inhibited processes. Blue or black ellipses represent membrane (transport) proteins, and green ellipses represent chloroplasts.

Chapter 4: The Localisation and Physiological Role of MRS2 Magnesium Transporters in *A. thaliana*

4.1 Introduction

4.1.1 Knowledge gaps with respect to MRS2 transporters in *A. thaliana*

As outlined in **Chapter 1, Section 1.3**, the CorA/MRS2/Alr1 superfamily is the most extensive family of Mg^{2+}-transporters identified to date, and members are found across all kingdoms of life [127]. Many of their members within plants are essential for plant growth and functioning. In addition to this, they may exhibit a unique regulatory mechanism, changing their open probability in direct response to changes in internal Mg^{2+}-concentrations (see **Chapter 1**, **Section 1.3.5**). Therefore, they may not only be subject to regulation by other proteins in response to MgD, but they may also take part in Mg^{2+}-sensing and -signalling themselves, essentially functioning as transceptors. However, knowledge gaps and inconsistencies in the data on MRS2 family members in *A. thaliana* make further progress difficult.

The quality of the data on the subcellular localisation of MRS2s from different publications is often suboptimal, in many cases stemming from transformation of protoplasts [119, 138, 154, 157, 242] or transient transformation of *Nicotiana benthamiana* [136, 153]. Few studies report results from viable *A. thaliana*, stably transformed with GFP fusion constructs [121, 156], and even fewer show even partial complementation of mutant phenotypes in these lines first [103]. In some cases, individual reports actively contradict each other (see **Table 1.2**). Considering the known problems interfering with the determination of protein localisations in this way, with up to 39% of localisation data from fluorescently tagged proteins disagreeing with data from mass spectrometry assays [243], much of this data seems unconvincing. Of course, it is possible for proteins to exhibit different subcellular localisations in different tissues or at different stages of development, but neither can this be shown using protoplasts or transient transformation assays, nor is it acknowledged by most authors; usually, one localisation is given for each MRS2 by each author, even if conflicting data exist.

In order to establish the localisation of these transporters more securely, phenotypes of *mrs2* mutant lines should be complemented by the respective MRS2::GFP fusion protein, demonstrating that the GFP-fused protein is functional and correctly targeted. Then, the localisation of GFP can be determined across different developmental stages and plant parts. Alternatively, or additionally, localisations could be asserted through other experiments, such as membrane fractionation followed by pull-down or mass spectrometry.

Another important knowledge gap exists with respect to regulation of MRS2s. As outlined above, these channels could have the ability to respond directly to Mg^{2+}-concentrations, but this is not the only way transporters can be regulated, or participate in regulatory networks. Changes in gene expression levels, either on the level of transcription or translation, or re-localisation of the protein under certain conditions, as for the IRT1 iron transporter [244], are all possible. Most studies report that the expression of *MRS2*-family genes does not depend on external levels of Mg^{2+} or duration of Mg^{2+}-stress experienced by plants [61, 102, 136]. However, Mao *et al.* report that the expression of *MRS2-4* is increased rapidly after transfer of plants to low-Mg^{2+} plates, specifically in roots, with the expression dropping to normal levels after one week [138], suggesting changes in expression-patterns might be very specific, possibly evading detection so far. These changes in transcript levels could not be confirmed by other authors [166]. Data on protein-level expression of MRS2s is exceedingly rare, making it impossible to exclude the possibility of post-transcriptional regulation of gene levels, such as changes to splicing, translation, post-translational modifications or degradation. It is not known whether *Arabidopsis* MRS2s interact with other proteins, besides the apparent ability to form heterodimers with other members of the family [167], despite the possibility of conformational changes triggering signalling events, as outlined in the previous section, which would be reminiscent of NRT1.1's function as a transceptor [245].

In summary, although the phenotypes caused by knockout (KO) of MRS2s have been relatively well characterized, current knowledge about their molecular functioning and their place in the wider Mg^{2+}-homeostasis network is lacking.

4.1.2 Aims of this chapter

To address some of the knowledge gaps outlined in the previous section, it is necessary to fully complement *Arabidopsis mrs2* mutants with fluorescently-tagged MRS2 proteins, generating stable transformants. These can then be used to investigate not only the subcellular localisation of the respective MRS2 family members, but also any changes in protein localisation, in real time.

The first part of this chapter describes the generation and characterisation of homozygous T-DNA insertion mutants for all functional MRS2 family members in the Col-0 accession. The second part describes the generation of GFP-fused expression constructs for a subgroup of MRS2s, transformation of the respective mutants, and assessment of complementation in transformant lines. In the third part, subcellular localisation of MRS2-3::GFP and MRS2-4::GFP is assessed via confocal microscopy. The overall aim was to conclusively confirm the subcellular localisations and/or tissue-level expression patterns of as many MRS2 family members as possible, as well as to lay the foundations for experiments investigating dynamic changes in subcellular localisation, protein-level expression and protein-protein interactions.

4.2 Results

4.2.1 Disruption of MRS2s causes growth impairments of varying severity

To investigate the roles of MRS2s in Mg^{2+}-homeostasis in *A. thaliana* further, as well as clarify their subcellular localisation, *mrs2* mutants were obtained. *Arabidopsis* lines with T-DNA insertions (SALK lines) within each true *MRS2* gene in Col-0, were obtained from the Nottingham *Arabidopsis* Stock Centre (NASC). Obtained lines are described in **Table 4.1**. Additionally, an *mrs2-1*/*5*/*10* triple knockout line (TKO) was received courtesy of the Knoop lab at Universität Bonn in Germany. All of these lines were subjected to genotyping by PCR (see **Chapter 2**, **Section 2.3.2**) and were found to contain T-DNA insertions in the correct *MRS2*. Each line not found to be homozygous already was self-fertilized and homozygous offspring selected.

During initial growth for seed bulking, none or very few seeds could be obtained for *mrs2-2* (SALK_082081C), *mrs2-6* (SALK_037061C), and *mrs2-11* (SALK_028422C). These lines were therefore not carried forward, due to the difficulty associated with using them. For *mrs2-1* (SALK_006797C), *mrs2-5* (SALK_105475C), *mrs2-7* (SALK_127086C), and *mrs2-10* (SALK_006528C and SALK_100361C), no difference in growth compared to WT plants could be seen. *mrs2-3* 1 and *mrs2-3* 2 (SALK_080443 and SALK_201976C, respectively) initially showed highly variable phenotypes, with some individuals growing extremely slowly and/or yielding few to no seeds. After propagation for two and three generations respectively, lines consistently showing slightly delayed growth and normal seed development were obtained. *mrs2-4* 1 and *mrs2-4* 2 (SALK_203866C and SALK_145997, respectively) both produced smaller plants at every stage of growth, with rosette leaves that tended to curl downward both in the direction of base-to-tip and side-to-side, with fewer seeds produced than for WT plants. Finally, TKO tended to grow more slowly than WT plants, producing fewer, shorter bolts and fewer flowers. **Figure 4.1** and **Figure S4.1** show images of representative individuals of some of the lines used going forward, after five weeks of growth on soil.

Table 4.1 - mrs2 mutant lines used in this work

Name	MRS2	SALK identifier	Observed phenotype
mrs2-1	MRS2-1	SALK_006797C	Wild-type
mrs2-2	MRS2-2	SALK_082081C	Normal growth, almost fully sterile
***mrs2-3* 1**	MRS2-3	SALK_080443	Slow growth
***mrs2-3* 2**	MRS2-3	SALK_201976C	Slow growth
***mrs2-4* 1**	MRS2-4	SALK_203866C	Small, curled leaves, fewer seeds
***mrs2-4* 2**	MRS2-4	SALK_145997	Small, curled leaves, fewer seeds
mrs2-5	MRS2-5	SALK_105475C	Wild-type
mrs2-6	MRS2-6	SALK_037061C	Normal growth, sterile
mrs2-7	MRS2-7	SALK_127086C	Wild-type
***mrs2-10* 1**	MRS2-10	SALK_006528C	Wild-type
***mrs2-10* 2**	MRS2-10	SALK_100361C	Wild-type
mrs2-11	MRS2-11	SALK_028422C	Early leaf senescence, few seeds

Names given to lines used, MRS2 family member disrupted in each line, SALK identifiers for each, as well as phenotypes observed during initial growth on soil.

At this stage, five MRS2s and their mutant lines were selected for further characterisation. The *mrs2-2*, *mrs2-6*, and *mrs2-11* lines did not produce enough seed to be used further. The *mrs2-1* and *mrs2-5* lines were abandoned since KO of these genes did not cause noticeable phenotypes. *mrs2-*7 was abandoned because 10 introns and 13 splice variants were reported on TAIR, making successful gene cloning and complementation of the observed phenotypes unlikely. *mrs2-10* single mutants were retained alongside TKO, with the intention to complement the phenotype in TKO by re-introducing *MRS2-10*. The *mrs2-4* and *mrs2-3* mutant lines were retained since they showed appreciable phenotypes. Next, the exact locations of the T-DNA insertions present in the genomes of those *mrs2* lines carried forward were determined. This was achieved by carrying out Sanger-sequencing on DNA fragments amplified from *mrs2* genomic DNA using the same primers used for initial genotyping (see **Chapter 2**, **Section 2.3.3**,). Results are visualized in **Figure 4.2**.

Aside from *mrs2-4 2*, which carries a T-DNA insertion not described on TAIR, although previously reported [103], insertions were found in the described locations. Since insertions found in *mrs2-3* lines lie in the 3' UTR of *MRS2-3*, these may represent partial KO lines.

This page is intentionally left blank

Blank pages are used throughout to allow legends to appear opposite display items in the paper copy of this document

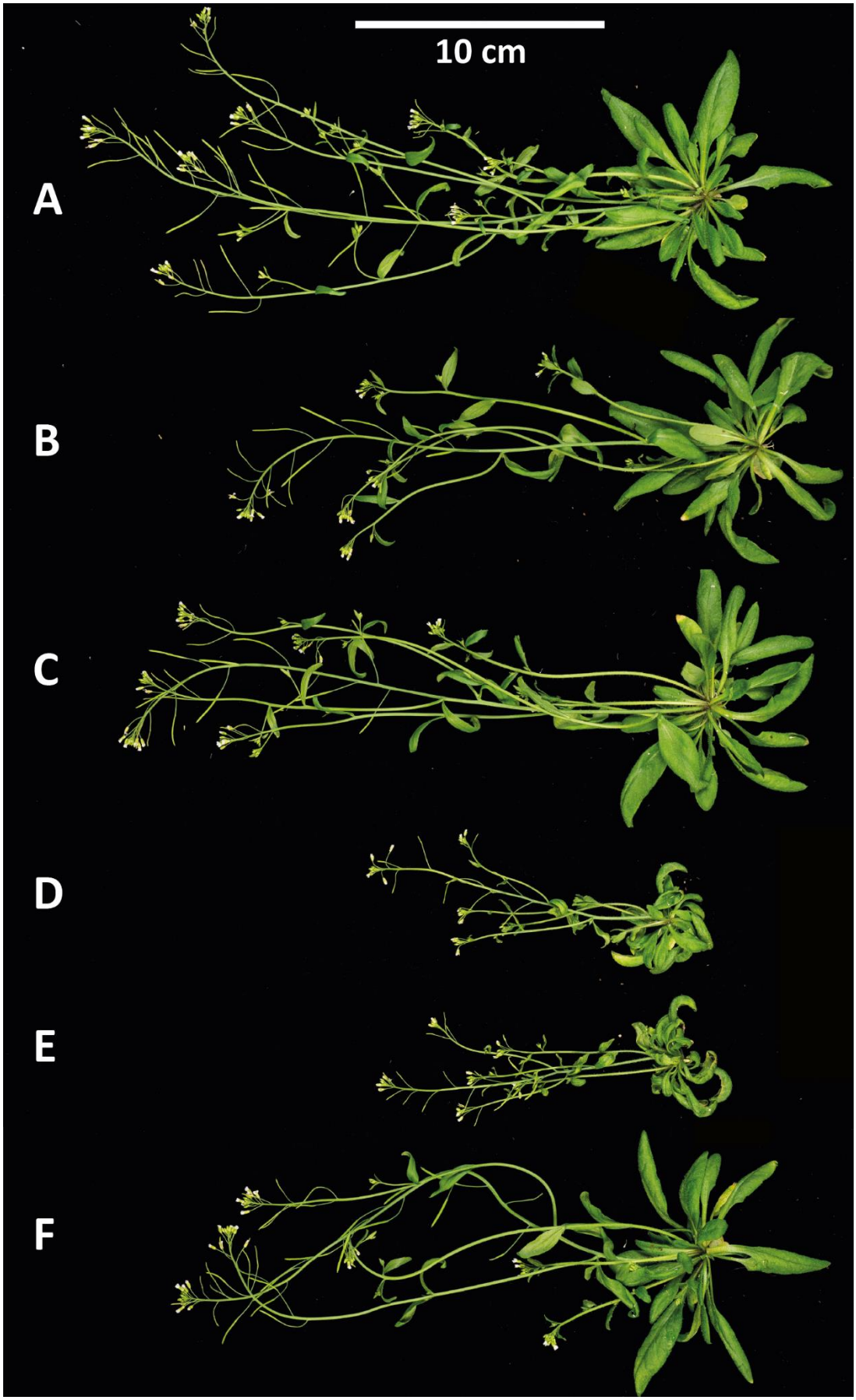
10 cm
A
B
C
D
E
F

Figure 4.1 – Growth of *mrs2* mutants on soil

mrs2 mutant lines were maintained on soil for five weeks, before aerial parts of representative individuals were removed, and images taken. A – Col-0, B – *mrs2-3* 1, C – *mrs2-3* 2, D – *mrs2-4* 1, E – *mrs2-4* 2, F – TKO.

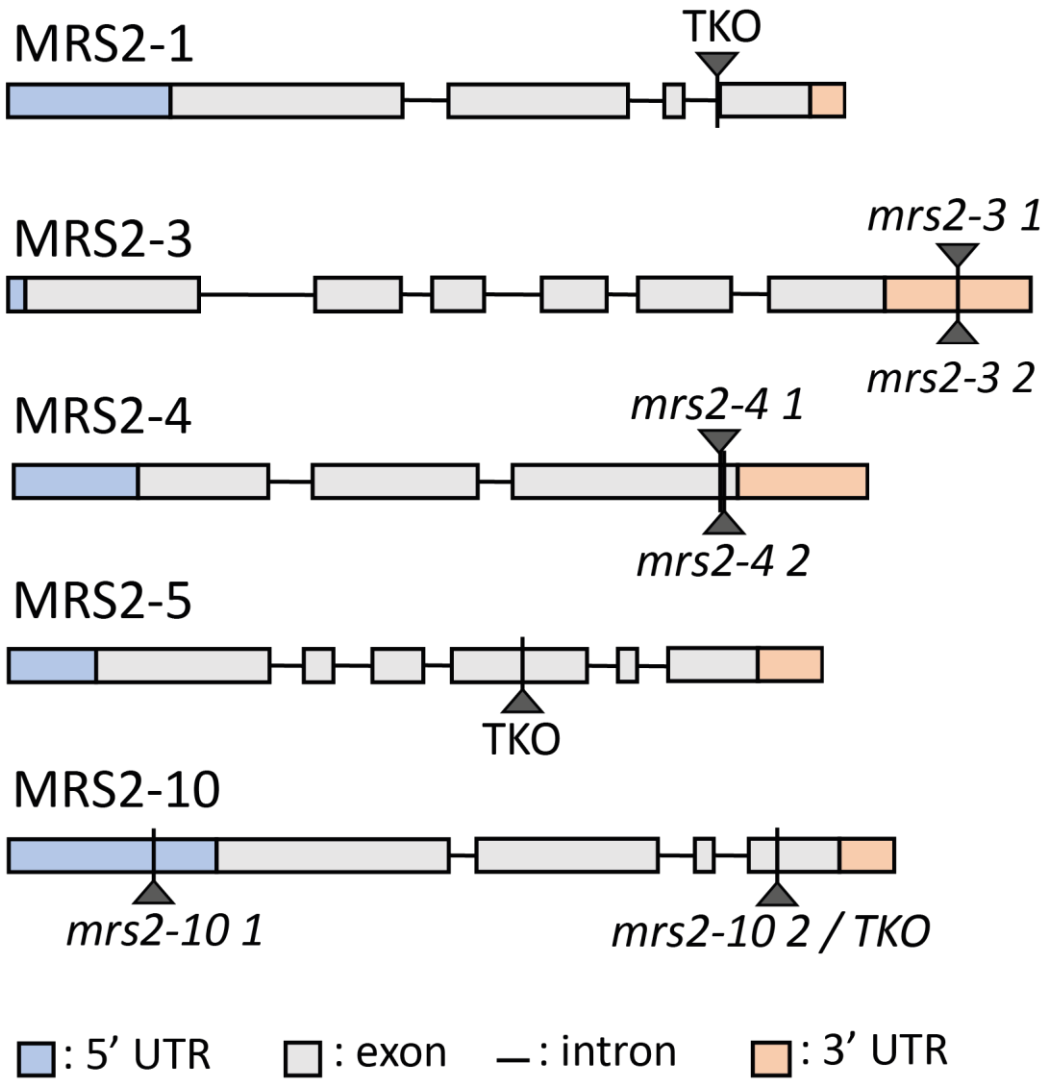

Figure 4.2 – Exact locations of T-DNA insertions present in *mrs2* mutant lines used in this work.

Representative gene models of *MRS2*s of interest are shown, giving the relative length of untranslated regions, introns and exons. Vertical lines with arrows give the location of the T-DNA insertion present in the line(s) given. Locations were ascertained by Sanger-sequencing using the LBb1.3-Ext primer, which anneals to the T-DNA insertion. **TKO** - Triple knock-out (*mrs2-1 mrs2-5 mrs2-10*).

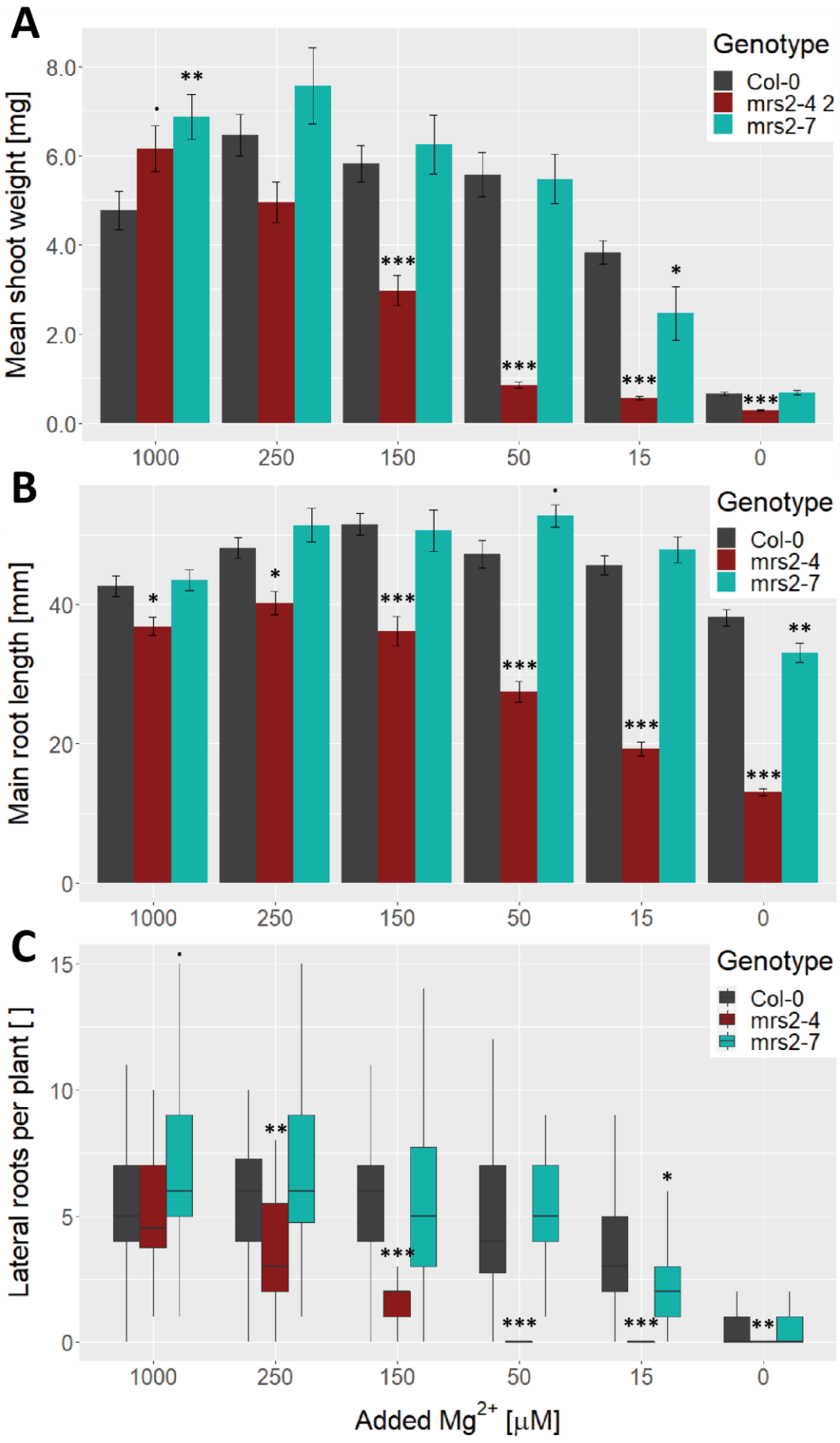
A
Mean shoot weight [mg]
8.0
6.0
4.0
2.0
0.0
Genotype
Col-0
mrs2-4 2
mrs2-7
1000
250
150
50
15
0
B
Main root length [mm]
40
20
0
Genotype
Col-0
mrs2-4
mrs2-7
C
Lateral roots per plant [ ]
15
10
5
0
Added Mg2+ [µM]

Figure 4.3 – Growth of WT *Arabidopsis* and *mrs2* mutants on media containing different Mg^{2+}-concentrations.

Seedlings of Col-0, *mrs2-4* 2 and *mrs2-7* were grown on agar plates containing HM made with washed agar, with different concentrations of added Mg^{2+}, until 14 DAG; various characteristics of the seedlings were determined. **A** – Mean shoot fresh weights of seedlings at 14 DAG. **B** – Main root length of seedlings at 10 DAG. **C** –numbers of lateral roots per plant at 10 DAG. Columns in **A** and **B** represent mean values (± SEM); Significant differences were determined using a two-way ANOVA followed by Tukey's HSD post-hoc test. Boxes in **C** represent first and third quartile, while the median is shown as a horizontal line. Significant differences between conditions in **C** were determined by a Dunn test, followed by a Kruskal-Wallis test. All data are from three independent replicates. Symbols above error bars denote significant differences between values observed for the respective line and Col-0 for the same Mg^{2+} concentration (▪ - $p < 0.1$; * - $p < 0.05$; ** - $p < 0.01$; *** - $p < 0.001$).

To quantify the observed phenotypes, relevant *mrs2* lines were grown on agar plates and shoot weight, main root length and number of lateral roots per seedling measured. First, *mrs2-4* 2 and *mrs2-7* were grown alongside Col-0 on plates containing different concentrations of Mg^{2+}. *mrs2-4* 2 was found to show growth impairments at much higher Mg^{2+}-concentrations than Col-0, with shoot weight being significantly reduced at or below 150 µM relative to Col-0 (**Figure 4.3 A**). Main root length was lower than for Col-0 at all concentrations; values followed a similar trend to that of WT plants, although they also started to decrease at higher concentrations (**Figure 4.3 B**). Numbers of lateral roots per plant were similar at 1000 µM Mg^{2+}, but decreased at 250 µM and below (**Figure 4.3 C**). The number of lateral roots per mm main root length showed the same trend as for Col-0, but the decrease observed for Col-0 on lower Mg^{2+} could be seen at much higher concentrations (**Figure 4.4**). For *mrs2-7*, reduced growth was only observed within a narrow range of concentrations, and reductions were comparatively small. Mean shoot weight was only reduced on 15 µM Mg^{2+}, as was the number of lateral roots per plant and the number of lateral roots per mm main root; main root length was only decreased relative to Col-0 on 0 µM Mg^{2+} (**Figure 4.3** and **4.4**).

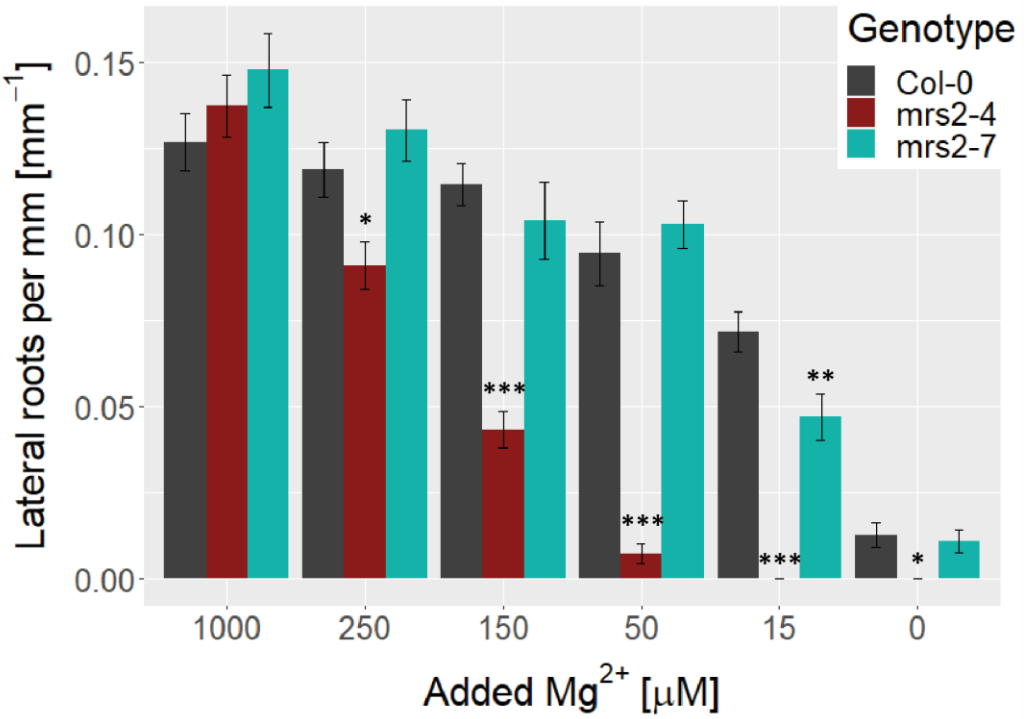

Figure 4.4 - Lateral roots per mm main root length for WT *Arabidopsis* and *mrs2* mutants grown on different Mg^{2+}-concentrations.

Seedlings of Col-0, *mrs2-4* 2 and *mrs2-7* were grown on agar plates containing HM made with washed agar, with different concentrations of added Mg^{2+}. At 10 DAG, length of the main root and number of lateral roots for each seedling were determined. The number of lateral roots was divided by the length of the main root, and values plotted grouped by concentration Columns represent mean values (± SEM) from three independent biological replicates. Significant differences between conditions were determined by two-way ANOVA followed by Tukey's HSD Symbols above error bars denote significant differences between values observed for the respective line and Col-0 for the same Mg^{2+} concentration (▪ - $p < 0.1$; * - $p < 0.05$; ** - $p < 0.01$; *** - $p < 0.001$).

It was deemed that phenotypes of remaining lines could be characterized by growing them on three different concentrations of Mg^{2+} only. A concentration of 100 µM added Mg^{2+} was chosen as the "low Mg^{2+}" condition, whereas 10 mM Mg^{2+} was used to test growth on excess Mg^{2+}. Results are summarized in **Figure 4.5**. Both *mrs2-3* mutant lines were found to accumulate significantly less biomass than WT on 1 mM Mg^{2+}, although only one of them (*mrs2-3* 2) also produced smaller seedlings on low Mg^{2+}. Seedlings of *mrs2-4* 1 were significantly smaller under all conditions, although the growth impairment on low and high Mg^{2+} was much more pronounced than on standard Mg^{2+}. Meanwhile, *mrs2-10* 1 showed significantly reduced growth on standard Mg^{2+} and increased growth on excess Mg^{2+}, while *mrs2-10* 2 did not; TKO showed growth impairment on low and standard Mg^{2+} and increased growth on excess Mg^{2+}.Although *mrs2-10* lines did not yield a consistent phenotype, TKO did differ significantly from WT plants in its growth. The TKO phenotype could likely be at least partially complemented by an *MRS2-10* transgene, since *mrs2-1 mrs2-5* mutant lines were previously found to show no obvious phenotypic differences from WT plants [136, 137]. It was therefore decided that the *mrs2-3*, *mrs2-4* and TKO lines were suitable for complementation with GFP-tagged expression constructs and subsequent localisation analysis.

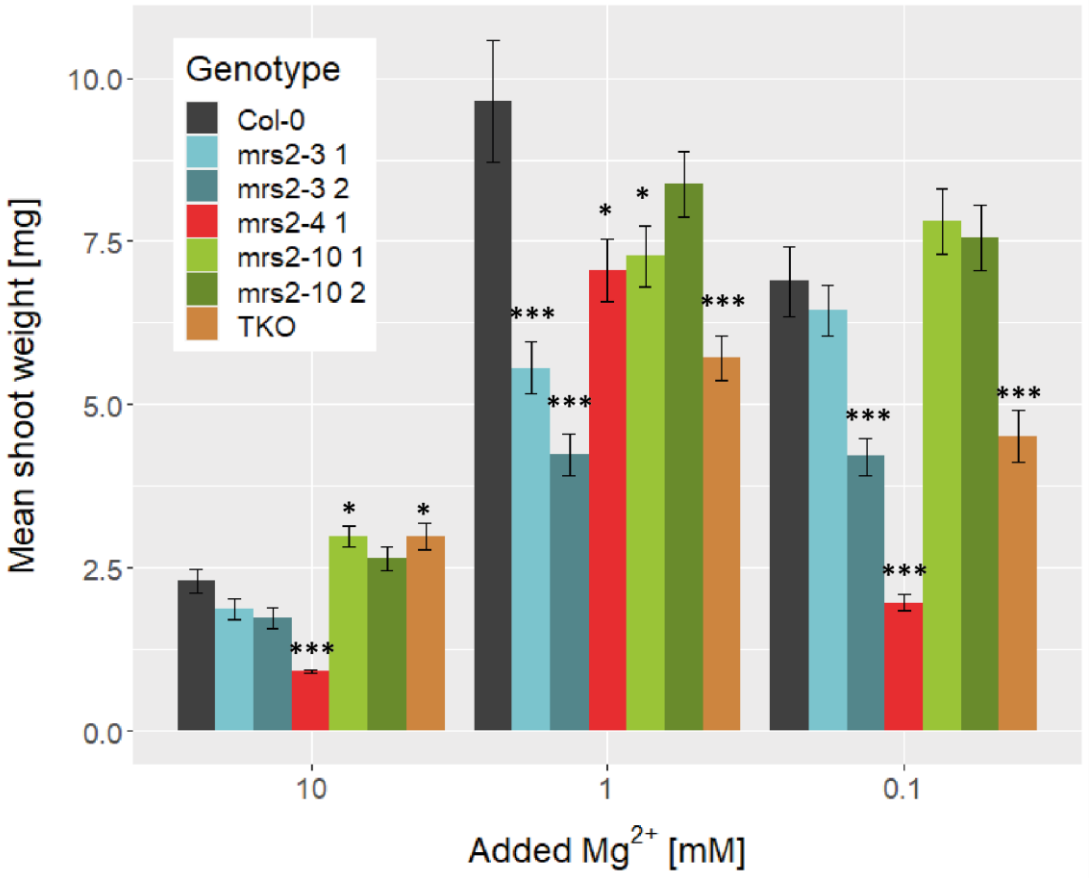

Figure 4.5 - Growth of WT *Arabidopsis* and *mrs2* mutants on different Mg^{2+}-concentrations.

Seedlings of Col-0 and various *mrs2* mutants were grown on agar plates containing HM made with unwashed agar, with different concentrations of added Mg^{2+}. At 14 DAG, shoot weight was determined for each seedling. Columns represent mean values (± SEM) from three independent biological replicates. Significant differences between conditions were determined by two-way ANOVA followed by Tukey's HSD. Symbols above error bars denote significant differences between values observed for the respective line and Col-0 for the same Mg^{2+} concentration (▪ - $p < 0.1$; * - $p < 0.05$; ** - $p < 0.01$; *** - $p < 0.001$). **TKO** - Triple knock-out (*mrs2-1 mrs2-5 mrs2-10*).

4.2.2 The phenotypes present in *mrs2-3* and *mrs2-4* can be partially complemented by GFP-tagged expression constructs

To determine the subcellular localisations of MRS2-3, MRS2-4 and MRS2-10, GFP-tagged expression constructs were introduced into the respective mutant lines. Cloning and transformation of *mrs2* mutant lines was carried out according to **Chapter 2**, **Section 2.7**. Coding sequences for each chosen MRS2 family member were amplified from cDNA prepared from WT seedlings, while promoter and terminator regions were amplified from genomic DNA, with sequences chosen being roughly equivalent to the sequences in the gene models from TAIR. For *MRS2-3*, the promoter region consisted of the 1151 bp immediately before the start codon; for *MRS2-4*, the length was 905 bp; for *MRS2-10*, 832 bp. p*MRS2-3*::*MRS2-3*::eGFP and p*MRS2-10*::*MRS2-10*::eGFP were cloned successfully, but for p*MRS2-4*::*MRS2-4*::eGFP, the correct sequence could not be obtained. Instead, the pMDC107 plasmid, containing the genomic sequence of *MRS2-4*, including the 2.5 kb upstream of the start codon, was obtained courtesy of Takehiro Kamiya at the University of Tokyo [103]. For each of the three plasmids used, transformants exhibiting the correct antibiotic resistance could be obtained. However, while GFP expression could be seen in *mrs2-3* and *mrs2-4* plants transformed with the respective *MRS2::GFP* constructs (referred to as *mrs2-3* + and *mrs2-4* +, respectively) (**Figure 4.6**), no GFP fluorescence could be detected in any of the individuals transformed with p*MRS2-10*::*MRS2-10*::eGFP.

Next, homozygous transformant lines showing uniform transgene expression were raised for *mrs2-3* + and *mrs2-4* +, resulting in the lines *mrs2-3* 1 + 6-4, *mrs2-3* 2 + 1-4, *mrs2-4* 1 + 3-4 and *mrs2-4* 2 + 3-4. To determine whether the previously observed phenotypes were complemented by introduction of the transgenes, two phenotyping experiments were carried out, comparing growth of WT plants to mutant lines and transformed mutant lines. The experimental conditions were similar to those used previously, however, the "excess Mg^{2+}" condition was changed to 5 mM Mg^{2+} instead of 10 mM, since 10 mM MgCl caused excessive growth impairment in WT plants. Results of the complementation experiments are shown in **Figure 4.7**.

Additionally, growth of the lines in question on soil was compared and images of plants taken, which are shown in **Figure 4.8** and **Figure 4.9**.

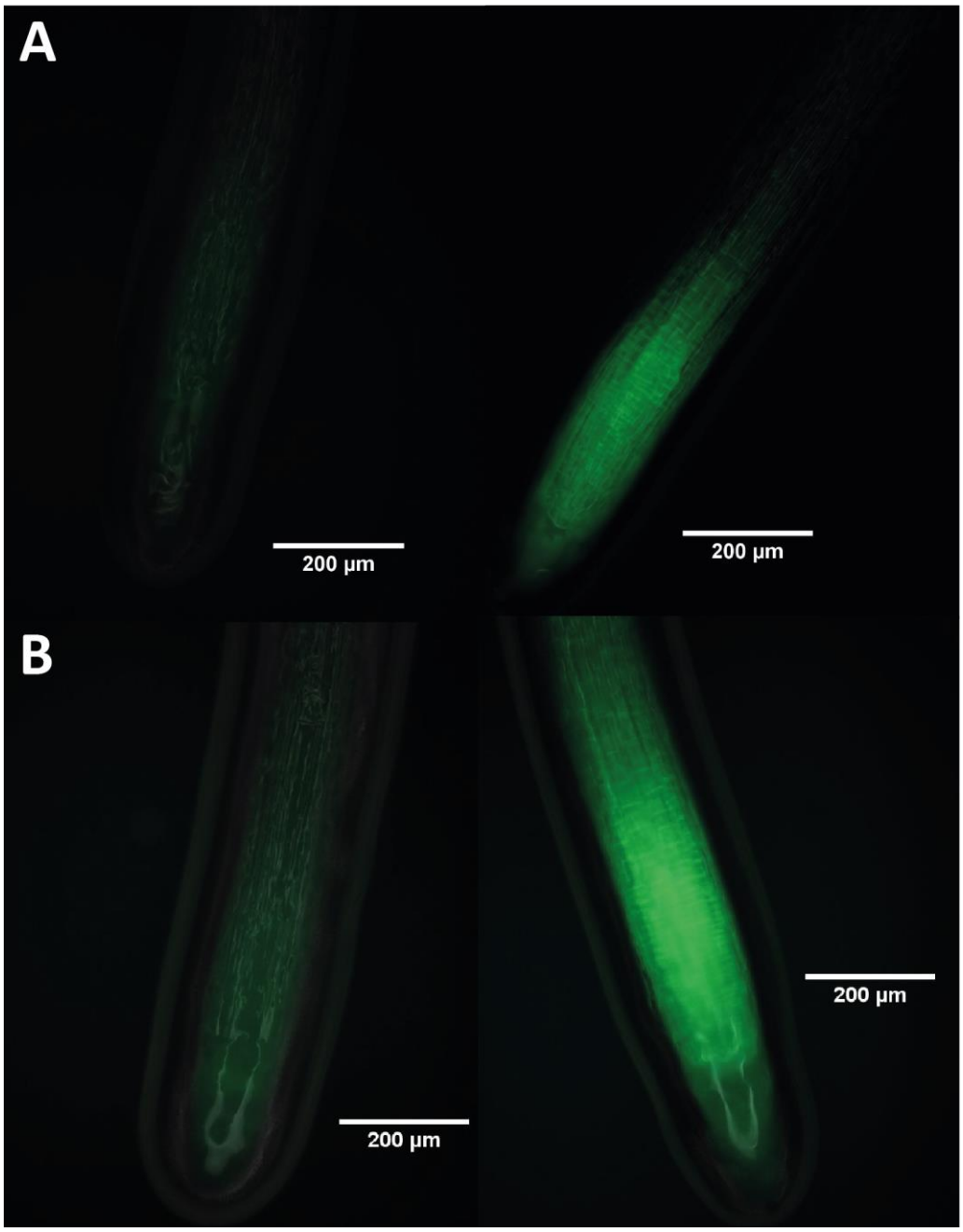

Figure 4.6 – GFP expression in *mrs2* lines transformed with GFP-tagged *MRS2* constructs

Seedlings of Col-0 and transformed lines were grown under the same conditions and images taken using a fluorescence microscope. BF images and images of GFP fluorescence were taken separately using the same conditions and merged. **A** – Col-0 (left) compared to *mrs2-3* 1 + 6-4. **B** – Col-0 (left) compared to *mrs2-4* 2 + 3-4.

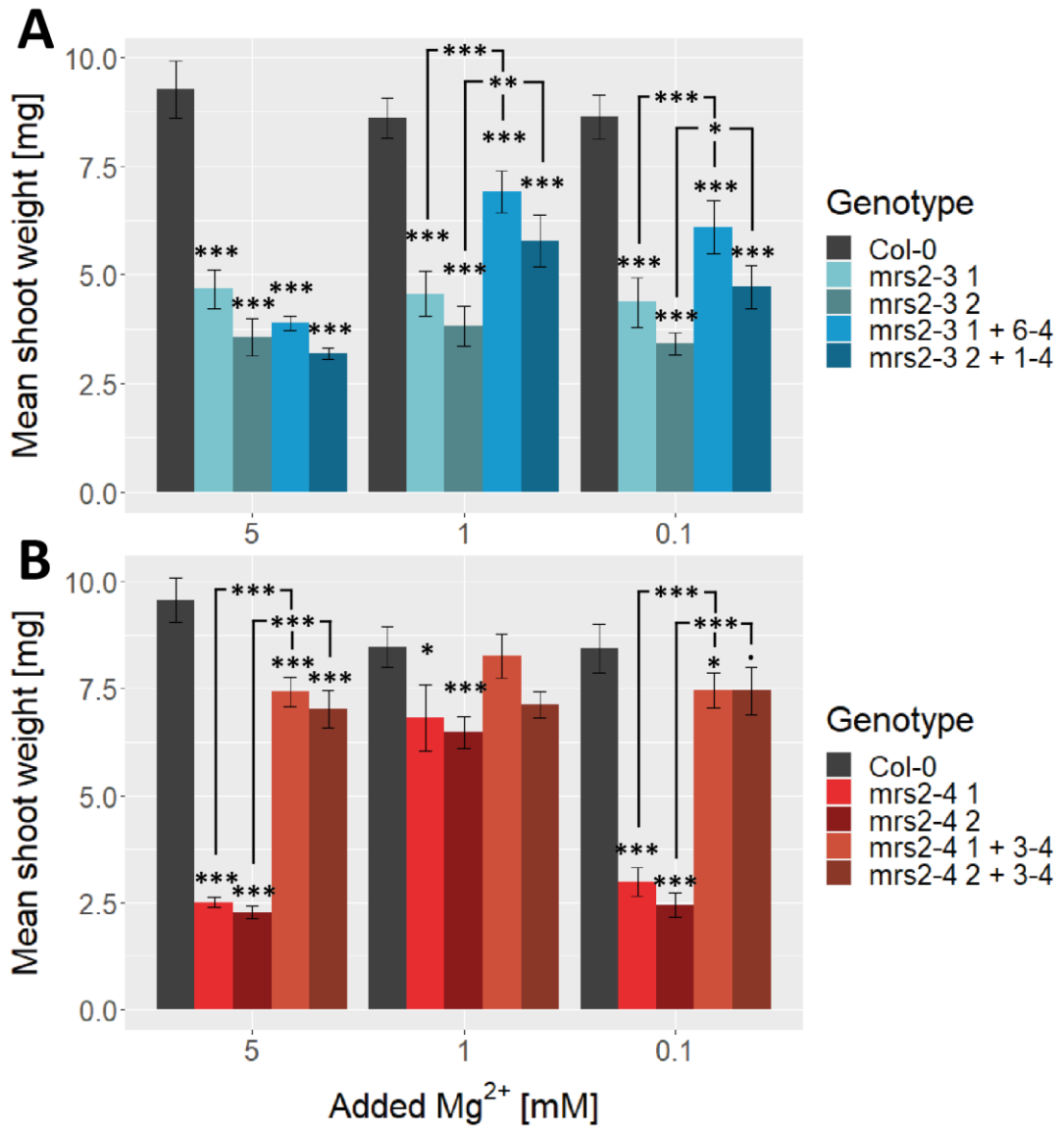

Figure 4.7 – Growth of *mrs2* mutant lines and lines transformed with GFP tagged *MRS2* constructs on different Mg^{2+}-concentrations

Seedlings of Col-0, *mrs2* mutants and transformed lines, were grown on agar plates containing HM made with unwashed agar, with different concentrations of added Mg^{2+}. At 14 DAG, shoot weight was determined for all seedlings from one plate at a time and average shoot weights determined. A – *mrs2-3* mutants and transformants. **B** – *mrs2-4* mutants and transformants. Columns represent mean values (± SEM) from three independent biological replicates. Significant differences between conditions were determined by two-way ANOVA followed by Tukey's HSD. Symbols above error bars denote significant differences between values observed for the respective line and Col-0 for the same Mg^{2+} concentration; brackets represent pairwise comparisons between mutant lines and transformed lines (▪ - $p < 0.1$; * - $p < 0.05$; ** - $p < 0.01$; *** - $p < 0.001$).

Both *mrs2-3* and *mrs2-3* + seedlings accumulated less biomass than WT seedlings under all conditions tested, however, on low and standard Mg^{2+}, transformed lines were significantly larger than mutant lines, implying that introduction of the transgene had beneficial effects on the mutants, likely by partially complementing the *mrs2-3* phenotype. On excess Mg^{2+}, both transformant lines were smaller than the respective mutant lines, although these differences were not statistically significant (**Figure 4.7 A**). After five weeks of growth on soil, *mrs2-3* + lines appeared to be smaller than both *mrs2-3* and WT plants as well, implying a detrimental effect of the transgene under certain conditions or at certain points in development. Despite this, both the mutant and transformed lines developed fully, were fertile, reached similar sizes at maturity, and produced roughly the same number of seeds as WT plants (**Figure 4.8**).

As can be seen in **Figure 4.7 B**, *mrs2-4* lines behaved similarly in this experiment as in the previous phenotyping experiments, with reduced shoot fresh weight at all Mg^{2+}-concentrations, but most significant reductions at low and excess Mg^{2+}, with mutant shoots less than 1/3 the weight of WT shoots under both of these conditions. While *mrs2-4* + shoots were still significantly smaller than WT shoots on low and excess Mg^{2+}, the difference between WT and transformed lines' shoot fresh weights was not significant at standard Mg^{2+}. Both *mrs2-4* + lines produced shoots of roughly three times the weight of the respective *mrs2-4* lines, closer to WT plants than the mutant plants the lines were derived from. Therefore, based on measurement of shoot biomass, complementation can be considered nearly complete. Similarly, *mrs2-4* + lines developed much better than *mrs2-4* lines on soil, with larger rosettes and bolts, as well as more seeds produced. Rosette leaves were no longer "curled" as in the mutant lines. Compared to WT plants, *mrs2-4* + lines developed slightly more and longer bolts, but slightly fewer and/or smaller rosette leaves than Col-0 (**Figure 4.9**).

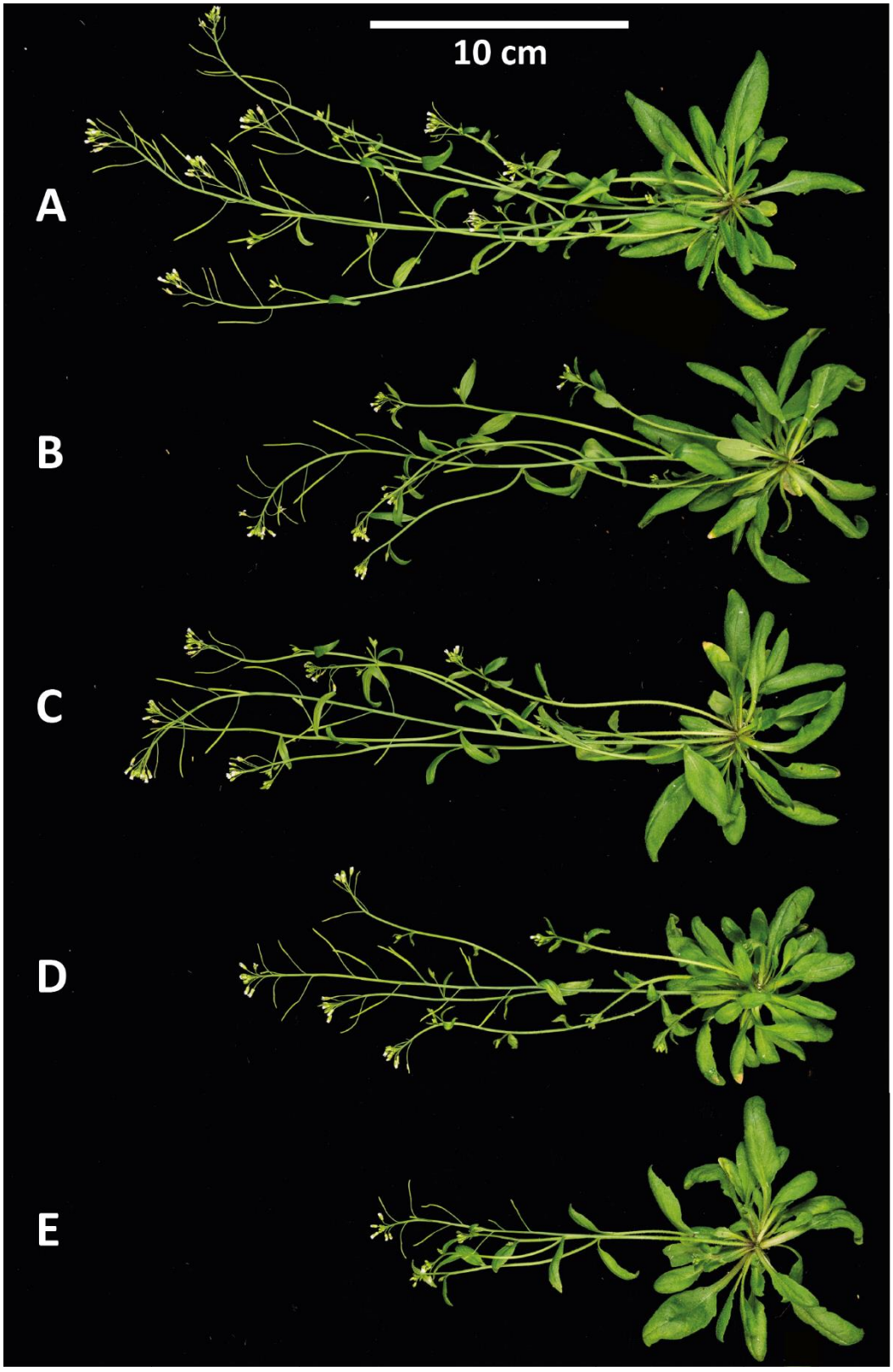

Figure 4.8 – Growth of *mrs2-3* and *mrs2-3* + lines on soil

Plants were maintained on soil for five weeks, before aerial parts of representative individuals were removed, and images taken. **A** – Col-0, **B** – *mrs2-3* 1, **C** – *mrs2-3* 2, **D** – *mrs2-3* 1 + 5-1, **E** – *mrs2-3* 1 + *6-4*, **F** – *mrs2-3 2* + 1-4.

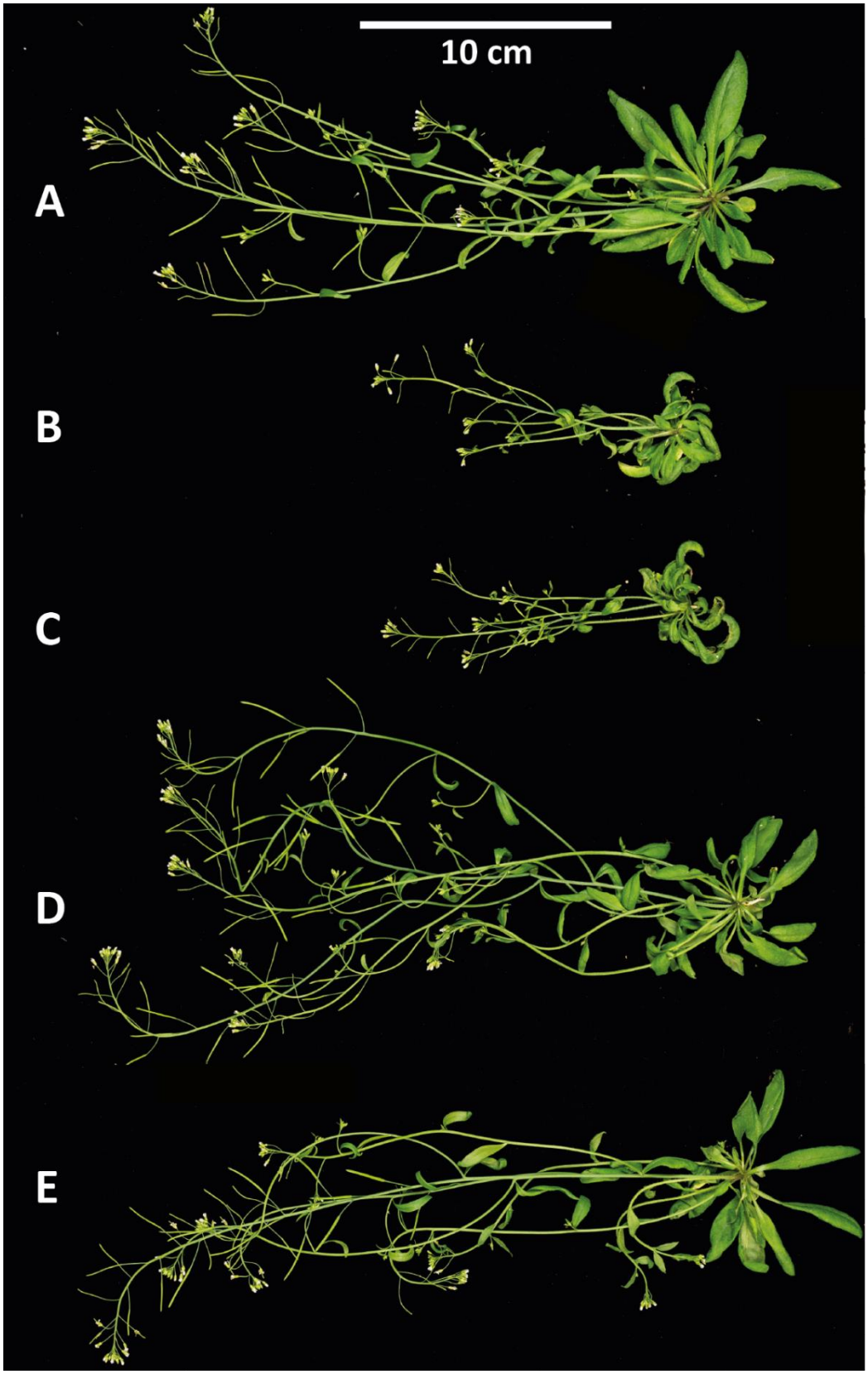

Figure 4.9 – Growth of *mrs2-4* and *mrs2-4* + lines on soil

Plants were maintained on soil for five weeks, before aerial parts of representative individuals were removed, and images taken. **A** – Col-0, **B** – *mrs2-4* 1, **C** – *mrs2-4* 2, **D** – *mrs2-4* 1 + 3-4, **E** – *mrs2-4* 2 + 3-4

Finally, to investigate both the impact of the T-DNA insertions in *mrs2-3* and *mrs2-4* lines and the transgenes in *mrs2-3* + and *mrs2-4* + lines on transcript abundances of *MRS2-3* and *MRS2-4*, respectively, qRT-PCR analysis was carried out.

Since the T-DNA insertions present in *mrs2-3* lines also lie within 500 bp of the start of the gene model of AT3G19650, this transcript was included in the analysis together with *MRS2-3*, to exclude the chance of a disruption of this transcript being responsible for the phenotypes observed for *mrs2-3* lines. Results are summarized in **Figure 4.10 A**. No difference in AT3G19650 transcript abundance could be observed between WT and *mrs2-3* or *mrs2-3* + lines. Although the difference in *MRS2-3* transcript abundance between WT and *mrs2-3* lines was not significant, confirming that these mutants did not constitute KOs for MRS2-3, the abundance observed for *mrs2-3* 1 was roughly two times as high as for Col-0, and three times for *mrs2-3* 2. *MRS2-3* transcript abundance in *mrs2-3* 1 + 6-4 was roughly six times that in Col-0, and *mrs2-3* 2 + 1-4 showed significantly increased *MRS2-3* abundance at 13-fold, demonstrating strong expression of the transgene beyond WT levels in these lines.

In *mrs2-4* 1 & 2, no expression of full-length *MRS2-4* could be detected (C_t - values > 30 in all samples). Expression was restored partially in *mrs2-4* 1 + 3-4, at about 0.15-fold the levels of WT expression, while in *mrs2-4* 2 + 3-4, expression was significantly greater than in Col-0 at 1.5-fold (**Figure 4.10 B**). These results are consistent with GFP-fluorescence observed during microscopy, which appeared dimmer in *mrs2-4* 1 + 3-4 than in *mrs2-3* 2 + 3-4.

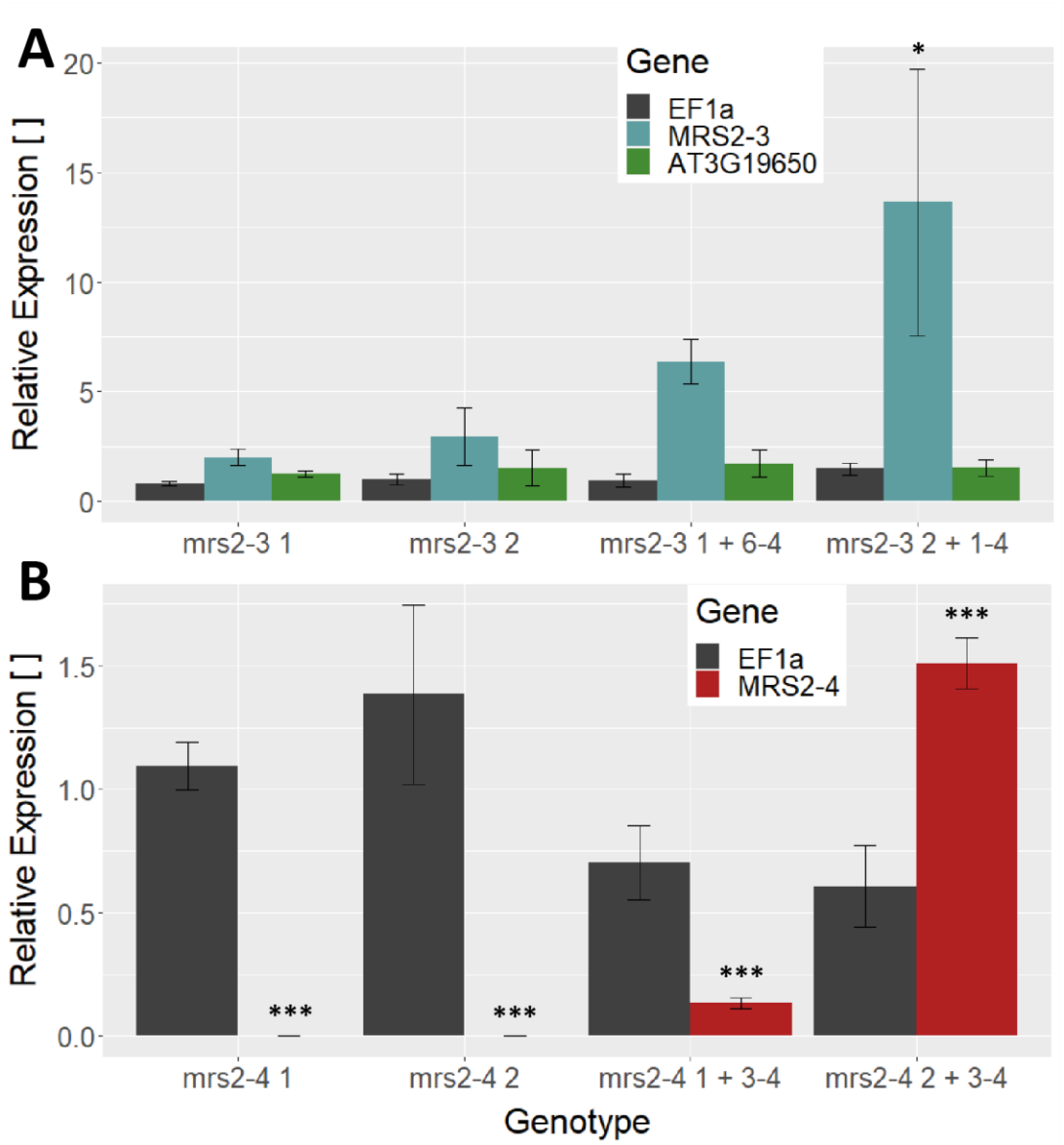

Figure 4.10 – Abundance of transcripts in *mrs2* lines and GFP-tagged lines

Gene expression in seedlings of Col-0, *mrs2* mutant lines and transformed lines was determined for the respective MRS2 transporter. AT3G19650 was included to ensure its expression was not influenced by the T-DNA insertions present in the *mrs2-3* lines. **A** - *mrs2-3* mutants and transformants. **B** – *mrs2-4* mutants and transformants. Expression levels for all transcripts were normalized to expression of ACTIN2 and expression of the respective transcripts in Col-0 Columns represent mean values (± SEM) from three independent biological replicates. Significant differences between conditions were determined by two-way ANOVA followed by Tukey's HSD. Symbols above error bars denote significant differences between values observed for the respective line and Col-0 (▪ - $p < 0.1$; * - $p < 0.05$; ** - $p < 0.01$; *** - $p < 0.001$).

4.2.3 MRS2-4::eGFP and MRS2-3::eGFP appear to localize to the cytoplasm and/or endomembrane system of the *A. thaliana* root tip

Both during fluorescence microscopy and confocal microscopy, GFP expression in *mrs2-3* + and *mrs2-4* + lines was observed primarily within the root tip, with expression decreasing beyond the maturation zone and becoming difficult to distinguish from autofluorescence. No GFP expression could be observed in shoots of seedlings of ages up to 14 DAG for either MRS2-3::eGFP or MRS2-4::eGFP. Efforts to determine subcellular localisations of MRS2-3 and MRS2-4 were therefore focussed on the root tip. In both cases, the FM™ 4-64 dye was used as a counterstain, to mark plasma membranes and allow determination of the localisation of MRS2-3::GFP and MRS2-4::GFP by comparison with the localisation of FM4-64.

To determine the localisation of MRS2-4::GFP, two complementary approaches were used: A Z-stack of an area close to the root tip was taken and a deconvolution algorithm applied to the image series in order to generate a high-resolution image with minimal interference (**Figure 4.11**); a wavelength-scan of a similar area was taken and a linear unmixing algorithm used to separate the emission of eGFP from that of FM™ 4-64, as well as background autofluorescence (**Figure 4.12**) (see **Chapter 2**, **Section 2.6.3**). In both cases, GFP fluorescence could be seen in the intracellular space; however, fluoresce was especially strong at the plasma membrane, co-localising with FM™ 4-64 fluorescence. This PM localisation appears to be especially pronounced within specific cell files, and within transverse cell membranes (**Figure 4.11 B**, **Figure 4.12**).

The localisation of MRS2-3::GFP was determined via the second method only, as shown in **Figure 4.13**. The GFP signal in these lines was stronger than in *mrs2-4* + lines, reflecting the greater expression of MRS2-3, and fluorescence could be seen in the intracellular space as well, showing the characteristic pattern of an ER-localized protein (**Figure 4.13**). Despite this, areas of especially strong fluorescence also co-localized with FM™ 4-64 fluorescence in plasma membranes of some cells, especially transverse cell membranes (white arrows in **Figure 4.13 C**).

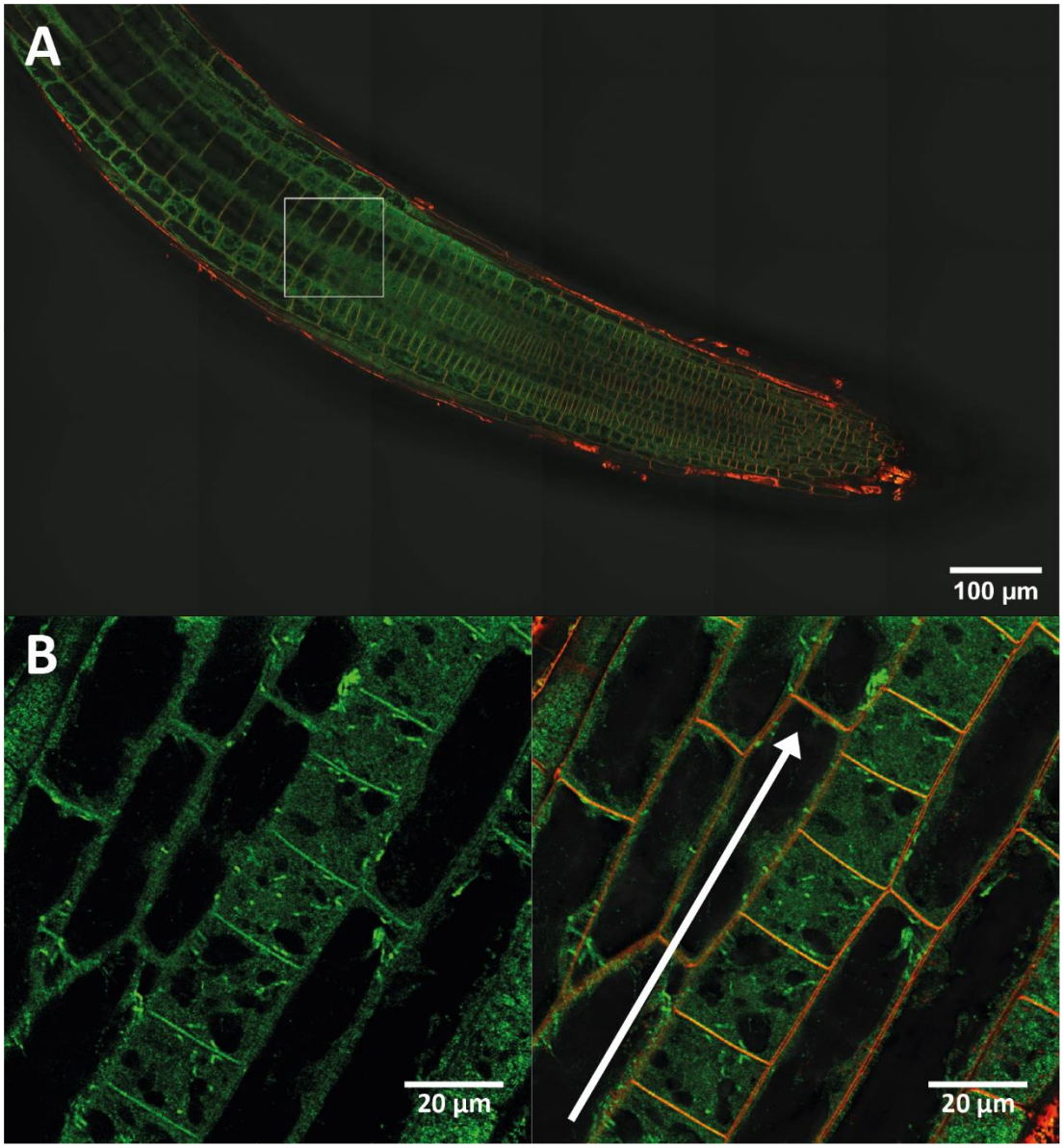

Figure 4.11 – GFP localisation in *mrs2-4* 2 + 3-4, after image deconvolution. Seedlings were grown on HM until 14 DAG, then stained with FM™ 4-64 dye. Images were taken using a confocal microscope. **A** – Tile-scan of the root tip area. **B** – Images of the area within the white square in **A**, at higher magnification. A Z-stack was taken, before applying a deconvolution algorithm. GFP fluorescence only (left); GFP and FM™ 4-64 fluorescence (right). The white arrow in the right image denotes the direction from the root tip towards the shoot.

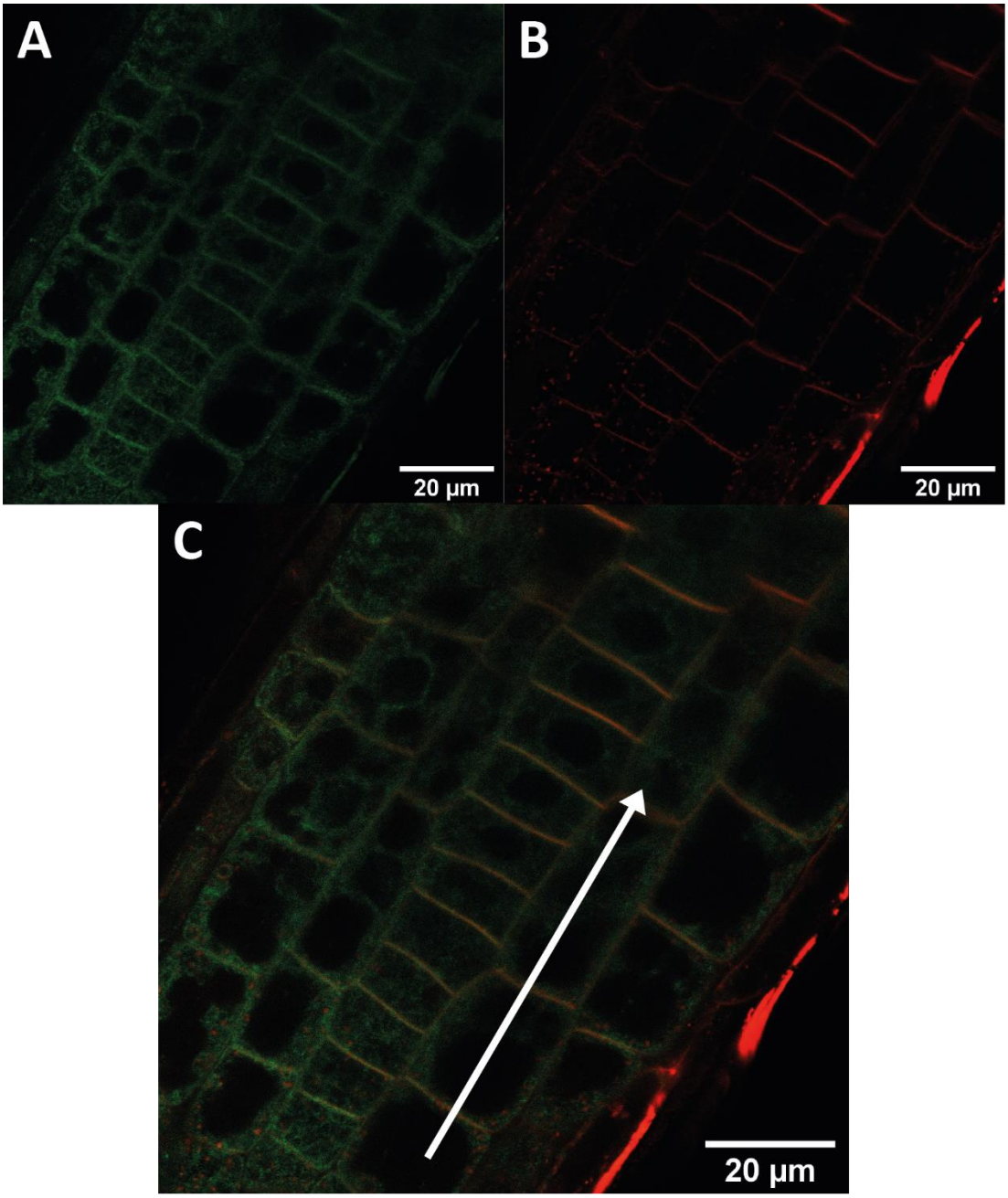

Figure 4.12 – GFP localisation in *mrs2-4* 2 + 3-4, after linear unmixing.
Seedlings were grown on HM until 14 DAG, then stained with FM™ 4-64 dye. Images were taken using a confocal microscope, as a lambda-scan. GFP fluorescence, FM™ 4-64 fluorescence, and autofluorescence signals were separated via a linear unmixing algorithm. **A** – GFP fluorescence. **B** - FM™ 4-64 fluorescence. **C** – GFP and FM™ 4-64 fluorescence, overlayed. The white arrow denotes the direction from the root tip towards the shoot.

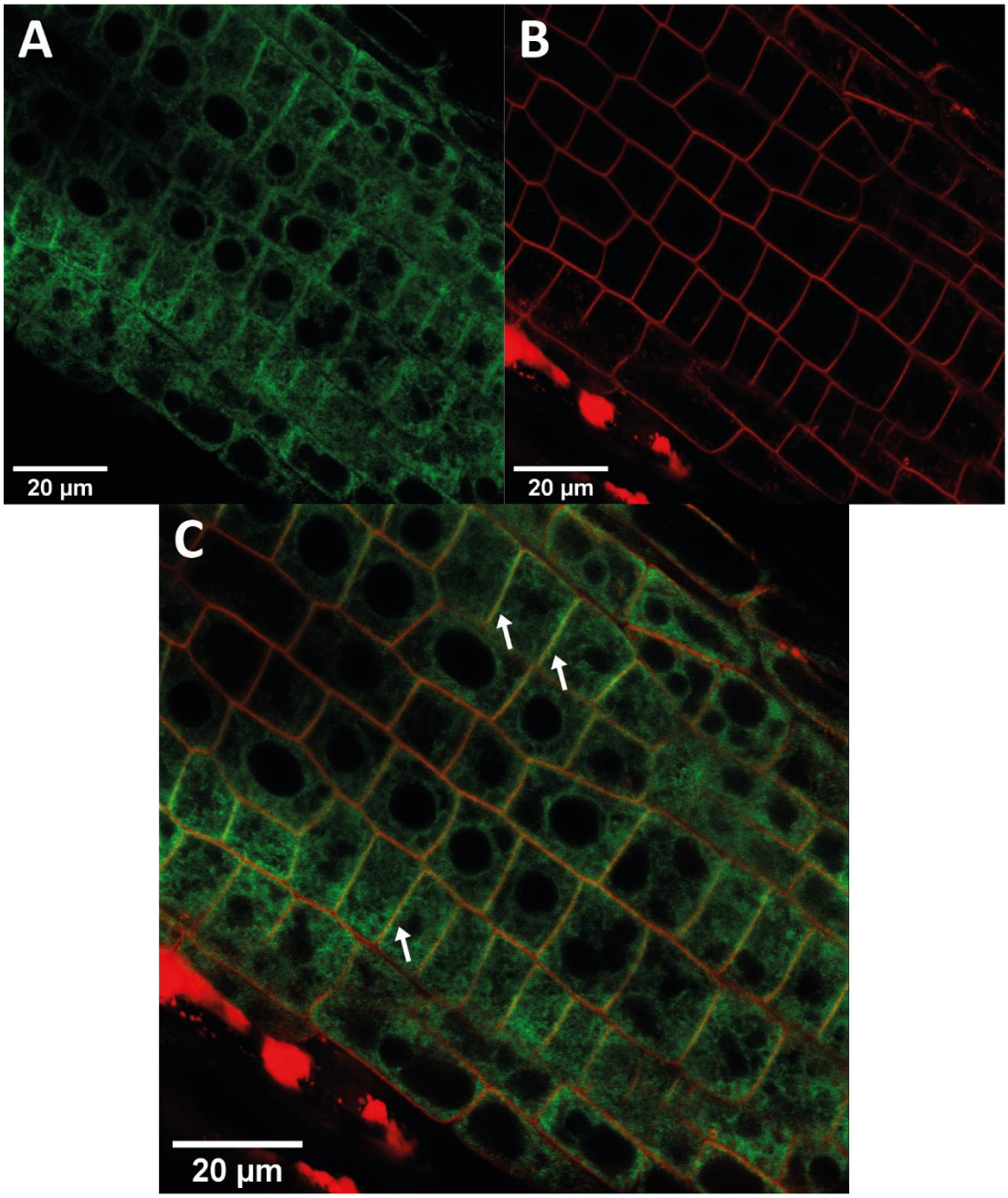

Figure 4.13 – GFP localisation in *mrs2-3* 2 + 1-4, after linear unmixing.
Seedlings were grown on HM until 14 DAG, then stained with FM™ 4-64 dye. Images were taken using a confocal microscope, as a lambda-scan. GFP fluorescence, FM™ 4-64 fluorescence, and autofluorescence signals were separated via a linear unmixing algorithm. **A** – GFP fluorescence. **B** - FM™ 4-64 fluorescence. **C** – GFP and FM™ 4-64 fluorescence, overlayed. White arrows indicate overlap between GFP and FM™ 4-64 fluorescence.

4.3 Discussion

4.3.1 Phenotypes observed for most *mrs2* mutant lines tested are in accordance with previous reports

SALK T-DNA insertion lines were obtained for all the *MRS2* family genes present and functional in *Arabidopsis* ecotype Col-0 over the course of this project. Where possible, lines that had not been previously characterized were chosen, to ensure that phenotypes are consistent across different KO lines for the same gene. For *MRS2*s causing sterility phenotypes specifically, weaker alleles could lead to mutant lines with distinct, complementable phenotypes that could nevertheless be propagated more easily.

Lines that were not previously characterized include *mrs2-2* (SALK_082081C), *mrs2-3* 1 (SALK_080443), *mrs2-3* 2 (SALK_201976C), *mrs2-7* (SALK_127086C), *mrs2-10* 1 (SALK_006528C) and *mrs2-11* (SALK_028422C). *mrs2-4* 1 (SALK_203866C) was un-characterized when it was obtained, but has since been described [161]. For almost all of the mutant lines used, phenotypes were similar to those previously described. Few to no seeds could be obtained for *mrs2-2* [140] and *mrs2-6* [153]. Reduced pigmentation and early leaf senescence were observed for *mrs2-11* [139, 157]. No observable phenotype could be seen for *mrs2-1*, *mrs2-5* or *mrs2-10* 2 [137]. *mrs2-7* exhibited sensitivity to low Mg^{2+}-concentrations [103, 136, 165], although the phenotype appeared to be comparatively mild. Both *mrs2-4* lines were found to be sensitive to both high and low Mg^{2+} [103, 138, 165].

The TKO line seemingly did not exhibit the low-Mg^{2+}-sensitive phenotype originally associated with it; however, both the control Mg^{2+}- and Ca^{2+}-concentration used in the experiment in **Figure 4.5** were lower than the standard concentrations from the original publication by Lenz *et al.* [137]. The “low” Mg^{2+}-concentration used in this work, however, was higher than the concentrations causing the more extreme growth impairment phenotypes in Lenz *et al*. Therefore, it is likely that the similar levels of growth impairment observed for TKO on 1 mM and 0.1 mM Mg^{2+} would resolve into growth similar to WT and strong growth impairment if the concentrations were exchanged for 1.5 mM and 50 µM, for example.

Another interesting result from the experiment summarized in **Figure 4.5** is the significantly increased growth of *mrs2-10* 1 and TKO relative to WT plants at high Mg^{2+}. It would stand to reason that KO of a PM-localized [121] Mg^{2+}-transporter expressed in roots [136] could confer protection from excess Mg^{2+}; however, this was not observed in Lenz *et al*. [137] or Visscher *et al*., [246]. This could be due to any number of factors, including the different Ca^{2+}-concentrations, the use of $MgSO_4$ rather than $MgCl_2$ to induce Mg^{2+} toxicity in Visscher *et al*., the light regime, and, most importantly, the growth medium. Growth under hydroponic conditions, as in Lenz *et al*. and Visscher *et al*. and growth on agar plates do not always correlate well. It is questionable which system is more similar to "natural" conditions, and therefore whether the conclusion that KO of *MRS2-10* is not protective against Mg^{2+} toxicity needs to be revised.

4.3.2 *mrs2-3* lines used in this work most likely represent partial knockouts

The biggest difference between previously-reported phenotypes and those observed in this assay was that seen for *mrs2-3* 1 and *mrs2-3* 2. There is only one publication investigating the role of MRS2-3 specifically, by Li *et al*. [154]. The authors used plants of the Landsberg (Ler) background, rather than Col-0, which left open the possibility for different results in Col-0 plants to be due to different functions of MRS2-3 in these ecotypes, or different levels of redundancy with other MRS2s.

When *mrs2-3* 1 and *mrs2-3* 2 were obtained, both lines initially produced few seeds, and offspring varied widely with respect to growth, which was initially interpreted as either the effects of bad seed quality or a stochastic phenotype, potentially caused by an incomplete KO. Observed phenotypes stabilized after several generations to give the slight to moderate growth impairment that can be seen in **Figure 4.5** and **Figure 4.7 A**. During qRT-PCR for *MRS2-3* transcript abundance, no working primers spanning the T-DNA insertion site could be obtained, confirming that the T-DNA insertions in these lines are present at the end of the untranslated region, potentially in a part of the gene that is not present in mature mRNA.

qRT-PCR had to be carried out using primers binding to the transcript before the T-DNA insertion, with results suggesting roughly 2-fold and 3.5-fold increased transcript abundances in *mrs2-3* 1 and *mrs2-3* 2, respectively (**Figure 4.10 A**). When qRT-PCR for *MRS2-4* was carried out using primers binding to the transcript before the T-DNA insertion in the sequence, transcript abundance was determined to be increased roughly two-fold in both *mrs2-4* mutants as well (data not shown). When primers were designed to bind after the T-DNA insertion, full-length transcript was found to be absent in the mutants (**Figure 4.10 B**). Since the T-DNA insertions present in *mrs2-4* 1 and -2 lie within the coding region, it is very unlikely that any amount of functional protein is produced in these lines. Although this cannot be said for *mrs2*-3 lines, increased mRNA levels in *mrs2-3* mutants nevertheless indicate a disturbance in normal expression. A change in the last few bases of the 3' UTR could lead to disruption of the terminator sequence and production of an abnormally long transcript, which takes longer to be degraded. An abnormally long transcript, or one with a change in the last few bases in general, could lead to improper translation termination, which could increase transcript levels by interfering with normal degradation of mRNA while at the same time causing a reduction in protein levels or production of a non-functional protein. In either case, the observable phenotypes present in these lines are unlikely to be caused by anything other than a disruption in *mrs2-3* protein levels. SALK T-DNA insertion lines often contain multiple T-DNA insertions [191], but the use of two different T-DNA insertion lines all but excludes the possibility of other insertions causing the observed phenotypes instead of the ones within *MRS2-3*, since both of the lines used would have to contain other insertions causing similar phenotypes. The insertions present in both lines are close to the gene model of another gene, AT3G19650, but transcript abundance of this gene was similar in both mutant lines and both *mrs2-3* + transformant lines tested (**Figure 4.10 A**), therefore the possibility of disruptions in this gene being responsible for the observed phenotypes can be excluded as well. Finally, although complementation in *mrs2-3* + lines is by no means complete, growth is still significantly restored compared to the original mutant lines (**Figure 4.7 A**), implying that the growth impairment in *mrs2-3* lines is due to disruption of *MRS2-3*.

To determine whether the phenotypes observed for *mrs2-3* 1 and *mrs2-3* 2 are genuinely caused by reduced MRS2-3 protein levels, assays testing protein abundance directly are necessary, such as western-blots or mass spectrometry; unfortunately, this was not possible within the scope of this project. Therefore, although the observed phenotypes are likely to be caused by disruption of *MRS2-3*, this remains a hypothesis rather than a certainty.

4.3.3 The phenotypes of *mrs2-3* lines may represent epigenetic adaptations

MRS2-3 is most well-known for its role in pollen development, with even heterozygous *mrs2-3* lines showing reduced male fertility due to abortion of pollen development; its role in this process has been relatively well-characterized. This same quality has made additional work on this MRS2 family member in intact *Arabidopsis* difficult, since it has not been possible to obtain or maintain homozygous mutants [154]. However, GUS fusion constructs show that *MRS2-3* is also expressed in the vasculature of both roots and leaves of *Arabidopsis* seedlings, including the root tip [136, 154]. On this basis, a role of MRS2-3 in Mg^{2+}-transport from root to shoot and/or within leaves, overshadowed by its role in pollen development, cannot be excluded. Over the course of this work, expression of MRS2-3::eGFP in leaves could not be confirmed, potentially due to absorption of emitted light by chlorophyll in the cell layers around the vasculature. Expression was found within the root tip though, including the differentiation and elongation zones, seemingly gradually decreasing further away from the root tip, potentially also due to greater thickness of non-expressing tissue above. A role of MRS2-3 in Mg^{2+}-transport could explain the phenotypes observed for *mrs2-3* mutants in this work. It is possible that the T-DNA insertions present in these lines are less detrimental to MRS2-3 expression within male reproductive organs than to its expression within vascular tissues, impairing Mg^{2+}-transport from root to shoot and concomitantly reducing growth without causing sterility. Such a role would throw new light on this transporter, however additional experiments are needed to confirm this; perhaps measurements of ion concentrations within *mrs2-3* and *mrs2-3* + lines, or ion uptake measurements similar to those carried out by Ogura *et al*. [166].

However, recent research by Xu *et al*. [161] highlights another explanation for the phenotype of *mrs2-3* lines (see **Chapter 1**, **Section 1.3.4**). If the fertility of *mrs2-3* mutant can be restored by slower development, similar to *mrs2-6*, and the *mrs2-3* lines investigated here represent partial KOs, this could explain the stochastic slow growth/infertility phenotype initially observed for these lines. Fast-growing individuals would produce no seeds, and therefore not be propagated, exhibiting a strong selective pressure on the population. After several generations of selection for individuals showing seed production while growing as quickly as possible, slightly, but sufficiently slowed development could have become "fixed" in the population on an epigenetic level, yielding lines with relatively uniformly slower growth than WT plants. Heritable epigenetic variation of traits of a similar magnitude has been observed and described before, and epigenetic traits can be inherited over five or more generations [247]. Therefore, the observed phenotype could have arisen without MRS2-3 playing a significant role in Mg^{2+}-uptake from the soil or -translocation to the shoot. This would also explain the partial complementation seen in *mrs2-3* + lines; epigenetic growth restriction may be only partially relieved at this stage, even if complementation was complete in theory. To test this hypothesis, *mrs2-3* lines should be crossed with *mrs2-4*, as for *mrs2-6* and *mrs2-4* in Xu *et al*. [161]. If MRS2-3 is important in Mg^{2+}-uptake and translocation, the double mutant should show a more severe phenotype than single mutants on their own, whereas if growth inhibition is due to epigenetic effects, growth in the double mutant should be no worse than in *mrs2-4* on its own. Additionally, both the *mrs2-3* lines and *mrs2-3* + lines could be propagated for several more generations and phenotypes followed. If growth were to remain stable in *mrs2-3* but improves in later generations of *mrs2-3* + without further intervention, this would also lend credibility to this hypothesis.

4.3.4 MRS2-4 functions within the plasma membrane of *Arabidopsis* roots

The data for MRS2-3 localisation generated here seem to agree with previous results; although data is not perfect, MRS2-3 appears to primarily be targeted to the endoplasmic reticulum (**Figure 4.13**). In some cells, observed GFP fluorescence appears to co-localize with FM™ 4-64 fluorescence, indicating plasma membrane localisation, but this could be due to imaging artifacts. Since complementation of the *mrs2-3* phenotype is not complete, there is no guarantee that this localisation is the correct one, and similarly it is not certain that this is the only localisation for MRS2-3 across all tissues and stages of development, but nevertheless this represents a confirmation of and improvement upon previous results [154].

For MRS2-4::GFP, the fluorescence signal was also present in the intracellular space, but a much greater portion of the total fluorescence was located at the plasma membrane (**Figure 4.11**, **Figure 4.12**). Additionally, the protein seems to be polarly distributed across the plasma membrane, with preferred targeting to transverse cell membranes of specific cell files. Judging by the appearance and location of these cell files, they may correspond to cells of the protoxylem [248]or protophloem [249], *i.e.*, the early vasculature system. PM targeting of MRS2-4::GFP can be seen in neighbouring cells as well, but it is less apparent. The almost complete complementation of the *mrs2-4* phenotype in the lines used to obtain these images confirms that MRS2-4 is in its functional state and place. Although the presence of imaging artifacts cannot be excluded, this localisation was confirmed using two different imaging and image enhancement methods; a two-channel, Z-stack image with deconvolution, as well as a wavelength-scan followed by linear unmixing; this dual confirmation significantly reduces the chance of artefacts. PM localisation has been reported twice before for MRS2-4 [138, 153]. The other serious candidate for the target of MRS2-4 is the endoplasmic reticulum, a claim achieved using the same method and the same plasmid as in this work [103]. However, the resolution achieved by Oda *et al*. appears considerably worse than here, and the complementation seen in their study appears less complete as well. It is well-known that tagged proteins can often fail to be exported from the ER properly and reach their normal destination.

Finally, the rapid Mg^{2+}-uptake mediated by MRS2-4 (and MRS2-7), as demonstrated by Ogura *et al*. [166] appears more likely for a PM-localized transporter than for one in the ER. The rapid drop in MRS2-4/MRS2-7 - mediated Mg^{2+}-uptake seen in their work could be the result of Mg^{2+}-gating of the channel, as discussed in **Chapter 1**, **Section 1.3.5**, but could also be the result of rapid internalisation and subsequent degradation of the channel, similar to that seen for the iron transporter IRT1 [244]. This could also explain the large portion of GFP fluorescence seen in the intracellular space for MRS2-4::GFP, as well as the conflicting results obtained for MRS2-4 localisation. It is noteworthy in this context that the Alr1 protein, a member of the same superfamily from yeast, becomes degraded under high-Mg^{2+} conditions [250].

In summary, I believe the data here shown demonstrate that MRS2-4 is localized within the plasma membrane, particularly in the vasculature of the *Arabidopsis* root, where it may be preferentially targeted to transverse cell membranes to aid with uptake of Mg^{2+} and transport towards the shoot. Additional experiments that could be carried out to further test these findings include confocal microscopy on cells subjected to plasmolysis, a common method used to confirm PM localisation [251, 252], potentially followed by disruption of the vacuole and PM in sequence [253]. Membrane fractionation, followed by mass spectrometry, could be used, although the low abundance of MRS2-4 could make this difficult. Time-course experiments following protein localisation and abundance in response to Mg^{2+}-application or -withdrawal should be carried out to test potential re-localisation and/or degradation of the protein. This is possible using the current transformant lines, for example by using a perfusion-setup similar to that described in Gjetting *et al*. [186].

This page is intentionally left blank

Blank pages are used throughout to allow legends to appear opposite display items in the paper copy of this document

Chapter 5: A forward Genetic Screen for Factors involved in Magnesium Homeostasis

5.1 Introduction

5.1.1 Mutagenesis techniques in *A. thaliana*

Forward genetic screens are based on random mutagenesis. In theory, a forward genetic screen can test whether damage to any of the genes in the genome influences a process or metric in question. To achieve this, it is necessary to create a population in which disruptions to every gene are represented, while each individual harbours a number of disruptions low enough to allow them to be viable. To do this, populations are treated with mutagens which produce disruptions within the genome at random, or as close to at random as possible. In practice, there are several different methods to achieve this, each of which has its own advantages, disadvantages and biases. Available mutagens can be divided into three categories: physical, biological and chemical. Before a forward genetic screen can be carried out, a mutagen has to be chosen from the available options.

X-rays were the first technique used to produce mutations artificially, in work by H. J. Muller in 1927 [254]. X-rays are an example of a physical mutagen, a category which also includes gamma rays [255, 256], fast neutrons [257] and heavy ions [258].Physical mutagens primarily cause double-stranded breaks in DNA, which are repaired by the organism via non-homologous end-joining. In some cases, this mechanism introduces errors, which can cause a range of changes to the genome, including point mutations, insertions and deletions (InDels), as well as inversions and translocations. Deletions are most common, and these can be very large, with deletions of 1000 kb being possible [255, 256, 258]. While large deletions can simplify mapping efforts, modern genome sequencing methods are sufficiently precise to reliably detect single-nucleotide variations (SNVs) [189, 190], negating this advantage. DNA deletions of dozens or hundreds of kb in size can cause multiple genes to be disrupted at the same time, on the other hand, potentially complicating attempts to identify the precise gene responsible for observed phenotypes. Mutations introduced via ionizing radiation have also been found to be non-random [256]. Finally, physical mutagens require specialized equipment and expertise, and are therefore not always accessible.

Biological mutagens include transposons and T-DNA. Transposons were first discovered by Barbara McClintock in the 1940s. There are multiple classes of transposons, which use different mechanisms, but all of them can be characterized as short sequences of DNA which have the ability to "jump" from one place in the genome to another. Transposons can disrupt genes if they integrate within a gene sequence, which can lead to mutants with observable and exploitable phenotypes. This approach has been used in the past [259]. However, the use of transposons is slow and cumbersome compared to other modern methods, and transposons can continue to move throughout the genome, which makes it possible for mutant lines to lose their phenotype from one generation to the next, or to acquire disruptions in different genes. T-DNA represents the biological mutagen of choice nowadays; this mutagenesis technique makes use of the ability of *Agrobacterium tumefaciens* to facilitate the integration of DNA-sequences into host genomes. This technique became feasible on a large scale around the turn of the millennium [260], and the most well-known example of its use is the establishment of the SALK T-DNA insertional mutant library, now used by nearly every *Arabidopsis* researcher on a frequent basis [191]. Although originally thought to be more common in highly-expressed sequences and regions of the genome, T-DNA insertions were actually determined to be close to truly random across the genome [261]. Similarly to transposons, the use of T-DNA as a mutagen is generally more work-intense and time-consuming than the use of physical or chemical mutagens. There are two main advantages to the use of T-DNA, and biological mutagens in general. First, the DNA-sequences used for insertional mutagenesis are very easy to detect within the genome via PCR-based methods. Second, the inserted sequences can be modified freely. This allows activation tagging screens to be carried out, during which enhancer sequences are randomly inserted into the target genome [262]. This alternative approach allows screening for the consequences of overexpression of genes, which means that genes normally causing a lethal phenotype on knockout can be found more easily. Additionally, genes normally acting in redundancy with other genes can still produce an observable phenotype when overexpressed. For example, activation-tagging has been used to identify mutants with increased tolerance to low-sulphur conditions [263] and a mutant showing sensitivity to phosphate starvation [264].

Chemical mutagens include compounds such as colchicine, N-nitroso-N-methylurea, and ethyl methanesulphonate (EMS). EMS is an alkylating agent which primarily acts on guanine residues in DNA, producing O^6-ethylguanine, which pairs with thymine (T) instead of cytosine (C). Therefore, during DNA repair or replication, a G/C pair will be replaced by an A/T pair. At lower frequency, EMS also generates G/C to C/G transitions. Both of these lead to point mutations, which are produced throughout the genome at random [265]. The sequence changes induced by EMS treatment can therefore lead to the emergence of null mutants if STOP codons or strongly disruptive base-changes are produced. While mutagens in the other categories almost exclusively cause complete loss-of-function mutations, using EMS, partial loss-of-function mutations are common as well, caused by small changes in promoter sequences, untranslated regions or protein sequences. This makes it more likely to isolate mutants in genes that would be lethal if knocked out completely. These small changes can also cause constitutive expression or activation, producing gain-of-function mutants. Chemical mutagenesis is generally more efficient, producing more mutations per genome than is possible with other mutagens and making it easier to achieve saturation [265]. EMS is commonly available and easy to use, and, as mentioned before, identification of the resulting SNVs in the genome no longer represents a great hurdle [189, 190]. These advantages have made EMS the most commonly-used chemical mutagen, and likely the most commonly-used mutagen in general [164, 189, 190, 213, 215, 218, 265, 266]. As such, EMS was also chosen as the mutagen for the forward genetic screen carried out in this work.

5.1.2 Luciferase as a reporter in genetic screens

As outlined in **Chapter 3**, **Section 3.1.2**, an approach based on a transcriptional reporter was chosen for the forward genetic screen carried out in this work, since use of a transcriptional reporter increases the likelihood of identifying components of a signalling-network and transcription factors, as well as mutations causing comparatively subtle effects.

A transcriptional reporter construct consists of a promoter producing changes in expression under conditions of interest, in this case under MgD, fused to an ORF encoding a protein the abundance of which can be determined [semi]quantitatively as easily as possible. Suitable proteins which have been used in the past include β-glucuronidase (GUS) [267, 268] and fluorescent proteins [213], but the most commonly used reporter is firefly luciferase (LUC) [190, 212, 214, 215]. LUC is an oxidase, which catalyses the reaction of luciferin to oxyluciferin [234, 269]. The reaction is dependent on oxygen (O_2) and MgATP, which makes it possible to determine MgATP- or oxygen-levels from emitted light intensities (see **Chapter 3**). Assuming that O_2 - and MgATP-levels are roughly constant, the amount of light emitted will depend on the abundance of luciferase, which makes this protein a useful transcriptional reporter. Its main advantage over other reporters is that both *LUC* mRNA and LUC protein are comparatively unstable, which means that detected luminescence intensity reflects current reporter expression more closely than for GFP-derived fluorescent proteins and GUS, which are usually highly stable. The LUC protein also takes a long time to recover activity after each reaction, which makes it possible to follow *LUC* expression in real time. Due to these advantages, firefly luciferase was chosen as the reporter in this work.

5.1.3 Aims of this chapter

The aim of this chapter was to carry out a forward genetic screen designed to identify genes associated with Mg^{2+}-homeostasis in *A. thaliana*, especially genes encoding Mg^{2+}-sensing- or -signalling-factors. The method used was adapted from the LumiMap pipeline published in Kato *et al.* [190], and is visualized in **Figure 5.1**. RNA-sequencing, comparison of sequencing data to published transcriptomic datasets and choice of candidate MgD reporter genes (steps 1. and 2. in **Figure 5.1**) are described in S**ection 5.2.1**. **Sections 5.2.2** to **5.2.4** describe the establishment of MgD reporter plants suitable for use in a forward genetic screen (step 3. in **Figure 5.1**). **Section 5.2.5** documents the forward genetic screen itself (steps 4. to 6.), while S**ection 5.2.6** describes the identification of potential causative variants in the identified mutants (steps 7. to 9.).

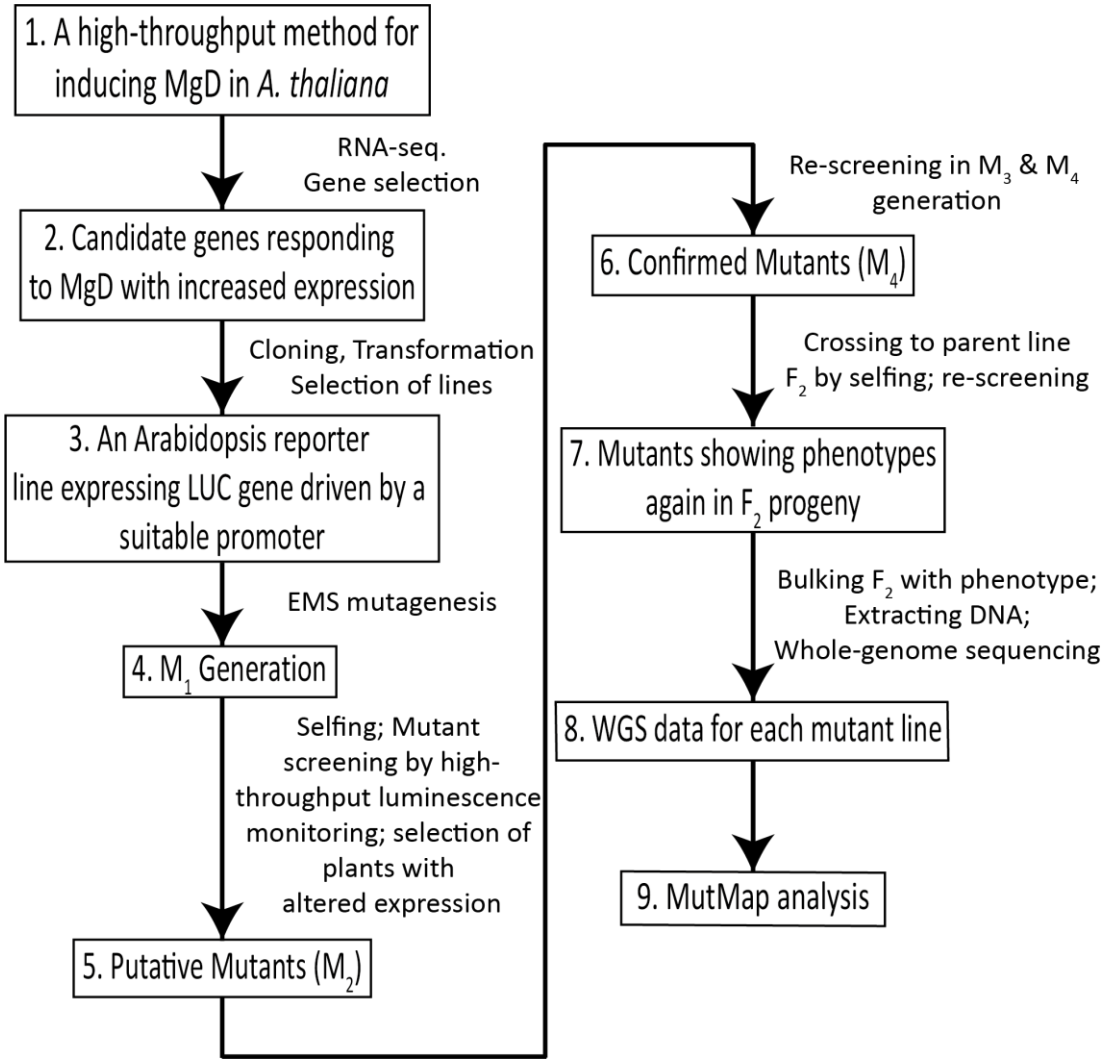

Figure 5.1 – Flow-chart for the forward genetic screen

The entire process of the forward genetic screen for genes involved in Mg^{2+}-homeostasis. Stages in the process are described in black boxes, whereas processes leading from one stage to the next are symbolized by black arrows and briefly described next to the respective arrow. Processes are adapted from Abe *et al.* [189] and Kato *et al.* [190].

5.2 Results

5.2.1 RNA-sequencing reveals candidates for MgD marker genes

To find genes with differential expression, and ultimately candidate MgD reporter genes, RNA-sequencing was carried out on RNA from seedlings grown on media containing different concentrations of added Mg^{2+}, according to the method developed and outlined in **Chapter 3**, S**ection 3.2.1**. RNA was extracted from shoots of seedlings grown on HM made with washed agar and containing 1000, 250, 150, 50 and 15 µM Mg^{2+} until 14 DAG, before being harvested around the middle of the light period and flash-frozen in liquid nitrogen. RNA quality was assessed before submission, and quality of the obtained data was assessed after sequencing and found to be high for all samples. Some measurements of data quality for all samples are shown in **Appendix B**, **Table S5.1**, and more in-depth graphical representations of data quality for one sample are shown in **Appendix A**, **Figure S5.1**.

Few DEGs were found within samples from slightly reduced Mg^{2+}-concentrations; the expression of six transcripts was significantly increased at 50 µM Mg^{2+} relative to 1000 µM, and that of three transcripts at 250 µM Mg^{2+}. The vast majority of changes was seen at 15 µM Mg^{2+}, with 249 transcripts significantly up-regulated, and 82 down-regulated (**Figure 5.2**). Genes showing differential expression during RNA-seq were also divided into subclusters according to their expression-profiles across different Mg^{2+}-concentrations. Each cluster contains genes with similar expression-profiles; all eight clusters are shown in **Figure 5.3**. Out of the subclusters containing genes with increased expression under MgD, subclusters two, five and seven contained genes showing a steep increase of expression between 50 and 15 µM Mg^{2+} (“steep” genes), whereas subclusters three, four and eight contained genes the expression of which increased gradually, starting at 250 µM Mg^{2+} (“incremental” genes). In both cases, the individual subclusters differed primarily with respect to the magnitude by which expression was increased.

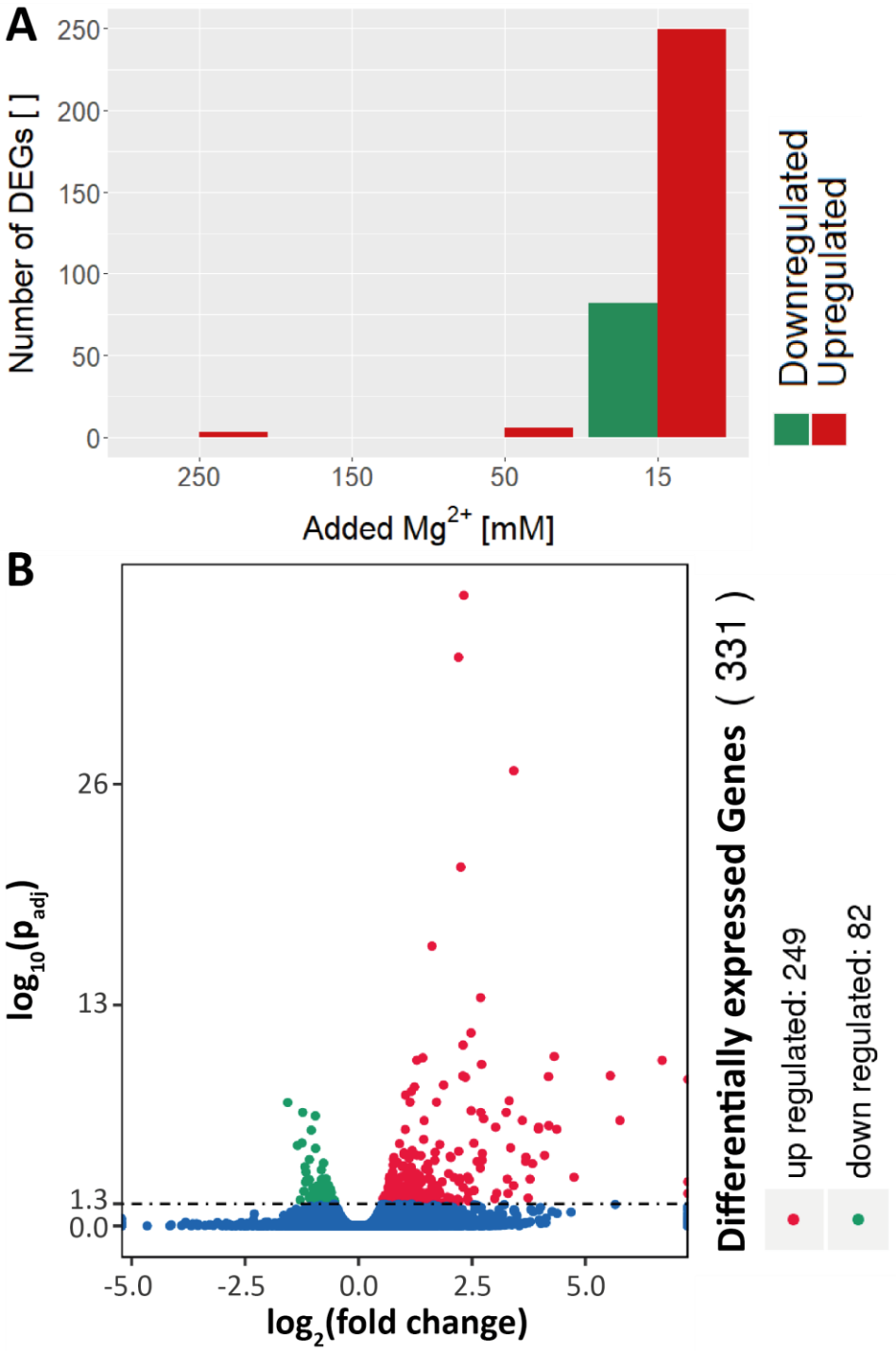

Figure 5.2 - Differentially expressed genes (DEGs) detected via RNAseq.

A. thaliana seedlings were grown on HM made with washed agar, on five different Mg^{2+}-concentrations, until 14 DAG. RNAseq was carried out on RNA extracted from shoot tissue. **A** – Number of DEGs detected during RNAseq at each Mg^{2+}-concentration used, relative to 1000 µM Mg^{2+}. **B** – Volcano-plot of gene expression at 15 µM Mg^{2+} relative to 1000 µM Mg^{2+}. The Y-axis gives the decadic logarithm of the adjusted probability of the respective gene being differentially expressed. The X-axis gives the binary logarithm of the fold-change in expression for the same gene.

This page is intentionally left blank

Blank pages are used throughout to allow legends to appear opposite display items in the paper copy of this document

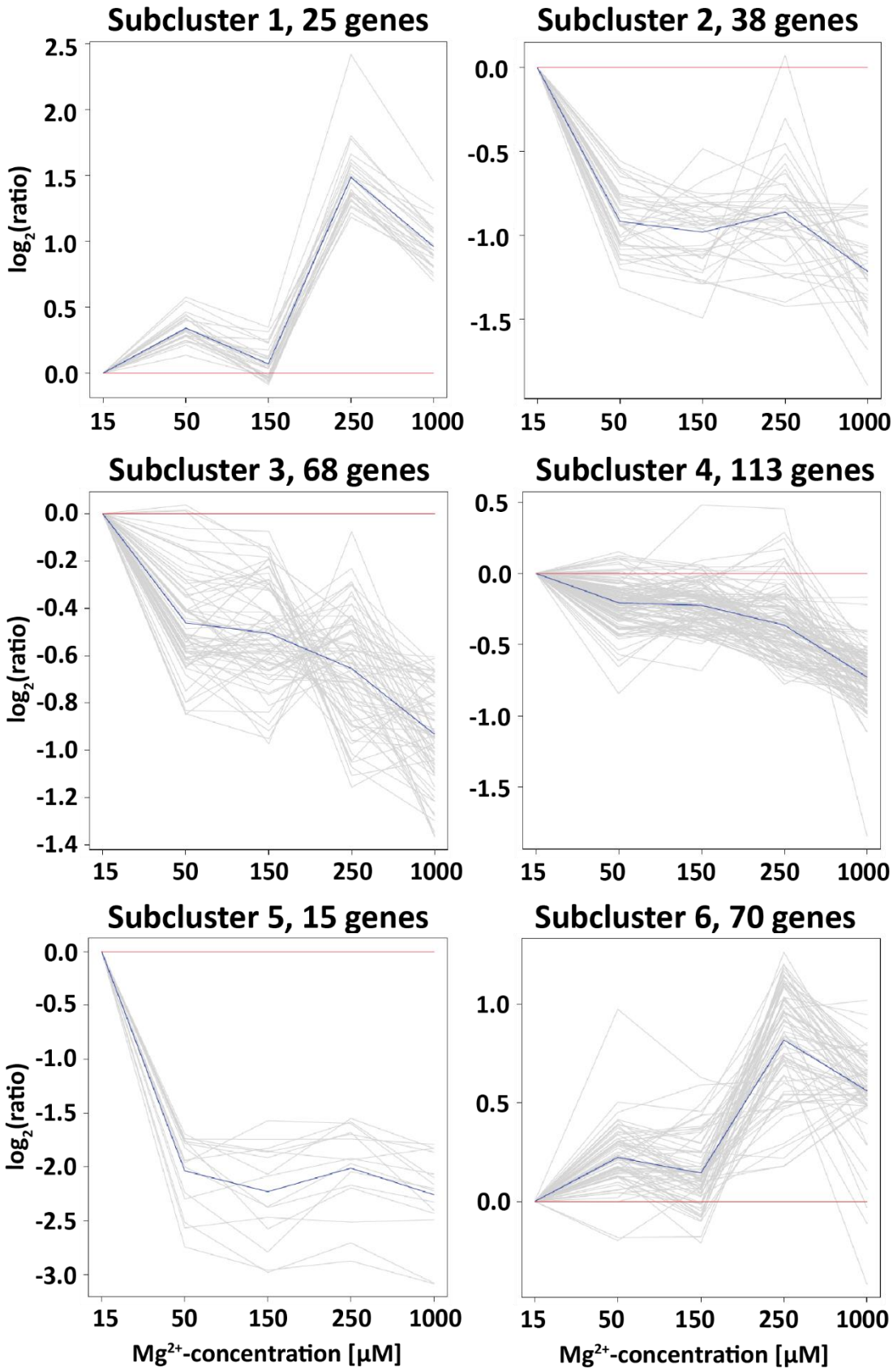
Subcluster 1, 25 genes
Subcluster 2, 38 genes
Subcluster 3, 68 genes
Subcluster 4, 113 genes
Subcluster 5, 15 genes
Subcluster 6, 70 genes
log2(ratio)
Mg2+-concentration [µM]
15
50
150
250
1000

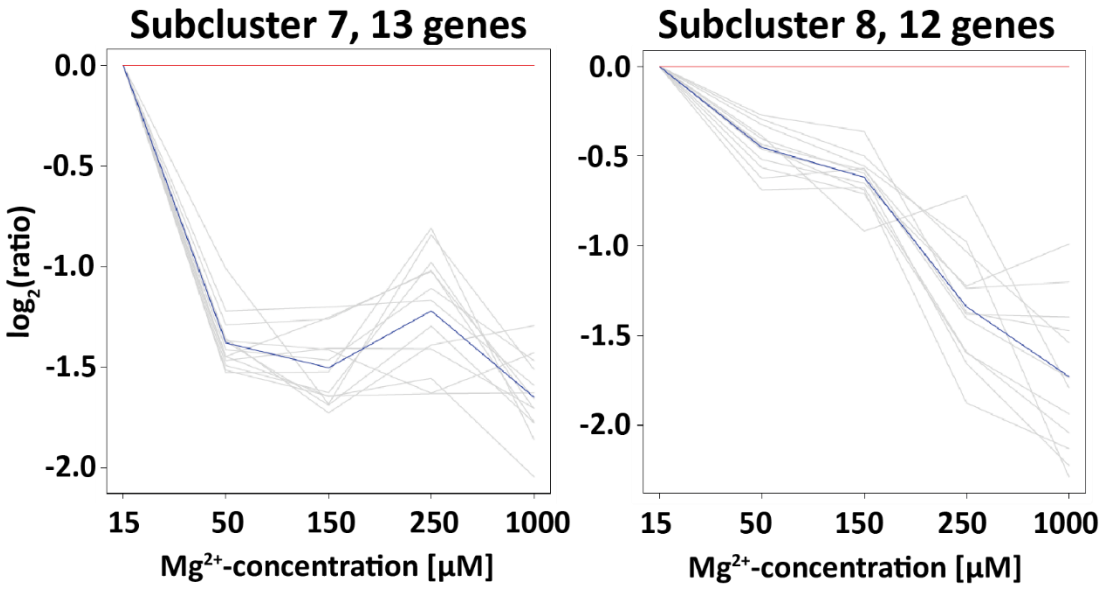

Figure 5.3 - Subcluster analysis of DEGs from RNAseq data

DEGs found during RNAseq analysis of *A. thaliana* grown on different Mg^{2+}-concentrations were ordered into clusters according to expression-patterns. The y-axis gives the binary logarithm of the expression at each condition relative to expression at 15 µM Mg^{2+} (*e.g.*, a value of -1.5 indicates that expression at the respective concentration equals 0.35 times that at 15 µM Mg^{2+}). Grey lines in charts represent relative expression of individual genes on different concentrations, blue lines represent average expression of genes within the respective cluster.

To further characterize the genes upregulated under MgD, gene ontology (GO) annotation was carried out on the list of genes showing significant increases in expression at 15 µM Mg^{2+}. GO terms that were significantly enriched in this set, compared to the genome as a whole, were determined to give an idea of the cellular processes most strongly influenced by this stress. **Table 5.1** gives the list of GO terms in the category "molecular function" that were significantly enriched in the dataset, while **Table S5.2** gives significantly-enriched terms for the category "biological process", and **Table S5.3** those for "localization". Unsurprisingly, the GO terms most significantly enriched in the dataset, both for molecular function and biological process, included terms around transport, particularly ion transport. Interestingly, sulphur compound transport and sulphate transport, nitrate transport and calcium ion transport were among the significantly enriched molecular functions (**Table 5.1**).

Table 5.1 – GO term annotation of genes upregulated in the RNAseq dataset

GO entry	Description	q-value	No. Genes
0022857	Transmembrane transporter activity	8.36E-10	37
0005215	Transporter activity	1.91E-09	41
0015075	Ion transmembrane transporter activity	1.50E-08	28
0008509	Anion transmembrane transporter activity	2.39E-08	17
0022892	Substrate-specific transporter activity	5.65E-08	32
0022891	Substrate-specific transmembrane transport	5.65E-08	30
0015103	Inorganic anion transmembrane transport	1.61E-06	10
0004601	Peroxidase activity	6.14E-06	10
0016684	Oxidoreductase activity, acting on peroxide	7.33E-06	10
0016209	Antioxidant activity	3.46E-05	10
0022804	Active transmembrane transporter activity	1.52E-04	19
0015112	Nitrate transmembrane transporter activity	2.12E-04	5
1901682	Sulphur compound transmembrane transport	0.0028467	4
0010177	2-(2'-methylthio)ethylmalate synthase	0.0089402	2
0016820	Hydrolase activity, transmembrane movement	0.012554	9
0042626	ATPase activity, coupled to transmembrane movement	0.012554	9
0043492	ATPase activity, coupled to movement of substances	0.012554	9
0005315	Inorganic phosphate transmembrane transport	0.031812	3
0015291	Secondary active transmembrane transport	0.03191	10
0015116	Sulphate transmembrane transporter activity	0.033005	3
0005507	Copper ion binding	0.033005	8
0072509	Divalent inorganic cation transmembrane transport	0.033597	5
0015405	P-P-bond-hydrolysis-driven transmembrane transport	0.037704	9
0015399	Primary active transmembrane transport	0.038231	9
0009055	Electron carrier activity	0.03902	5
0015085	Calcium ion transmembrane transport	0.040042	4
0015369	Calcium:proton antiporter activity	0.040042	2
0022836	Gated channel activity	0.041474	5

Gene Ontology（GO, http://www.geneontology.org/） is a major bioinformatics initiative to unify the representation of gene and gene product attributes across all species. GO terms were attributed to the genes found to be upregulated during RNAseq analysis; GO terms enriched in the dataset were determined by calculating adjusted p-values for the likelihoods of finding this number of genes associated with the respective term in a set of this size. This table gives GO terms enriched in the dataset for the category “molecular function”. **GO entry** – Number of the respective term in the GO database. **q-value** – Adjusted probability of this level of enrichment to occur randomly. **No. Genes** – Number of genes in the dataset carrying the respective GO annotation.

Several other terms present in **Table 5.1** point to the presence of oxidative stress (peroxidase activity, oxidoreductase activity, antioxidant activity), confirming that ROS production is one of the primary problems associated with MgD. Within the category “localisation”, significantly-enriched terms were mostly associated with the extracellular space, as well as various membranes; the seven significantly-enriched terms were “extracellular region”, “cell periphery”, “cell wall”, “external encapsulating structure”, “extrinsic component of mitochondrial inner membrane”, “membrane” and “plasma membrane” (**Table S5.3**).

Additionally, the RNAseq data was compared to previously-obtained and published transcriptomic datasets obtained for MgD, as previously in **Chapter 3**, **Section 3.2.1**. The 249 genes showing significantly increased expression in this work were compared to the datasets described in **Table 3.1.** A Venn-diagram visualising overlap between data generated in this work (**F**) and datasets **A-D** was generated, shown in **Figure 5.4**. 153 of the 249 genes from the data in this work (**F** in **Figure 5.4**), *i.e.*, 61.4%, were present in at least one other dataset. Out of these, 37 genes (14.9%) were present in exactly one other dataset, 38 (15.3%) were present in two others, 52 (20.9%) in three others, 25 (9.7%) in four, and one single gene (0.4%) was present in all five other transcriptomic data sets from **Table 3.1**. All genes found to be present in four or five other datasets are listed in **Table 5.2**

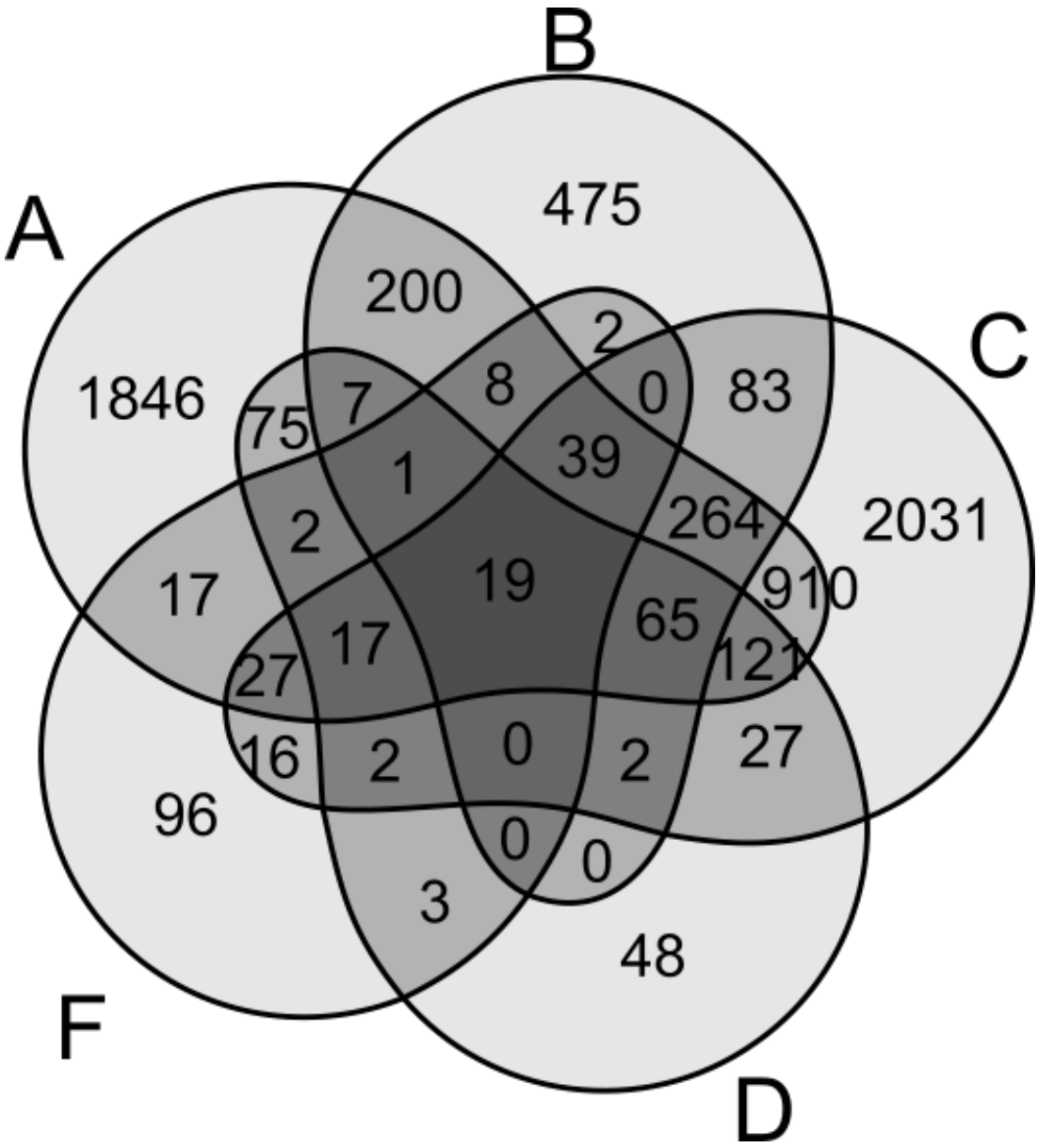

Figure 5.4 - Venn-diagram giving overlap between genes upregulated in the RNAseq data and those from previous transcriptomic datasets for MgD

Datasets **A-D** are listed in **Table 3.1**, labelled according to letters from the "Name" column; dataset "F" constitutes the genes upregulated in the RNAseq data obtained in this work. Shading of each area correspond to number of datasets overlapping to give the genes represented by the area, with darker areas containing genes occurring in more datasets. Numbers in areas give the number of genes in the subset.

This page is intentionally left blank

Blank pages are used throughout to allow legends to appear opposite display items in the paper copy of this document

Table 5.2 – Genes upregulated in RNAseq data obtained in this work and more than four other previous transcriptomic datasets for MgD.

#	Gene ID	Gene Name	Gene Description (TAIR)
1	**AT5G62480**	ATGSTU9	Tau class glutathione transferase
2	**AT1G05680**	UGT74E2	UDP-glucosyltransferase; may integrate ROS and auxin signalling
3	**AT1G26390**	ATBBE4	FAD-binding Berberine protein
4	**AT1G30700**	ATBBE8	FAD-binding Berberine protein
5	**AT1G61800**	GPT2	Glucose 6-phosphate/phosphate transporter 2
6	**AT2G02010**	GAD4	Glutamate decarboxylase 4
7	**AT2G03760**	SOT12	Brassinosteroid sulphotransferase
8	**AT2G04040**	DTX1	Detoxifying efflux carrier for toxic compounds, including Cd^{2+}; MATE efflux family protein
9	**AT2G04050**	DTX3	MATE efflux family protein
10	**AT2G04070**	DTX4	MATE efflux family protein; Expression induced by high boron
11	**AT2G14610**	PR1	Expression of this gene is salicylic-acid responsive
12	**AT2G18660**	PNP-A	Plant natriuretic peptide A. May function in defence
13	**AT2G20720**	-	Pentatricopeptide repeat superfamily protein
14	**AT2G38340**	DREB19	Involved in response to drought
15	**AT2G41730**	HRG1	H_2O_2 response gene; Expression activated by high boron
16	**AT2G45220**	PME17	Pectin methylesterase involved in pectin remodelling
17	**AT2G45570**	CYP76C2	Member of CYP76C
18	**AT2G47000**	ABCB4	Auxin efflux transporter
19	**AT3G28510**	-	AAA-type ATPase
20	**AT3G48850**	PHT3;2	Mitochondrial PO_4^{3-} transporter
21	**AT3G51860**	CAX3	Cation exchanger 3
22	**AT3G63380**	ACA12	ATPase E1-E2 type family protein
23	**AT4G05020**	NDB2	Mitochondrial NADH dehydrogenase
24	**AT4G14630**	GLP9	Germin-like protein
25	**AT4G37370**	CYP81D8	Member of CYP81D
26	**AT5G39580**	PER62	Class III cell wall peroxidase

The list of genes upregulated at 15 μM Mg^{2+} compared to 1000 μM Mg^{2+} in the RNAseq dataset obtained during this work was compared to those upregulated in the datasets from **Table 3.1**. Only one gene, #1 in this table, was present in all five other datasets; the other 25 genes in this table were present in four others.

To choose candidate genes for use as MgD reporters in a forward genetic screen, it was necessary to find genes that would produce a change in reporter expression of sufficient magnitude. Subcluster five from **Figure 5.2** contains genes with the greatest fold-change in expression among those showing "steep" upregulation between 50 and 15 μM Mg^{2+}; subcluster eight contains genes with the greatest fold-change among genes showing "incremental" upregulation at lower Mg^{2+}-concentrations. As such, genes from both of these clusters were considered potential candidates. **Table 5.3** lists all genes from subcluster five, along with their expression at 15 μM Mg^{2+}, fold-change in expression between 1000 and 15 μM Mg^{2+}, the number of other transcriptomic datasets each gene was found to be upregulated in, and a short description for each. **Table 5.4** lists genes from subcluster eight. "Absolute" levels of expression, fold-change of expression under MgD and presence in other MgD transcriptomic data sets, were all considered when choosing candidate MgD reporter genes, prioritising genes with high expression, large fold-change in expression and presence in multiple other datasets. Additionally, (putative) function was taken into account, and both the Klepikova atlas [224] and the *Arabidopsis* eFP browser [225] were searched for expression of potential candidate genes under other stress conditions. Genes with functions potentially related to the symptoms of MgD and/or unknown functions were prioritized, as well as those known to be upregulated under as few (other) stress conditions as possible. Three candidate MgD reporter genes were chosen, two from subcluster five and one from subcluster eight, which are listed in **Table 5.4**.

Table 5.3 – Genes contained within subcluster five of the RNAseq dataset

Gene ID	FPKM (15)	fold up	Sets	Gene description (TAIR)
AT1G05680	11.10	5.88	4	UDP-glucosyltransferase; May integrate ROS and auxin
AT1G13480	4.91	12.97	2	Hypothetical protein (DUF1262)
AT1G26390	12.40	6.47	4	FAD-binding Berberine protein
AT2G04050	22.94	12.59	4	MATE efflux family protein
AT2G04070	5.91	10.90	4	MATE efflux family protein; Expression induced by high boron
AT2G18190	2.46	81.92	3	AAA-type ATPase
AT2G18193	13.57	18.75	3	AAA-type ATPase
AT2G45220	19.18	6.81	4	Pectin methylesterase involved in pectin remodelling
AT4G12490	230.42	5.50	3	Member of AZI family; lipid transfer protein; chloroplast localized
AT4G12735	6.72	5.72	3	Encodes a peroxisomal protein
AT4G14630	6.74	10.23	4	Germin-like protein
AT4G25200	2.63	87.79	3	AtHSP23.6-mito, nuclear gene encoding mitochondrial protein
AT5G13210	8.26	5.13	3	Uncharacterized conserved protein UCP015417
AT5G24640	6.38	20.40	2	H_2O_2 response gene, sensor/responder of H_2O_2
AT5G55150	4.43	54.02	3	F-box SKIP23-like protein (DUF295)

FPKM (15) – Expression of the respective transcript at 15 μM in fragments per kilobase million (FPKM). **fold up** – the fold change in expression measured for the respective transcripts at 15 μM added Mg^{2+} relative to 1000 μM Mg^{2+}. **Sets** – number of transcriptomic datasets from **Table 3.1** in which the transcript was found to be upregulated.

Table 5.4 – Genes contained within subcluster eight of the RNAseq dataset

Gene ID	FPKM (15)	fold up	Sets	Gene description (TAIR)
AT2G14580	3.77	4.65	0	Pathogenesis related, PR1-like
AT2G14610	34.56	5.51	4	Protein expression is SA-responsive
AT2G32860	22.45	3.18	0	BGLU33, beta glucosidase 33
AT3G05727	239.16	2.80	0	Defensin-like (DEFL) family protein; Activated by OXS2 under salt stress
AT3G51860	16.85	4.06	4	CAX3 / Cation exchanger 3
AT4G01390	9.96	2.21	0	TRAF-like family protein
AT4G22485	39.13	5.16	0	Protease inhibitor/seed storage/LTP family protein
AT4G22505	40.61	4.78	0	Bifunctional inhibitor/lipid-transfer /seed storage 2S albumin family
AT4G22520	13.74	5.33	0	Bifunctional inhibitor/lipid-transfer /seed storage 2S albumin family
AT4G30140	32.32	3.59	0	Member of GDSL lipase/esterase family that functions as cutinase
AT5G38940	9.74	2.66	0	RmlC-like cupins superfamily; putative Mn^{2+}-binding site
AT5G64110	12.90	4.91	3	Peroxidase superfamily protein PER70

FPKM (15) – Expression of the respective transcript at 15 μM in fragments per kilobase million (FPKM). fold up – the fold change in expression measured for the respective transcripts at 15 μM added Mg^{2+} relative to 1000 μM Mg^{2+}. **Sets** – number of transcriptomic datasets from **Table 3.1** in which the transcript was found to be upregulated.

The first candidate chosen was *AT2G04050*, which encodes DTX3, a protein in the multidrug and toxic compound extrusion (MATE) family. It is one of three MATE family transporter-encoding transcripts found to be significantly upregulated in the RNAseq data. All three were found in four of the other transcriptomic datasets examined, and their genomic loci are close to each other in the genome, as can be seen from their gene identifiers (**Table 5.2**). Two of the three transcripts were present in subcluster five (**Table 5.3**), but *AT2G04050/DTX3* was chosen over *AT2G04070/DTX4* due to its higher expression and fold-change in expression.

Table 5.5 – Potential MgD reporters chosen from the RNAseq data

Gene ID	"Name"	FPKM (15)	fold up	Sets
AT2G04050	**DTX3**	22.94	12.59	4
AT2G18193	**AAA**	13.57	18.75	3
AT5G64110	**PER70**	12.90	4.91	3

Genes from subclusters five or eight were chosen based on "absolute" expression values, fold upregulation at 15 μM added Mg^{2+} relative to 1000 μM Mg^{2+}, presence in previously-published MgD data sets, putative function and differential expression under other stress conditions. **FPKM (15)** – Expression of the respective transcript at 15 μM in fragments per kilobase million (FPKM). fold up – the fold change in expression measured for the respective transcripts at 15 μM added Mg^{2+} relative to 1000 μM Mg^{2+}. **Sets** – number of transcriptomic datasets from **Table 3.1** in which the transcript was found to be upregulated.

Additionally, the expression of *DTX4* is known to respond to excess boron, unlike *DTX3*. GO terms (http://www.geneontology.org/) for biological processes associated with DTX3 include "porphyrin-compound containing metabolic process" and "xenobiotic detoxification by transmembrane export across the plasma membrane", indicating it may be involved in detoxifying the products of chlorophyll degradation, which constitutes a function that would be relevant under MgD, although not exclusively. Gene expression is induced by salt stress in roots and by UVB-stress in leaves, according to the *Arabidopsis* eFP browser [225]. Increased expression of *DTX3* and *DTX4* under MgD has been confirmed previously by Kamiya *et al.* [105].

The second candidate is *AT2G18193*, which encodes a poorly-annotated AAA-type ATPase, henceforth referred to as "AAA" for convenience. It was present in subcluster five in the RNAseq data, and was found in three other transcriptomic datasets, similar to the closely-related gene *AT2G18190* (**Table 5.3**) No data on the expression of the *AAA* transcript could be found in the *Arabidopsis* eFP browser for *AT2G18193*, while *AT2G18190* appears to be upregulated under salt-stress. Similarly, the singular GO terms associated with *AT2G18190* is "response to salt stress", whereas *AT2G18193* is associated with a variety of GO terms.

Terms associated with *AAA* include “root morphogenesis”, “response to oxidative stress”, “carbohydrate derivative metabolic process”, “response to inorganic substance”, and “plant epidermis development”, *i.e.*, processes known or thought to be influenced under MgD. Therefore, *AT2G18193* was chosen over *AT2G18190* as a candidate MgD-marker not just because its higher base-line expression (**Table 5.3**), but also due to the association with processes related to MgD.

The third candidate chosen in this work was selected from subcluster eight, to provide additional diversity with respect to the potential reporter genes chosen. Most of these genes were not found in any of the other transcriptomic datasets tested (**Table 5.4**); only *AT2G14610/PR1*, *AT3G51860/CAX3* and *AT5G64110/PER70* were found in four, four and three other datasets, respectively. Since *PR1* is a known pathogenesis-related gene and *CAX3* has been investigated and found to be responsive to Ca^{2+}-excess and phosphate deficiency before by Kamiya *et al.* [105], *PER70* constituted the only reasonable choice. GO terms listed for this gene are “response to oxidative stress” and “response to stress”, but responses found in the *Arabidopsis* eFP browser [225] seem smaller than that found in this work, leaving open the possibility for this gene’s expression to be partially induced by ROS, but only fully induced in the presence of MgD, potentially similar to *OsSGR* [96].

To confirm the increase in expression seen for the three candidates under MgD, as well as the accuracy of the RNAseq data obtained, qRT-PCR was carried out, using retained aliquots of the same RNA-samples submitted for RNAseq analysis. Transcript abundance of *DTX3*, *AAA* and *PER70*, as well as *AT2G20720/PPR*, in shoots of seedlings grown on different concentrations of Mg^{2+} were tested.

PPR was included in the analysis since primers for this transcript had already been obtained, and its expression under MgD had been tested previously (see **Chapter 3**, **Section 3.2.1**). *ACT2* and *EF1α* were used as reference transcripts once again. Results of the experiment are summarized in **Figure 5.5**. Although the fold-changes in expression of the individual transcripts determined during qRT-PCR (**Figure 5.5 A**) differed slightly from those obtained during RNAseq (**Figure 5.5 B**), significant increases in expression could be seen for each transcript tested, confirming results obtained during RNAseq.

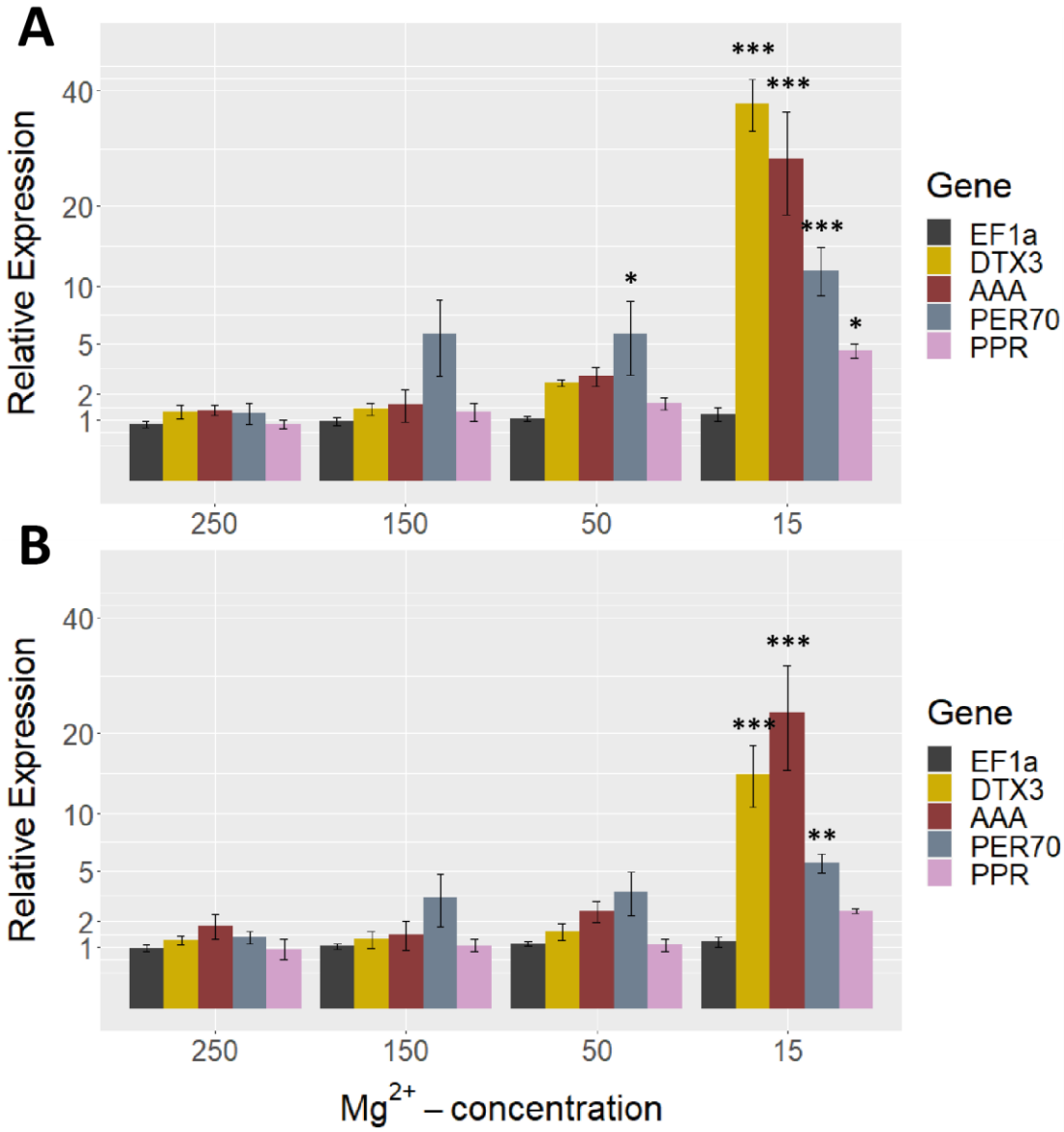

Figure 5.5 – Validation of RNAseq data by qRT-PCR

A – qRT-PCR was carried out on aliquots of RNA from the same samples as those submitted for RNAseq analysis. Transcripts tested were those from **Table 5.5**, as well as PPR, which had been tested previously. **B** – Expression values (in FPKM) for the genes tested in **A** at all concentrations were obtained from the RNAseq data. Expression-levels for all transcripts in **A** and **B** were normalized to expression of ACTIN2 and expression of the respective transcripts at 1000 µM according to the $\Delta\Delta C_T$ method. The dimensions of the Y-Axis are scaled to match the square root of the associated values. Columns represent mean values (± SEM) from three independent experiments, each repeated as three technical replicates. Symbols above error bars denote significant differences between expression on 1000 µM Mg^{2+} and the respective concentration, as determined by a two-way ANOVA, followed by Tukey's HSD post-hoc test (▪ - $p < 0.1$; * - $p < 0.05$; ** - $p < 0.01$; *** - $p < 0.001$).

5.2.2 Reporter plants react specifically to MgD with increased luciferase expression

To create MgD reporter plants, putative promoters of *DTX3*, *AAA* and *PER70* were amplified from genomic DNA and used to create *LUC* expression constructs. For *DTX3*, a sequence of 2754 bases immediately preceding the START codon listed in the gene model was amplified. For *AAA*, the sequence chosen was 1366 bp long, and for *PER70*, 3062 bases preceding the coding sequence were chosen. Each of these sequences was cloned into the acceptor site of the pGW_luc destination vector separately, using the Gateway method [270] (see **Chapter 2**, **Section 2.7**). Next, *A.thaliana* plants were transformed with each of the constructs via floral dip, and transformants were selected by testing for glufosinate (BASTA™) resistance in the T_1 generation. LUC expression was confirmed in the T_2 generation by spraying seedlings on plates with a solution containing 1 mM luciferin and recording light emission (see C**hapter 2**, **Section 2.6.1**). Homozygous transformant lines showing approximately uniform and universal luciferase expression were obtained in the T_3 generation for each promoter-luciferase construct. The transformant lines showing strongest and most universal luciferase expression were termed *pDTX3::LUC* 14-1, *pAAA::LUC* 2-4 and *pPER70::LUC* 5-1, respectively. To test Mg^{2+}-dependence of the luciferase-expression in each of these lines, they were grown on agar plates containing HM with different concentrations of Mg^{2+} until 8 DAG. At the end of the growth period, luciferase expression within seedlings was quantified as before. For both *pDTX3::LUC* 14-1 (**Figure 5.6**) and *pAAA::LUC* 2-4 (**Figure 5.7**), LUC expression was detected primarily in shoots, and a clear increase in LUC expression could be seen under MgD. For *pPER70::LUC*, a significant portion of luciferase expression was detected in roots, and no obvious increase in expression was seen under MgD (**Figure S5.2**).

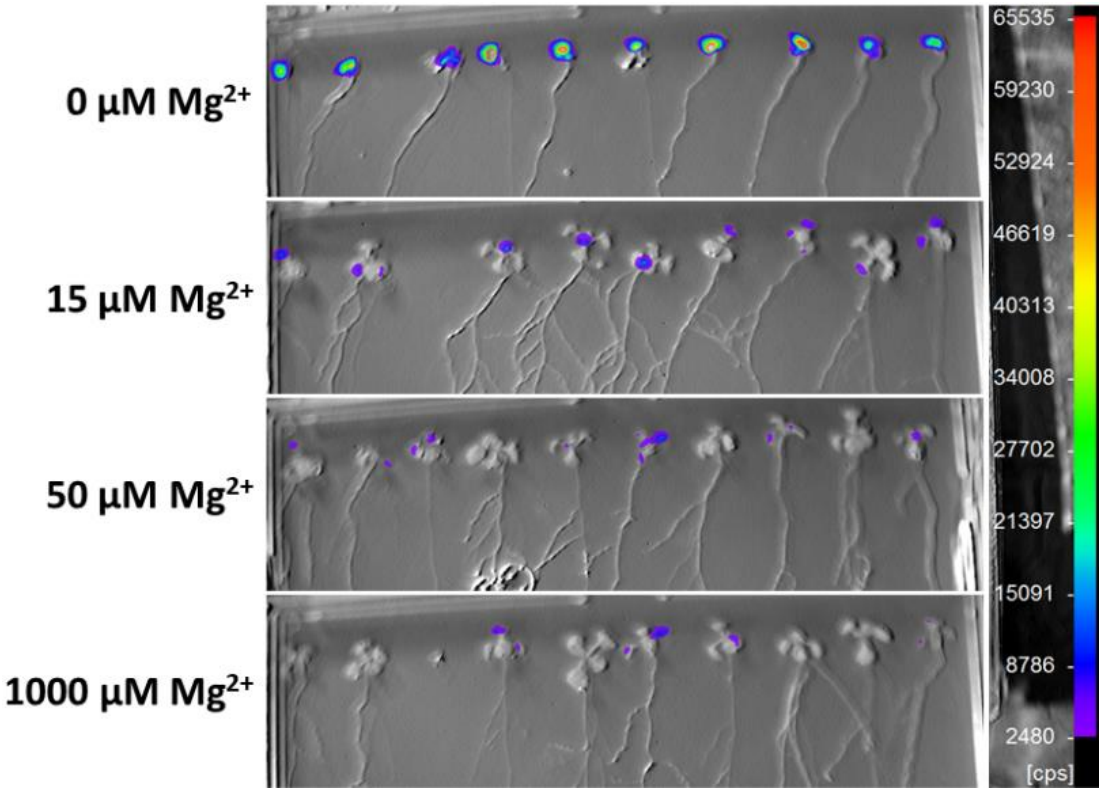

Figure 5.6 – *pDTX3::LUC* expression on different concentrations of Mg^{2+}
Seedlings of *pDTX3::LUC* 14-1 were grown on agar plates containing HM made with washed agar with different concentrations of added Mg^{2+} until 8 DAG, then luciferase expression was visualized by spraying seedlings with a solution containing luciferin and measuring light emission using a photon-counting camera. **cps** – [photon] counts per second.

LUC expression in *pDTX3::LUC* 14-1 was only reliably increased at 0 µM Mg^{2+}, when plant growth was significantly impaired (**Figure 5.6**), whereas *pAAA::LUC* 2-4 plants showed detectably increased luc expression at 15 µM Mg^{2+}, a concentration with minimal effects on plant growth (**Figure 5.7**). Additionally, growth of *pAAA::LUC* 2-4 appeared more vigorous and uniform, and *AAA* was deemed a superior MgD reporter gene due to the unique set of potentially MgD-related biological processes it is thought to be involved in. Therefore, *pAAA::LUC* 2-4 was chosen as the reporter line to be taken forward.

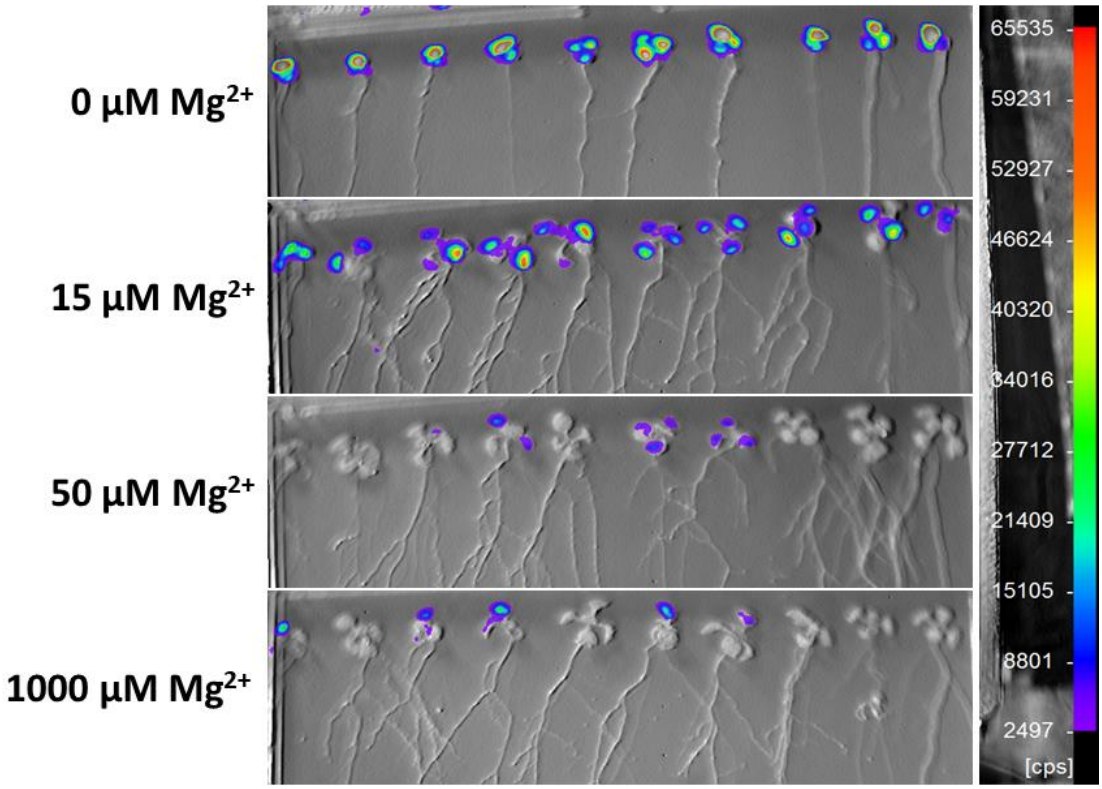

Figure 5.7 – *pAAA::LUC* expression on different concentrations of Mg^{2+}
Seedlings of *pAAA::LUC* 2-4 were grown on agar plates containing HM made with washed agar with different concentrations of added Mg^{2+} until 8 DAG, then luciferase expression was visualized by spraying seedlings with a solution containing luciferin and measuring light emission using a photon-counting camera. **cps** – [photon] counts per second.

To confirm that expression of luciferase was genuinely increased at the transcript level in *pAAA::LUC* 2-4, and to ensure that expression of the endogenous *AT2G18193/AAA* gene was not disrupted by the presence of the reporter transgene, qRT-PCR analysis was carried out. Col-0 and *pAAA::LUC* seedlings were grown on plates containing HM with 1000, 100, 50, 15 and 7.5 µM added Mg^{2+} until 14 DAG, before shoots were sampled and expression of *AAA* and *LUC* was tested. *ACT2* and *EF1α* were used as reference transcripts, as before. Results are summarized in **Figure 5.8**.

The expression of the second reference transcript, *EF1α*, was significantly increased relative to *ACT2* at lower Mg^{2+}-concentrations for both Col-0 (**Figure 5.8 A**) and *pAAA::LUC* 2-4 (**B**), but the increase was small compared for that seen for *AAA* and *LUC*. If expression was normalized to *EF1α*, or the geometric mean of their expression, the increase in *AAA* and *LUC* expression would still be statistically significant. As such, this issue does not influence the results. For both Col-0 and *pAAA::LUC* 2-4, *AAA* expression was significantly increased at 15 and 7.5 µM Mg^{2+} relative to 1000 µM Mg^{2+}. The increase was lower for *pAAA::LUC* 2-4 (904-fold at 15 µM Mg^{2+}, 1484-fold at 7.5 µM Mg^{2+}) than for Col-0 (1610-fold at 15 µM Mg^{2+}, 1779-fold at 7.5 µM Mg^{2+}), but due to the relatively large margins of error, the differences were not statistically significant. No *LUC* expression was detected in Col-0, while *LUC* expression in *pAAA::LUC* 2-4 was detected under all conditions. *LUC* expression in this line was increased 212-fold at 15 µM Mg^{2+} relative to 1000 µM Mg^{2+}, and 113-fold at 7.5 µM Mg^{2+}. It is noteworthy that *AAA* expression in Col-0 was remarkably similar to 1000 µM Mg^{2+} at 100 and 50 µM Mg^{2+}, before increasing dramatically at lower concentrations, with the expression at 15 and 7.5 µM Mg^{2+} very similar to each other once again. This further indicates a binary, "switch-like" pattern of expression.

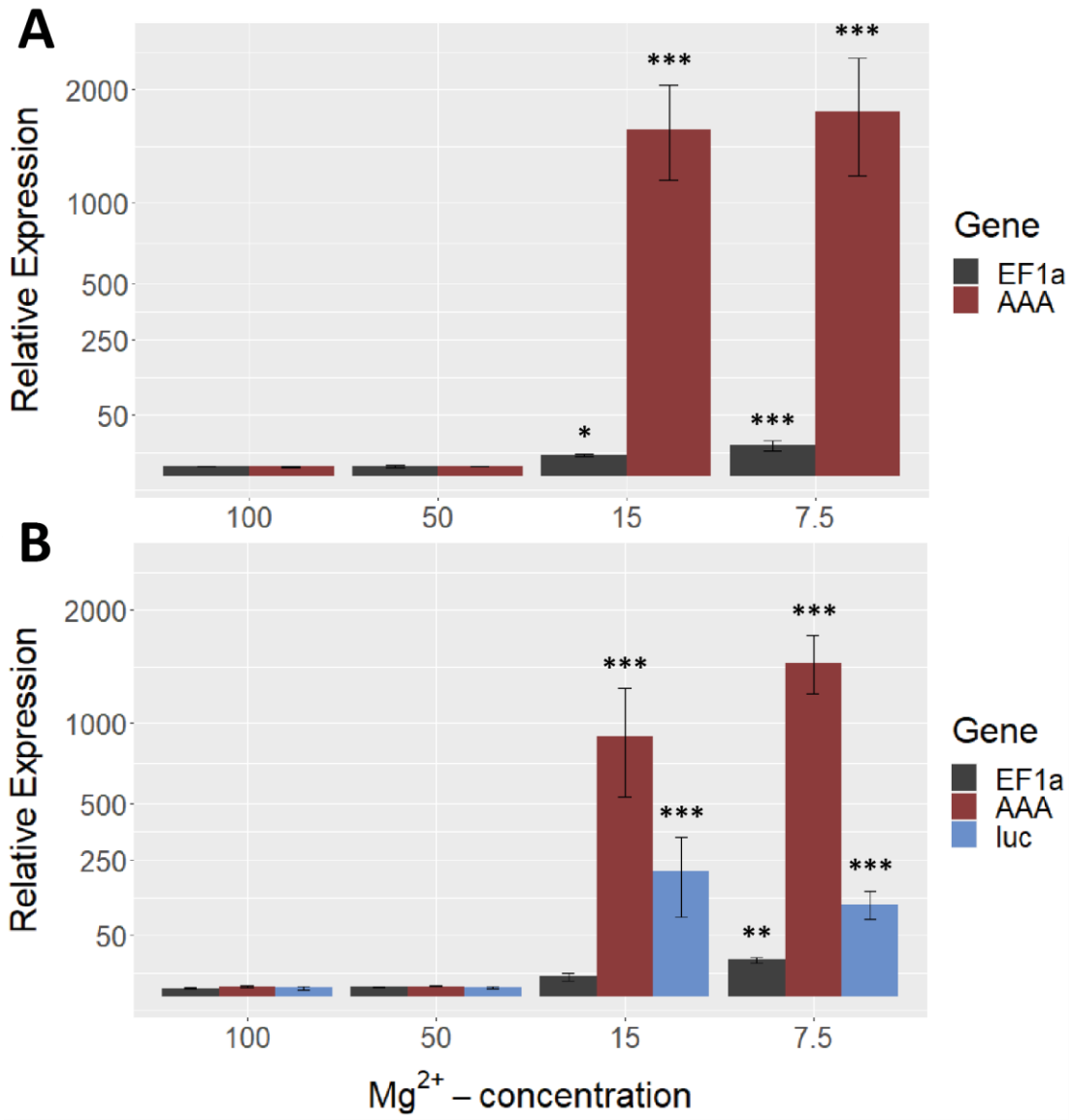

Figure 5.8 – qRT-PCR analysis of *AAA* and *pAAA::LUC* expression

Seedlings were grown on agar plates containing HM made with washed agar, with different concentrations of added Mg^{2+}, until 14 DAG. **A** – *AT2G18193/AAA* expression levels in Col-0 seedlings; no *LUC* expression was detected. **B** – expression of *AAA* and *LUC* transcripts in *pAAA::LUC* 2-4 seedlings. Expression levels for all transcripts in **A** and **B** were normalized to expression of *ACTIN2* and expression of the respective transcripts at 1000 µM according to the $\Delta\Delta C_T$ method. The dimensions of the Y-Axis are scaled to match the square root of the associated values. Columns represent mean values (± SEM) from three independent experiments, each repeated as three technical replicates. Symbols above error bars denote significant differences between expression on 1000 µM Mg^{2+} and the respective concentration, as determined by a two-way ANOVA, followed by Tukey's HSD post-hoc test (▪ - $p < 0.1$; * - $p < 0.05$; ** - $p < 0.01$; *** - $p < 0.001$).

5.2.3 AT2G18193 ("AAA") is a member of the BCS1 clade of AAA ATPases

It has been established that the expression of *AAA* varies at different Mg^{2+}-concentrations. However, it is not known whether the expression of this gene reacts specifically or directly to magnesium-concentrations. Expression could be regulated in response to downstream symptoms of MgD or react non-specifically to various other stresses, as little to no reliable data on expression of this gene exists. Knowledge about the specificity of *AAA* upregulation is necessary since it could influence the likelihood of identifying genuine Mg^{2+}-related mutants during the forward genetic screen. It was therefore clear that luciferase-expression in reporter plants would have to be tested under a number of different conditions. However, it was not possible to test all conceivable conditions. Therefore, a literature search for information on the candidate gene *AT2G18193* was carried out, with the aim of finding conditions likely to elicit upregulation of its expression.

Based on sequence information, AT2G18193 has been determined by molecular modelling algorithms to be an AAA-type ATPase, belonging to the BCS1-clade [271]. Since other members of this clade could have functions and expression-profiles similar to *AAA*, the search was extended to all members of the BCS1 clade. When the UniprotKB database (https://www.uniprot.org/) was queried for protein sequences of BCS1-clade AAA ATPases in *A. thaliana*, 97 sequences were found, but many among them represented duplicates or sequences of questionable quality. When only manually-reviewed entries were permitted, 23 sequences were found. Most of the genes and proteins associated with these entries were still poorly-annotated. To get an idea of the possible functions of these proteins, GO terms for the category "cellular process" associated with each of them were retrieved. Gene identifiers for all confirmed BCS1-clade AAA ATPases found, as well as associated GO terms for "cellular process", are listed in **Table 5.6**. **Table S5.4** gives GO terms for "localisation".

Five of the genes found were annotated as "response to salt stress" (# 2, 11, 12, 14 and 22 in **Table 5.6**). Five members appear to be associated with defense responses to pathogens (# 3, 4 13, 20, 24). Three members are associated with developmental processes (# 3, 9, 16) and eight members were not yet associated with any GO terms (# 5, 6, 7, 8, 17, 18, 19, 21).

Many members appear to respond to or modulate the response to various phytohormones, including salicylic acid (SA) (# 13, 20, 23), abscisic acid (ABA) (# 10, 20, 22, 23), and jasmonic acid (JA) (# 3, 16, 20, 23).

A phylogenetic tree of *A. thaliana* BCS1 AAA ATPases was constructed, using all the verified protein sequences of BCS1 AAA ATPases available in the UniprotKB database, plus two other known AAA ATPases from *A. thaliana*, FtsH2 and APP1, included as an outgroup to root the tree [272, 273]. The full tree is shown in **Figure 5.9**; sequence identity scores for all members are given in **Table S5.5**.

Members of the BCS1 clade were found to be much more similar to each other than to the other included AAA ATPases. Many of the associated genes lie very close to each other in the genome, as indicated by the gene identifiers, with the nearest neighbours being most similar to each other in most cases, pointing towards recent gene duplications. AAA itself has one such neighbour, AT2G18190 (# 2), with which it shares 81% protein sequence identity. Besides this, AAA is most similar to the AT5G17XX-group above it in the tree, as well as to AT3G50930 (AtBCS1) and AT3G50940 below it, with high sequence identities of 42.7 to 49.0%. Although it does not constitute a guarantee, sequence identities of this level can point to highly similar molecular functions; for example, MRS2 magnesium-channels from plants can complement for absence of their yeast homologues despite sequence identities around 20% [135, 136]. AT5G17740 and -50 are annotated on TAIR as reacting to salt-drought- and osmotic stress, whereas AT5G17760 appears to respond to SA and cycloheximide exposure according to the *Arabidopsis* eFP browser [225]. Finally, transcript of *AT1G43910*, which is slightly more distantly related to AAA, accumulates in shoots under potassium starvation; the protein appears to influence ABA signalling. According to these data, expression of *AAA* should be tested under salt-stress conditions and after exposure to K^+ deficiency. Additionally, *CAX3/AT3G51860*, a putative transcriptional MgD-reporter was tested under different nutrient stress conditions, and was found to respond to P deficiency and calcium excess [105], both of which can cause symptoms similar to those of MgD. Therefore, both of these conditions should be tested as well.

Table 5.6 – GO annotation of BCS1-clade AAA ATPases in *A. thaliana*

#	Gene ID	GO annotation; cellular processes
1	AT1G43910	Cellular response to potassium ion starvation
2	AT2G18190	Response to salt stress
3	AT2G18193	Root morphogenesis, response to oxidative stress, carbohydrate derivative metabolic process, secondary metabolic process, response to inorganic substance, plant epidermis development, response to jasmonic acid, defense response to other organism, cell differentiation
4	AT2G46620	Response to alcohol, response to chitin, defense response to bacterium, defense response to fungus, signal transduction, response to lipid, regulation of defense response, immune system process
5	AT3G28510	-
6	AT3G28520	-
7	AT3G28540	-
8	AT3G28560	-
9	AT3G28570	Meristem development, shoot system development, root morphogenesis
10	AT3G28580	Response to abscisic acid, response to singlet oxygen
11	AT3G28600	Response to salt stress
12	AT3G28610	Response to salt stress
13	AT3G50930	Plant-type hypersensitive response, response to bacterium, response to molecule of bacterial origin, cell death, response to UV, salicylic acid mediated signaling pathway
14	AT3G50940	Response to salt stress
15	AT4G25835	Porphyrin-containing compound metabolic process, tetrapyrrole biosynthetic process
16	AT4G30250	Response to jasmonic acid, floral whorl development, plant organ formation, pattern specification process, floral organ development, phyllome development, meiotic cell cycle process
17	AT5G17730	-
18	AT5G17740	-
19	AT5G17750	-
20	AT5G17760	Cellular catabolic process, defense response to fungus, protein catabolic process, defense response to bacterium, response to jasmonic acid, response to heat, response to abscisic acid, response to salicylic acid, response to inorganic substance
21	AT5G40000	-
22	AT5G40010	Response to abscisic acid, fruit development, response to cold, response to water deprivation, response to salt stress, seed maturation
23	AT5G57480	Oxoacid metabolic process, defense response to fungus, response to abscisic acid, secondary metabolic process, response to water deprivation, response to bacterium, response to salicylic acid

A search for BCS1-clade AAA-type ATPases present in *A.thaliana* in the UniprotKB database (https://www.uniprot.org/) was carried out. Only manually-reviewed entries were accepted, a total of 23 of which were found. Locus identifiers for the associated genes were collected, and GO terms associated with each were obtained.GO annotations of the category “cellular processes” are displayed.

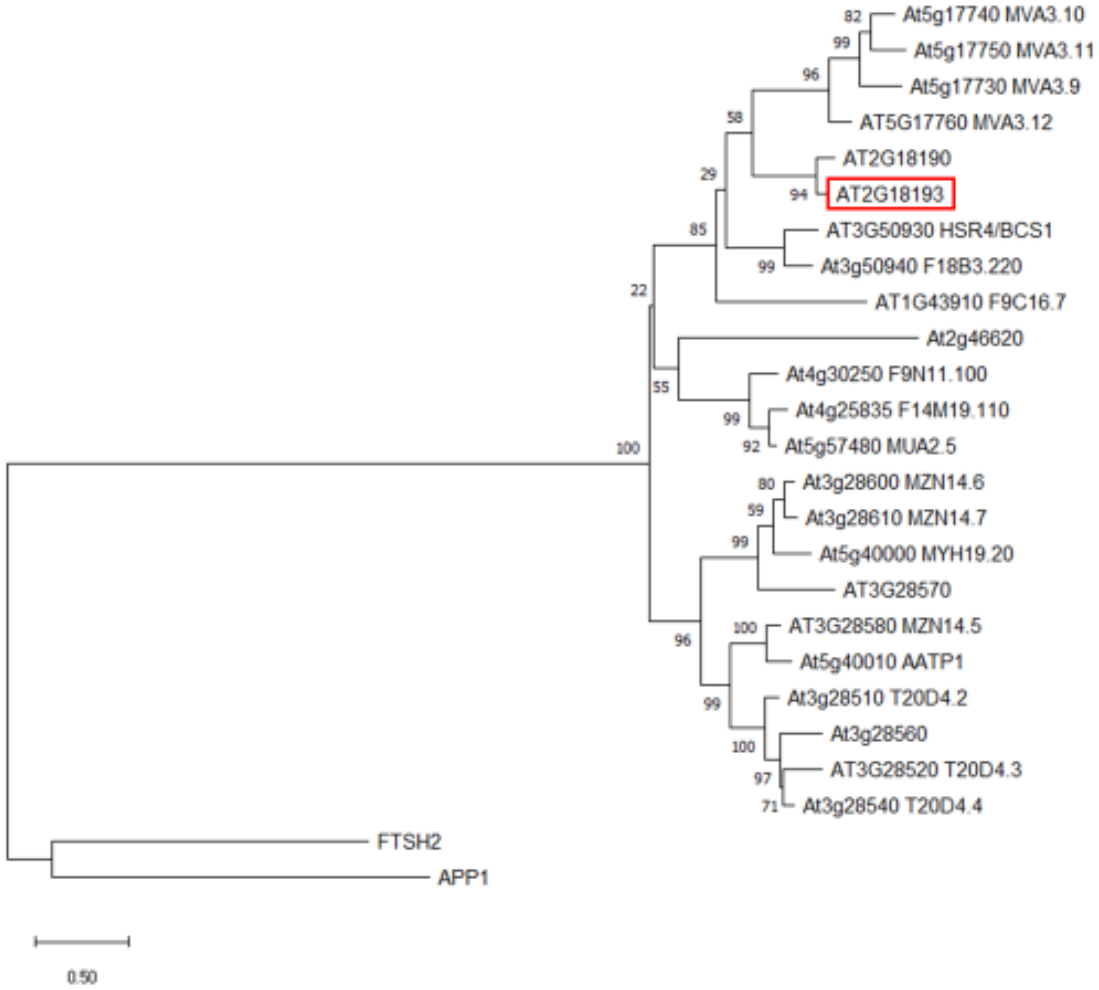

Figure 5.9 – Phylogenetic tree of the BCS1-clade AAA ATPases in *A. thaliana*
Amino acid sequences associated with the genes listed in **Table 5.6** were used to construct a phylogenetic tree. The evolutionary history was inferred using the Neighbour-Joining method. The percentage of replicate trees in which the associated taxa clustered together in the bootstrap test (500 replicates) are shown next to the branches. The tree is drawn to scale, with branch lengths in the same units as those of the evolutionary distances used to infer the phylogenetic tree. The evolutionary distances were computed using the Poisson correction method. All ambiguous positions were removed for each sequence pair (pairwise deletion option). Analysis was conducted in MEGA X. AAA/At2g18193 is highlighted by a red box.

5.2.4 *pAAA::LUC* reporter expression appears to react specifically to MgD

Luciferase expression in *pAAA::LUC* 2-4 seedlings was tested under all the nutrient stress conditions of interest identified in the previous section. Seedlings of *pAAA::LUC* 2-4 were grown on agar plates containing HM with altered compositions designed to induce the stresses of interest; in addition to MgD (15 µM Mg^{2+}), phosphate deficiency (10 µM PO_4^{3-}), salt stress (60 mM NaCl), K^+ deficiency (2.5 µM K^+) and Ca^{2+} excess (25 mM Ca^{2+}) were tested. After growth until 10 DAG, LUC expression in seedlings was visualized as before (**Figure 5.10**). Despite growth being visibly affected under all stress conditions tested, increased LUC expression could only be detected under MgD. This indicates that expression of *AAA/AT2G18193*, or at least of the reporter construct in *pAAA::LUC* 2-4, may react specifically to MgD. It was therefore concluded that these reporter plants were suitable for use in a forward genetic screen. LUC reporter expression was also tested on agar plates without sucrose containing different Mg^{2+}-concentrations, since the presence of sucrose in agar plates may interfere with the symptoms of MgD (see **Chapter 3, Section 3.3.4**). LUC expression in *pAAA::LUC* 2-4 was still increased at 15 µM Mg^{2+} relative to higher Mg^{2+}-concentrations (**Figure S5.3**), further indicating that 0.5% added sucrose in agar plates does not mitigate the symptoms of MgD.

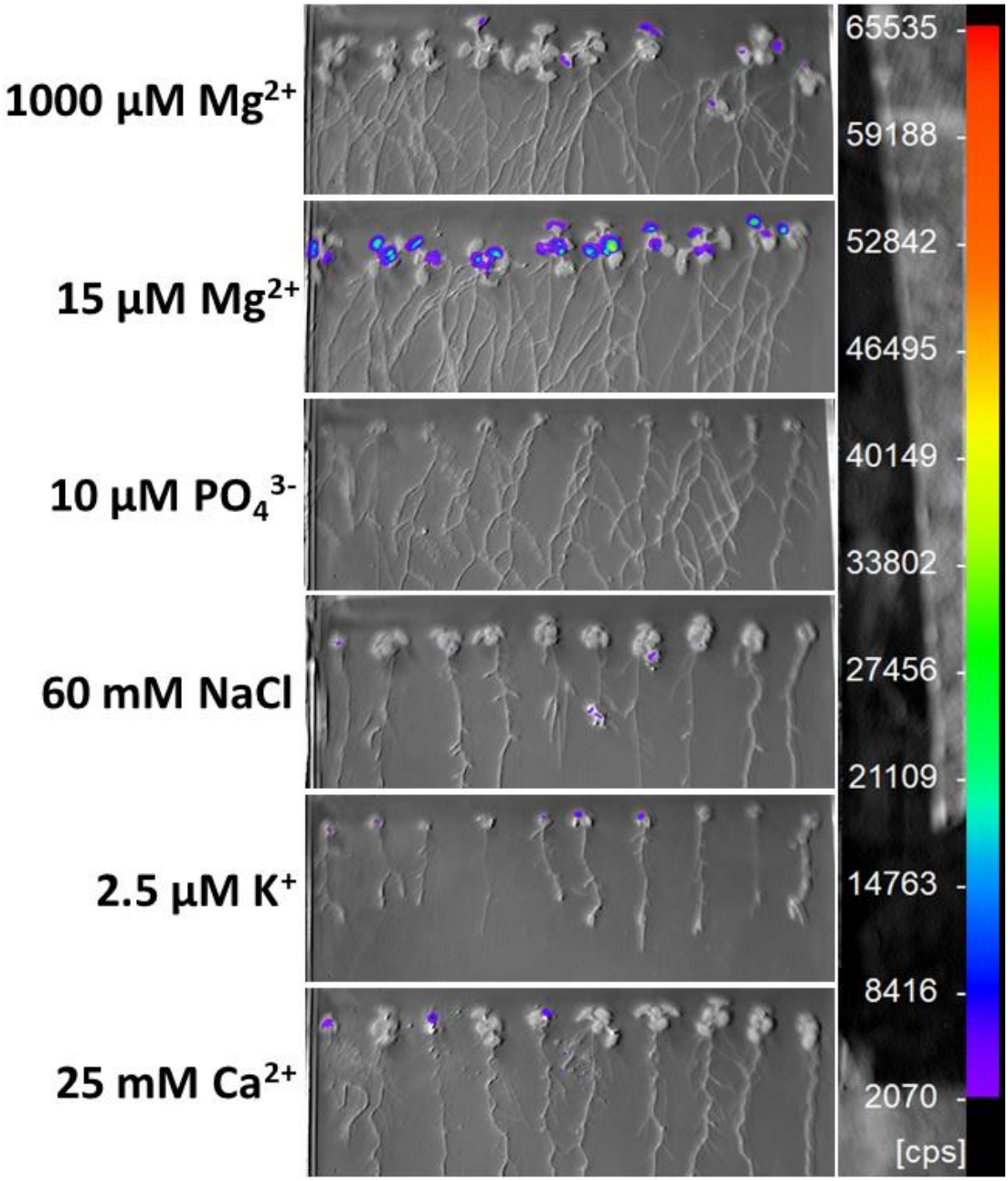

Figure 5.10 – *pAAA::LUC* reporter expression under different nutrient stresses
Seedlings of *pAAA::LUC* 2-4 were grown on agar plates containing HM made with washed agar with altered ion concentrations until 10 DAG, then luciferase expression was visualized by spraying seedlings with a solution containing luciferin and measuring light emission using a photon-counting camera. **cps** – [photon] counts per second.

5.2.5 A forward genetic screen for factors involved in Mg^{2+} homeostasis

To start the forward genetic screen, seeds of *pAAA::LUC* 2-4 were mutagenized by being submerged in a solution containing 65 mM EMS for six hours, using a protocol adapted from Kim *et al.* [265]. Seeds were then dried, and sprinkled onto soil immediately. Mature M_1 plants were allowed to self-fertilize, then grouped into "pools" of roughly ten individuals at a time, collecting seeds from each pool together This yielded a total of fifty pools of seeds from roughly 500 M_1 individuals.

Germination rate is often used as a simple measure for the effect of mutagenesis on viability of the mutagenized progeny, whereas the rate of plants exhibiting white coloration due to damage to genes necessary for chlorophyll production ("albino mutants") can be used to assess the frequency of mutations present in the population [274, 275]. Therefore, germination and the rate of albino mutants were determined in a mixed population consisting of seeds from pools 1-16. Germination rate was 96.7% for the parent line, but 82.8% for M_2 seeds. No albino mutants could be found among seedlings of the parent line, but 74 out of 2070 M_2 seedlings investigated (3.58%) showed no or very little green coloration. Therefore, EMS mutagenesis was deemed effective, while seed viability was deemed sufficiently high to carry out a forward genetic screen.

To identify M_2 seedlings with altered LUC expression, two different, complementary approaches were used. In each case, seeds from mutagenized populations were plated alongside un-mutagenized *pAAA::LUC* seeds ("parent line" seeds), and screened for LUC expression after growth on agar plates until 10DAG, as before. When plates with seeds from mutagenized populations were set up, the middle two seeds in both rows were replaced with seeds from the parent line, to provide a control for expected LUC expression. To find individuals with increased reporter expression, seeds were placed on plates containing HM with 50 µM added Mg^{2+}. After image acquisition, the detection threshold was set sufficiently high to exclude any light emission detected from any of the parent line seedlings on the plate. Any of the mutagenized seedlings for which significant emission could still be seen were considered to be expressing the reporter at higher levels than the un-mutagenized parent line and selected.

To find individuals that had lost reporter expression, seeds were placed on square plates containing HM with 15 µM Mg^{2+}.Seedlings for which no LUC expression could be detected were selected.

Examples of plates from both "sides" of the screen are shown in **Figure 5.11**. In both cases, selected seedlings were placed on soil trays and allowed to self-fertilize. For each pool of M_2 seedlings tested, 300 seeds were screened for increased LUC expression and loss of LUC expression each. 16 pools were screened, which means that a total of 5000 seeds were tested for both increased and lost LUC expression.

Out of all candidate M_2 seedlings transferred to soil trays, 30 individuals selected for loss of LUC expression and 43 individuals selected for increased LUC expression survived and produced seeds. To determine whether the changes in LUC expression were caused by a genuine mutation, M_3 seeds from each candidate were screened for LUC expression again, as before. For each candidate, at least 80 seeds were tested under the same conditions as before, and the percentages of seedlings showing altered LUC expression were determined. Since a dominant mutation, present as a single copy in the genome, would be passed on to 75% of all offspring, and a recessive mutation would be passed on to all offspring, only candidates producing offspring out of which more than 70% showed altered LUC expression were carried forward. **Figure 5.12** shows example images from the M_3 re-screen for the lines later termed MgMt 2 and MgMt 3.

This process was repeated in the M_4 generation, both to increase the robustness of the approach and because for some lines, insufficient M_3 seeds had germinated to determine the ratio of seedlings showing altered expression with any certainty. After this, none of the lines initially selected for loss of reporter expression on 15 µM Mg^{2+} remained. However, eleven lines selected for increased reporter expression on 50 µM Mg^{2+} were carried forward, each showing altered LUC expression in at least 70% of seedlings in the M_3 and M_4 generations. The results of this part of the forward genetic screen are visualized in **Figure 5.13**. Out of the eleven lines carried forward, ten appeared to carry homozygous, recessive mutations, while one appeared to be carrying a dominant mutation.

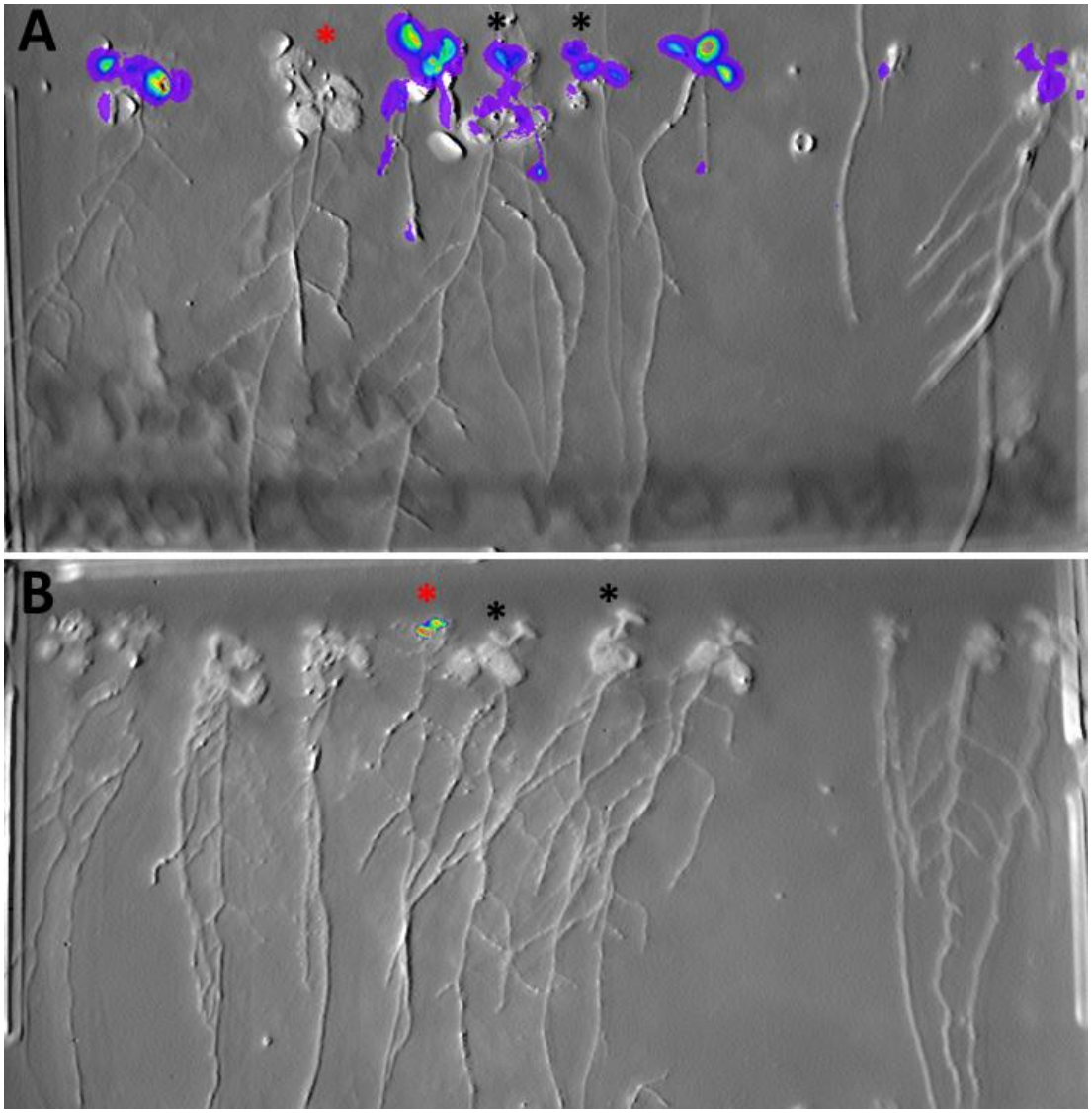

Figure 5.11 – Example images from the forward genetic screen (M_2)

Seedlings of *pAAA::LUC* 2-4 (M_2) were grown alongside seedlings of the un-mutagenized parent line on agar plates containing HM made with washed agar until 10 DAG, then LUC expression was visualized by spraying seedlings with a solution containing luciferin and measuring light emission using a photon-counting camera. **A** – During the screen for loss of reporter expression, seedlings were grown on plates containing 15 µM Mg^{2+}; detection limits were set to roughly 1000 cps. Seedlings showing no detectable luciferase expression were selected. **B** – During the screen for increased reporter expression, seedlings were grown on plates containing 50 µM Mg^{2+}; detection limits were set such that no expression was detected from control seedlings. Seedlings showing detectable expression were selected. Black stars in **A** and **B** denote control seedlings (*pAAA::LUC* 2-4), while red stars denote candidates that were selected and transferred to soil trays.

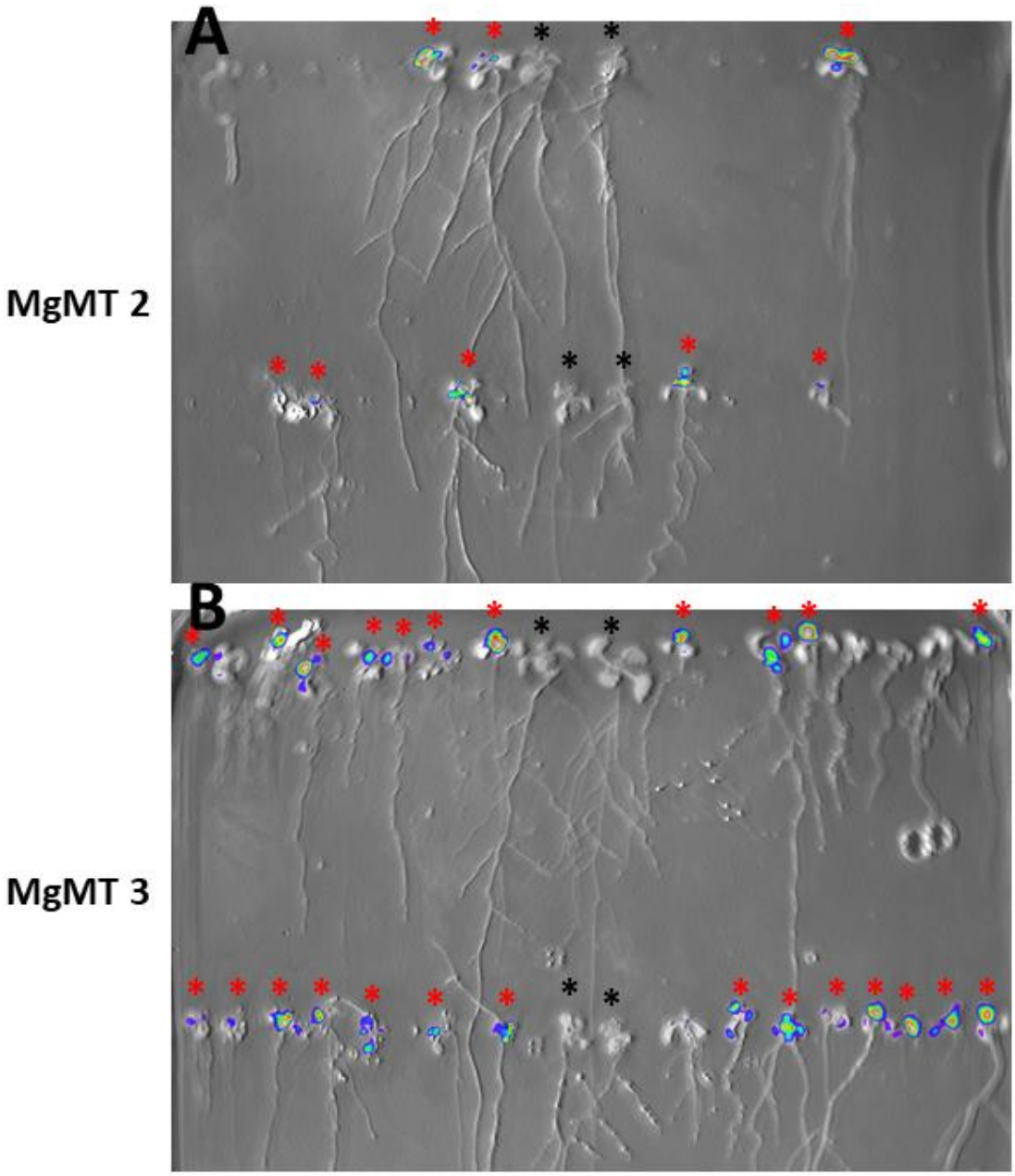

Figure 5.12 - Example images from the forward genetic screen (M_3)

Seeds from putative mutants (M_3) were grown alongside seedlings of the un-mutagenized parent line *pAAA::LUC* 2-4 on agar plates containing HM made with washed agar until 10 DAG, then LUC expression was visualized by spraying seedlings with a solution containing luciferin and measuring light emission using a photon-counting camera. Seedlings showing changes in reporter expression similar to the M_2 individual they were derived from were counted and compared to numbers of seedlings showing "normal" reporter expression. **A** – MgMt 2. **B** – MgMt 3. Black stars in **A** and **B** denote control seedlings (*pAAA::LUC* 2-4), while red stars denote seedlings showing increased reporter expression.

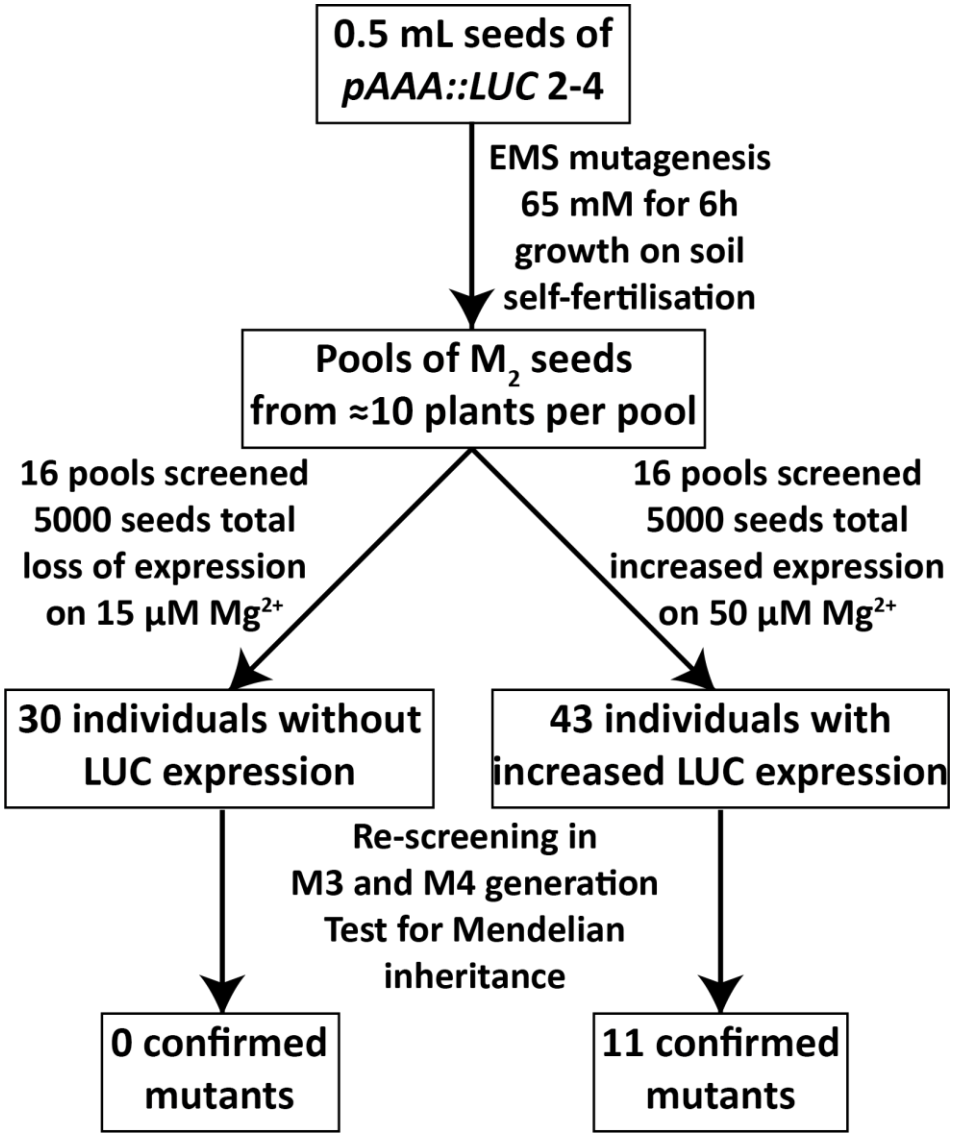

Figure 5.13 - Workflow and outcomes of the forward genetic screen

The process of the forward genetic screen for genes involved in Mg^{2+}-homeostasis carried out in this project, from mutagenesis to discovery of confirmed mutant lines. Stages in the process are described in black boxes, whereas processes leading from one stage to the next are symbolized by black arrows and briefly described next to the respective arrow.

5.2.6 Potentially causative SNVs were determined for seven candidates arising from the forward genetic screen

As described in the introduction, identification of the mutations present in each mutant line was carried out using the MutMap approach [189, 190]. Therefore, the confirmed mutant lines identified previously were crossed with the un-mutagenized "parent line" *pAAA::LUC* 2-4. Nine mutant lines were back-crossed successfully and yielded F_1 seeds, which were tested for LUC expression and growth yet again. All crosses yielded some offspring that were phenotypically similar to WT plants (some examples shown in **Appendix A**, **Figure S5.4**), although in all cases, seedlings showing mutant phenotypes were found together with those exhibiting WT phenotypes. This was attributed to imperfect efficiency of the crossing procedure, with seedlings showing mutant phenotypes representing self-fertilized seeds contaminating the pools of crossed seeds. For the eight lines carrying recessive mutations, seedlings having lost the increased LUC expression phenotype were therefore selected and carried forward, while for the putative dominant line, seedlings growing comparatively well, but retaining increased LUC expression were selected.

All selected seedlings were put to soil and allowed to self-fertilize, then resulting F_2 seeds were screened for LUC expression again. F_2 seedlings showing increased LUC expression similar to M_3 and/or M_4 seedlings before back-crossing were counted for each line. All recessive lines yielded around 25% seedlings showing the original phenotypes again, consistent with Mendelian inheritance for a single recessive allele. For the line thought to harbour a dominant mutation, approximately 50% of all offspring showed increased reporter expression, which is not consistent with Mendelian inheritance. Regardless, for all mutant lines, as well as for the parent line *pAAA::LUC* 2-4, at least 20 seedlings showing increased LUC expression were sampled, pooling all selected seedlings for one line. DNA was extracted from the resulting ten pools, and whole-genome sampling (WGS) carried out according to **Chapter 2**, **Section 2.3.4**. At this stage, all remaining lines were known to harbour a mutation responsible for the observed phenotype, with the potential exception of the line with the dominant mutation.

Therefore, mutants were referred to as MgMt ("magnesium mutant") 2 to -10, with the name MgMt 1 reserved for a line that was initially not back-crossed successfully.

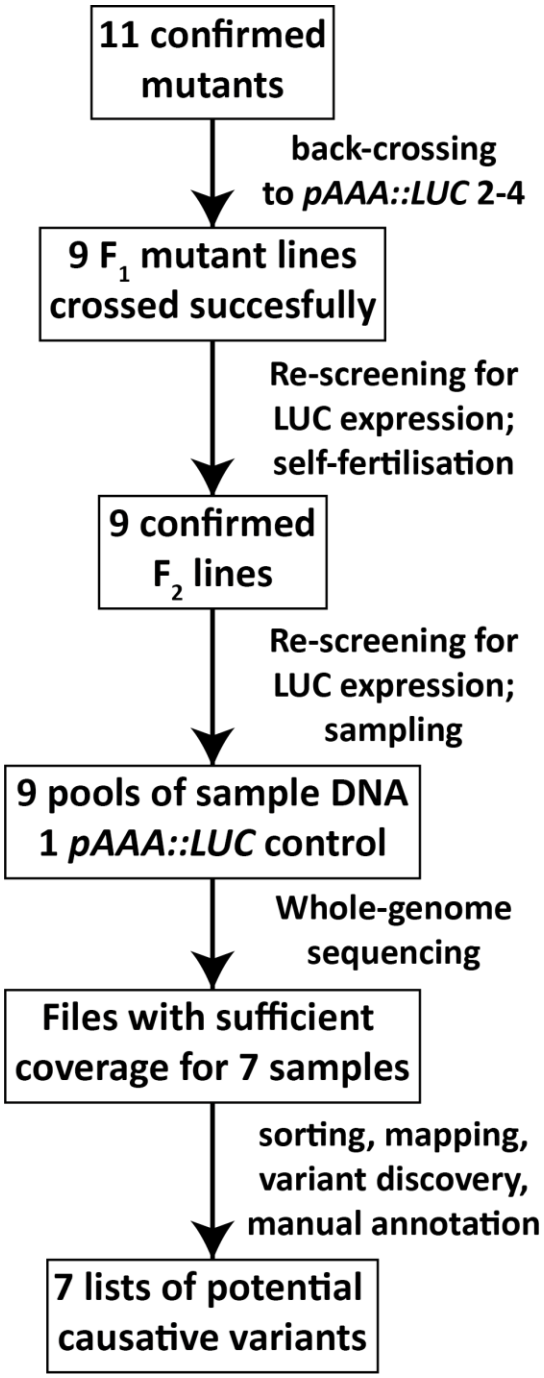

Figure 5.14 – Workflow and outcomes of variant discovery in mutants

The process of the forward genetic screen for genes involved in Mg^{2+}-homeostasis carried out in this project, from confirmed mutants to discovery of potentially causative variants in each line. Stages in the process are described in black boxes, whereas processes leading from one stage to the next are symbolized by black arrows and briefly described next to the respective arrow.

Single nucleotide variations (SNVs) present in each sample were determined from WGS data according to **Chapter 2**, **Section 2.10.3**. Briefly, sequencing data from each sample, including the *pAAA::LUC* 2-4 control, were compared to the TAIR10 *A. thaliana* reference genome and SNVs obtained. SNVs present in the control were removed from all samples, but due to low coverage of the control genome, many false-positives remained. Therefore, SNVs present in more than two samples were discarded as well, accounting for two pairs of lines (MgMt 2 and -3, as well as MgMt 9 and -10) originating from the same pools, respectively. After this step, analysis of data for MgMt 10 was abandoned due to low sequencing coverage as well.

Next, locus information was obtained for each SNV, and those not within 3 kb of a transcriptional start site were discarded. SNVs occurring in the submitted DNA at less than 90% frequency were discarded, since these could not be causative of a phenotype occurring in all sampled seedlings. The line seemingly harbouring a dominant mutation, MgMt 8 was abandoned at this stage, since in this line, the causative mutation could be present at much lower frequencies in sampled DNA. At 66% or 75% frequency, too many SNVs were present to feasibly be able to assign causality.

Remaining SNVs clustered on one or two chromosomes in all seven remaining samples, with few variants present at high frequencies occurring outside of those clusters, which were several Mb wide. Finally, remaining SNVs were annotated manually, first discarding those within transposable element genes, yielding lists of potentially causative variants. Then those within introns, those causing synonymous mutations, and “low strength candidates” were excluded. In this context, low strength candidates were defined as those occurring at less than 100% frequency while also causing only a change to a very similar amino acid, more than 1 kb from a transcriptional start site, or similar. This yielded shortlists of potentially causative variants. **Table 5.7** gives the chromosomes with SNV clusters, as well as the lengths of long and short variant lists for each mutant line. Additionally, the entire mapping process is visualized in **Figure 5.14**. Shortlists of potentially causative mutations in each mutant line are given in **Tables 5.8** to **5.13**, except for MgMt 7, which is listed in **Table S5.6**.

To get an additional indication of candidate strength, each list of the potentially causative variants was compared with the MgD-related transcriptomic datasets from **Table 3.1**. The number of sets each gene potentially disrupted by an SNV was present in was determined, and is also given in **Tables 5.8** to **5.13** and **Table S5.6**.

Table 5.7 – Variant clusters and numbers in mutants with good coverage

Candidate	Chromosome(s)[a]	All Variants[b]	Variant Shortlist[c]
MgMt 2	5	29	15
MgMt 3	2, 5	9	3
MgMt 4	3, 4	22	12
MgMt 5	5, 4	6	4
MgMt 6	5	21	11
MgMt 7	2	51	30
MgMt 9	4	14	9

a – Chromosome(s) containing significant numbers of validated variants. **b** – Variants remaining in the respective mutant line after exclusion of those in intergenic regions, false-positives, variants below 90% frequency. **c** – Variants remaining after manual exclusion of remaining synonymous mutations, those in introns, and low-strength candidates.

Several seedlings showing increased LUC expression in the F_2 generation were put to soil for each mutant line in order to document the observed phenotypes. **Figure 5.15**, **Figure 5.16** and **Figure 5.17** show phenotypes of all seven retained mutant lines before and after back-crossing. Some lines, specifically MgMt 6, -7 and -9, showed visibly improved growth after back-crossing, with MgMt 7 and -9 indistinguishable from WT or pAAA::luc plants after back-crossing. MgMt 2 and -3 both exhibited yellowed leaves, especially in interveinal areas (**Figure 5.18**).

Figure 5.15 - Growth of M_2 mutant lines and F_2 back-crossed lines on soil

Plants were maintained on soil for five weeks, before aerial parts of representative individuals were removed and images taken. **A** – pAAA::luc 2-4; **B** – MgMt 2; **C** – MgMt 2 back-cross F_2; **D** – MgMt 3; **E** – MgMt 3 back-cross F_2; **F** – MgMt 4; **G** – MgMt 4 back-cross F_2.

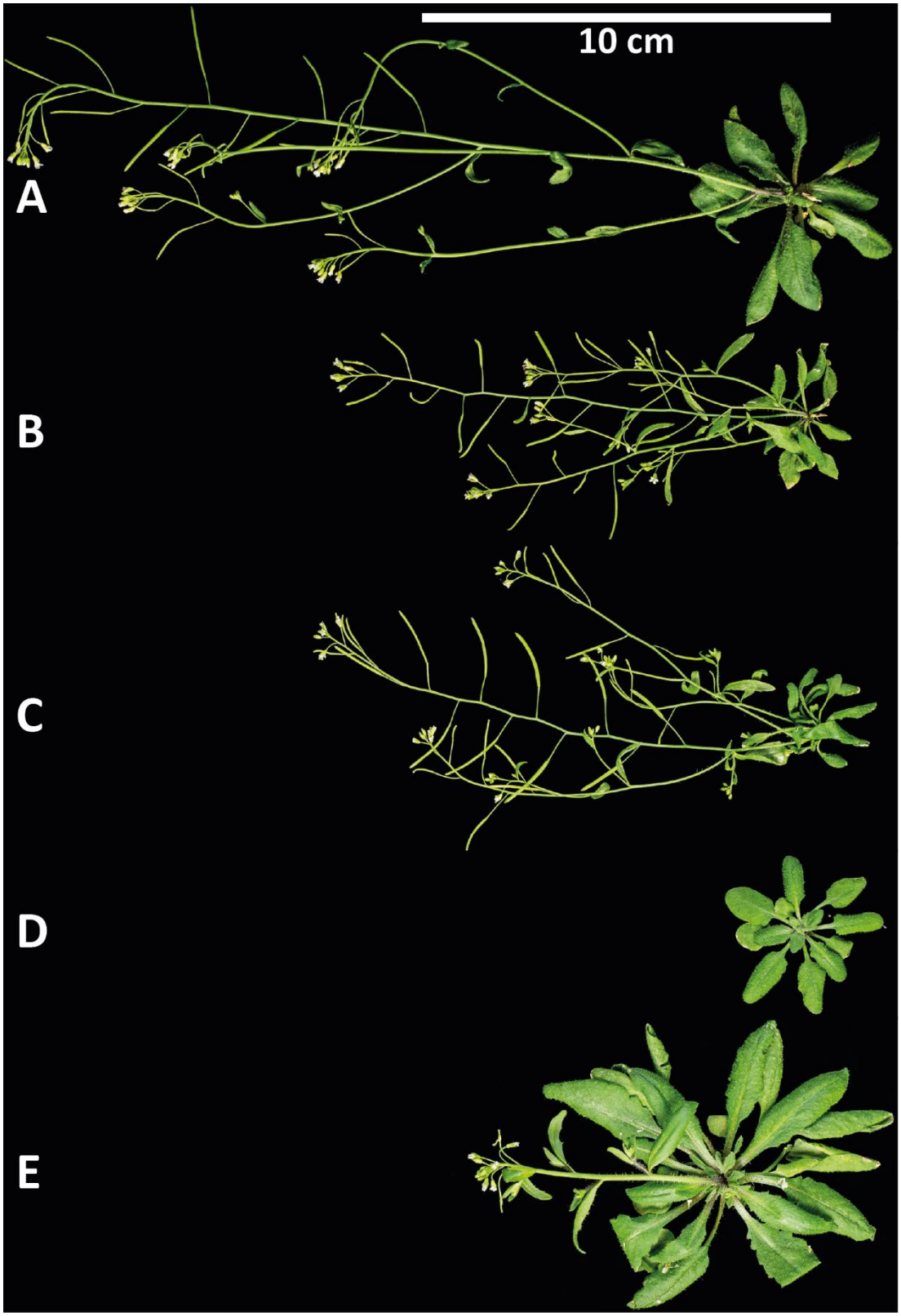

Figure 5.16 – Growth of M_2 mutant lines and F_2 back-crossed lines on soil

Plants were maintained on soil for five weeks, before aerial parts of representative individuals were removed and images taken. **A** – pAAA::luc 2-4; **B** – MgMt 5; **C** – MgMt 5 back-cross F_2; **D** – MgMt 6; **E** – MgMt 6 back-cross F_2.

This page is intentionally left blank

Blank pages are used throughout to allow legends to appear opposite display items in the paper copy of this document


10 cm
A
B
C
D
E

Figure 5.17 - Growth of M_2 mutant lines and F_2 back-crossed lines on soil

Plants were maintained on soil for five weeks, before aerial parts of representative individuals were removed and images taken. **A** – pAAA::luc 2-4; **B** – MgMt 7; **C** – MgMt 7 back-cross F_2; **D** – MgMt 9; **E** – MgMt 9 back-cross F_2.

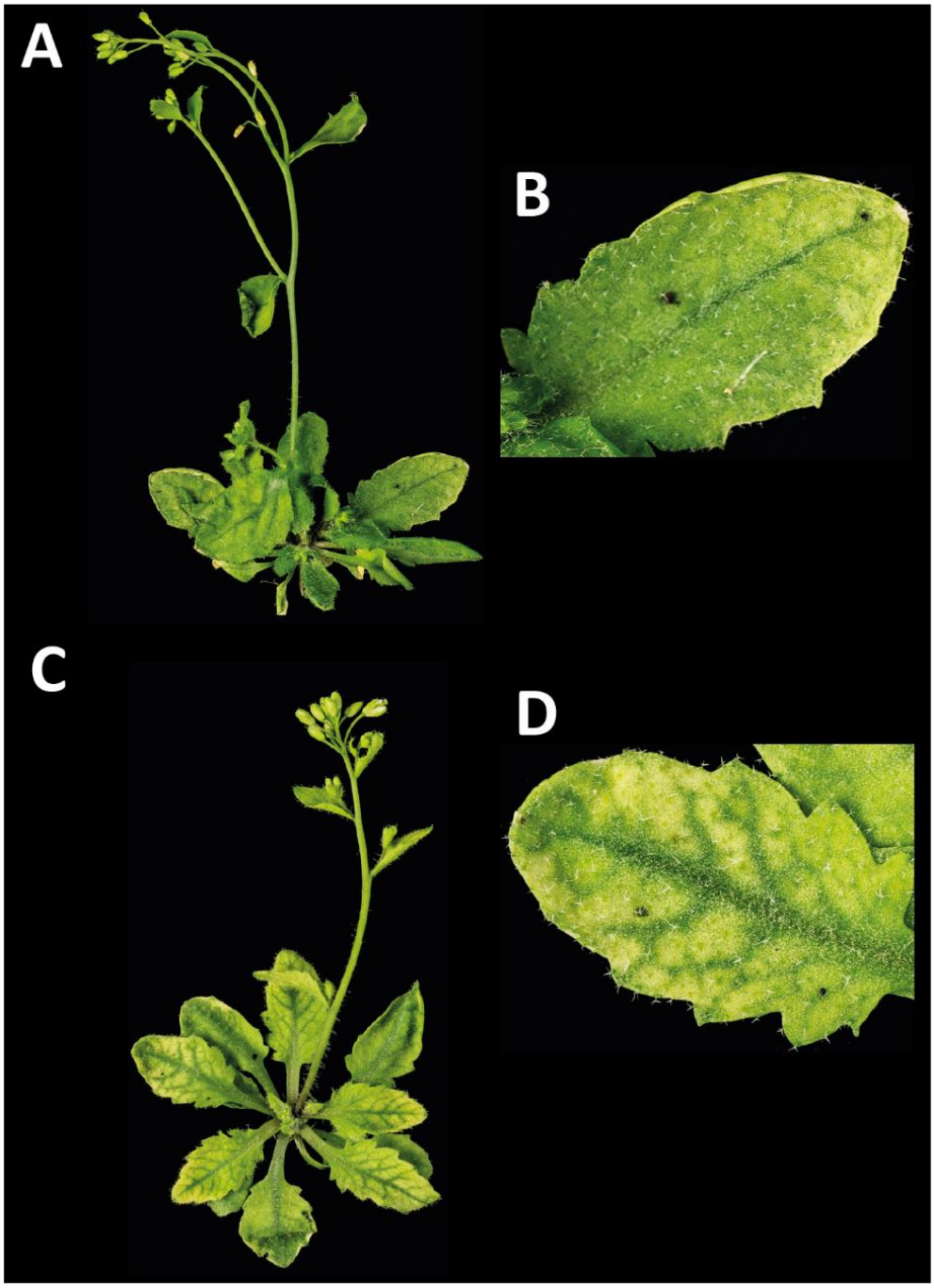

Figure 5.18 – Leaf yellowing phenotypes observed in MgMt 2 and MgMt 3

Plants were maintained on soil for five weeks, before aerial parts of representative individuals were removed and images taken. **A** – Whole MgMt 2 plant; **B** – Close-up image of a representative leaf of MgMt 2; **C** – Whole MgMt 3 plant; **D** – Close-up image of a representative leaf of MgMt 2.

Table 5.8 – Shortlist of potentially causative variants in MgMt 2

Position	Gene ID	Freq.	Lies in	Base change	Gene Annotation	No
16536	**AT5G01040**	100.0%	Promoter	-	LAC8; putative laccase	0
744897	**AT5G03150**	100.0%	Promoter	-	JKD, nuclear-localized putative TF	0
1047141	**AT5G03890**	100.0%	Promoter	-	PADRE protein	2
2956496	**AT5G09510**	100.0%	Exon	?	Ribosomal S19 family protein	3
3777800	**AT5G11720**	100.0%	Exon	Gly->Ser	AGLU1; Glycosyl hydrolases family 31	0
3809879	**AT5G11810**	100.0%	Exon	Gly->Ser	Rhomboid family protein	0
4294929	**AT5G13390**	100.0%	Exon	Cys->Tyr	NEF1	1
5196746	**AT5G15920**	100.0%	Exon	Leu->Gln	SMC5	1
7549111	**AT5G22720**	100.0%	Exon	?	FBXL; Encodes an F-box protein.	0
7549111	**AT5G22700**	100.0%	Promoter	-	LOW protein: F-box/FBD/LRR-like	0
4755734	**AT5G14730**	94.4%	Promoter	-	Unknown protein	3
1086693	**AT5G04040**	94.1%	Promoter	-	SDP1; triacylglycerol lipase	0
1130508	**AT5G04140**	93.3%	Exon	Glu->Lys	FD-GOGAT;	0
5516366	**AT5G16770**	92.2%	Exon	Asp->Asn	MYB9; Member of R2R3 factor family	0
5686309	**AT5G17280**	92.2%	5' UTR	-	Oxidoreductase-like protein	0

Position - Position of the SNV on the chromosome. **Freq.** - Frequency of the variant across sequencing reads. **Lies in** - Position of the SNV relative to the gene model in the "Gene ID" column; "Promoter" denotes presence within 2 kb of the transcriptional start site. **Base change** - Change to the amino acid sequence caused by the SNV in question; "?" denotes uncertainty due to poorly-defined gene sequence. **No** - Number of transcriptomic datasets from **Table 3.1** in which the respective gene was found to be upregulated.

Table 5.9 – Shortlist of potentially causative variants in MgMt 3

Position	Gene ID	Freq.	Lies in	Base change	Gene Annotation	No
18678877	**AT2G45300**	100%	Splice site	-	3-phosphoshikimate 1-carboxyvinyltransferase	0
7305160	**AT2G16860**	95.0%	Exon	?	SYF2; GCIP-interacting family protein	0
9174995	**AT5G26230**	91.0%	Promoter	-	Membrane-associated kinase regulator 1	0

Position - Position of the SNV on the chromosome. **Freq.** - Frequency of the variant across sequencing reads. **Lies in** - Position of the SNV relative to the gene model in the "Gene ID" column; "Promoter" denotes presence within 2 kb of the transcriptional start site. **Base change** - Change to the amino acid sequence caused by the SNV in question; "?" denotes uncertainty due to poorly-defined gene sequence. **No** - Number of transcriptomic datasets from **Table 3.1** in which the respective gene was found to be upregulated.

Table 5.10 – Shortlist of potentially causative variants in MgMt 4

Position	Gene ID	Freq.	Lies in	Base change	Gene Annotation	No
2454066	**AT3G07680**	100.00%	Promoter	-	Golgi-localized p24 protein.	0
9682091	**AT4G17300**	100.00%	Exon	Asp->Asn	OVA8; Asparaginyl-tRNA synthetase	0
11474114	**AT4G21580**	96.15%	Promoter	-	Organic solute transporter ostalpha	2
10276160	**AT4G18670**	95.83%	Exon	Pro->Ser	LRX5; Leucine rich extensin protein	0
8616267	**AT4G15090**	95.24%	Exon	Asp->Asn	FAR1; far red light response signaling.	0
8932034	**AT3G24510**	95.00%	Exon	Asn->Lys	Defensin-like (DEFL) family protein	1
10107827	**AT4G18282**	94.74%	3' UTR	-	Uncharacterized ORF	0
10018908	**AT3G27160**	94.44%	3' UTR	-	GHS1; Plastid ribosomal pr. S21	0
16029581	**AT4G33240**	94.44%	Exon	Pro->Ser	FAB1a; PtdIns3P	0
5982753	**AT4G09440**	94.12%	Promoter	-	Hypothetical protein (DUF577)	0
10359705	**AT4G18905**	92.86%	Promoter	-	WD40 repeat-like superfamily	1
10749681	**AT3G28680**	92.59%	Exon	Gly->Asp	Ser carboxypeptidase S28 family protein	1

Position - Position of the SNV on the chromosome. **Freq.** - Frequency of the variant across sequencing reads. **Lies in** - Position of the SNV relative to the gene model in the "Gene ID" column; "Promoter" denotes presence within 2 kb of the transcriptional start site. **Base change** - Change to the amino acid sequence caused by the SNV in question; "?" denotes uncertainty due to poorly-defined gene sequence. **No** - Number of transcriptomic datasets from **Table 3.1** in which the respective gene was found to be upregulated.

Table 5.11 – Shortlist of potentially causative variants in MgMt 5

Position	Gene ID	Freq.	Lies in	Base change	Gene Annotation	No
2391161	**AT5G07560**	94.0%	Promoter	-	GRP20; Lipid-binding oleosin	1
10024147	**AT5G28010**	92.0%	Promoter	-		0
12801535	**AT4G24840**	91.0%	Promoter	-	COG2; oligomeric golgi complex subunit-like	0
26316266	**AT1G69870**	86.0%	Exon	Ser->Phe	NRT1.7; low affinity nitrate transporter	3

Position - Position of the SNV on the chromosome. **Freq.** - Frequency of the variant across sequencing reads. **Lies in** - Position of the SNV relative to the gene model in the "Gene ID" column; "Promoter" denotes presence within 2 kb of the transcriptional start site. **Base change** - Change to the amino acid sequence caused by the SNV in question; "?" denotes uncertainty due to poorly-defined gene sequence. **No** - Number of transcriptomic datasets from **Table 3.1** in which the respective gene was found to be upregulated.

Table 5.12 – Shortlist of potentially causative variants in MgMt 6

Position	Gene ID	Freq.	Lies in	Base change	Gene Annotation	No
14463243	**AT5G36740**	100.0%	Splice site	-	N-acyltransferase with RING/FYVE/PHD-domain	0
15334961	**AT5G38360**	100.0%	Promoter	-	Alpha/beta-Hydrolases superfamily	0
15938443	**AT5G39810**	100.0%	Promoter	-	AGAMOUS-like 98	2
16085046	**AT5G40240**	100.0%	Promoter	-	UMAMIT40; nodulin MtN21-like family	1
18158336	**AT5G44980**	100.0%	Promoter	-	F-box/RNI-like/FBD-like domains-containing	2
19763770	**AT5G48730**	100.0%	Splice site	-	Pentatricopeptide repeat (PPR) protein	0
18402087	**AT5G45410**	96.0%	Exon	Thr->Ile	Plastid protein of unknown function.	2
15289273	**AT5G38270**	95.0%	Exon	Gly->Glu	FDB37; F-box family protein	0
16602918	**AT5G41500**	93.0%	Promoter	-	F-box domain	0
20037529	**AT5G49430**	93.0%	Exon	?	WD40/YVTN repeat domain	0
15367494	**AT5G38390**	91.0%	Splice site	-	F-box/RNI-like superfamily	0

Position - Position of the SNV on the chromosome. **Freq.** - Frequency of the variant across sequencing reads. **Lies in** - Position of the SNV relative to the gene model in the "Gene ID" column; "Promoter" denotes presence within 2 kb of the transcriptional start site. **Base change** - Change to the amino acid sequence caused by the SNV in question; "?" denotes uncertainty due to poorly-defined gene sequence. **No** - Number of transcriptomic datasets from **Table 3.1** in which the respective gene was found to be upregulated.

Table 5.13 – Shortlist of potentially causative variants in MgMt 9

Position	Gene ID	Freq.	Lies in	Base change	Gene Annotation	No
5964761	AT4G09420	100.0%	Promoter	-	TIR-NBS15; Disease resistance protein	
15205157	AT4G31340	95.0%	Promoter	-	Myosin heavy chain-like protein	
5579450	AT4G08740	95.0%	Exon	Ser->Asn	Hypothetical protein	
11439592	AT4G21490	94.0%	Promoter	-	NAD(P)H dehydrogenase B3	
11799739	AT4G22330	92.0%	3' UTR	-	AtCES1; ceramide synthase	
12069075	AT4G23020	92.0%	Promoter	-	TRM11; hypothetical protein	
7332146	AT4G12370	91.0%	Exon	Arg->Cys	F-box/kelch-repeat protein	
7483062	AT4G12700	90.0%	Exon	Asp->Asn	Calcium ion-binding protein	
7538571	AT4G12860	90.0%	Exon	Gly->Glu	EF hand calcium-binding protein family	

Position - Position of the SNV on the chromosome. **Freq.** - Frequency of the variant across sequencing reads. **Lies in** - Position of the SNV relative to the gene model in the "Gene ID" column; "Promoter" denotes presence within 2 kb of the transcriptional start site. **Base change** - Change to the amino acid sequence caused by the SNV in question; "?" denotes uncertainty due to poorly-defined gene sequence. **No** - Number of transcriptomic datasets from **Table 3.1** in which the respective gene was found to be upregulated.

5.3 Discussion

5.3.1 Mg^{2+}-responsive genes identified during RNAseq can be divided into two categories

As can be seen from the subcluster analysis carried out on the RNAseq data generated in this work, displayed in **Figure 5.3**, subclusters one and six contain transcripts showing decreased expression at lower Mg^{2+}, while the other six subclusters contain transcripts showing increased expression. The six subclusters containing up-regulated transcripts can be divided into two categories: Subclusters three, four and eight are made up of transcripts showing "incremental" increases in expression, *i.e.*, expression is inversely correlated with medium Mg^{2+}-concentration throughout the spectrum of concentrations used. Subclusters two, five and seven contain transcripts showing a "steep" increase in expression between 50 and 15 µM Mg^{2+}, while expression at all higher Mg^{2+}-concentrations is roughly similar. This pattern was confirmed by qRT-PCR for some members, with *DTX3*, *AAA* (subcluster seven) and *PPR* (subcluster two) showing increases in expression only at 15 µM Mg^{2+}, while *PER70* (subcluster eight) showed a significant increase in expression at 50 and 15 µM Mg^{2+}, with non-significant, but appreciable increases in expression visible at even higher Mg^{2+} (**Figure 5.5**). The data generated for *AAA* specifically (**Figure 5.8**) suggest that the expression of this gene does not increase further when supplied Mg^{2+} is reduced further. Although the data are not sufficient to draw firm conclusions, the existence of a set of genes showing a "MgD on/off" pattern of expression is an exciting possibility.

When the set of genes upregulated under MgD in this work was compared to datasets from previous publications, it became apparent that the genes from subcluster five (**Table 5.3**) are present in more of the other datasets than those from subcluster eight (**Table 5.4**). When genes from subclusters two, five and seven are combined to form the set of genes showing "steep" upregulation (66 genes) and this set is compared with the other transcriptomic datasets, each gene is found in 2.8 datasets on average, with a median of three.

Only five members of this set (7.6%) are found in none of the other datasets. Doing the same for subclusters three, four and eight yields a set of 193 “incremental” transcripts, each found in 1.1 other datasets on average, with a median of one. 93 of them (48.2%) occur in no other dataset (data not shown). Therefore, most of the “incremental” transcripts are not universally MgD-responsive. They may be responding to conditions particular to some of the experiments carried out. Alternatively, changes in expression for many of them could be too small to be detected in other experiments, but since the total number of DEGs found in some other experiments is more than ten times higher than here (see **Chapter 3**, S**ection 3.2.1**), this seems unlikely. Since the genes occurring in the “steep” set are far more universally MgD-dependent, they are more likely to represent the core MgD transcriptomic dataset sought after in this study.

GO terms enriched for the set of “incremental” MgD-responsive transcripts did not differ greatly from those enriched for the whole set of genes upregulated under MgD in this study (data not shown). One noteworthy change is the occurrence of “phosphate ion homeostasis” in the category “biological process”. However, among the set of “steep” MgD-responsive genes, no significantly-enriched terms could be found except the single term “response to stimulus” for the category “biological process”. This may be due to the relatively small size of this set of genes (66 genes) reducing the likelihood of statistically significant results. However, the major problem is that the most relevant GO terms for this analysis are barely defined or annotated for *A. thaliana*. For example, only one gene in *Arabidopsis* carries the GO annotations “response to magnesium ion” and “cellular response to magnesium ion”: *PCAP1/AT4G20260*. This gene was not upregulated in any of the transcriptomic datasets tested, including the one obtained in this work. As such, the absence of (other) GO terms in the set of “steep” transcripts may be another indication that these genes do respond to MgD specifically.

5.3.2 The BCS1-clade AAA-type ATPases may have diversified to respond to a range of different stress-conditions in plants

AAA ATPases are a subfamily of AAA+-proteins, which is itself a subfamily of P-loop NTPases. They carry out a large variety of functions; in fact, "AAA" stands for "ATPases associated with diverse cellular activities" [271, 276]. The BCS1-clade of AAA ATPases derives its name from BCS1, a protein that differs from other AAA ATPases in both structure and function. BCS1 is present in the mitochondrial membrane, and is required for the functional assembly of integral proteins of the respiratory electron transport chain: the Rip1 complex in yeast, and respiratory complex III in humans, respectively [277]. The protein forms homo-heptamers in yeast, forming two aqueous pockets on either side of the membrane, then uses the energy from ATP-hydrolysis to transport its substrates across the membrane in their folded states in an "airlock-like" translocation mechanism [278].

The BCS1-clade of AAA-type ATPases is represented in animals and fungi by only one or two members per species. In plants, there are often many paralogues of BCS1 (36 in *A. thaliana*), which differ from their homologues in animals and fungi with respect to their N-termini [271]. This points toward a functional diversification of BCS1 AAA ATPases in plants. This could be due to the sedentary nature of plants, which have to cope with environmental stresses rather than moving away from them, but fungi are generally sedentary as well, and also possess only few members of the clade. It is also possible that the difference is due to the presence of chloroplasts in plants, which require highly complex, correctly-folded integral membrane proteins for their own electron transport chains. Indeed, GO annotation assigns chloroplast localisation to seven out of the 23 BCS1 clade members investigated here, (# 1, 9, 11, 14, 15, 17, 19) while only four are annotated as present in mitochondria (**Table S5.4**). "Plasma membrane" occurs eight times within the set, "endoplasmic reticulum" five times, "plasmodesma" two times, "Golgi apparatus" once and "extracellular region" once.

Five BCS1 clade members carry multiple annotations, and three carry none. Determination of the localisations of membrane proteins can sometimes be unreliable, so in practice, more (or fewer) BCS1 clade members may carry out their functions in chloroplasts. Nevertheless, it is likely that their diversification in plants has also led to some members being present in other cellular membranes.

As mentioned, many members of BCS1 appear to respond to salt stress. Assuming that their function is similar to their yeast and human homologues, this would make sense, since salt stress can impair protein folding [279, 280]. Increase in expression of proteins that can support protein folding could help mitigate the symptoms of salt stress. However, some members of this clade are also involved in modulating the response to plant hormones, such as AtBCS1/AtOM66/AT3G50930. This protein has been shown to be able to stimulate SA biosynthesis and signalling, with SA levels and expression of SA biosynthesis genes increased in ATOM66 overexpressor lines. They also exhibited reduced leaf starch content and superoxide accumulation in response to drought [281]. As shown in **Chapter 3**, starch accumulation is one of the earliest consequences of MgD, and superoxide is the ROS species primarily evolved in leaves affected by MgD. The sequence of ATOM66 is one of the most similar to AAA (**Figure 5.9**, **Table S5.5**). Despite its presence in the mitochondrial outer membrane, the abundance of proteins of the mitochondrial respiratory complex was unchanged in ATOM66 overexpressor lines, which further indicates that the function of BCS1-clade proteins in plants differs from their function in other kingdoms of life [281]. Expression of *ATOM66* also reacts to antimycin A (AA), an inhibitor of oxidative phosphorylation, which could indicate a response to disruptions of cellular energy-levels or to increased ROS evolution, both of which are caused by AA treatment. AT3G28510 (#5 in **Table 5.6** and **Table S5.5**) was also found to be upregulated in the RNAseq dataset generated here, and in four of the other transcriptomic datasets examined (**Table 5.2**). Interestingly, it is annotated as localized in the endoplasmic reticulum like AAA, whereas the third BCS1-clade AAA ATPase upregulated under MgD, AT2G18190, is not yet associated with a cellular localisation term.

In summary, it seems like most members of the BCS1-clade of AAA ATPases in *A. thaliana* are involved in responses to biotic and/or abiotic stress factors. There is also evidence that at least some members have roles in the modulation of hormone signalling pathways and/or developmental processes. Therefore, the BCS1-clade of AAA ATPases may have diversified in plants to respond to various stresses and regulate signalling pathways. It is possible that these proteins influence biological processes by modulating the abundance of membrane proteins in a mechanism similar to their yeast and human homologues, but since homologies are mostly restricted to the AAA ATPase domains [271, 281], their functions in plants might be different. Functional characterisation of more members of the clade will be necessary in order to confirm their role in plants. It might be necessary to investigate multiple knockouts due to potential redundancies; for example, the "mild" phenotype observed in *atom66* lines [281] may be due to the presence of the highly similar neighbouring clade member *AT3G50940*. Ultimately, the function of these proteins will have to be established by confirming protein interactions via methods such as pull-down assays, bimolecular fluorescence complementation, and *in vitro* functional assays. X-ray crystallography or cryo-electron microscopy could help to assign similarities and differences in their structure relative to their homologues.

5.3.3 *AAA/AT2G18193* may be a "master regulator" of responses to MgD

There is a large difference between the upregulation of *AAA* in the RNAseq data (19-fold, **Table 5.5**) and during the experiment for luciferase and *AAA* abundance (roughly 1600-fold, **Figure 5.8**), despite the conditions used being similar in theory. The value was higher during confirmation of RNAseq results by qRT-PCR (roughly 30-fold, **Figure 5.5**), which is generally more accurate than RNAseq, but the difference remains. This could be due to multiple factors, including the agar wash procedure used in this work (see **Chapter 2**, **Section 2.1.4**) producing inconsistencies in actual Mg^{2+}-concentrations within plates. Additionally, these two experiments were carried out roughly two years apart, and conditions in growth rooms, such as light intensity and temperature, may have changed slightly. The low absolute expression of *AAA* could also lead to large changes in observed fold-change values due to small errors or genuine differences in expression under control conditions. *AAA* is the most highly upregulated transcript in the transcriptomics datasets by Hermans *et al.*, 2010b [102] (552-fold) and Niu *et al* [104] (highest expression at low Mg^{2+} out of the transcripts that were not detected at control Mg^{2+}), and is within the top 30 most highly upregulated genes in Oda *et al.* [103] (67-fold). The transcript is not present in the data provided by Kamiya *et al.* [105], which likely means that the microarray used did not contain a probe able to detect this transcript. Therefore, *AAA* exhibits one of the strongest inductions under MgD out of all genes in the genome, and both of the values determined here appear to be within the possible range.

The upregulation of AAA appears to be highly specific to MgD (**Figure 5.10**). Of course, the expression of the *LUC* reporter construct may not reflect the expression of the endogenous *AAA* gene in all cases. Endogenous *AAA* expression should therefore be tested under these and other stress conditions via qRT-PCR. Ideally, abundance of the endogenous protein should be confirmed as well, potentially via western-blot. These experiments were beyond the scope of this project, but they should not represent a great hurdle. In terms of other stress conditions, exposure to flg22 and other biotic stresses would be especially interesting, since *ATOM66* expression was found to react to flg22 [281] and AAA is associated with the GO terms "defense" and "response to other organism" (**Table 5.6**).

Next, exposure to chemicals such as cycloheximide or AA could be tested, since many other BCS1-clade members were found to respond to one or both of these. However, these chemicals do not reflect stresses plants normally encounter in nature, so a reaction to Cycloheximide or AA would not necessarily imply that upregulation is not normally MgD-specific. Rather, these treatments could help pin-point the exact stimulus responsible for *AAA* upregulation in a series of experiments similar to those carried out by Peng *et al.* [96] for *OsSGR*.

The GO terms for "cellular process" associated with AAA coincide with some of the symptoms of MgD (**Table 5.6**). Oxidative stress and changes to carbohydrate metabolism are some of the most characteristic symptoms of MgD, and root morphogenesis is altered under these conditions as well (see **Chapter 3**). MgD also activates parts of the biotic stress response, as exemplified by the GO term "defense response" being enriched in the RNAseq data (**Table S5.2**), which could explain the the term "defense response to other organism" being associated with AAA. It seems unlikely that this is a coincidence, especially since one of the most similar proteins, ATOM66, was shown to reduce superoxide abundance and starch accumulation when overexpressed. It seems possible, therefore, that AAA could initiate and/or coordinate responses to multiple or all of the described symptoms of MgD.

5.3.4 Forward genetic screens for loss of reporter expression are prone to false-positives

During the forward genetic screen carried out here, 30 M_2 individuals which had apparently lost expression of the *LUC* transgene were identified, and 43 individuals were selected due to increased LUC expression. Subsequently, eleven of the candidates showing increased LUC expression could be confirmed as harbouring genuine mutations, whereas none of the candidates selected for loss of expression were ultimately retained. This can easily be explained by considering the factors that could lead to increases or decreases in expression, respectively, aside from genuine mutations.

Silencing of transgenes via RNA-directed DNA methylation is common in plants and can occur from one generation to the next stochastically [230, 282]. The luciferin spraying method used to test LUC expression during the screening process is not perfect, and uneven coverage or incomplete penetration of luciferin into cells could lead to individual seedlings not showing light emission despite expressing LUC. And finally, inherent biological variation as well as inconsistencies in plate Mg^{2+}-concentrations could lead to some seedlings not exhibiting increased *AAA*/*LUC* expression despite the reporter pathway being intact. In contrast, when testing for increased LUC expression, false-positives could only conceivably arise from stochastic variation in low-Mg^{2+} tolerance or transgene expression. Gain-of-function mutations in the promoter sequence of the transgene could cause false-positives for increased LUC expression, but loss-of-function mutations in the promoter could have the same effect for loss of expression, and loss-of-function mutations are generally more common.

The M_2 seedlings selected during the screen for absence of *LUC* expression all produced offspring some of which continued to exhibit reduced or absent LUC expression, but none of them passed on the phenotype to enough offspring to be consistent with Mendelian inheritance. Since stochastic differences in transgene expression and incomplete coverage during spraying would cause none of the offspring to show this phenotype, while loss-of-function mutations within the transgene promoter would be passed on normally, the cause for most of these false-positives is most likely silencing of the transgene.

Although chance is undoubtedly a large factor when it comes to the success or failure of a forward genetic screen, this problem highlights the importance of a set-up that minimizes the chance for errors. Selection for a positive phenotype, *i.e.*, increased reporter expression, is preferable to selection for a negative phenotype, *i.e.*, loss of reporter expression. Ideally, inconsistencies arising from human error would be eliminated, for example by using an automated set-up for luciferin spraying or avoiding reliance on the agar wash procedure used here (see **Chapter 2, Section 2.1.4**).

5.3.5 Mutants identified during the forward genetic screen contain multiple potentially causative mutations

Seven candidates arising from the screen have had their genome sequenced successfully (MgMt 2, 3, 4, 5, 6, 7 and 9), while another two have been back-crossed to *pAAA::LUC* 2-4 successfully and showed recovery of the initial phenotype in the F_2 generation, but have not yielded sequencing data of sufficient quality (MgMt 8 and 10). Two mutant lines could not be back-crossed successfully initially, (MgMt 1 and 11), out of which F_1 seeds are now available for one line (MgMt 1). Unfortunately, causative mutations could not be determined unambiguously for any of these lines. Determination of causative variants has been problematic mostly due to two factors, namely the inferior quality of the WGS data received and the abundance of SNVs in these mutant lines.

Since the frequency at which individual SNVs occur in DNA pools subjected to WGS is the key factor in determining the causative SNV in MutMap analysis [189], high and consistent sequencing depth during WGS is crucial. The target sequencing depth for the WGS analysis carried out in this work was 30x across the whole genome, however, the control and MgMt 10 samples exhibited many regions that were not covered at all. Even in other samples, coverage was closer to 5x in some regions. This means that sampling errors during creation of pools of F_2 seedlings showing mutant phenotypes, *i.e.*, inclusion of a seedling not actually homozygous for the causative SNV, is more likely to have a large influence on the outcome of sequencing. Even a single read from WT DNA would push the frequency of an SNV to 80% at 5x coverage, and would therefore mask a potentially causative SNV. The same is true for sequencing errors, *i.e.*, even if an SNV in the DNA is present at 100%, a single sequencing error could mask it from the set of SNVs considered for causality. This effect is felt even more strongly for dominant mutations, which would only be present in 66% of the sampled DNA, statistically. Since non-causative SNVs should be present at 50% frequency, these two rates become impossible to distinguish if margins of error are too high due to low coverage. This is why MgMt 8, thought to carry a dominant mutation, was excluded from analysis.

Nevertheless, lists of potentially causative SNVs could be obtained for seven of the candidates, narrowed down to a few SNVs each for most (**Tables 5.8** to **5.14**, **Table S5.6**). It is possible to speculate about the most likely candidate(s) for some of them.

MgMt 2 produces small plants showing leaf yellowing, particularly at the edges, tips and interveinal areas of leaves (**Figure 5.15, Figure 5.18**). The shortlist of potentially causative SNVs contains 15 entries, ten of which are present in 100% of the sequenced DNA (**Table 5.8**). Three of the strongest candidates are a Cys->Tyr change in the gene model for *AT5G13390/NEF1* at 100% frequency, and a Glu->Lys change in the gene model of *AT5G04140/Fd-GOGAT*, as well as a mutation of unknown effect within the predicted CDS of *AT5G22720/FBXL*. NEF1 (NO EXINE FORMATION 1) is predicted to be a protein of the mitochondrial inner membrane involved in maintaining plastid integrity [283]. Knockout mutants are small and show defects in plastid formation, as well as altered lipid abundance in reproductive tissues. These phenotypes are certainly consistent with those observed for MgMt 2, and defects in plastid formation could exacerbate the symptoms of MgD, although this protein is unlikely to be directly involved in processes maintaining Mg^{2+}-homeostasis. Fd-GOGAT is a glutamate synthase; mutants show defects in iron uptake, resulting in yellow-leaf phenotypes [284] similar to those observed for MgMt 2. Finally, FBXL (F-BOX/FBD/LRR-LIKE) is a poorly-annotated protein containing an F-box domain; overexpressor lines have been found to exhibit defects in cotyledon vein patterning [285]. The gene appears to be expressed throughout the vasculature of *Arabidopsis*.

MgMt 3 produces small plants as well, but the interveinal chlorosis phenotype is even stronger than for MgMt 2. (**Figure 5.15, Figure 5.18**). MgMt 3 contains only a single SNV present at 100% frequency in the WGS results (**Table 5.9**); a G to A change close to a splice site in the sequence of *AT2G45300*. This gene is thought to encode 3-phosphoshikimate 1-carboxyvinyltransferase, an enzyme important for chorismate biosynthesis through the shikimate pathway. However, it has not been functionally characterized. SHIKIMATE KINASE-LIKE 1 (SKL1), a protein originally thought to be involved in the shikimate pathway, has been shown to participate in chloroplast development in actuality [286].

Mutants showed strongly reduced ability to develop chloroplasts and concomitantly developed mostly white leaves. There is also a G to A SNV in an exon of *AT2G16860/SYF2*, a member of a spliceosome complex, which is reminiscent of SMU1, identified during a screen for mutants impaired in Mg^{2+}-homeostasis and described in Feng *et al.* [164], present at 95% frequency.

The shortlist of variants generated for MgMt 5 contains no SNVs occurring at 100% frequency (**Table 5.11**). One potentially causative SNV present at 94% frequency may be within the promoter sequence of *AT5G07560/GRP20*, a glycine-rich protein in the lipid-binding oleosin family, while another may be in the promoter of AT5G28010, a predicted Polyketide cyclase/dehydrase and lipid transport superfamily protein. Interestingly, there is also an SNV causing a Ser->Phe base change in *AT1G69870/NRT1.7* present at 86% frequency in the sequencing data for this line. *NRT1.7* was found to be upregulated in three of the MgD transcriptomic datasets investigated in this work, implying that it does have a role in the response to MgD. Since this protein is expressed in the phloem and thought to be important for source-to-sink remobilisation of nitrate [287], this is not unlikely. The low frequency the SNV in *NRT1.7* was observed with makes it seem unlikely that this SNV is causing the phenotype observed in MgMt 5, however. It is possible that the causative SNP in this line was "missed" altogether, since no SNV at 100% frequency remains.

All SNV shortlists generated for other MgMt lines contain plausible candidates, but at this stage, it is impossible to determine which ones are most likely to be truly causative of the phenotypes observed for each line.

Chapter 6: General Discussion

6.1 Summary of research findings

In this chapter, results generated over the course of this project will be discussed and related to existing literature. Open questions will be highlighted, and possible directions for further research provided. First, however, summaries of the research carried out are given for each of the three results chapters.

Chapter 3: An investigation of the physiological consequences of magnesium-deficiency in A. thaliana

The expression of putative MgD marker genes was compared between *A. thaliana* seedlings transferred to low-Mg^{2+} media (Mg^{2+}withdrawal) or grown on low Mg^{2+} continuously using qRT-PCR, and changes in expression were found to be similar between the two methods. Growth of plants on different concentrations of Mg^{2+} was quantified. The physiological symptoms of MgD were characterized for plants grown on continuous low Mg^{2+}, and the occurrence of starch accumulation, ROS stress, and reduced chlorophyll abundance was confirmed. The concentration of Mg^{2+} required to elicit each symptom was found to be inversely correlated to the time of Mg^{2+}-withdrawal required to elicit the same symptom in previous studies, confirming that continuous MgD elicits the same symptoms in the same "order" of severity as Mg^{2+} withdrawal, and therefore lending credibility to the established model of MgD (**Figure 1.6**). This work served to establish a method for inducing MgD of known severity in *A. thaliana* seedlings at high throughput, laying the foundation for a further exploration of the symptoms of MgD as well as establishing a basis for carrying out a forward genetic screen for factors involved in Mg^{2+}-homeostasis.

Additionally, the symptoms of MgD upstream of those characterized previously were investigated with the help of genetically-encoded, ratiometric sensors. The sequence encoding the MARIO FRET-sensor was cloned and transgenic *A. thaliana* expressing the sensor generated. Most lines generated were subject to silencing of the transgene, with the only MARIO-expressing line showing incorrect targeting of the protein. However, correct functioning of the sensor, as expressed in *Arabidopsis*, could be confirmed *in vitro*. The MgATP FRET-sensor ATeam and the ratiometric pH-sensor pHusion were used to investigate changes in cytosolic MgATP-concentrations, as well as cytosolic and apoplastic pH, respectively. The results show that levels of MgATP, as well as cytoplasmic and apoplastic pH and PM pH differentials increase under continuous MgD in *A. thaliana*, and this information was used to create an alternative model of the consequences of MgD. The model is visualized in **Figure 3.20**.

Chapter 4: The localisation and physiological role of MRS2 magnesium transporters in A. thaliana

SALK T-DNA insertion lines for all functional MRS2s in *A. thaliana* were obtained, and presence of T-DNA insertions was confirmed by PCR. Visual and fertility phenotypes were observed and found to be similar to published results for all lines tested, except for *mrs2-3* mutants, which initially showed stochastic slow growth and fertility defects. After propagation for several generations, however, these lines showed uniformly slow growth and normal fertility. *mrs2-3*, *mrs2-4*, *mrs2-7*, *mrs2-10* and *mrs2-1 mrs2-5 mrs2-10* triple knock-out (TKO) lines were carried forward and characterized further. Shoot weight after growth on low, replete, and excess Mg^{2+} was compared between mutants and WT. One *mrs2-4* and *mrs2-7* line each were characterized under a range of Mg^{2+}-concentrations, including root growth parameters.

To investigate the sub-cellular localisation and tissue distribution of select MRS2s, creation of *pMRS2-3::MRS2-3::GFP*, *pMRS2-4::MRS2-4::GFP* and *pMRS2-10::MRS2-10::GFP* expression constructs was attempted, but *pMRS2-4::MRS2-4::GFP* could not be assembled successfully. *mrs2-3* mutants were transformed with *pMRS2-3::MRS2-3::GFP*, *mrs2-10* mutants and TKO were transformed with *pMRS2-10::MRS2-10::GFP* and *mrs2-4* mutants with a previously-used *pMRS2-4::MRS2-4::GFP* plasmid [103]. GFP expression was detected for plants transformed with *pMRS2-3::MRS2-3::GFP* and *pMRS2-4::MRS2-4::GFP*, but not for those with *pMRS2-10::MRS2-10::GFP*. In both cases, GFP fluorescence was detected primarily in the division and elongation zones of the root tip.

Complementation of mutant phenotypes was assessed for transformed *mrs2-3* and *mrs2-4* lines; partial complementation was found for *mrs2-3* transformants, and nearly complete complementation for *mrs2-4* transformants. Confocal laser-scanning microscopy revealed that MRS2-4::GFP was targeted primarily to transverse cell membranes of cells of the early vasculature in root tips, while MRS2-3::GFP seemed to localize primarily in the endomembrane system. An epigenetic mechanism for the initially stochastic phenotypes and partial complementation observed for *mrs2-3* lines was proposed.

RNA-sequencing was carried out using RNA from *A. thaliana* seedlings grown on different concentrations of Mg^{2+}. A collection of MgD transcriptome data was generated by combining the obtained data and previously published MgD transcriptomic datasets. The use of multiple intermediate Mg^{2+}-concentrations allowed differentially-expressed genes within the RNAseq dataset obtained here to be divided into two distinct categories according to expression-patterns. The expression of "incremental" transcripts is inversely correlated with Mg^{2+}-concentrations across all concentrations, whereas expression of "steep" transcripts increases sharply below a threshold of roughly 50 µM Mg^{2+}. Implications for functional relevance and specificity to MgD were discussed.

The MgD transcriptome collection was used to choose three putative MgD marker genes, which were in turn used to create MgD reporter plants. Reporter expression was tested for plants grown on different Mg^{2+}-concentrations, and an increase in reporter expression was found for plants transformed with two of the constructs. *pAAA::LUC*, containing the promoter of the putative AAA-type ATPase *AT2G18193*, was found to produce the strongest increase in expression and was selected for further characterisation. Reporter expression was tested under several other selected nutrient deficiency and excess conditions and was not found to be increased under any of the other stress conditions tested.

A forward genetic screen was carried out using *pAAA::LUC* reporter plants, in which 5,000 M_2 seedlings were screened for loss of reporter expression and increased reporter expression each. None of the initial candidates showing loss of reporter expression could be confirmed as genuine mutants, but eleven candidates were identified from the screen for increased reporter expression. Identification of causative mutations was attempted according to the MutMap/LumiMap pipeline [189, 190]. Due to the abundance of genetic variants in the mutant DNA and inconsistencies during WGS, no single mutations clearly responsible for the mutant phenotypes could be identified. However, lists of potentially causative variants could be generated for seven of the candidates, and genomic regions containing the causative mutations could be identified for most of them.

6.2 Open questions and possibilities for further research

6.2.1 Comparisons of multiple transcriptomic datasets can improve understanding of MgD responses and assist marker gene discovery

Over the course of this project, a total of six different transcriptomic datasets including data on gene expression under MgD were gathered and compared, creating a "collection" of MgD transcriptome data, consisting of data acquired over the course of this work (see **Chapter 5**, **Section 5.2.1**) and data from previous studies (see **Chapter 3**, **Table 3.1**). So far, only transcripts showing increased expression were investigated, both due to the requirement of a gene showing increased expression as the reporter for the forward genetic screen and due to the higher number of upregulated genes under MgD [227]. It would be simple to generate a second collection of transcripts showing decreased expression, using the same sources. This approach has enabled a more informed choice of reporter for the forward genetic screen, and the discovery of a subset of MgD-induced genes with increased chance of being robustly, and potentially specifically, associated with MgD (see **Chapter 5, Section 5.3.1**). This collection can be used to validate and contextualize other studies on the MgD transcriptome.

A recent study by Ogura *et al.* [87] includes transcriptome data on leaves and roots exposed to MgD by Mg^{2+}-withdrawal, including multiple time-points. These recent data were not included in the transcriptome collection, because the authors separate leaves into "mature leaves" and "expanding leaves", which would have complicated inclusion into the existing collection. Two of the most characteristic responses observed in Ogura *et al.* are the increased expression of genes with functions in antioxidant processes, such as those encoding subunits of glutathione S-transferase tau and glutaredoxins, as well as the activation of the systemic acquired resistance (SAR) pathway. Lists of genes associated with these functions are provided, and these were cross-referenced with the transcriptome collection generated here. Results for genes with functions in antioxidant processes are shown in **Table 6.1**, and for those in SAR in **Table 6.2**.

The antioxidant-related genes from **Table 6.1** are well-represented in the six transcriptomic datasets in the collection, occurring in an average of 3.27 of them, median 3. Similarly, the SAR-related genes from **Table 6.2** occur in 2.52 other datasets on average, median 3.

This serves to highlight the universal emergence of ROS stress in plants exposed to MgD, and the importance of mitigating the same. The activation of defence responses in *Arabidopsis* exposed to MgD has been observed previously as well [227], and includes multiple important activators of SA signalling [87]. Possible causes of this coupling between MgD and defence responses has not been explained so far, and is worthy of further investigation.

On the other hand, Ogura *et al.* provide a table of known and putative Mg^{2+} transport proteins in *A. thaliana*, none of which were found to show increased expression under MgD in their data [87]. Cross-referencing this table with the MgD collection created here shows that none of these genes occur in any of the datasets, except for five of the 28 genes, which are each represented in a single set (0.18 sets average, median 0) (**Table S6.1**). This remarkably low representation highlights the seemingly complete absence of regulation of Mg^{2+}-transporters at the transcriptional level.

Table 6.1 - Presence of genes associated with antioxidant processes from Ogura *et al.* in the MgD transcriptome collection

Gene ID	Name	Description	Sets
AT2G29490	*GSTU1*	Glutathione S-transferase tau 1	2
AT2G29460	*GSTU4*	Glutathione S-transferase tau 4	5
AT3G09270	*GSTU8*	Glutathione S-transferase tau 8	3
AT5G62480	*GSTU9*	Glutathione S-transferase tau 9	6
AT1G74590	*GSTU10*	Glutathione S-transferase tau 10	3
AT1G78380	*GSTU19*	Glutathione S-transferase tau 19	0
AT1G78340	*GSTU22*	Glutathione S-transferase tau 22	4
AT1G17170	*GSTU24*	Glutathione S-transferase tau 24	4
AT1G17180	*GSTU25*	Glutathione S-transferase tau 25	4
AT1G03850	*GRXS13*	Glutaredoxin 13	2
AT1G28480	*GRX480*	Glutaredoxin 480	3

The list of genes associated with antioxidant processes in Ogura *et al.* [87] was cross-referenced with the MgD transcriptome collection created in this work, returning the number of transcriptomic datasets from the collection each of the genes is upregulated in, given in the "**Sets**" column.

Brumbarova *et al.* [188] carried out co-expression analysis on *Arabidopsis* with respect to 13 different nutrient availability anomalies, *i.e.*, nutrient stress conditions, with the aim of identifying transcriptional regulators both unique and common to different nutrient stress conditions. Two MgD transcriptomes were incorporated into the study, those by Hermans *et al*., 2010a [101] and by Niu *et al*., 2016 [104]. In both cases, data from roots were used; a list of potential transcriptional marker genes for MgD was generated. Remarkably, despite root data being used to generate this list of marker genes, the overlap with the transcriptome collection, which includes only data from gene expression in shoots, is substantial. Each of the 20 proposed MgD marker genes is present in 3.25 transcriptomic datasets from the collection on average, with a median of 3 (**Table 6.3**). Expression of these genes therefore increases under MgD in roots and shoots. However, the descriptions for many of these genes imply responsiveness to other stress-conditions, which would prevent them from being useful as MgD-specific marker genes.

Table 6.2 - Presence of genes associated with systemic acquired resistance from Ogura *et al.* in the MgD transcriptome collection

Gene ID	Name	Description	Sets
AT1G74710	*EDS16*	Isochorismate synth.; mutants impaired in SA	4
AT2G46370	*JAR1*	Jasmonate-amido synthetase, GH3 family	0
AT5G65600	*LECRK-IX.2*	Concanavalin A-like lectin protein kinase	2
AT1G22070	*TGA3*	bZIP Transcription factor	0
AT5G45110	*NPR3*	Regulation of defense responses	2
AT3G52430	*PAD4*	Lipase-like gene, SA signaling	4
AT1G19250	*FMO1*	EDS1-regulated but SA-independent	4
AT5G52810	*SARD4*	NAD(P)-binding Rossmann-fold superfamily	3
AT3G56400	*WRKY70*	WRKY Transcription Factor; Group III	3
AT4G12470	*AZI1*	Priming of SA induction, systemic immunity	3
AT4G23170	*EP1(AED19)*	Induced in response to SA	2
AT3G57260	*BGL2 (PR2)*	Beta 1,3-glucanase	4
AT5G10760	*AED1*	Eukaryotic aspartyl protease family	3
AT1G75040	*PR5*	Thaumatin-like, response to pathogens	4
AT5G03350	*LLP1 (AED9)*	Legume lectin family protein	3
AT2G38470	*WRKY33*	WRKY transcription factor; salt stress	1
AT5G40990	*GLIP1*	Component of plant resistance. Antimicrobial	2
AT4G37150	*MES9*	Carboxylesterase activity, SAR	2
AT3G04720	*PR4*	Response to ethylene and turnip crinkle virus	1
AT3G48090	*EDS1*	R gene-mediated disease resistance	3
AT1G59870	*PEN3*	ATP binding cassette transporter	2
AT2G13810	*ALD1*	AGD2-like defense response protein 1	3
AT2G18660	*PNP-A*	Plant Natriuretic Peptide A; SAR, PR like	5
AT2G43570	*CHI (AED15)*	Chitinase	3
AT4G01370	*MPK4*	MAP kinase, inv. in response to pathogens	0
AT5G64930	*CPR5*	Regulator of expression of PR genes; SAR	0
AT5G55460	*ATLTP4.5*	Bifunctional inhibitor/lipid-transfer protein	2
AT2G14610	*PR1*	PR1 gene expression is induced in response to a variety of pathogens, SA responsive	5
AT5G55450	*ATLTP4.4*	Bifunctional inhibitor/lipid-transfer protein	3

The list of genes associated with SAR in Ogura *et al.* [87] was cross-referenced with the MgD transcriptome collection created in this work, returning the number of transcriptomic datasets from the collection each of the genes is upregulated in, given in the "**Sets**" column.

The three genes represented in most of the datasets, specifically (*UGT74E2*, *SOT12* and *HRG2*, each present in five out of six datasets) all are annotated as responding to other stress conditions; *UGT74E2* and *HRG2* to H_2O_2, *i.e.*, ROS, and *SOT12* to pathogens, once again showing that the responses to ROS stress and pathogenesis are prevalent under MgD.

The transcriptome collection generated here can be queried to generate a measure of the likelihood that any set of genes is involved in the response to MgD. However, there is currently no way to take into account potential functions of queried genes under other (stress) conditions. Although the increase in expression of *AAA/AT2G18193* so far seems to be MgD-specific, in general, it is exceedingly unlikely to find a gene which responds only to a single stress condition using the methods employed here, and it seems likely that *AAA* does respond to one or more other conditions itself.

Interactions between different nutrients, and nutrient stress conditions, have become the focus of research on abiotic stress over recent years [288, 289], reflected in the coining of the terms “ionome” and “ionomics” [290]. Indeed, to truly understand the response to a stress condition, it cannot be observed in isolation, but must be compared and contrasted with others. Comparing multiple transcriptomic datasets is preferable to looking at one set, but to improve understanding of the responses to abiotic stress, to discover improved marker genes and reporter candidates, and to be able to predict gene functions from transcriptional profiles, it will be necessary to create larger collections and databases incorporating information from multiple stress conditions. Progress is being made at this, with more and more transcriptome data becoming available [188, 291]. With the rise of machine-learning methods, large sets of data can be analysed to reveal effects and conclusions that would not be obvious otherwise, and many approaches lend themselves to prediction of gene functions, for example [292]. Machine learning approaches have already made progress in distinguishing responses to different stress conditions [293], identifying transcription factors involved in drought resistance [294], and elucidating functions of microRNAs in abiotic stress responses [295], among others.

Table 6.3 - Presence of putative MgD marker genes from Brumbarova *et al.* in the MgD transcriptome collection

Gene ID	Name	Description	Sets
AT1G05680	*UGT74E2*	UDP-glucosyltransferase, induced by H_2O_2	5
AT1G18300	*NUDT4*	Nudix hydrolase homolog 4	2
AT1G35140	*HSP17.6A*	HSP20-like chaperones superfamily	2
AT1G76650	*CML38*	Calmodulin-like 38	4
AT2G03760	*SOT12*	Induced by SA, JA and bacterial pathogens	5
AT2G46400	*WRKY46*	Osmotic/salt stress-dependent lateral root inhibition	4
AT3G22370	*AOX1A*	Marker for mitochondrial retrograde response	4
AT3G46230	*HSP17.4*	Induced by heat, cold, salt, drought and high-light	3
AT3G54530		Hypothetical protein	2
AT4G01360	*BPS3*	Protein related to BYPASS1 (BPS1)	3
AT4G08555		Hypothetical protein	3
AT4G12735		Encodes a peroxisomal protein	4
AT4G34135	*UGT73B2*	Flavonol 7-O-glucosyltransferase	3
AT4G34410	*RRTF1*	Involved in salt stress tolerance, ROS inhibition	3
AT4G37220	*CYP81D8*	Member of CYP81D	2
AT4G37370	*HRG2*	H_2O_2 response gene, root meristem activity	5
AT5G24640		Similar to ACC oxidase	3
AT5G43450	*HSP23.5*	HSP20-like chaperones superfamily protein	3
AT5G55150	*ATFDR2*	F-box SKIP23-like protein (DUF295)	4
AT5G59820	*RHL41*	Zinc finger protein involved in high light and cold acclimation	3

The list of genes given as potential MgD marker genes within *Arabidopsis* roots in Brumbarova *et al*. [188] was cross-referenced with the MgD transcriptome collection created in this work, returning the number of transcriptomic datasets from the collection each of the genes is upregulated in, given in the "**Sets**" column.

6.2.2 Similarities and interactions between MgD and other stress conditions

It is well-known that Ca^{2+}-excess can mimic the effects of MgD, and it is not unlikely that in many ways, plants react to the Mg^{2+}/Ca^{2+}-ratio rather than levels of either ion. As a consequence, excess supply of Ca^{2+} is sometimes used to induce MgD [103, 105], although it is not entirely clear how well a combination of high Ca^{2+} and low Mg^{2+} mimics the effects of low Mg^{2+} alone. This relationship likely exists partially due to Ca^{2+} and Mg^{2+} being imported together through non-specific cation channels, such as the *rca* channel [114], and CNGC10 [117, 118] (see **Chapter 1**, **Section 1.3.2**). Indeed, high levels of Mg^{2+} are known to lead to decreased Ca^{2+}-levels in roots and shoots [106]. The binding properties of EF-hand proteins represent another source of interactions between Mg^{2+} and Ca^{2+} [110, 112, 296] (see **Chapter 1**, **Section 1.2.5**). Quantitative trait loci identified using association genetics often influence both Ca^{2+}-and Mg^{2+}-concentrations, but opposite effects have been observed [297-299]. The same is true for mutants with altered ionomes [216]. Disruptions to the Casparian strip have been found to influence Mg^{2+}-, but not Ca^{2+}-concentrations in *Arabidopsis* [268], but interestingly, an equivalent mutation influenced both Ca^{2+}- and Mg^{2+}-concentrations in *Brassica rapa* [218].

This discrepancy may be due to different ion levels in the two species under normal conditions, differences in the role or organisation of the Casparian strip, or specificities in the growth conditions used. All in all, it appears that there exist sets of genes and proteins that influence both Ca^{2+} and Mg^{2+} together, while others can lead to changes in levels of one of the two ions specifically, sometimes at the expense of the other. The second set of genes and proteins may become active primarily when the Mg^{2+}/Ca^{2+} ratio becomes imbalanced, restoring homeostasis if possible. The *CATION EXCHANGER* family may represent such genes and proteins in *Arabidopsis*, with disruptions in *CAX1* producing tolerance to media with high Mg^{2+}/Ca^{2+} ratios [300], and *CAX3* increasing in expression in response to low Mg^{2+} and high Ca^{2+} [105]. *CAX3* was present in the set of genes responding to MgD in an "incremental" manner in this work, a set including many genes associated with ion transport; many of these genes and associated proteins may have a role in restoring disrupted ion levels caused by reduced medium Mg^{2+} (see **Chapter 5**, **Section 5.3.1**).

One GO term in the category “biological process” significantly enriched in the set of “incremental” genes is “phosphate ion homeostasis”. The interplay between phosphate (Pi) deficiency and MgD is apparent on many levels, but unlike Mg^{2+} and Ca^{2+}, Mg^{2+} and Pi do not seem to compete for uptake by plants. While Mg^{2+} and Pi can form insoluble precipitates, this is not likely to take place at concentrations conducive to plant growth [229]. Similarly, anions and cations are not likely to compete for binding sites within transport proteins, enzymes, cell walls and soil particles.

Pi deficiency leads to inhibition of primary root growth, which enables increased growth of lateral roots and root hairs [301]. This response is thought to increase Pi uptake by increasing root surface area and allowing plants to explore the soil more efficiently, specifically within the topsoil, where Pi is primarily found. Since Pi is a very immobile ion within soils, a dense, highly-branched root system is necessary to forage for this nutrient. The adaptations of root system architecture to low Pi are influenced by blue light [302] and iron availability [152]. MgD causes the opposite effect on root growth, inhibiting lateral root emergence while leaving primary root growth intact, presumably to reach Mg^{2+}-supplies within lower soil strata [108, 228] (**Chapter 3**, **Figures 3.5** and **3.6** and **Section 3.3.2**). This inherent conflict means that a compromise between Mg^{2+}-uptake and Pi-uptake is necessary. Niu *et al.* [229] found that high Mg^{2+}-levels reduced primary root growth and Pi concentrations within plants on low-Pi media further. Both Mg^{2+} and Pi appear to affect auxin distribution in root tips by altering the expression of AUX and PIN transporters, implying that auxin mediates the establishment of a compromise between acquisition of Mg^{2+} and Pi.

Once within the plant, Pi and Mg^{2+} appear to act synergistically, rather than antagonistically. Phosphorus contents in leaves were reduced after Mg^{2+} withdrawal in Ogura *et al.* [87]. Phosphorus (P) was the macronutrient most strongly affected by Mg^{2+}-withdrawal besides Mg^{2+} itself, with effects first seen in mature leaves, followed by expanding leaves. At the same time, P contents in roots were increased, suggesting that root-to-shoot transport of P is inhibited under MgD, with some P re-mobilized from mature to expanding leaves.

This may explain the enrichment of genes associated with phosphate ion transport in the transcriptome data obtained here (see **Chapter 5**, **Section 5.3.1**). Most importantly, though, although considerably less is known about the effect of Pi deficiency in leaves than in roots, the symptoms caused by Pi deficiency and MgD are strikingly similar. Pi deficiency appears to cause similar effects on the electron transport chain [223] as MgD [97], with photosystem II more strongly affected, especially during exposure to light, and accumulation of energy in the electron transport chain activating alternative energy-dispersing processes such as non-photochemical quenching and cyclic electron flow. Photo-oxidative stress results, as well as reduced expression of proteins with functions related to photosynthesis and carbon fixation [303]. Pi deficiency causes sucrose and starch accumulation in leaves as well [304, 305]. Mutants accumulating high levels of sucrose in leaves and roots were found to be hypersensitive to Pi deficiency, and a large portion of genes upregulated under Pi deficiency were constitutively upregulated in these mutants [264, 306]. Therefore, a great deal of the symptoms of MgD apply to Pi deficiency as well, and additional transcriptomic, proteomic and physiological studies examining the similarities, differences and interactions between MgD and Pi deficiency may help to further elucidate the mechanisms and disruptions underlying the symptoms of both deficiencies.

Boron and copper levels were reduced in leaves exposed to MgD in the study by Ogura *et al.* as well [87], which is interesting considering one of the GO terms enriched in the RNAseq data obtained in this work was “Copper ion binding” (**Table 5.1**), and two of the genes represented in five of the transcriptomes in the collection are induced by high boron (**Table 5.2**, # 10 and 15), potentially pointing to interactions between these ions.

6.2.3 Including new results in the MgD "timeline"

In this work, an increase in the concentrations of MgATP and total ATP, in the ATP/ADP ratio and the PM pH differential was observed in leaves of plants grown under MgD continuously for two weeks (see **Chapter 3**). An alternative model of the events occurring during MgD was generated to account for this, based on possible changes in SWEET transporter activity, as opposed to that of SUC transporters (**Figure 3.20**). However, this only represents one possibility for how the observed changes could arise, and unlike with the previous model, which provided a plausible cause for how BvSUT/AtSUC transporters could be inhibited by reduced MgATP-levels [90] (**Figure 1.5**), there is currently no mechanism for how SWEET transporters could be inhibited by low Mg^{2+}. Additionally, the observed results represent changes occurring in one species, at one stage in development, under one specific set of conditions, and very much await validation. It is therefore first necessary to confirm the observed changes further, before establishing a possible mechanism for their occurrence.

As mentioned before (see **Chapter 3**, **Section 3.3.5**), a good first step might be to return to the method of "Mg^{2+} withdrawal" and to generate a time-course of symptoms after removal of Mg^{2+} from the nutrient solution. This could serve to integrate the new symptoms into the "timeline" of symptoms of MgD (**Figure 1.6**). Recent studies, such as that by Ogura *et al.* [87], have been extending knowledge about early events in MgD, and using similar methods, distinguishing between mature and expanding leaves in similar ways, and/or correlating altered nucleotide pools and pH levels with mineral nutrient profiles as well as downstream symptoms could prove especially informative. Other species, such as rice [96], sugar beet [56] and *Vicia faba* [88], all of which have seen studies investigating the symptoms of MgD, would represent equally interesting targets.

A major shortcoming of the methods used here, which has not been discussed so far, is their low spatial resolution. All measurements on ATP-levels, MgATP-levels and pH have been carried out on entire leaves and roots. Inhibition of sucrose export, according to the previous model, however, would require MgATP-levels to be reduced in phloem companion cells only [90]. It is possible, therefore, that this could be the case despite a general increase in MgATP. Using higher-resolution methods, such as confocal microscopy, it may be possible to distinguish between different areas with the required accuracy. Alternatively, ATeam, and/or pH reporters could be expressed in phloem companion cells specifically, potentially under the control of the *SUC2* promoter itself [93, 94].

Finally, if MARIO can be expressed consistently in *Arabidopsis* plants and calibrated properly, assessment of concentrations of [Mg^{2+}] within tissues of plants exposed to MgD could provide further context to the observed symptoms.

6.2.4 The role of sucrose transporters in MgD and phosphate deficiency

Although sucrose accumulation is one of the major disruptions occurring under MgD and Pi deficiency, the role of sucrose transporters in this process is not clear so far.

Sucrose accumulation in the *sweet11 sweet12* double mutant [238] appears similar to sucrose accumulation under MgD (see **Chapter 3**, **Section 3.3.5**), however, this does not confirm that inhibition of these transporters is the cause of sucrose accumulation under MgD. Nevertheless, it could be informative to test the sensitivity of this mutant to MgD and Pi deficiency. The *hps1* mutant, which was identified for its hypersensitivity to Pi deficiency, was later found to overexpress the SUC2 sucrose/H^+ symporter, leading to accumulation of sucrose in root and shoot tissues on media containing sucrose [264]. As mentioned above, this mutant was found to exhibit alterations to its transcriptome very similar to those observed under Pi deficiency. Similarly, the *pho3* mutant, which harbours a defective copy of *SUC2*, is hypersensitive to Pi deficiency and displays many of the phenotypes associated with Pi deficiency. This could be the case for the *sweet11 sweet12* mutant as well.

Investigations of similarities and differences in the transcriptomic changes seen in these mutants compared to plants exposed to MgD and Pi deficiency could further elucidate the extent to which these deficiencies are caused by sucrose accumulation, and how much of the changes are shared between them. If sucrose accumulation is the main cause of the symptoms of MgD, it could be possible to alter the transporters involved in a way that could increase plant resistance to MgD and/or Pi deficiency, by preventing inhibitory post-translational modifications, reductions in expression, or similar changes. Alternatively, it is possible that SUC transporters, or SUC2 specifically, are inhibited by Pi deficiency, whereas SWEET transporters are inhibited during MgD. However, both the SWEET and SUC families are large, and their expression changes across developmental stages, which may complicate this analysis. **Table 6.4** lists some sugar transporters and gives the number of transcriptomic datasets from the collection they were found to be upregulated in.

In Ogura *et al*. [87], *SUC1*, *SUC3* and *SUC7* were found to be increased in expression at day 8 of Mg^{2+}-withdrawal in expanding leaves of *A.thaliana*. *SWEET11* and *SWEET12* were down-regulated, but *SWEET13* and *SWEET15/SAG29* were up-regulated. Chen *et al.* [238] observe an induction of *SWEET13* in the *sweet11 sweet12* double mutant, suggesting that expression of this transporter can be induced to compensate for excessive sucrose accumulation. As can be seen in **Table 6.4**, only *SUC1*, *SUC7* and *SWEET15/SAG29* were increased in expression in more than one of the transcriptomic datasets investigated here. Interestingly, both *SUC7* and *SWEET15/SAG29* are primarily expressed in siliques according to the Klepikova atlas [224]. *SWEET15* expression can be induced by the WHIRLY2 transcription factor, overexpression of which causes early senescence and also inhibits *SWEET11* expression [307]. It is therefore possible that *SWEET15* and/or *SUC7* are involved in senescence-like responses during MgD, perhaps as part of carbon reallocation processes.

Table 6.4 - Presence of sugar transporter genes in the MgD transcriptome collection

Gene ID	Name	Description	Sets
AT3G48740	*SWEET11*	SWEET sucrose efflux transporter.	0
AT5G23660	*SWEET12*	SWEET sucrose efflux transporter.	1
AT5G50800	*SWEET13*	Involved in pollen, anther, seed and seedling development and modulating of the GA response.	0
AT5G13170	*SWEET15/SAG29*	SWEET sucrose efflux transporter.	3
AT3G16690	*SWEET16*	Nodulin MtN3 family protein	0
AT1G71880	*SUC1*	Sucrose-proton symporter 1	2
AT1G22710	*SUC2*	Sucrose-proton symporter 2	0
AT2G02860	*SUC3*	Sucrose-proton symporter 3	1
AT1G66570	*SUC7*	Sucrose-proton symporter 7	3
AT5G26340	*MSS1*	High-affinity hexose/H^+ symporter	4

A list of genes associated with sugar transport was compiled and cross-referenced with the MgD transcriptome collection created in this work, returning the number of transcriptomic datasets from the collection each of the genes is upregulated in, given in the "**Sets**" column.

AT5G26340/MSS1, also known as sugar transport protein 13 (STP13), shows increased expression in the transcriptomic dataset acquired here, as well as in Hermans *et al*., 2010b [227], Niu *et al*. [104] and Oda *et al*. [103]. This transporter is part of a third family of plant sugar transporters, the STP family of hexose/H^+ symporters [95]. Out of the three families (SWEET, SUC and STP), least research is available on the STP family. STP13, specifically, appears to be involved in uptake of sugars from the apoplast in response to biotic stress [308]. More recently, it has been suggested that this transporter has roles in the integration of biotic and abiotic stresses under the control of the transcription factor MYB96 [309].

Sucrose transporters, specifically the SWEET family, have recently been linked to disease resistance [310, 311]. During infection, some pathogens can cause SWEET transporters to be activated, releasing sugars for the pathogens to feed on. On the other hand, plants inhibit release of sugars into the apoplast to deprive pathogens of sustenance [308].

Since the biotic stress pathway, specifically SAR, is induced under MgD (see **Section 6.2.1**) [87], this raises a question of cause and effect. Either MgD causes starch accumulation, which activates the SAR response, or the SAR response becomes activated under MgD and leads to retention of sugars to counteract a perceived infection. The *sweet11 sweet12* mutant has been found to show increased activation of the SAR pathway, increasing resistance to *C. higgensianum* infection via sugar-mediated defense priming [312], suggesting that the former is the case. Therefore, the often-observed, but rarely-discussed upregulation of defense-associated genes during MgD can most likely be attributed to sugar-mediated defense priming as well.

In summary, the links between sugar transporters, sucrose accumulation and MgD, as well as Pi deficiency, are becoming increasingly apparent, and some patterns are starting to emerge. However, the causes behind the initial sucrose accumulation in leaves of plants exposed to MgD and Pi deficiency are still unclear. Proteomic studies, investigation of post-translational modifications to sugar transporters, and further work on *sweet*, *suc* and *stp* mutants may provide more information in the future.

6.2.5 The localisation, function and regulation of MRS2-3 and MRS2-4

The results obtained in **Chapter 4** highlight the problems associated with determination of the subcellular localisation of proteins using fluorescent tagging. Despite indications to the contrary from (partial) complementation of the *mrs2-3* mutant phenotype by *pMRS2-3::MRS2-3::GFP* (**Figure 4.7**), it is possible that MRS2-3::GFP is not localized correctly in these lines. ER localisation, specifically, is often the result of failure to export fluorescently-tagged proteins due to interference of the tag with targeting sequences, correct folding, or membrane integration [243]. On the other hand, the low abundance of MRS2-4, and consequentially MRS2-4::GFP, created difficulties distinguishing GFP fluorescence from autofluorescence. This represents another common problem encountered during experiments using fluorescently-tagged proteins [243].

Although PM localisation of MRS2-4 could be determined with relatively high confidence, follow-up experiments investigating the dynamics of MRS2-4 fluorescence under different external Mg^{2+}-concentrations, for example, may be difficult.

Determination of subcellular localisations of MRS2-family proteins only makes up one step toward further elucidation of their functions and regulation. As outlined in the introduction (**Sections 1.3.4** and **1.3.5**), questions remain regarding the existence of Mg^{2+}-gating in this protein family, as well as their interaction-partners. Patch-clamp experiments, similar to those carried out for ScMrs2p, could be used to investigate gating mechanisms in *Arabidopsis* MRS2s [132]. Cryo-electron microscopy could be used to confirm any changes in conformation between Mg^{2+}-bound and Mg^{2+}-free states, as has been done for CorA [128]. Knowledge about the structure of the α6b-helices and variable α4-α5 linker regions of plant MRS2s, *i.e.*, those sequence elements that are absent in non-plant homologues of MRS2s [167], could be especially useful. High-resolution structural models could allow predictions about the role of these sequences in modulating channel conductance or facilitating protein-protein interactions.

Co-immunoprecipitation analysis could facilitate the determination of proteins interacting with MRS2s in theory. However, it is unlikely that these methods could be successfully applied using the available *Arabidopsis* lines containing GFP-tagged MRS2s. Although protocols for co-immunoprecipitation analysis on plant membrane proteins have been developed, and could be followed by mass spectrometry analysis [313], interactions between MRS2s and regulatory proteins, if present, would likely be too transient, rare and/or conditional on internal states to be detected reliably. *MRS2-3::GFP* - containing lines would have to be investigated more closely before being used in further experiments, to determine whether structure and localisation of MRS2-3 in these lines is correct, as described in **Chapter 4, Section 4.3.3**. Additionally, abundance of MRS2-4::GFP, and possibly MRS2-3::GFP, is likely too low to facilitate such experiments. If individual, specific candidates for interactions with MRS2s were known, this method could be used to investigate them, but more data are required before this is possible.

6.2.6 Further work is required to complete the forward genetic screen and characterize identified mutants

MgMt 3 is currently the only mutant line identified during the forward genetic screen for which it seems feasible to progress to the next stage of characterisation, which would involve attempts at complementing the phenotype via the introduction of a transgene containing a wild-type copy of *AT2G45300*. Additionally, phenotypes present in this line should be characterized and compared to those of a knockout mutant of *AT2G45300*. Homozygous SALK T-DNA insertion lines with insertions in the CDS of this gene (SALK_024713C and SALK_086083C) are available. In this context, Mg^{2+}-dependent phenotypes would be especially important.

Mg^{2+}-dependency of the phenotypes observed in MgMt lines needs to be confirmed in general, and can be done easily by comparing characteristics like shoot weight and root growth of MgMt lines to that of Col-0 and/or *pAAA::LUC* 2-4 plants on different Mg^{2+}-concentrations. Unfortunately, due to time limitation, this was not within the scope of this project. However, most MgMt lines appeared smaller than control seedlings when grown on agar plates until 14 DAG, including MgMt 6 and -9 after the back-cross, which later developed plants of similar or larger sizes than *pAAA::LUC* 2-4 (**Figure 5.16**, **Figure 5.17**). This could indicate that the low Mg^{2+}-concentrations within the plates used for screening may have hampered their growth, while they would otherwise grow normally.

To identify causative SNVs in mutant lines other than MgMt 3, it will be necessary to carry out WGS again, at higher sequencing depth than that achieved in this project. 50x coverage across the genome could narrow down lists of potential candidates while providing additional confidence in the results obtained. However, many of the lines investigated here still exhibit regions of the genome containing multiple SNVs occurring at 100% frequency in the sequencing-results, meaning these SNVs are genetically linked. It may be preferable to perform a second back-cross before a second attempt at WGS, which may break the linkage and “resolve” those SNVs. If few high-confidence SNVs remain for each line, complementation experiments can show causality next, paving the way for further characterisation of mutant phenotypes and functions of causative genes.

During the forward genetic screen carried out in this work, 16 pools of M_2 seeds underwent the screening-procedure, with 300 seeds per pool screened for LUC expression, for a total of 5000 seeds screened for increased LUC expression and loss of LUC expression each. Haughn and Somerville [314] estimate that 125,000 M_1 seedlings need to be screened to have a 95% chance to find an individual with a mutation in any given base-pair in an EMS-based screen. Jander *et al.* [266] determined that under the conditions used in that study, 45,000 M_1 lines would have been sufficient to achieve the same. Of course, it is not necessary to find mutations in every single base pair to identify knock-out or knock-down mutations within every gene in the genome. Assuming that the sequence of a gene contains 100 bases that would impair the function of that gene sufficiently to cause an appreciable phenotype (N), a 3% chance to find a mutant in any base-pair in the genome (P_1) will give a 95% chance to find a knock-out for any gene (P_2), according to $P_2 = 1 - (1 - P_1)^N$. Using the mutation frequency determined by Jander *et al.*, (1.6×10^{-5} per base) for F, and the new rate of required mutations per base pair in the genome P = 3%, we can solve $P = 1 - (1 - F)^N$ to give the number of M_1 lines necessary to find knock-outs in every gene, which gives N = 1903 M_1 lines. This is just a rough estimate, but since only 16 pools consisting of roughly ten individuals each were screened in this project, equating to roughly 160 M_1 individuals, it is close to certain that far from all the possible candidates have been identified during this screen.

The attempt at carrying out a forward genetic, luciferase reporter-based screen for factors involved in Mg^{2+}-homeostasis made here should therefore be seen as a proof of concept. Along with a second back-cross and WGS of the mutant lines identified here, it would be beneficial to repeat the M_2 screening process with more pools of seeds, at least the additional 34 pools generated here, but potentially more pools from a second round of EMS mutagenesis. It might be more time-efficient not to attempt another screen for loss of luciferase expression at this stage, and screen for increased expression only to avoid false-positives. Further, before this, it might be prudent to validate and further test the specificity of *AAA* induction to MgD to increase the likelihood of discovering genuine MgD-related genes, as outlined in **Section 5.3.3**.

Appendix A: Supplementary Figures

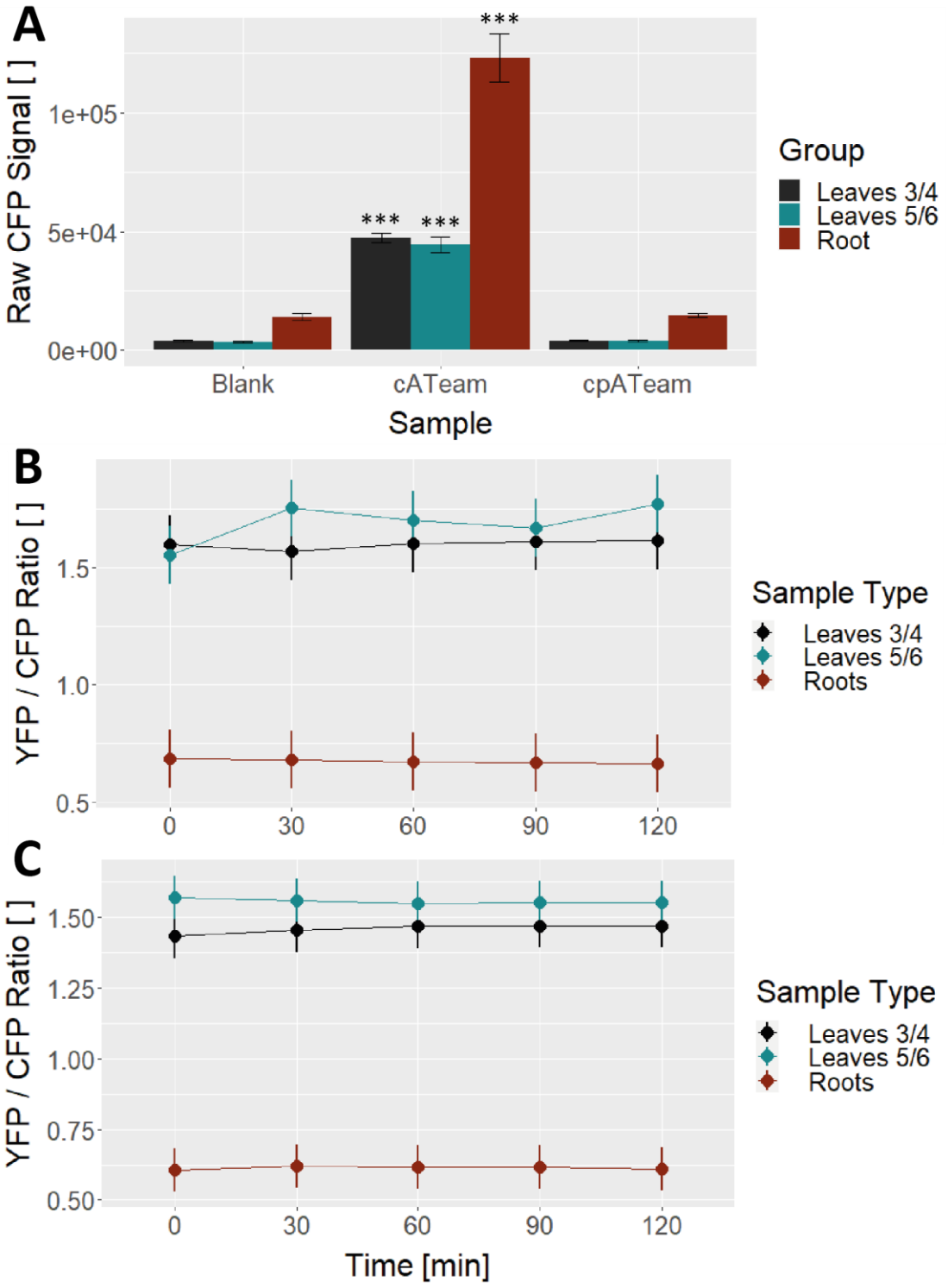
A
Raw CFP Signal [ ]
1e+05
5e+04
0e+00
***
***
***
Blank
cATeam
cpATeam
Sample
Group
Leaves 3/4
Leaves 5/6
Root
B
YFP / CFP Ratio [ ]
1.5
1.0
0.5
0
30
60
90
120
Sample Type
Leaves 3/4
Leaves 5/6
Roots
C
YFP / CFP Ratio [ ]
1.50
1.25
1.00
0.75
0.50
0
30
60
90
120
Time [min]
Sample Type
Leaves 3/4
Leaves 5/6
Roots

Figure S2.1 – Validation of the plate-reader assay for measuring changes in ATeam FRET ratios in seedlings grown on different Mg^{2+}-concentrations.

A. thaliana (Col-0) seedlings were grown on agar-plates containing HM made with washed agar, with different concentrations of added Mg^{2+}, until 14 DAG, before leaves and roots were separated and transferred to the wells of a 96-well plate, filled with liquid HM of the same concentration. The plate was transferred to a plate reader and emission values for CFP and YFP recorded, using excitation wavelengths for CFP. **A** – Average CFP emission values observed for Blank (Col-0), cATeam and cpATeam samples in the plate-reader assay, for the three sample types. Data represent mean values (± SEM) from one experiment, including three technical replicates. Symbols above error bars denote significant differences between expression on 1000 µM Mg^{2+} and the respective condition, as determined by a two-way ANOVA followed by Tukey's HSD post-hoc test (▪ - $p < 0.1$; * - $p < 0.05$; ** - $p < 0.01$; *** - $p < 0.001$). **B, C** – Average FRET ratios (YFP/CFP emission after excitation of CFP) for the three sample types after dark-incubation for different times, for plants grown on 15 µM Mg^{2+} (**B**) or 50 µM Mg^{2+} (**C**). Mean and confidence intervals for each plant part and time-point are displayed, from a mixed-effect linear model generated using the data. Data generated during one experiment, carried out as three technical replicates.

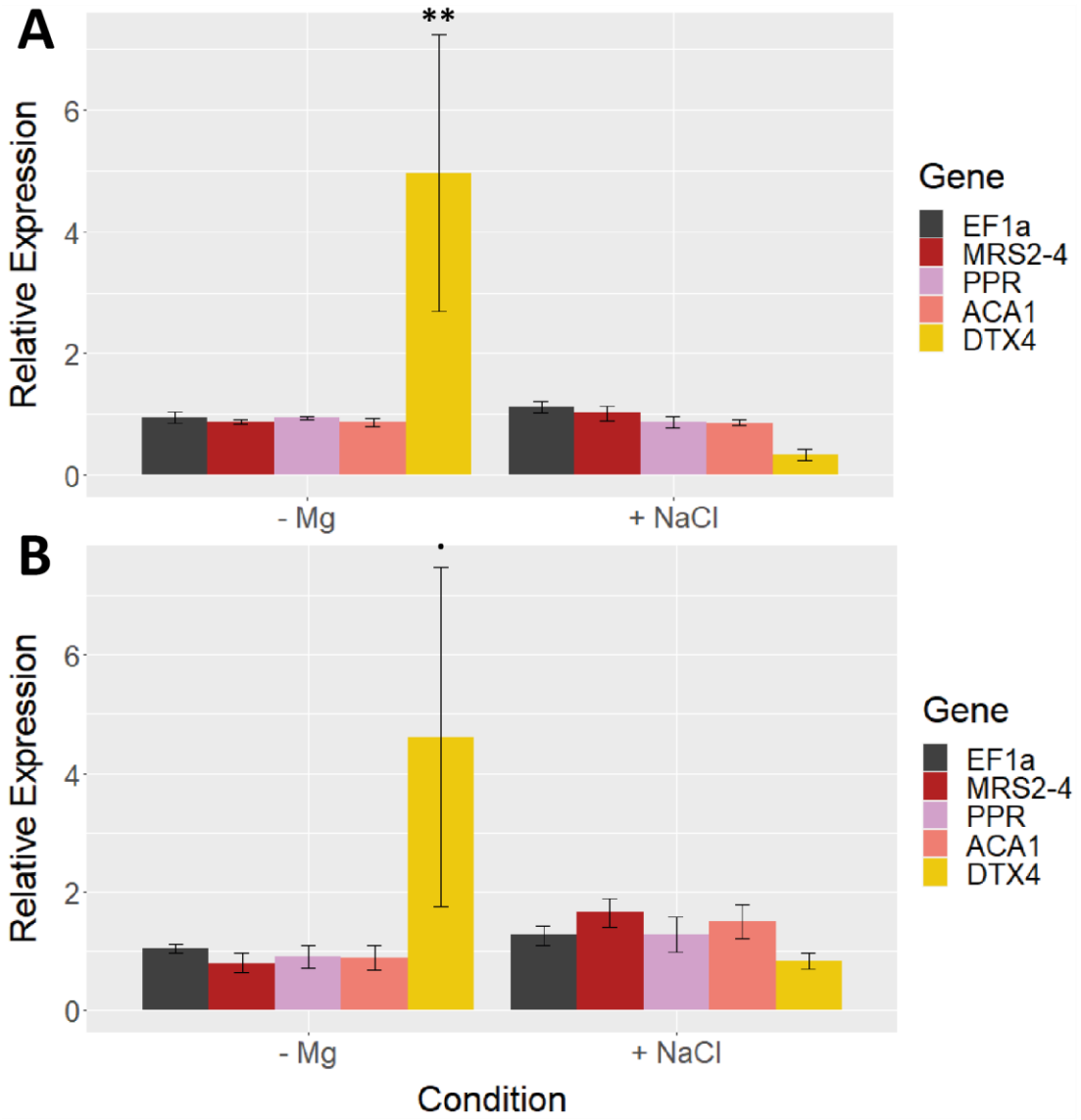

Figure S3.1 – Relative expression of candidate MgD-responsive genes in roots of seedlings after transfer to low Mg^{2+} or excess NaCl.

Col-0 seedlings were grown on Mg^{2+}-replete plates until 14 DAG and then transferred to plates without added Mg^{2+} (- Mg), with 60 mM NaCl (+ NaCl) or 1000 µM Mg^{2+}. Gene expression in roots of seedlings after 3 days (**A**) and 7 days (**B**) was determined by qRT-PCR. Expression levels for all transcripts were normalized to expression of ACTIN2 and expression of the respective transcripts at 1000 µM according to the $\Delta\Delta C_T$ method. Data represent mean values (± SEM) from three independent experiments, each repeated as three technical replicates. Symbols above error bars denote significant differences between expression on 1000 µM Mg^{2+} and the respective condition, as determined by a two-way ANOVA followed by Tukey's HSD post-hoc test (▪ - $p < 0.1$; * - $p < 0.05$; ** - $p < 0.01$; *** - $p < 0.001$).

Figure S3.2 – Growth of mrs2-4 1 + cpMARIO on soil.

Plants of each genotype were grown on soil for five weeks, before aerial parts were removed, and images taken. **A** – Col-0, **B** – *mrs2-4* 1, **C** – *mrs2-4* 1 + *cpMARIO*.

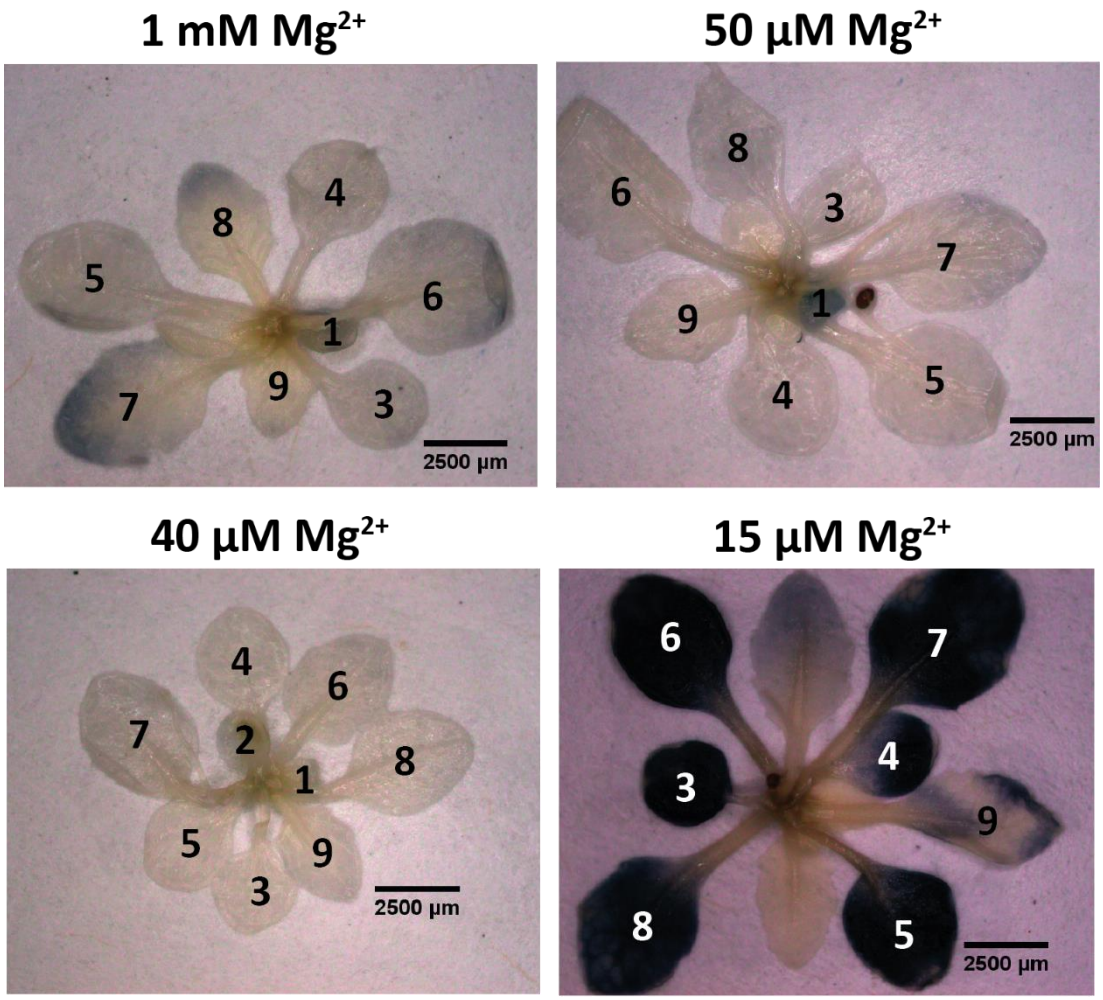

Figure S3.3 – Starch staining of plants grown on different Mg^{2+}-concentrations, without sucrose

A. thaliana (Col-0) seedlings were grown on agar-plates containing HM made with washed agar, with different concentrations of added Mg^{2+}, until 14 DAG, before being subjected to a starch staining protocol using Lugol's solution. Representative image of a stained seedling from each concentration tested. Leaves are numbered according to order of emergence.

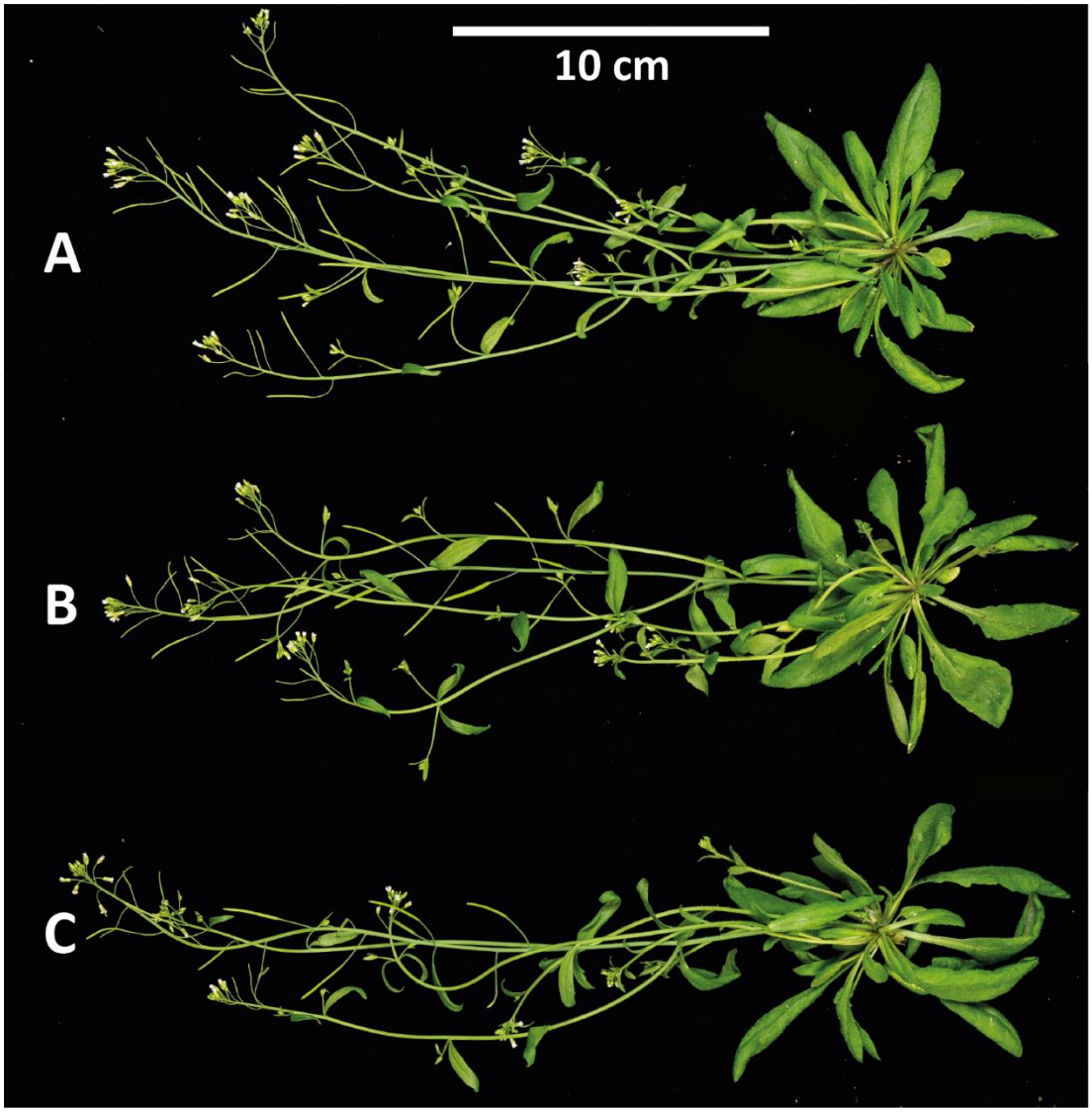

Figure S4.1 – Growth of mrs2-10 mutants compared to Col-0.

Plants of each genotype were grown on soil for five weeks, before aerial parts were removed, and images taken. **A** – Col-0, **B** – *mrs2-10* 1, **C** – *mrs2-10* 2.

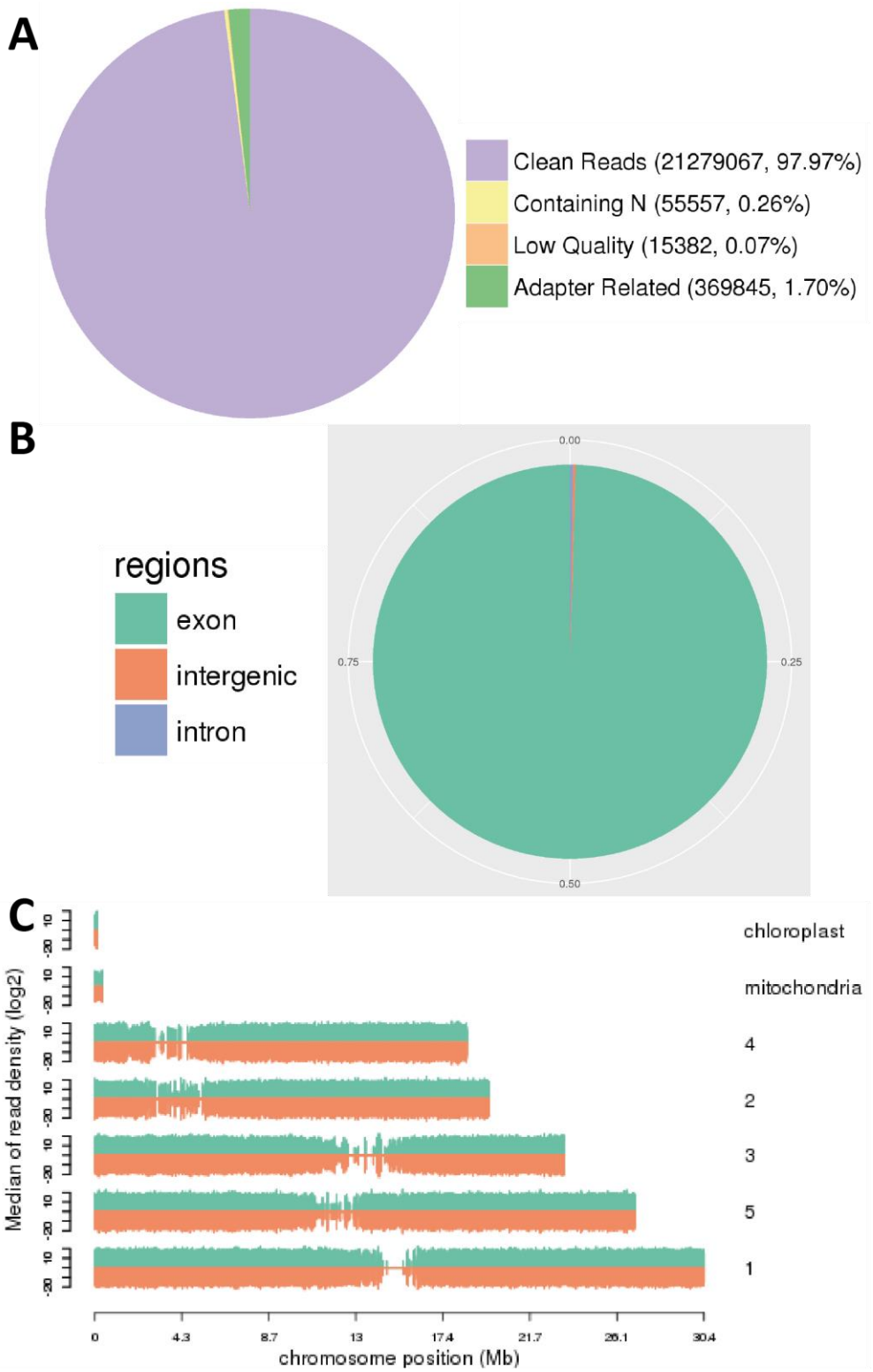

Figure S5.1 -Further quality control characteristics for sample 15_1

A – Characteristics of reads for sample 15_1, including percentages of clean reads and filtered reads, sorted by reasons for exclusion of reads, displayed as a bar chart. **B** – Frequency of different genomic regions of transcripts reads were aligned to, displayed as a pie chart. **C** – Density of reads aligned to each position along the chromosomes of *A. thaliana*, including chloroplast and mitochondrial chromosomes.

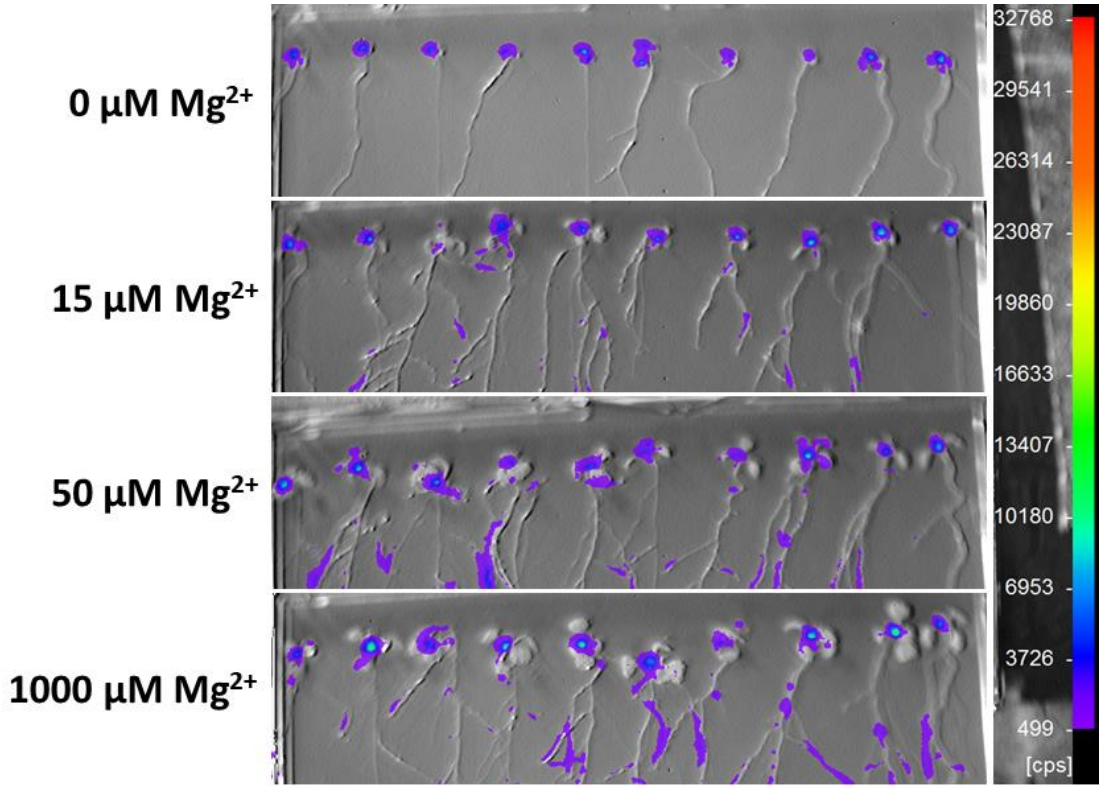

Figure S5.2 – *pPER70::LUC* expression on different concentrations of Mg^{2+}
Seedlings of *pPER70::LUC* 5-1 were grown on agar-plates containing HM made with washed agar with different concentrations of added Mg^{2+} until 8 DAG, then luciferase expression was visualized by spraying seedlings with a solution containing luciferin and measuring light emission using a photon-counting camera. **cps** – [photon] counts per second.

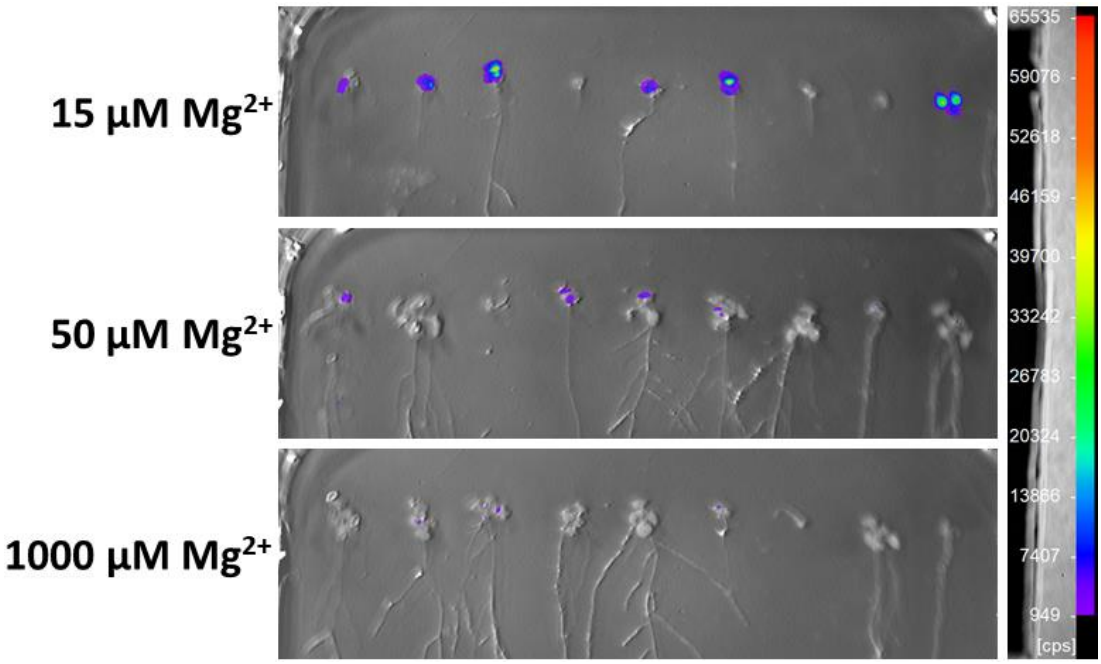

Figure S5.3 – *pAAA::LUC* expression on media without sucrose

Seedlings of *pAAA::LUC* 2-4 were grown on agar-plates containing HM made with washed agar without sucrose with different concentrations of added Mg^{2+} until 11 DAG, then luciferase expression was visualized by spraying seedlings with a solution containing luciferin and measuring light emission using a photon-counting camera. **cps** – [photon] counts per second.

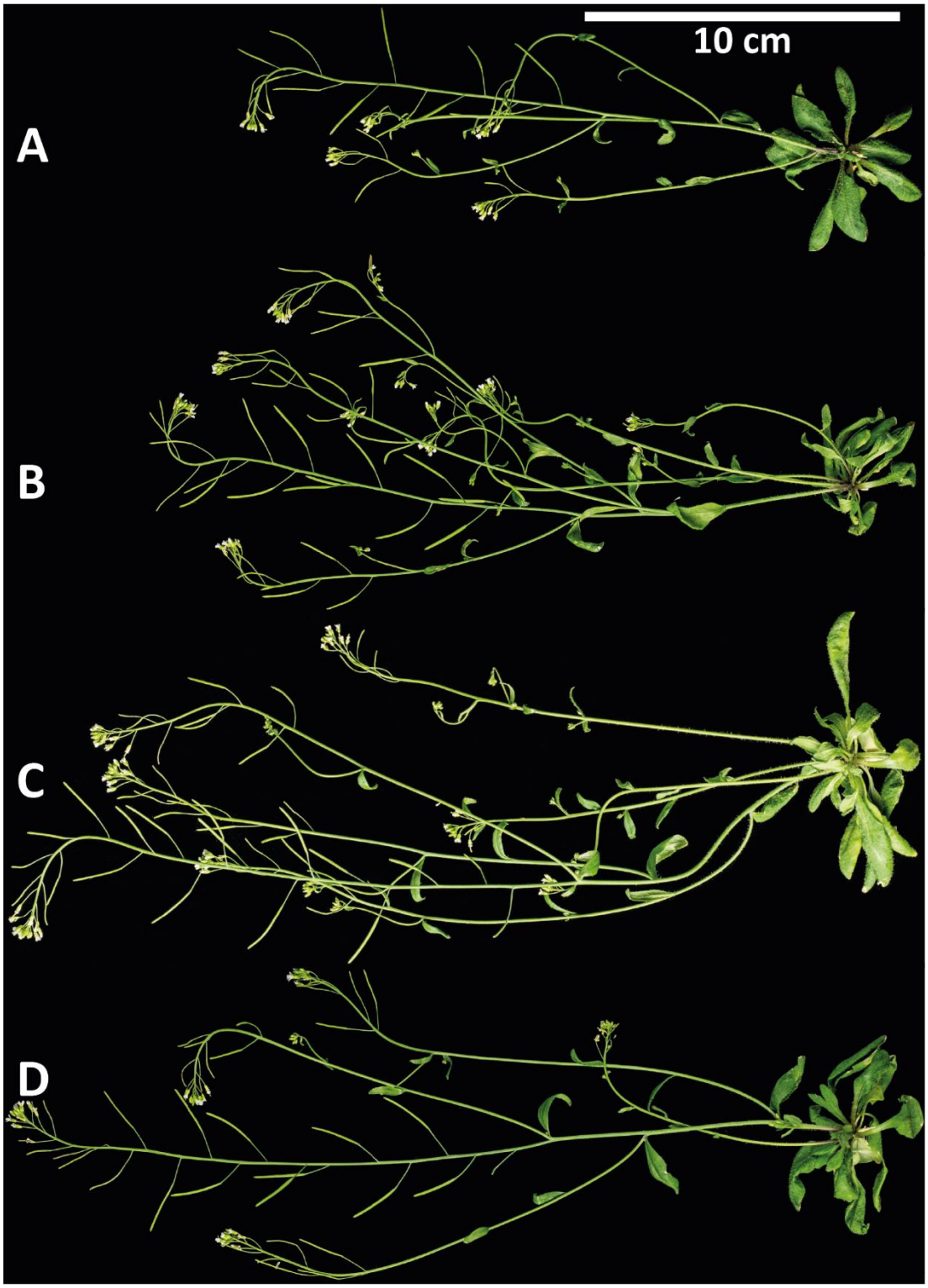

Figure S5.4 - Growth of F_1 back-crossed lines on soil

Plants were maintained on soil for five weeks, before aerial parts of representative individuals were removed and images taken. **A** – *pAAA::LUC* 2-4; **B** – MgMt 2 X F_1; **C** – MgMt 5 X F_1; **D** – MgMt 6 X F_1.

Appendix B: Supplementary Tables

Table S2.1 - Measured Ion-concentrations in media containing different forms of agar and different amounts of added Mg^{2+}.

Mg^{2+} added [µM]	Agar used	Measured Ion concentrations [µM]				
		PO_4^{3-}	K^+	Na^+	Ca^{2+}	Mg^{2+}
0	Washed	275	2899	2205	848	5.0
15	Washed	283	3020	2260	878	12.9
50	Washed	292	2946	2225	875	36.1
1000	Washed	168	2831	1890	882	675.1
0	HGA	867	2244	5532	1445	46.5
15	HGA	931	2427	5934	780	44.3
50	HGA	906	2400	5882	780	67.7
1000	HGA	995	2367	5560	961	764
0	Unwashed	999	2258	6311	726	31.4
15	Unwashed	1050	2319	6740	738	42.3
15	Unwashed	1048	2418	6727	746	40.4
1000	Unwashed	1164	2259	6061	927	757
1000	Unwashed	1170	2455	6415	978	814
0	None	274	1949	2313	805	5.20
15	None	268	1917	2415	810	15.1
50	None	272	1901	2397	803	41.1
1000	None	265	1892	1989	825	726

Values were obtained by ICP-OES analysis after Agar-equilibration using agar-plates made with different types of agar and different concentrations of added Mg^{2+}. Washed: Type A agar, subjected to an EDTA-washing procedure (see section). HGA: High gel-strength agar. Unwashed: Type A agar, used unaltered. None: Nutrient solutions made without added agar.

Table S5.1 – Quality control characteristics of RNA-seq. data

Sample name	Clean reads	Clean bases	Error rate	Q30	GC content	Total mapped	Multiple mapped
15_1	42558134	6.4 Gb	0.03%	93.8%	45.5%	93.1%	0.95%
15_2	44094670	6.6 Gb	0.03%	93.1%	45.3%	92.6%	1.14%
15_3	47360912	7.1 Gb	0.03%	93.6%	45.5%	93.1%	1.06%
50_1	43153036	6.5 Gb	0.03%	93.1%	45.5%	92.5%	1.15%
50_2	40442864	6.1 Gb	0.03%	93.3%	45.4%	92.6%	1.02%
50_3	47539340	7.1 Gb	0.03%	92.9%	45.0%	91.3%	1.09%
150_1	44838154	6.7 Gb	0.03%	92.6%	45.5%	91.2%	0.94%
150_2	45753906	6.9 Gb	0.03%	92.9%	45.4%	91.3%	0.97%
150_3	43815440	6.6 Gb	0.03%	93.8%	45.0%	92.9%	0.99%
250_1	40990422	6.1 Gb	0.03%	92.9%	45.4%	92.4%	0.99%
250_2	49122314	7.4 Gb	0.03%	92.3%	45.0%	90.8%	1.05%
250_3	41946484	6.3 Gb	0.03%	93.0%	45.0%	92.6%	1.02%
1000_1	42799160	6.4 Gb	0.03%	93.2%	45.3%	93.0%	1.05%
1000_2	45686622	6.9 Gb	0.03%	92.4%	45.3%	91.1%	1.04%
1000_3	40137236	6.0 Gb	0.03%	93.7%	45.0%	93.0%	0.99%

Sample name – Defines the sample described in the column, names consist of added concentration and biological repeat. **Clean reads** – the number of reads remaining after filtering of erroneous reads. **Clean bases** – total number of bases present in clean reads. **Error rate** – average sequencing error rate. **Q30** – percentage of bases displaying a Phred score greater than 30. **GC content** – percentage of the bases G and C within the total base number. **Total mapped** – percentage of reads aligning to the reference genome (TAIR10). **Multiple mapped** – percentage of reads aligning to the reference genome in multiple places.

Table S5.2 – GO term annotation of genes upregulated in the RNA-seq. dataset

GO entry	Description	q-value	No. Genes
GO:0006820	Anion transport	9.37E-15	36
GO:0006811	Ion transport	6.35E-14	47
GO:0050896	Response to stimulus	1.99E-12	120
GO:0071705	Nitrogen compound transport	3.33E-10	34
GO:0051179	Localization	3.98E-10	75
GO:0006810	Transport	8.36E-10	70
GO:1902578	Single-organism localization	8.36E-10	66
GO:0042221	Response to chemical	1.44E-09	79
GO:0044765	Single-organism transport	1.57E-09	65
GO:0051234	Establishment of localization	1.71E-09	70
GO:0006950	Response to stress	1.77E-09	81
GO:0015711	Organic anion transport	1.21E-08	20
GO:0015849	Organic acid transport	2.09E-08	19
GO:0046942	Carboxylic acid transport	2.09E-08	19
GO:0006865	Amino acid transport	3.19E-08	18
GO:1901700	Response to oxygen-containing compound	2.51E-07	54
GO:0015698	Inorganic anion transport	1.61E-06	16
GO:0071702	Organic substance transport	1.84E-06	42
GO:0010035	Response to inorganic substance	2.82E-06	37
GO:0009605	Response to external stimulus	5.41E-06	48
GO:0050801	Ion homeostasis	5.64E-06	15
GO:0009404	Toxin metabolic process	6.58E-06	14
GO:0001101	Response to acid chemical	6.98E-06	39
GO:0006952	Defense response	1.20E-05	40
GO:0055081	Anion homeostasis	2.02E-05	6

GO terms were attributed to the genes found to be upregulated during RNAseq analysis; GO terms enriched in the dataset were determined by calculating adjusted p-values for the likelihoods of finding this number of genes associated with the respective term in a set of this size. This table gives the top 25 GO terms of the category “biological process” most significantly enriched in the dataset. **GO entry** – Number of the respective term in the GO database. **q-value** – Adjusted probability of this level of enrichment to occur randomly. **No. Genes** – Number of genes in the dataset carrying the respective GO annotation.

Table S5.3 – GO term annotation of genes upregulated in the RNA-seq. dataset

GO entry	Description	q-value	No. Genes
GO:0005576	Extracellular region	7.07E-08	56
GO:0071944	Cell periphery	2.02E-05	69
GO:0005618	Cell wall	2.36E-04	20
GO:0030312	External encapsulating structure	2.36E-04	20
GO:0031314	Extrinsic component of mitochondrial inner membrane	2.64E-02	2
GO:0016020	Membrane	3.77E-02	71
GO:0005886	Plasma membrane	4.99E-02	51

GO terms were attributed to the genes found to be upregulated during RNAseq analysis; GO terms enriched in the dataset were determined by calculating adjusted p-values for the likelihoods of finding this number of genes associated with the respective term in a set of this size. This table gives GO terms enriched in the dataset for the category “localization”. **GO entry** – Number of the respective term in the GO database. **q-value** – Adjusted probability of this level of enrichment to occur randomly. **No. Genes** – Number of genes in the dataset carrying the respective GO annotation.

Table S5.4 - GO annotation of BCS1-clade AAA ATPases in A. thaliana

#	Gene ID	GO annotation; cellular processes
1	AT1G43910	Plasmodesma, endoplasmic reticulum, golgi apparatus, chloroplast
2	AT2G18190	-
3	AT2G18193	Endoplasmic reticulum
4	AT2G46620	Extracellular region
5	AT3G28510	Endoplasmic reticulum, plasma membrane
6	AT3G28520	Plasmodesma, mitochondrion, cytoplasm
7	AT3G28540	Mitochondrion
8	AT3G28560	-
9	AT3G28570	Chloroplast
10	AT3G28580	Endoplasmic reticulum
11	AT3G28600	Plasma membrane, chloroplast
12	AT3G28610	Plasma membrane
13	AT3G50930	Mitochondrial outer membrane, mitochondrial envelope, plasma membrane
14	AT3G50940	Chloroplast
15	AT4G25835	Chloroplast
16	AT4G30250	Plasma membrane
17	AT5G17730	Chloroplast
18	AT5G17740	Plasma membrane
19	AT5G17750	Chloroplast
20	AT5G17760	Cytoplasm, plasma membrane
21	AT5G40000	Plasma membrane
22	AT5G40010	Mitochondrion, endoplasmic reticulum, nucleus
23	AT5G57480	-

A search for BCS1-clade AAA-type ATPases present in *A.thaliana* in the UniprotKB database (https://www.uniprot.org/) was carried out. Only manually-reviewed entries were accepted, a total of 23 of which were found. Locus identifiers for the associated genes were collected, and GO terms associated with each were obtained.GO annotations of the category “localisation” are displayed.

Table S5. 5 – Identity matrix for the BCS1-clade of AAA ATPases in A. thaliana

#	Gene	4	1	20	17	18	19	2	3	13	14	16	15	23	9	21	11	12	8	10	22	5	6	7	-	-
4	At2g46620	100	30.3	35.3	31.3	30.1	36.8	29.5	32.6	32.7	32.5	35.2	35.5	36.4	33.2	33.9	34.0	33.9	21.2	36.6	34.9	34.3	31.3	33.3	16.7	15.3
1	At1g43910	30.3	100	41.5	39.4	39.3	39.2	40.8	41.5	40.8	42.2	34.3	33.5	33.9	35.3	35.9	36.9	37.2	20.6	34.6	35.9	35.9	34.1	35.3	17.0	16.9
20	At5g17760	35.3	41.5	100	60.4	60.5	62.7	48.1	48.4	45.4	44.9	38.1	39.3	38.7	38.2	38.3	39.0	39.6	23.4	36.7	36.5	35.4	37.4	39.0	18.5	17.3
17	At5g17730	31.3	39.4	60.4	100	64.9	65.9	44.3	45.8	43.4	42.0	37.4	37.9	37.0	35.9	34.5	36.0	36.4	20.3	33.4	34.6	35.0	34.2	33.9	17.3	16.8
18	At5g17740	30.1	39.3	60.5	64.9	100	73.0	42.9	42.7	41.7	42.8	36.5	35.7	34.9	36.9	36.8	38.8	39.8	26.6	35.6	35.3	33.5	34.6	36.1	17.5	15.4
19	At5g17750	36.8	39.2	62.7	65.9	73.0	100	45.1	45.5	45.0	42.4	38.2	39.5	37.9	38.4	40.2	41.2	41.2	22.6	37.0	38.2	37.2	37.1	37.6	19.8	17.2
2	At2g18190	29.5	40.8	48.1	44.3	42.9	45.1	100	81.0	45.8	50.0	37.6	38.5	38.6	39.5	38.6	36.6	38.5	25.3	37.0	35.8	37.2	36.3	37.2	18.2	17.8
3	At2g18193	32.6	41.5	48.4	45.8	42.7	45.5	81.0	100	45.8	49.0	38.4	39.0	37.9	40.4	40.2	38.4	39.6	27.4	39.0	38.0	38.1	37.6	39.2	19.4	17.8
13	At3g50930	32.7	40.8	45.4	43.4	41.7	45.0	45.8	45.8	100	73.2	39.0	38.9	39.9	42.3	40.2	41.2	41.7	22.8	39.9	38.4	36.8	35.2	37.3	18.3	16.2
14	At3g50940	32.5	42.2	44.9	42.0	42.8	42.4	50.0	49.0	73.2	100	41.3	41.0	41.0	41.7	40.9	40.8	41.5	24.5	39.2	38.2	39.0	36.6	40.3	19.0	17.1
16	At4g30250	35.2	34.3	38.1	37.4	36.5	38.2	37.6	38.4	39.0	41.3	100	67.6	71.0	39.8	43.1	41.9	41.0	27.2	42.0	40.6	39.8	38.4	40.3	20.5	15.7
15	At4g25835	35.5	33.5	39.3	37.9	35.7	39.5	38.5	39.0	38.9	41.0	67.6	100	81.4	39.5	40.8	39.3	39.9	28.4	40.1	39.6	37.9	37.0	38.8	18.9	17.7
23	At5g57480	36.4	33.9	38.7	37.0	34.9	37.9	38.6	37.9	39.9	41.0	71.0	81.4	100	40.1	42.3	39.3	40.4	27.6	41.2	40.0	38.0	36.3	37.9	19.4	16.3
9	At3g28570	33.2	35.3	38.2	35.9	36.9	38.4	39.5	40.4	42.3	41.7	39.8	39.5	40.1	100	56.9	59.3	60.0	28.6	48.4	49.4	48.5	44.3	46.5	18.6	17.8
21	At5g40000	33.9	35.9	38.3	34.5	36.8	40.2	38.6	40.2	40.2	40.9	43.1	40.8	42.3	56.9	100	71.5	69.7	33.5	48.4	50.2	49.7	48.7	50.8	18.4	17.4
11	At3g28600	34.0	36.9	39.0	36.0	38.8	41.2	36.6	38.4	41.2	40.8	41.9	39.3	39.3	59.3	71.5	100	84.3	32.6	49.6	50.5	49.9	47.3	48.4	17.4	17.2
12	At3g28610	33.9	37.2	39.6	36.4	39.8	41.2	38.5	39.6	41.7	41.5	41.0	39.9	40.4	60.0	69.7	84.3	100	35.8	49.9	50.6	49.8	49.0	50.2	17.5	16.8
8	At3g28560	21.2	20.6	23.4	20.3	26.6	22.6	25.3	27.4	22.8	24.5	27.2	28.4	27.6	28.6	33.5	32.6	35.8	100	40.5	39.0	58.9	53.3	62.7	13.5	16.1
10	At3g28580	36.6	34.6	36.7	33.4	35.6	37.0	37.0	39.0	39.9	39.2	42.0	40.1	41.2	48.4	48.4	49.6	49.9	40.5	100	76.0	59.9	54.3	57.7	19.0	21.0
22	At5g40010	34.9	35.9	36.5	34.6	35.3	38.2	35.8	38.0	38.4	38.2	40.6	39.6	40.0	49.4	50.2	50.5	50.6	39.0	76.0	100	58.4	52.4	56.2	17.4	19.7
5	At3g28510	34.3	35.9	35.4	35.0	33.5	37.2	37.2	38.1	36.8	39.0	39.8	37.9	38.0	48.5	49.7	49.9	49.8	58.9	59.9	58.4	100	66.2	74.3	19.9	21.3
6	At3g28520	31.3	34.1	37.4	34.2	34.6	37.1	36.3	37.6	35.2	36.6	38.4	37.0	36.3	44.3	48.7	47.3	49.0	53.3	54.3	52.4	66.2	100	73.8	19.5	21.3
7	At3g28540	33.3	35.3	39.0	33.9	36.1	37.6	37.2	39.2	37.3	40.3	40.3	38.8	37.9	46.5	50.8	48.4	50.2	62.7	57.7	56.2	74.3	73.8	100	19.4	20.9
-	FTSH2	16.7	17.0	18.5	17.3	17.5	19.8	18.2	19.4	18.3	19.0	20.5	18.9	19.4	18.6	18.4	17.4	17.5	13.5	19.0	17.4	19.9	19.5	19.4	100	29.6
-	APP1	15.3	16.9	17.3	16.8	15.4	17.2	17.8	17.8	16.2	17.1	15.7	17.7	16.3	17.8	17.4	17.2	16.8	16.1	21.0	19.7	21.3	21.3	20.9	29.6	100

The identity matrix was calculated using the Clustal omega web app (https://www.ebi.ac.uk/Tools/msa/clustalo/), using the protein sequences of AAA-type ATPases in *A. thaliana* used in **Figure 5.9**. Each protein sequence included is numbered according to **Table 5.6**; columns containing the same numbers represent the same protein sequences. Each cell in the matrix gives the percent of identical amino acids in the sequence between the proteins in the respective row and column. The row and column containing AAA/AT2G18193 are highlighted in grey.

Table S5. 6 (next page) - Shortlist of potentially causative variants in MgMt 7

Position - Position of the SNV on the chromosome. **Freq.** - Frequency of the variant across sequencing reads. **Lies in** - Position of the SNV relative to the gene model in the "Gene ID" column; "Promoter" denotes presence within 2 kb of the transcriptional start site. **Base change** - Change to the amino acid sequence caused by the SNV in question; "?" denotes uncertainty due to poorly-defined gene model. **No** - Number of transcriptomic datasets from **Table 3.1** the respective gene was found to be upregulated in.

Position	Gene ID	Freq.	Lies in	Base change	Gene Annotation	No
5417560	**AT2G13126**	100%	Promoter	-	Hypothetical protein	0
11601305	**AT2G27150**	100%	Promoter	-	AAO3	1
11601305	**AT2G27145**	100%	Promoter	-	LCR9	0
11627322	**AT2G27200**	100%	Exon	Gly->Asp	LSG1-1	1
13186951	**AT2G30985**	100%	Exon	Arg->Trp	Hypothetical protein	0
13547918	**AT2G31865**	100%	Exon	?	PARG2	3
15354626	**AT2G36630**	100%	Exon	?	Sulfite exporter TauE	2
15393102	**AT2G36720**	100%	5' UTR	-	N-acyltransferase with zinc finger domain	0
15537744	**AT2G36990**	100%	Exon	Gly->Arg	SIG6; chloroplast sigma factor 6	0
15725026	**AT2G37450**	100%	5' UTR	-	UMAMIT13; nodulin MtN21-like	0
16461947	**AT2G39420**	100%	Exon	-	MAGL8	1
16785076	**AT2G40190**	100%	Promoter	-	LEW3	0
16997397	**AT2G40740**	100%	Exon	Thr->Ile	WRKY55	3
17089653	**AT2G40950**	100%	Exon	Gly->Asp	bZIP17	2
17096705	**AT2G40960**	100%	Exon	Ser->Phe	Nucleic acid binding R3H protein	0
17727996	**AT2G42580**	97.0%	Promoter	-	TTL3	0
11321280	**AT2G26610**	96.0%	Splice site	-	WD-40 repeat family protein	0
15700369	**AT2G37420**	96.0%	5' UTR	-	Microtubule motor family protein	0
16459008	**AT2G39415**	96.0%	Promoter	-	F-box family protein	0
9112622	**AT2G21280**	95.0%	Exon	Leu->Phe	SULA	0
14602117	**AT2G34660**	95.0%	Promoter	-	ABCC2	2
15757147	**AT2G37555**	95.0%	Exon	?	Natural antisense transcript	1
13676346	**AT2G32200**	95.0%	Promoter	-	Cysteine-rich protein	2
16288727	**AT2G39000**	95.0%	Promoter	-	GNAT4	0
13420662	**AT2G31510**	95.0%	Exon	?	ARI7	0
10393293	**AT2G24450**	94.0%	Exon	Pro->Leu	FLA3	1
12141110	**AT2G28390**	94.0%	Exon	?	MON1; SAND family	0
15390236	**AT2G36710**	93.0%	Exon	?	Pectin lyase-like protein	1
15455685	**AT2G36850**	93.0%	Exon	Arg->Lys	Glucan-synthase-like	1
7736812	**AT2G17790**	92.0%	Exon	Gly->Glu	ZIP3	1

Table S6. 1 - Presence of genes associated with Mg^{2+} transport from Ogura *et al*. in the MgD transcriptome collection

Gene ID	Name	Description	Sets
AT1G16010	MRS2-1	Magnesium transporter 2 (MGT2)	0
AT5G64560	MRS2-2	Magnesium transporter 9 (MGT9)	0
AT3G19640	MRS2-3	Magnesium transporter 4 (MGT4)	0
AT3G58970	MRS2-4	Magnesium transporter 6 (MGT6)	0
AT2G03620	MRS2-5	Magnesium transporter 3 (MGT3)	0
AT4G28580	MRS2-6	Magnesium transporter 5 (MGT5)	0
AT5G09690	MRS2-7	Magnesium transporter 7 (MGT7)	0
AT1G80900	MRS2-10	Magnesium transporter 1 (MGT1)	1
AT5G22830	MRS2-11	Magnesium transporter 10 (MGT10)	0
AT1G29830		Magnesium transporter CorA-like family protein	0
AT5G09720		Magnesium transporter CorA-like family protein	0
AT1G29820		Magnesium transporter CorA-like family protein	0
AT2G42950		Magnesium transporter CorA-like family protein	1
AT2G04305		Magnesium transporter CorA-like family protein	0
AT2G47600	MHX1	Magnesium/proton exchanger 1	0
AT1G61790	OST3/6	Oligosaccharyltransferase subunit 3/6	0
AT4G29870		Oligosaccharyltransferase complex/magnesium transporter family protein	0
AT1G11560		Oligosaccharyltransferase complex/magnesium transporter family protein	0
AT2G19340		Oligosaccharyltransferase complex/magnesium transporter family protein	0
AT3G23870		Magnesium transporter NIPA	1
AT4G13800		Magnesium transporter NIPA	0
AT5G11960		Magnesium transporter, putative	0
AT3G26670		Magnesium transporter, putative	1
AT1G71900		Magnesium transporter, putative	0
AT1G34470		Magnesium transporter, putative	0
AT4G09640		Magnesium transporter, putative	0
AT2G21120		Magnesium transporter, putative	1
AT4G38730		Magnesium transporter, putative	0
AT5G03345	PRCE2	PSI-interacting root-cell enriched 2	0

The list of genes associated with Mg^{2+}-transport in Ogura *et al.* was cross-referenced with the MgD transcriptome collection created in this work, returning the number of transcriptomic datasets from the collection each of the genes is upregulated in, given in the "**Sets**" column.

Bibliography

1. Laeter, J.R.d., et al., *Atomic weights of the elements. Review 2000 (IUPAC Technical Report).* Pure and Applied Chemistry, 2003. **75**(6): p. 683-800.
2. Allred, A.L., *Electronegativity values from thermochemical data.* Journal of Inorganic and Nuclear Chemistry, 1961. **17**(3): p. 215-221.
3. Maguire, M.E. and J.A. Cowan, *Magnesium chemistry and biochemistry.* Biometals, 2002. **15**(3): p. 203-210.
4. Ikeda, T., M. Boero, and K. Terakura, *Hydration properties of magnesium and calcium ions from constrained first principles molecular dynamics.* The Journal of Chemical Physics, 2007. **127**(7): p. 074503.
5. Schwierz, N., *Kinetic pathways of water exchange in the first hydration shell of magnesium.* The Journal of Chemical Physics, 2020. **152**(22): p. 224106.
6. Diebler, H., et al., *Kinetics and mechanism of reactions of main group metal ions with biological carriers.* Pure and Applied Chemistry, 1969. **20**(1): p. 93-116.
7. Eigen, M., *Fast elementary steps in chemical reaction mechanisms.* Pure and Applied Chemistry, 1963. **6**(1): p. 97-116.
8. Cowan, J.A., *Structural and catalytic chemistry of magnesium-dependent enzymes.* Biometals, 2002. **15**(3): p. 225-235.
9. KLEIN, D.J., P.B. MOORE, and T.A. STEITZ, *The contribution of metal ions to the structural stability of the large ribosomal subunit.* RNA, 2004. **10**(9): p. 1366-1379.
10. Dudev, T., J.A. Cowan, and C. Lim, *Competitive Binding in Magnesium Coordination Chemistry: Water versus Ligands of Biological Interest.* Journal of the American Chemical Society, 1999. **121**(33): p. 7665-7673.
11. Waldron, K.J., et al., *Metalloproteins and metal sensing.* Nature, 2009. **460**(7257): p. 823-830.
12. Irving, H. and R.J.P. Williams, *ORDER OF STABILITY OF METAL COMPLEXES.* Nature, 1948. **162**(4123): p. 746-747.
13. Andreini, C., et al., *Metal ions in biological catalysis: from enzyme databases to general principles.* Journal of Biological Inorganic Chemistry, 2008. **13**(8): p. 1205-1218.
14. Yazaki, Y., et al., *Estimation of Cytoplasmic free Mg2+-Levels and Phosphorylation Potentials in Mung Bean Root-Tips by in vivo P31 NMR-Spectroscopy.* Plant and Cell Physiology, 1988. **29**(6): p. 919-924.
15. Gout, E., et al., *Interplay of Mg2+, ADP, and ATP in the cytosol and mitochondria: Unravelling the role of Mg2+ in cell respiration.* Proceedings of the National Academy of Sciences, 2014. **111**(43): p. E4560-E4567.
16. Igamberdiev, A.U. and L.A. Kleczkowski, *Membrane potential, adenylate levels and Mg2+ are interconnected via adenylate kinase equilibrium in plant cells.* Biochimica et Biophysica Acta (BBA) - Bioenergetics, 2003. **1607**(2): p. 111-119.
17. Kleczkowski, L.A. and A.U. Igamberdiev, *Magnesium Signaling in Plants.* International Journal of Molecular Sciences, 2021. **22**(3).

18. Igamberdiev, A.U. and R.D. Hill, *Elevation of cytosolic Ca2+ in response to energy deficiency in plants: the general mechanism of adaptation to low oxygen stress.* Biochemical Journal, 2018. **475**(8): p. 1411-1425.
19. Ionescu, M.I., *Adenylate Kinase: A Ubiquitous Enzyme Correlated with Medical Conditions.* Protein J, 2019. **38**(2): p. 120-133.
20. Hartwig, A., *Role of magnesium in genomic stability.* Mutation Research/Fundamental and Molecular Mechanisms of Mutagenesis, 2001. **475**(1): p. 113-121.
21. Waldron, K.J. and N.J. Robinson, *How do bacterial cells ensure that metalloproteins get the correct metal?* Nature Reviews Microbiology, 2009. **7**(1): p. 25-35.
22. Canelas, H.M., L.M. De Assis, and F.B. De Jorge, *DISORDERS OF MAGNESIUM METABOLISM IN EPILEPSY.* Journal of neurology, neurosurgery, and psychiatry, 1965. **28**(4): p. 378-381.
23. DiNicolantonio, J.J., J.H. O'Keefe, and W. Wilson, *Subclinical magnesium deficiency: a principal driver of cardiovascular disease and a public health crisis.* Open Heart, 2018. **5**(1): p. e000668.
24. Al Alawi, A.M., S.W. Majoni, and H. Falhammar, *Magnesium and Human Health: Perspectives and Research Directions.* International Journal of Endocrinology, 2018. **2018**: p. 9041694.
25. Fazekas, T., et al., *Magnesium and the heart: Antiarrhythmic therapy with magnesium.* Clinical Cardiology, 1993. **16**(11): p. 768-774.
26. Papaceit, J., et al., *Severe heart arrhythmia secondary to magnesium depletion.* Revista espanola de anestesiologia y reanimacion, 1990. **37**(1): p. 28-31.
27. Battifora, H., et al., *The kidney in experimental magnesium deprivation. a morphologic and biochemical study.* Am J Pathol, 1966. **48**(3): p. 421-37.
28. Heggtveit, H.A., L. Herman, and R.K. Mishra, *CARDIAC NECROSIS AND CALCIFICATION IN EXPERIMENTAL MAGNESIUM DEFICIENCY. A LIGHT AND ELECTRON MICROSCOPIC STUDY.* The American journal of pathology, 1964. **45**(5): p. 757-782.
29. Rosanoff, A., C.M. Weaver, and R.K. Rude, *Suboptimal magnesium status in the United States: are the health consequences underestimated?* Nutrition Reviews, 2012. **70**(3): p. 153-164.
30. Guerrero-Romero, F. and M. Rodríguez-Morán, *Magnesium improves the beta-cell function to compensate variation of insulin sensitivity: double-blind, randomized clinical trial.* European Journal of Clinical Investigation, 2011. **41**(4): p. 405-410.
31. Nielsen, F.H., *Magnesium deficiency and increased inflammation: current perspectives.* Journal of inflammation research, 2018. **11**: p. 25-34.
32. Mauskop, A. and B.M. Altura, *Role of magnesium in the pathogenesis and treatment of migraines.* Clinical Neuroscience, 1998. **5**(1): p. 24-27.
33. Schimatschek, H.F. and R. Rempis, *Prevalence of hypomagnesemia in an unselected German population of 16,000 individuals.* Magnesium Research, 2001. **14**(4): p. 283-290.
34. Huijgen, H.J., et al., *Magnesium Levels in Critically Ill PatientsWhat Should We Measure?* American Journal of Clinical Pathology, 2000. **114**(5): p. 688-695.

35. Vormann, J., *Magnesium: nutrition and metabolism.* Molecular Aspects of Medicine, 2003. **24**(1): p. 27-37.
36. Sales, C.H., et al., *There is chronic latent magnesium deficiency in apparently healthy university students.* Nutricion hospitalaria, 2014. **30**(1): p. 200-204.
37. ter Borg, S., et al., *Micronutrient intakes and potential inadequacies of community-dwelling older adults: a systematic review.* British Journal of Nutrition, 2015. **113**(8): p. 1195-1206.
38. Mejía-Rodríguez, F., et al., *Iron, zinc, copper and magnesium deficiencies in Mexican adults from the National Health and Nutrition Survey 2006.* salud pública de méxico, 2013. **55**(3): p. 275-284.
39. Cakmak, I., *Magnesium in crop production, food quality and human health.* Plant and Soil, 2013. **368**(1): p. 1-4.
40. Fan, M.-S., et al., *Evidence of decreasing mineral density in wheat grain over the last 160 years.* Journal of Trace Elements in Medicine and Biology, 2008. **22**(4): p. 315-324.
41. Garvin, D.F., R.M. Welch, and J.W. Finley, *Historical shifts in the seed mineral micronutrient concentration of US hard red winter wheat germplasm.* Journal of the Science of Food and Agriculture, 2006. **86**(13): p. 2213-2220.
42. White, P.J. and M.R. Broadley, *Historical variation in the mineral composition of edible horticultural products.* Journal of Horticultural Science & Biotechnology, 2005. **80**(6): p. 660-667.
43. Marles, R.J., *Mineral nutrient composition of vegetables, fruits and grains: The context of reports of apparent historical declines.* Journal of Food Composition and Analysis, 2017. **56**: p. 93-103.
44. Guerrero-Romero, F., et al., *Oral magnesium supplementation improves glycaemic status in subjects with prediabetes and hypomagnesaemia: A double-blind placebo-controlled randomized trial.* Diabetes & Metabolism, 2015. **41**(3): p. 202-207.
45. Tarleton, E.K., et al., *Role of magnesium supplementation in the treatment of depression: A randomized clinical trial.* PLOS ONE, 2017. **12**(6): p. e0180067.
46. Sojka, J.E., *Magnesium Supplementation and Osteoporosis.* Nutrition Reviews, 1995. **53**(3): p. 71-74.
47. Jee, S.H., et al., *The effect of magnesium supplementation on blood pressure: a meta-analysis of randomized clinical trials*.* American Journal of Hypertension, 2002. **15**(8): p. 691-696.
48. White, P.J. and M.R. Broadley, *Biofortification of crops with seven mineral elements often lacking in human diets – iron, zinc, copper, calcium, magnesium, selenium and iodine.* New Phytologist, 2009. **182**(1): p. 49-84.
49. Cakmak, I. and A.M. Yazici, *Magnesium: a forgotten element in crop production.* Better Crops with Plant Food, 2010. **94**(2): p. 23-25.
50. Cleland, W.W., et al., *Mechanism of Rubisco: the carbamate as general base.* Chemical reviews, 1998. **98**(2): p. 549-562.
51. Gutteridge, S. and A.A. Gatenby, *Rubisco synthesis, assembly, mechanism, and regulation.* The Plant Cell, 1995. **7**(7): p. 809.
52. Mukerji, S., *Corn leaf phosphoenolpyruvate carboxylases: activation by magnesium ions.* Plant Science Letters, 1974. **2**(4): p. 243-248.

53. Wedding, R.T. and M.K. Black, *Role of magnesium in the binding of substrate and effectors to phosphoenolpyruvate carboxylase from a CAM plant.* Plant physiology, 1988. **87**(2): p. 443-446.
54. Raines, C.A., J.C. Lloyd, and T.A. Dyer, *New insights into the structure and function of sedoheptulose-1,7-bisphosphatase; an important but neglected Calvin cycle enzyme.* Journal of Experimental Botany, 1999. **50**(330): p. 1-8.
55. King, R.W. and J.A. Zeevaart, *Enhancement of Phloem Exudation from cut Petioles by Chelating Agents.* Plant Physiology, 1974. **53**(1): p. 96-103.
56. Hermans, C., et al., *Magnesium deficiency in sugar beets alters sugar partitioning and phloem loading in young mature leaves.* Planta, 2005. **220**(4): p. 541-549.
57. Chen, Z.C., et al., *Functional dissection and transport mechanism of magnesium in plants.* Seminars in Cell & Developmental Biology, 2018. **74**: p. 142-152.
58. Senbayram, M., et al., *Role of magnesium fertilisers in agriculture: plant–soil continuum.* Crop and Pasture Science, 2015. **66**(12): p. 1219-1229.
59. Mayland, H.F. and S.R. Wilkinson, *Soil Factors Affecting Magnesium Availability in Plant-Animal Systems: A Review.* Journal of Animal Science, 1989. **67**(12): p. 3437-3444.
60. Sillanpää, M., *Micronutrients and the nutrient status of soils: a global study*. 1982: Food & Agriculture Org.
61. Hermans, C., et al., *An update on magnesium homeostasis mechanisms in plants.* Metallomics, 2013. **5**(9): p. 1170-83.
62. Ishijima, S., et al., *Magnesium uptake of Arabidopsis transporters, AtMRS2-10 and AtMRS2-11, expressed in Escherichia coli mutants: Complementation and growth inhibition by aluminum.* Biochimica Et Biophysica Acta-Biomembranes, 2015. **1848**(6): p. 1376-1382.
63. Ishijima, S., et al., *The homologous Arabidopsis MRS2/MGT/CorA-type Mg2+ channels, AtMRS2-10 and AtMRS2-1 exhibit different aluminum transport activity.* Biochimica Et Biophysica Acta-Biomembranes, 2018. **1860**(11): p. 2184-2191.
64. Chen, Z.C., et al., *Up-Regulation of a Magnesium Transporter Gene OsMGT1 Is Required for Conferring Aluminum Tolerance in Rice.* Plant Physiology, 2012. **159**(4): p. 1624-1633.
65. Bose, J., O. Babourina, and Z. Rengel, *Role of magnesium in alleviation of aluminium toxicity in plants.* Journal of Experimental Botany, 2011. **62**(7): p. 2251-2264.
66. Marschner, H. and P. Marschner, *Marschner's Mineral Nutrition of Higher Plants*. 2012: Academic Press.
67. Gransee, A. and H. Führs, *Magnesium mobility in soils as a challenge for soil and plant analysis, magnesium fertilization and root uptake under adverse growth conditions.* Plant and Soil, 2013. **368**(1): p. 5-21.
68. Yeo, A., *Predicting the interaction between the effects of salinity and climate change on crop plants.* Scientia Horticulturae, 1999. **78**(1-4): p. 159-174.
69. Munns, R. and M. Tester, *Mechanisms of salinity tolerance.* Annu Rev Plant Biol, 2008. **59**: p. 651-81.

70. Wang, Z., et al., *Magnesium Fertilization Improves Crop Yield in Most Production Systems: A Meta-Analysis.* Frontiers in Plant Science, 2020. **10**: p. 10.
71. Grzebisz, W. and J. Potarzycki, *Effect of Magnesium Fertilization Systems on Grain Yield Formation by Winter Wheat (Triticum aestivum L.) during the Grain-Filling Period.* Agronomy, 2022. **12**(1): p. 12.
72. Geng, G., et al., *Effect of magnesium fertilization on seed yield, seed quality, carbon assimilation and nutrient uptake of rapeseed plants.* Field Crops Research, 2021. **264**: p. 108082.
73. Church, B. and R. Skinner, *The pH and nutrient status of agricultural soils in England and Wales 1969–83.* The Journal of Agricultural Science, 1986. **107**(1): p. 21-28.
74. McGrath, S. and P.J. Loveland, *Soil geochemical atlas of England and Wales*. 1992: Blackie Academic & Professional.
75. Lark, R.M., E.L. Ander, and M.R. Broadley, *Combining two national-scale datasets to map soil properties, the case of available magnesium in England and Wales.* European Journal of Soil Science, 2019. **70**(2): p. 361-377.
76. Hauer-Jakli, M. and M. Trankner, *Critical Leaf Magnesium Thresholds and the Impact of Magnesium on Plant Growth and Photo-Oxidative Defense: A Systematic Review and Meta-Analysis From 70 Years of Research.* Frontiers in Plant Science, 2019. **10**: p. 15.
77. Wang, J., et al., *Selecting optimal calibration samples using proximal sensing EM induction and γ-ray spectrometry data: An application to managing lime and magnesium in sugarcane growing soil.* Journal of Environmental Management, 2021. **296**: p. 113357.
78. Li, N., et al., *Determining optimal digital soil mapping components for exchangeable calcium and magnesium across a sugarcane field.* CATENA, 2019. **181**: p. 104054.
79. Bagdassarian, K.S., et al., *Versatile method for quantifying and analyzing morphological differences in experimentally obtained images.* Plant Signaling & Behavior, 2019: p. 1693092.
80. Zhao, D., et al., *Soil exchangeable cations estimation using Vis-NIR spectroscopy in different depths: Effects of multiple calibration models and spiking.* Computers and Electronics in Agriculture, 2021. **182**: p. 105990.
81. Wadoux, A.M.J.C., B. Minasny, and A.B. McBratney, *Machine learning for digital soil mapping: Applications, challenges and suggested solutions.* Earth-Science Reviews, 2020. **210**: p. 103359.
82. Romani, A. and A. Scarpa, *REGULATION OF CELL MAGNESIUM.* Archives of Biochemistry and Biophysics, 1992. **298**(1): p. 1-12.
83. Igamberdiev, A.U. and L.A. Kleczkowski, *Implications of adenylate kinase-governed equilibrium of adenylates on contents of free magnesium in plant cells and compartments.* Biochemical Journal, 2001. **360**: p. 225-231.
84. Ishijima, S., et al., *Light-induced increase in free Mg2+ concentration in spinach chloroplasts: Measurement of free Mg2+ by using a fluorescent probe and necessity of stromal alkalinization.* Archives of Biochemistry and Biophysics, 2003. **412**(1): p. 126-132.

85. Gout, E., et al., *Interplay of Mg2+, ADP, and ATP in the cytosol and mitochondria: Unravelling the role of Mg2+ in cell respiration.* Proceedings of the National Academy of Sciences of the United States of America, 2014. **111**(43): p. E4560-E4567.
86. Hermans, C. and N. Verbruggen, *Physiological characterization of Mg deficiency in Arabidopsis thaliana.* Journal of Experimental Botany, 2005. **56**(418): p. 2153-2161.
87. Ogura, T., et al., *Short-Term Magnesium Deficiency Triggers Nutrient Retranslocation in Arabidopsis thaliana.* Frontiers in Plant Science, 2020. **11**(563).
88. Cakmak, I., C. Hengeler, and H. Marschner, *Changes in phloem export of sucrose in leaves in response to phosphorus, potassium and magnesium deficiency in bean plants.* Journal of Experimental Botany, 1994. **45**(9): p. 1251-1257.
89. Kobayashi, N.I., et al., *Magnesium deficiency damages the youngest mature leaf in rice through tissue-specific iron toxicity.* Plant and Soil, 2018. **428**(1-2): p. 137-152.
90. Verbruggen, N. and C. Hermans, *Physiological and molecular responses to magnesium nutritional imbalance in plants.* Plant and Soil, 2013. **368**(1-2): p. 87-99.
91. Kühn, C. and C.P.L. Grof, *Sucrose transporters of higher plants.* Current Opinion in Plant Biology, 2010. **13**(3): p. 287-297.
92. Bush, D.R., *Proton-Coupled Sugar and Amino Acid Transporters in Plants.* Annual Review of Plant Physiology and Plant Molecular Biology, 1993. **44**(1): p. 513-542.
93. Truernit, E. and N. Sauer, *The promoter of the Arabidopsis thaliana SUC2 sucrose-H+ symporter gene directs expression of beta-glucuronidase to the phloem: evidence for phloem loading and unloading by SUC2.* Planta, 1995. **196**(3): p. 564-70.
94. Srivastava, A.C., et al., *Functional Characterization of the Arabidopsis AtSUC2 Sucrose/H+ Symporter by Tissue-Specific Complementation Reveals an Essential Role in Phloem Loading But Not in Long-Distance Transport.* Plant Physiology, 2008. **148**(1): p. 200-211.
95. Zakhartsev, M., et al., *Metabolic model of central carbon and energy metabolisms of growing Arabidopsis thaliana in relation to sucrose translocation.* BMC Plant Biology, 2016. **16**(1): p. 262.
96. Peng, Y.Y., et al., *Magnesium deficiency triggers SGR-mediated chlorophyll degradation for magnesium remobilization.* Plant Physiology, 2019: p. pp.00610.2019.
97. Hermans, C., et al., *Physiological characterisation of magnesium deficiency in sugar beet: acclimation to low magnesium differentially affects photosystems I and II.* Planta, 2004. **220**(2): p. 344-355.
98. Cakmak, I. and E.A. Kirkby, *Role of magnesium in carbon partitioning and alleviating photooxidative damage.* Physiologia Plantarum, 2008. **133**(4): p. 692-704.

99. Kobayashi, N.I. and K. Tanoi, *Critical Issues in the Study of Magnesium Transport Systems and Magnesium Deficiency Symptoms in Plants.* International Journal of Molecular Sciences, 2015. **16**(9): p. 23076-23093.
100. Sun, Y., et al., *The Magnesium Transporter MGT10 Is Essential for Chloroplast Development and Photosynthesis in Arabidopsis thaliana.* Molecular Plant, 2017. **10**(12): p. 1584-1587.
101. Hermans, C., et al., *Early transcriptomic changes induced by magnesium deficiency in Arabidopsis thaliana reveal the alteration of circadian clock gene expression in roots and the triggering of abscisic acid-responsive genes.* New Phytol, 2010. **187**(1): p. 119-31.
102. Hermans, C., et al., *Systems analysis of the responses to long-term magnesium deficiency and restoration in Arabidopsis thaliana.* New Phytol, 2010. **187**(1): p. 132-44.
103. Oda, K., et al., *The Arabidopsis Mg Transporter, MRS2-4, is Essential for Mg Homeostasis Under Both Low and High Mg Conditions.* Plant and Cell Physiology, 2016. **57**(4): p. 754-763.
104. Niu, Y.F., et al., *Physiological and Transcriptome Responses to Combinations of Elevated CO2 and Magnesium in Arabidopsis thaliana.* Plos One, 2016. **11**(2): p. 21.
105. Kamiya, T., et al., *Establishment of an in planta magnesium monitoring system using CAX3 promoter-luciferase in Arabidopsis.* Journal of Experimental Botany, 2011. **63**(1): p. 355-363.
106. Niu, Y.F., et al., *Magnesium availability regulates the development of root hairs in Arabidopsis thaliana (L.) Heynh.* Plant Cell and Environment, 2014. **37**(12): p. 2795-2813.
107. Liu, M., et al., *Auxin Acts Downstream of Ethylene and Nitric Oxide to Regulate Magnesium Deficiency-Induced Root Hair Development in Arabidopsis thaliana.* Plant and Cell Physiology, 2018. **59**(7): p. 1452-1465.
108. Xiao, Q.Y., et al., *Natural genetic variation of Arabidopsis thaliana root morphological response to magnesium supply.* Crop & Pasture Science, 2015. **66**(12): p. 1249-1258.
109. Day, I.S., et al., *Analysis of EF-hand-containing proteins in Arabidopsis.* Genome Biology, 2002. **3**(10): p. research0056.1.
110. Grabarek, Z., *Insights into modulation of calcium signaling by magnesium in calmodulin, troponin C and related EF-hand proteins.* Biochimica et Biophysica Acta (BBA) - Molecular Cell Research, 2011. **1813**(5): p. 913-921.
111. Astegno, A., et al., *Arabidopsis calmodulin-like protein CML36 is a calcium (Ca2+) sensor that interacts with the plasma membrane Ca2+-ATPase isoform ACA8 and stimulates its activity.* J Biol Chem, 2017. **292**(36): p. 15049-15061.
112. Batistic, O. and J. Kudla, *Plant calcineurin B-like proteins and their interacting protein kinases.* Biochim Biophys Acta, 2009. **1793**(6): p. 985-92.
113. Tang, R.J., et al., *Tonoplast CBL-CIPK calcium signaling network regulates magnesium homeostasis in Arabidopsis.* Proceedings of the National Academy of Sciences of the United States of America, 2015. **112**(10): p. 3134-3139.
114. Shaul, O., *Magnesium transport and function in plants: the tip of the iceberg.* Biometals, 2002. **15**(3): p. 309-323.

115. Tanoi, K., et al., *The analysis of magnesium transport system from external solution to xylem in rice root.* Soil Science and Plant Nutrition, 2011. **57**(2): p. 265-271.
116. Shaul, O., et al., *Cloning and characterization of a novel Mg2+/H+ exchanger.* Embo Journal, 1999. **18**(14): p. 3973-3980.
117. Guo, K.M., et al., *The cyclic nucleotide-gated channel AtCNGC10 transports Ca2+and Mg2+in Arabidopsis.* Physiologia Plantarum, 2010. **139**(3): p. 303-312.
118. Li, X.L., et al., *Arabidopsis AtCNGC10 rescues potassium channel mutants of E-coli, yeast and Arabidopsis and is regulated by calcium/calmodulin and cyclic GMP in E-coli.* Functional Plant Biology, 2005. **32**(7): p. 643-653.
119. Conn, S.J., et al., *Magnesium transporters, MGT2/MRS2-1 and MGT3/MRS2-5, are important for magnesium partitioning within Arabidopsis thaliana mesophyll vacuoles.* New Phytol, 2011. **190**(3): p. 583-94.
120. Ge, H., et al., *A metal tolerance protein, MTP10, is required for the calcium and magnesium homeostasis in Arabidopsis.* Plant Signaling & Behavior, 2022: p. 2025322.
121. Li, L.G., et al., *A novel family of magnesium transport genes in Arabidopsis.* Plant Cell, 2001. **13**(12): p. 2761-2775.
122. Knoop, V., et al., *Transport of magnesium and other divalent cations: evolution of the 2-TM-GxN proteins in the MIT superfamily.* Molecular Genetics and Genomics, 2005. **274**(3): p. 205-216.
123. Payandeh, J., R. Pfoh, and E.F. Pai, *The structure and regulation of magnesium selective ion channels.* Biochimica Et Biophysica Acta-Biomembranes, 2013. **1828**(11): p. 2778-2792.
124. Payandeh, J. and E.F. Pai, *A structural basis for Mg2+ homeostasis and the CorA translocation cycle.* The EMBO Journal, 2006. **25**(16): p. 3762-3773.
125. Lunin, V.V., et al., *Crystal structure of the CorA Mg2+ transporter.* Nature, 2006. **440**(7085): p. 833-837.
126. Eshaghi, S., et al., *Crystal Structure of a Divalent Metal Ion Transporter CorA at 2.9 Angstrom Resolution*. Science, 2006. **313**(5785): p. 354-357.
127. Palombo, I., D.O. Daley, and M. Rapp, *Why Is the GMN Motif Conserved in the CorA/Mrs2/Alr1 Superfamily of Magnesium Transport Proteins?* Biochemistry, 2013. **52**(28): p. 4842-4847.
128. Matthies, D., et al., *Cryo-EM Structures of the Magnesium Channel CorA Reveal Symmetry Break upon Gating.* Cell, 2017. **164**(4): p. 747-756.
129. Stetsenko, A. and A. Guskov, *Cation permeability in CorA family of proteins.* Scientific Reports, 2020. **10**(1): p. 840.
130. Nemchinova, M., et al., *Asymmetric CorA Gating Mechanism as Observed by Molecular Dynamics Simulations.* Journal of Chemical Information and Modeling, 2021. **61**(5): p. 2407-2417.
131. Maeshima, K., et al., *A Transient Rise in Free Mg2+ Ions Released from ATP-Mg Hydrolysis Contributes to Mitotic Chromosome Condensation.* Current Biology, 2018. **28**(3): p. 444-451.e6.
132. Schindl, R., et al., *Mrs2p forms a high conductance Mg2+ selective channel in mitochondria.* Biophysical Journal, 2007. **93**(11): p. 3872-3883.

133. Kolisek, M., et al., *Mrs2p is an essential component of the major electrophoretic Mg2+ influx system in mitochondria.* Embo Journal, 2003. **22**(6): p. 1235-1244.
134. Khan, M.B., et al., *Structural and functional characterization of the N-terminal domain of the yeast Mg2+ channel Mrs2.* Acta Crystallographica Section D-Biological Crystallography, 2013. **69**: p. 1653-1664.
135. Schock, I., et al., *A member of a novel Arabidopsis thaliana gene family of candidate Mg2+ ion transporters complements a yeast mitochondrial group II intron-splicing mutant.* Plant Journal, 2000. **24**(4): p. 489-501.
136. Gebert, M., et al., *A root-expressed magnesium transporter of the MRS2/MGT gene family in Arabidopsis thaliana allows for growth in low-Mg2+ environments.* Plant Cell, 2009. **21**(12): p. 4018-30.
137. Lenz, H., et al., *Magnesium Deficiency Phenotypes Upon Multiple Knockout of Arabidopsis thaliana MRS2 Clade B Genes Can be Ameliorated by Concomitantly Reduced Calcium Supply.* Plant and Cell Physiology, 2013. **54**(7): p. 1118-1131.
138. Mao, D.D., et al., *Arabidopsis Transporter MGT6 Mediates Magnesium Uptake and Is Required for Growth under Magnesium Limitation.* Plant Cell, 2014. **26**(5): p. 2234-2248.
139. Liang, S., et al., *Mutations in the Arabidopsis AtMRS2-11/AtMGT10/VAR5 Gene Cause Leaf Reticulation.* Frontiers in Plant Science, 2017. **8**: p. 12.
140. Chen, J., et al., *Magnesium transporter AtMGT9 is essential for pollen development in Arabidopsis.* Cell Research, 2009. **19**(7): p. 887-898.
141. Li, H., et al., *Identification, and Functional and Expression Analyses of the CorA/MRS2/MGT-Type Magnesium Transporter Family in Maize.* Plant and Cell Physiology, 2016. **57**(6): p. 1153-1168.
142. Li, H.Y., et al., *The maize CorA/MRS2/MGT-type Mg transporter, ZmMGT10, responses to magnesium deficiency and confers low magnesium tolerance in transgenic Arabidopsis.* Plant Molecular Biology, 2017. **95**(3): p. 269-278.
143. Li, H.Y., et al., *Molecular and functional characterization of the magnesium transporter gene ZmMGT12 in maize.* Gene, 2018. **665**: p. 167-173.
144. Saito, T., et al., *Expression and Functional Analysis of the CorA-MRS2-ALR-Type Magnesium Transporter Family in Rice.* Plant and Cell Physiology, 2013. **54**(10): p. 1673-1683.
145. Chen, Z.C., et al., *A Magnesium Transporter OsMGT1 Plays a Critical Role in Salt Tolerance in Rice.* Plant Physiology, 2017. **174**(3): p. 1837-1849.
146. Li, J., et al., *Diel magnesium fluctuations in chloroplasts contribute to photosynthesis in rice.* Nature Plants, 2020.
147. Zhang, L.D., et al., *OsMGT1 Confers Resistance to Magnesium Deficiency By Enhancing the Import of Mg in Rice.* International Journal of Molecular Sciences, 2019. **20**(1): p. 13.
148. Zhang, L., et al., *Molecular identification of the magnesium transport gene family in Brassica napus.* Plant Physiology and Biochemistry, 2019. **136**: p. 204-214.
149. Tong, M., et al., *Identification and functional analysis of the CorA/MGT/MRS2-type magnesium transporter in banana.* PLOS ONE, 2020. **15**(10): p. e0239058.

150. Zhao, Z.F., et al., *Phylogenetic and expression analysis of the magnesium transporter family in pear, and functional verification of PbrMGT7 in pear pollen.* Journal of Horticultural Science & Biotechnology, 2018. **93**(1): p. 51-63.
151. Heidari, P., et al., *Magnesium transporter Gene Family: Genome-Wide Identification and Characterization in Theobroma cacao, Corchorus capsularis, and Gossypium hirsutum of Family Malvaceae.* Agronomy, 2021. **11**(8).
152. Wang, Y.J., et al., *Comparative genomics revealed the gene evolution and functional divergence of magnesium transporter families in Saccharum.* Bmc Genomics, 2019. **20**: p. 18.
153. Xu, X.-F., et al., *Magnesium Transporter 5 plays an important role in Mg transport for male gametophyte development in Arabidopsis.* The Plant Journal, 2015. **84**(5): p. 925-936.
154. Li, J., et al., *An endoplasmic reticulum magnesium transporter is essential for pollen development in Arabidopsis.* Plant Science, 2015. **231**: p. 212-220.
155. Froehlich, J.E., et al., *Proteomic Study of the Arabidopsis thaliana Chloroplastic Envelope Membrane Utilizing Alternatives to Traditional Two-Dimensional Electrophoresis.* Journal of Proteome Research, 2003. **2**(4): p. 413-425.
156. Li, L.G., et al., *A mitochondrial magnesium transporter functions in Arabidopsis pollen development.* Molecular Plant, 2008. **1**(4): p. 675-685.
157. Drummond, R.S.M., et al., *A putative magnesium transporter AtMRS2-11 is localized to the plant chloroplast envelope membrane system.* Plant Science, 2006. **170**(1): p. 78-89.
158. Ishijima, S., et al., *Functional reconstitution and characterization of the Arabidopsis Mg2+ transporter AtMRS2-10 in proteoliposomes.* Biochimica et Biophysica Acta (BBA) - Biomembranes, 2012. **1818**(9): p. 2202-2208.
159. Ishijima, S., R. Shiomi, and I. Sagami, *Functional analysis of whether the glycine residue of the GMN motif of the Arabidopsis MRS2/MGT/CorA-type Mg2+ channel protein AtMRS2-11 is critical for Mg2+ transport activity.* Archives of Biochemistry and Biophysics, 2021. **697**: p. 108673.
160. Rengel, Z., et al., *Magnesium alleviates plant toxicity of aluminium and heavy metals.* Crop & Pasture Science, 2015. **66**(12): p. 1298-1307.
161. Xu, X.-F., et al., *Slowing Development Facilitates Arabidopsis mgt Mutants to Accumulate Enough Magnesium for Pollen Formation and Fertility Restoration.* Frontiers in Plant Science, 2021. **11**(2299).
162. Hermans, C., et al., *Low magnesium status in plants enhances tolerance to cadmium exposure.* New Phytologist, 2011. **192**(2): p. 428-436.
163. Mao, D.-D., et al., *AtMGT7: An Arabidopsis Gene Encoding a Low-Affinity Magnesium Transporter.* Journal of Integrative Plant Biology, 2008. **50**(12): p. 1530-1538.
164. Feng, Z., et al., *An SMU Splicing Factor Complex Within Nuclear Speckles Contributes to Magnesium Homeostasis in Arabidopsis thaliana.* Plant Physiology, 2020: p. pp.00109.2020.

165. Yan, Y.W., et al., *Magnesium Transporter MGT6 Plays an Essential Role in Maintaining Magnesium Homeostasis and Regulating High Magnesium Tolerance in Arabidopsis.* Frontiers in Plant Science, 2018. **9**: p. 13.
166. Ogura, T., et al., *Magnesium uptake characteristics in Arabidopsis revealed by 28Mg tracer studies.* Planta, 2018.
167. Schmitz, J., et al., *Membrane protein interactions between different Arabidopsis thaliana MRS2-type magnesium transporters are highly permissive.* Biochimica Et Biophysica Acta-Biomembranes, 2013. **1828**(9): p. 2032-2040.
168. Punshon, T., et al., *Methodological approaches for using synchrotron X-ray fluorescence (SXRF) imaging as a tool in ionomics: examples from Arabidopsis thaliana.* Metallomics, 2013. **5**(9): p. 1133-1145.
169. Liu, M., et al., *Fluorescent probes for the detection of magnesium ions (Mg2+): from design to application.* Rsc Advances, 2018. **8**(23): p. 12573-12587.
170. Yu, T., et al., *A novel and simple fluorescence probe for detecting main group magnesium ion in HeLa cells and Arabidopsis.* Biosensors and Bioelectronics, 2016. **86**: p. 677-682.
171. Gruskos, J.J., G. Zhang, and D. Buccella, *Visualizing Compartmentalized Cellular Mg2+ on Demand with Small-Molecule Fluorescent Sensors.* Journal of the American Chemical Society, 2016. **138**(44): p. 14639-14649.
172. Schneckenburger, H., *Förster resonance energy transfer–what can we learn and how can we use it?* Methods and Applications in Fluorescence, 2019. **8**(1): p. 013001.
173. PIETRASZEWSKA-BOGIEL, A. and T.W.J. GADELLA, *FRET microscopy: from principle to routine technology in cell biology.* Journal of Microscopy, 2011. **241**(2): p. 111-118.
174. Allen, G.J., et al., *Cameleon calcium indicator reports cytoplasmic calcium dynamics in Arabidopsis guard cells.* The Plant Journal, 1999. **19**(6): p. 735-747.
175. Deuschle, K., et al., *Rapid metabolism of glucose detected with FRET glucose nanosensors in epidermal cells and intact roots of Arabidopsis RNA-silencing mutants.* The Plant cell, 2006. **18**(9): p. 2314-2325.
176. Bischof, H., et al., *Live-Cell Imaging of Physiologically Relevant Metal Ions Using Genetically Encoded FRET-Based Probes.* Cells, 2019. **8**(5): p. 25.
177. Lindenburg, L.H., et al., *MagFRET: The First Genetically Encoded Fluorescent Mg2+ Sensor.* Plos One, 2013. **8**(12): p. 10.
178. Daw, C.C., et al., *Lactate Elicits ER-Mitochondrial Mg2+ Dynamics to Integrate Cellular Metabolism.* Cell, 2020. **183**(2): p. 474-489.e17.
179. Lazarou, T.S. and D. Buccella, *Advances in imaging of understudied ions in signaling: A focus on magnesium.* Current Opinion in Chemical Biology, 2020. **57**: p. 27-33.
180. Wu, Y., et al., *Magnesium efflux from Drosophila Kenyon cells is critical for normal and diet-enhanced long-term memory.* eLife, 2020. **9**: p. e61339.
181. Imamura, H., et al., *Visualization of ATP levels inside single living cells with fluorescence resonance energy transfer-based genetically encoded indicators.* Proceedings of the National Academy of Sciences, 2009. **106**(37): p. 15651-15656.

182. De Col, V., et al., *ATP sensing in living plant cells reveals tissue gradients and stress dynamics of energy physiology.* eLife, 2017. **6**: p. e26770.
183. Voon, C.P., et al., *ATP compartmentation in plastids and cytosol of Arabidopsis thaliana revealed by fluorescent protein sensing.* Proceedings of the National Academy of Sciences, 2018. **115**(45): p. E10778-E10787.
184. Martynov, V.I., et al., *Genetically encoded fluorescent indicators for live cell pH imaging.* Biochimica et Biophysica Acta (BBA) - General Subjects, 2018. **1862**(12): p. 2924-2939.
185. Miesenböck, G., D.A. De Angelis, and J.E. Rothman, *Visualizing secretion and synaptic transmission with pH-sensitive green fluorescent proteins.* Nature, 1998. **394**(6689): p. 192-195.
186. Gjetting, S.K., et al., *Live imaging of intra- and extracellular pH in plants using pHusion, a novel genetically encoded biosensor.* Journal of Experimental Botany, 2012. **63**(8): p. 3207-3218.
187. Martinière, A., et al., *Uncovering pH at both sides of the root plasma membrane interface using noninvasive imaging.* Proceedings of the National Academy of Sciences, 2018. **115**(25): p. 6488-6493.
188. Brumbarova, T. and R. Ivanov, *The Nutrient Response Transcriptional Regulome of Arabidopsis.* iScience, 2019. **19**: p. 358-368.
189. Abe, A., et al., *Genome sequencing reveals agronomically important loci in rice using MutMap.* Nature Biotechnology, 2012. **30**(2): p. 174-178.
190. Kato, H., et al., *Lumi-Map, a Real-Time Luciferase Bioluminescence Screen of Mutants Combined with MutMap, Reveals Arabidopsis Genes Involved in PAMP-Triggered Immunity.* Molecular Plant-Microbe Interactions®, 2020. **33**(12): p. 1366-1380.
191. Alonso, J.M., et al., *Genome-Wide Insertional Mutagenesis of Arabidopsis thaliana.* Science, 2003. **301**(5633): p. 653.
192. Murashige, T. and F. Skoog, *A Revised Medium for Rapid Growth and Bio Assays with Tobacco Tissue Cultures.* Physiologia Plantarum, 1962. **15**(3): p. 473-497.
193. Sinclair, S.A., et al., *Systemic Upregulation of MTP2- and HMA2-Mediated Zn Partitioning to the Shoot Supplements Local Zn Deficiency Responses.* The Plant cell, 2018. **30**(10): p. 2463-2479.
194. Kruskal, W.H. and W.A. Wallis, *Use of Ranks in One-Criterion Variance Analysis.* Journal of the American Statistical Association, 1952. **47**(260): p. 583-621.
195. Dunn, O.J., *Multiple Comparisons Using Rank Sums.* Technometrics, 1964. **6**(3): p. 241-252.
196. Bolger, A.M., M. Lohse, and B. Usadel, *Trimmomatic: a flexible trimmer for Illumina sequence data.* Bioinformatics (Oxford, England), 2014. **30**(15): p. 2114-2120.
197. Li, H. and R. Durbin, *Fast and accurate short read alignment with Burrows-Wheeler transform.* Bioinformatics, 2009. **25**(14): p. 1754-60.
198. Danecek, P., et al., *Twelve years of SAMtools and BCFtools.* GigaScience, 2021. **10**(2).

199. Koboldt, D.C., et al., *VarScan: variant detection in massively parallel sequencing of individual and pooled samples.* Bioinformatics, 2009. **25**(17): p. 2283-2285.
200. Feike, D., et al., *The Starch Granule-Associated Protein EARLY STARVATION1 Is Required for the Control of Starch Degradation in Arabidopsis thaliana Leaves.* The Plant Cell, 2016. **28**(6): p. 1472-1489.
201. Wagner, S., et al., *Multiparametric real-time sensing of cytosolic physiology links hypoxia responses to mitochondrial electron transport.* New Phytologist, 2019. **224**(4): p. 1668-1684.
202. Clough, S.J. and A.F. Bent, *Floral dip: a simplified method for Agrobacterium - mediated transformation of Arabidopsis thaliana.* The Plant Journal, 1998. **16**(6): p. 735-743.
203. Anders, S. and W. Huber, *Differential expression analysis for sequence count data.* Genome Biology, 2010. **11**(10): p. R106.
204. Mi, H., et al., *PANTHER version 14: more genomes, a new PANTHER GO-slim and improvements in enrichment analysis tools.* Nucleic Acids Res, 2019. **47**(D1): p. D419-d426.
205. Young, M.D., et al., *Gene ontology analysis for RNA-seq: accounting for selection bias.* Genome Biology, 2010. **11**(2): p. R14.
206. Xie, C., et al., *KOBAS 2.0: a web server for annotation and identification of enriched pathways and diseases.* Nucleic acids research, 2011. **39**(Web Server issue): p. W316-W322.
207. Gao, C.-H., G. Yu, and P. Cai, *ggVennDiagram: An Intuitive, Easy-to-Use, and Highly Customizable R Package to Generate Venn Diagram.* Frontiers in Genetics, 2021. **12**(1598).
208. Hall, B.G., *Building Phylogenetic Trees from Molecular Data with MEGA.* Molecular Biology and Evolution, 2013. **30**(5): p. 1229-1235.
209. Ramesh, A. and W.C. Winkler, *Magnesium-sensing riboswitches in bacteria.* Rna Biology, 2010. **7**(1): p. 77-83.
210. Cromie, M.J. and E.A. Groisman, *Promoter and Riboswitch Control of the Mg2+ Transporter MgtA from Salmonella enterica.* Journal of Bacteriology, 2010. **192**(2): p. 604-607.
211. McCluskey, K., et al., *Unprecedented tunability of riboswitch structure and regulatory function by sub-millimolar variations in physiological Mg2+.* Nucleic Acids Research, 2019. **47**(12): p. 6478-6487.
212. Kim, M.J., et al., *The Arabidopsis AP2/ERF transcription factor RAP2.11 modulates plant response to low-potassium conditions.* Mol Plant, 2012. **5**(5): p. 1042-57.
213. Wang, R.C., et al., *A Genetic Screen for Nitrate Regulatory Mutants Captures the Nitrate Transporter Gene NRT1.1.* Plant Physiology, 2009. **151**(1): p. 472-478.
214. Kim, S.A., et al., *The iron deficiency response in Arabidopsis thaliana requires the phosphorylated transcription factor URI.* Proceedings of the National Academy of Sciences, 2019. **116**(50): p. 24933-24942.
215. Sharma, R. and K.-C. Yeh, *The dual benefit of a dominant mutation in Arabidopsis IRON DEFICIENCY TOLERANT1 for iron biofortification and heavy*

metal phytoremediation. Plant Biotechnology Journal, 2020. **18**(5): p. 1200-1210.
216. Lahner, B., et al., *Genomic scale profiling of nutrient and trace elements in Arabidopsis thaliana.* Nat Biotech, 2003. **21**(10): p. 1215-1221.
217. Kamiya, T., et al., *The MYB36 transcription factor orchestrates Casparian strip formation.* Proc Natl Acad Sci U S A, 2015. **112**(33): p. 10533-8.
218. Alcock, T.D., et al., *Magnesium and calcium overaccumulate in the leaves of a schengen3 mutant of Brassica rapa.* Plant Physiology, 2021. **186**(3): p. 1616-1631.
219. Cakmak, I. and H. Marschner, *Magnesium deficiency enhances resistance to paraquat toxicity in bean leaves.* Plant, Cell & Environment, 1992. **15**(8): p. 955-960.
220. Ceylan, Y., et al., *Magnesium applications to growth medium and foliage affect the starch distribution, increase the grain size and improve the seed germination in wheat.* Plant and Soil, 2016. **406**(1): p. 145-156.
221. Trankner, M., et al., *Magnesium deficiency decreases biomass water-use efficiency and increases leaf water-use efficiency and oxidative stress in barley plants.* Plant and Soil, 2016. **406**(1-2): p. 409-423.
222. Cakmak, I. and H. Marschner, *Magnesium Deficiency and High Light Intensity Enhance Activities of Superoxide Dismutase, Ascorbate Peroxidase, and Glutathione Reductase in Bean Leaves.* Plant Physiology, 1992. **98**(4): p. 1222-1227.
223. Carstensen, A., et al., *The Impacts of Phosphorus Deficiency on the Photosynthetic Electron Transport Chain.* Plant Physiology, 2018. **177**(1): p. 271-284.
224. Klepikova, A.V., et al., *A high resolution map of the Arabidopsis thaliana developmental transcriptome based on RNA-seq profiling.* The Plant Journal, 2016. **88**(6): p. 1058-1070.
225. Winter, D., et al., *An "Electronic Fluorescent Pictograph" Browser for Exploring and Analyzing Large-Scale Biological Data Sets.* PLOS ONE, 2007. **2**(8): p. e718.
226. Czechowski, T., et al., *Genome-Wide Identification and Testing of Superior Reference Genes for Transcript Normalization in Arabidopsis.* Plant Physiology, 2005. **139**(1): p. 5-17.
227. Hermans, C., et al., *Systems analysis of the responses to long-term magnesium deficiency and restoration in Arabidopsis thaliana.* New Phytologist, 2010. **187**(1): p. 132-144.
228. Cristescu, S.M., et al., *Current methods for detecting ethylene in plants.* Annals of Botany, 2013. **111**(3): p. 347-360.
229. Niu, Y., et al., *Phosphorus and magnesium interactively modulate the elongation and directional growth of primary roots in Arabidopsis thaliana (L.) Heynh.* Journal of Experimental Botany, 2015. **66**(13): p. 3841-3854.
230. Vaucheret, H., et al., *Transgene-induced gene silencing in plants.* The Plant Journal, 1998. **16**(6): p. 651-659.
231. Peragine, A., et al., *SGS3 and SGS2/SDE1/RDR6 are required for juvenile development and the production of trans-acting siRNAs in Arabidopsis.* Genes & development, 2004. **18**(19): p. 2368-2379.

232. Carter, K.P., et al., *Critical Comparison of FRET-Sensor Functionality in the Cytosol and Endoplasmic Reticulum and Implications for Quantification of Ions.* Analytical Chemistry, 2017. **89**(17): p. 9601-9608.
233. Gouveia-Neto, A.S., et al., *Abiotic stress diagnosis via laser induced chlorophyll fluorescence analysis in plants for biofuel.* Biofuel Production-Recent Developments and Prospects, 2011: p. 3-22.
234. DeLuca, M. and W.D. McElroy, *Kinetics of the firefly luciferase catalyzed reactions.* Biochemistry, 1974. **13**(5): p. 921-925.
235. Liang, C., et al., *Impacts of high ATP supply from chloroplasts and mitochondria on the leaf metabolism of Arabidopsis thaliana.* Frontiers in plant science, 2015. **6**: p. 922-922.
236. Straube, H., et al., *Enhanced nucleotide analysis enables the quantification of deoxynucleotides in plants and algae revealing connections between nucleoside and deoxynucleoside metabolism.* The Plant Cell, 2020. **33**(2): p. 270-289.
237. Kesten, C., et al., *Pathogen-induced pH changes regulate the growth-defense balance in plants.* The EMBO Journal, 2019. **38**(24): p. e101822.
238. Chen, L.-Q., et al., *Sucrose Efflux Mediated by SWEET Proteins as a Key Step for Phloem Transport.* Science, 2012. **335**(6065): p. 207-211.
239. Zhang, C., et al., *Two evolutionarily duplicated domains individually and post-transcriptionally control SWEET expression for phloem transport.* New Phytologist, 2021. **232**(4): p. 1793-1807.
240. Chen, Q., et al., *Phosphorylation of SWEET sucrose transporters regulates plant root:shoot ratio under drought.* Nature Plants, 2022. **8**(1): p. 68-77.
241. Sadoine, M., et al., *Affinity Series of Genetically Encoded Förster Resonance Energy-Transfer Sensors for Sucrose.* ACS Sensors, 2021. **6**(5): p. 1779-1784.
242. Liang, W.W., et al., *MicroRNA-mediated responses to long-term magnesium-deficiency in Citrus sinensis roots revealed by Illumina sequencing.* Bmc Genomics, 2017. **18**: p. 16.
243. Tanz, S., et al., *Fluorescent protein tagging as a tool to define the subcellular distribution of proteins in plants.* Frontiers in Plant Science, 2013. **4**.
244. Brumbarova, T., P. Bauer, and R. Ivanov, *Molecular mechanisms governing Arabidopsis iron uptake.* Trends in Plant Science, 2015. **20**(2): p. 124-133.
245. Maghiaoui, A., A. Gojon, and L. Bach, *NRT1.1-centered nitrate signaling in plants.* Journal of Experimental Botany, 2020. **71**(20): p. 6226-6237.
246. Visscher, A.M., et al., *Growth Performance and Root Transcriptome Remodeling of Arabidopsis in Response to Mars-Like Levels of Magnesium Sulfate.* Plos One, 2010. **5**(8): p. 16.
247. Johannes, F., et al., *Assessing the Impact of Transgenerational Epigenetic Variation on Complex Traits.* PLOS Genetics, 2009. **5**(6): p. e1000530.
248. Kondo, Y., T. Tamaki, and H. Fukuda, *Regulation of xylem cell fate.* Frontiers in Plant Science, 2014. **5**.
249. Bauby, H., et al., *Protophloem Differentiation in Early Arabidopsis thaliana Development.* Plant and Cell Physiology, 2007. **48**(1): p. 97-109.
250. Graschopf, A., et al., *The yeast plasma membrane protein Alr1 controls Mg2+ homeostasis and is subject to Mg2+-dependent control of its synthesis and degradation.* Journal of Biological Chemistry, 2001. **276**(19): p. 16216-16222.

251. Dyachok, J., et al., *Plasma Membrane-Associated SCAR Complex Subunits Promote Cortical F-Actin Accumulation and Normal Growth Characteristics in Arabidopsis Roots.* Molecular Plant, 2008. **1**(6): p. 990-1006.
252. Junková, P., et al., *Mapping of Plasma Membrane Proteins Interacting With Arabidopsis thaliana Flotillin 2.* Frontiers in Plant Science, 2018. **9**: p. 991.
253. Serna, L., *A simple method for discriminating between cell membrane and cytosolic proteins.* New Phytol, 2005. **165**(3): p. 947-52.
254. Muller, H.J., *Artificial Transmutation of the Gene.* Science, 1927. **66**(1699): p. 84-87.
255. Du, Y., et al., *Frequency and Spectrum of Mutations Induced by Gamma Rays Revealed by Phenotype Screening and Whole-Genome Re-Sequencing in Arabidopsis thaliana.* International Journal of Molecular Sciences, 2022. **23**(2): p. 654.
256. Yang, C., B.J. Mulligan, and Z.A. Wilson, *Molecular genetic analysis of pollen irradiation mutagenesis in Arabidopsis.* New Phytologist, 2004. **164**(2): p. 279-288.
257. Kumawat, S., et al., *Expanding Avenue of Fast Neutron Mediated Mutagenesis for Crop Improvement.* Plants, 2019. **8**(6): p. 164.
258. Kazama, Y., et al., *Characterization of highly efficient heavy-ion mutagenesis in Arabidopsis thaliana.* BMC Plant Biology, 2011. **11**(1): p. 161.
259. Martienssen, R.A., *Functional genomics: Probing plant gene function and expression with transposons.* Proceedings of the National Academy of Sciences, 1998. **95**(5): p. 2021-2026.
260. Krysan, P.J., J.C. Young, and M.R. Sussman, *T-DNA as an Insertional Mutagen in Arabidopsis.* The Plant Cell, 1999. **11**(12): p. 2283-2290.
261. Kim, S.-I. and S.B. Gelvin, *Genome-wide analysis of Agrobacterium T-DNA integration sites in the Arabidopsis genome generated under non-selective conditions.* The Plant Journal, 2007. **51**(5): p. 779-791.
262. Gou, X. and J. Li, *Activation Tagging*, in *Plant Signalling Networks: Methods and Protocols*, Z.-Y. Wang and Z. Yang, Editors. 2012, Humana Press: Totowa, NJ. p. 117-133.
263. Wu, Y., et al., *Isolation and characterization of low-sulphur-tolerant mutants of Arabidopsis.* Journal of Experimental Botany, 2010. **61**(12): p. 3407-3422.
264. Lei, M., et al., *Genetic and Genomic Evidence That Sucrose Is a Global Regulator of Plant Responses to Phosphate Starvation in Arabidopsis* Plant Physiology, 2011. **156**(3): p. 1116-1130.
265. Kim, Y., K. Schumaker, and J.-K. Zhu, *EMS Mutagenesis of Arabidopsis.* Methods in molecular biology (Clifton, N.J.), 2006. **323**: p. 101-3.
266. Jander, G., et al., *Ethylmethanesulfonate Saturation Mutagenesis in Arabidopsis to Determine Frequency of Herbicide Resistance.* Plant Physiology, 2003. **131**(1): p. 139-146.
267. Lee, Y., et al., *A Mechanism for Localized Lignin Deposition in the Endodermis.* Cell, 2013. **153**(2): p. 402-412.
268. Pfister, A., et al., *A receptor-like kinase mutant with absent endodermal diffusion barrier displays selective nutrient homeostasis defects.* Elife, 2014. **3**.

269. Aflalo, C., *Biologically Localized Firefly Luciferase: A Tool to Study Cellular Processes*, in *International Review of Cytology*, K.W. Jeon and M. Friedlander, Editors. 1991, Academic Press. p. 269-323.
270. Hartley, J.L., G.F. Temple, and M.A. Brasch, *DNA cloning using in vitro site-specific recombination.* Genome Res, 2000. **10**(11): p. 1788-95.
271. Frickey, T. and A.N. Lupas, *Phylogenetic analysis of AAA proteins.* Journal of Structural Biology, 2004. **146**(1): p. 2-10.
272. Zaltsman, A., N. Ori, and Z. Adam, *Two Types of FtsH Protease Subunits Are Required for Chloroplast Biogenesis and Photosystem II Repair in Arabidopsis.* The Plant Cell, 2005. **17**(10): p. 2782-2790.
273. Yu, Q.Q., et al., *A P-Loop NTPase Regulates Quiescent Center Cell Division and Distal Stem Cell Identity through the Regulation of ROS Homeostasis in Arabidopsis Root.* Plos Genetics, 2016. **12**(9): p. 21.
274. Ivanov, V., *Estimation of induced mutation rate in Arabidopsis.* Arabidopsis information service, 1973.
275. Mednik, I., *On methods evaluating the frequencies of induced mutations in Arabidopsis based on embryo test data.* Arabidopsis Inf Serv, 1988. **26**: p. 67-72.
276. Ammelburg, M., T. Frickey, and A.N. Lupas, *Classification of AAA+ proteins.* Journal of structural biology, 2006. **156**(1): p. 2-11.
277. Wagener, N. and W. Neupert, *Bcs1, a AAA protein of the mitochondria with a role in the biogenesis of the respiratory chain.* Journal of Structural Biology, 2012. **179**(2): p. 121-125.
278. Kater, L., et al., *Structure of the Bcs1 AAA-ATPase suggests an airlock-like translocation mechanism for folded proteins.* Nature Structural & Molecular Biology, 2020. **27**(2): p. 142-149.
279. Liu, J.-X. and S.H. Howell, *Managing the protein folding demands in the endoplasmic reticulum of plants.* New Phytologist, 2016. **211**(2): p. 418-428.
280. Sahi, C., et al., *Beyond osmolytes and transporters: novel plant salt-stress tolerance-related genes from transcriptional profiling data.* Physiologia Plantarum, 2006. **127**(1): p. 1-9.
281. Zhang, B., et al., *The mitochondrial outer membrane AAA ATPase AtOM66 affects cell death and pathogen resistance in Arabidopsis thaliana.* Plant J, 2014. **80**(4): p. 709-27.
282. Eamens, A., et al., *RNA silencing in plants: yesterday, today, and tomorrow.* Plant Physiol, 2008. **147**(2): p. 456-68.
283. Ariizumi, T., et al., *Disruption of the novel plant protein NEF1 affects lipid accumulation in the plastids of the tapetum and exine formation of pollen, resulting in male sterility in Arabidopsis thaliana.* The Plant Journal, 2004. **39**(2): p. 170-181.
284. Cui, M., et al., *Glutamate synthase 1 is involved in iron-deficiency response and long-distance transportation in Arabidopsis.* Journal of Integrative Plant Biology, 2020. **62**(12): p. 1925-1941.
285. Cui, X., et al., *Overexpression of an F-box protein gene disrupts cotyledon vein patterning in Arabidopsis.* Plant Physiology and Biochemistry, 2016. **102**: p. 43-52.

286. Xu, H., et al., *SKL1 Is Essential for Chloroplast Development in Arabidopsis.* Frontiers in Plant Science, 2018. **9**(179).
287. Fan, S.-C., et al., *The Arabidopsis nitrate transporter NRT1.7, expressed in phloem, is responsible for source-to-sink remobilization of nitrate.* The Plant cell, 2009. **21**(9): p. 2750-2761.
288. Fan, X., et al., *Cross-Talks Between Macro- and Micronutrient Uptake and Signaling in Plants.* Frontiers in Plant Science, 2021. **12**.
289. Lešková, A., H. Javot, and R.F.H. Giehl, *Metal crossroads in plants: modulation of nutrient acquisition and root development by essential trace metals.* Journal of Experimental Botany, 2021. **73**(6): p. 1751-1765.
290. Salt, D.E., I. Baxter, and B. Lahner, *Ionomics and the study of the plant ionome.* Annu Rev Plant Biol, 2008. **59**: p. 709-33.
291. Forieri, I., et al., *System analysis of metabolism and the transcriptome in Arabidopsis thaliana roots reveals differential co-regulation upon iron, sulfur and potassium deficiency.* Plant, Cell & Environment, 2017. **40**(1): p. 95-107.
292. Mahood, E.H., L.H. Kruse, and G.D. Moghe, *Machine learning: A powerful tool for gene function prediction in plants.* Applications in plant sciences, 2020. **8**(7): p. e11376-e11376.
293. Shaik, R. and W. Ramakrishna, *Machine Learning Approaches Distinguish Multiple Stress Conditions using Stress-Responsive Genes and Identify Candidate Genes for Broad Resistance in Rice* Plant Physiology, 2013. **164**(1): p. 481-495.
294. Gupta, C., et al., *Using Network-Based Machine Learning to Predict Transcription Factors Involved in Drought Resistance.* Frontiers in Genetics, 2021. **12**.
295. Asefpour Vakilian, K., *Machine learning improves our knowledge about miRNA functions towards plant abiotic stresses.* Scientific Reports, 2020. **10**(1): p. 3041.
296. Erickson, J.R. and T.S. Moerland, *A competition assay of magnesium affinity for EF-hand proteins based on the fluorescent indicator magnesium green.* Analytical biochemistry, 2005. **345**(2): p. 343-345.
297. Broadley, M.R., et al., *Phylogenetic variation in the shoot mineral concentration of angiosperms.* Journal of Experimental Botany, 2004. **55**(396): p. 321-336.
298. Broadley, M.R., et al., *Shoot calcium and magnesium concentrations differ between subtaxa, are highly heritable, and associate with potentially pleiotropic loci in Brassica oleracea.* Plant Physiology, 2008. **146**(4): p. 1707-1720.
299. Alcock, T.D., et al., *Identification of Candidate Genes for Calcium and Magnesium Accumulation in Brassica napus L. by Association Genetics.* Frontiers in Plant Science, 2017. **8**: p. 13.
300. Bradshaw, H., *Mutations in CAX1 produce phenotypes characteristic of plants tolerant to serpentine soils.* New Phytologist, 2005. **167**(1): p. 81-88.
301. Shen, J., et al., *Phosphorus dynamics: from soil to plant.* Plant Physiol, 2011. **156**(3): p. 997-1005.

302. Yeh, C.-M., et al., *Blue Light Regulates Phosphate Deficiency-Dependent Primary Root Growth Inhibition in Arabidopsis.* Frontiers in Plant Science, 2020. **10**.
303. Hernández, I. and S. Munné-Bosch, *Linking phosphorus availability with photo-oxidative stress in plants.* Journal of Experimental Botany, 2015. **66**(10): p. 2889-2900.
304. Ajmera, I., T.C. Hodgman, and C. Lu, *An Integrative Systems Perspective on Plant Phosphate Research.* Genes, 2019. **10**(2): p. 139.
305. Hermans, C., et al., *How do plants respond to nutrient shortage by biomass allocation?* Trends in Plant Science, 2006. **11**(12): p. 610-617.
306. Lloyd, J.C. and O.V. Zakhleniuk, *Responses of primary and secondary metabolism to sugar accumulation revealed by microarray expression analysis of the Arabidopsis mutant, pho3.* Journal of Experimental Botany, 2004. **55**(400): p. 1221-1230.
307. Huang, C., et al., *Triple-localized WHIRLY2 influences leaf senescence and silique development via carbon allocation.* Plant Physiology, 2020. **184**(3): p. 1348-1362.
308. Yamada, K., et al., *Regulation of sugar transporter activity for antibacterial defense in Arabidopsis.* Science, 2016. **354**(6318): p. 1427-1430.
309. Lee, H.G. and P.J. Seo, *Transcriptional activation of SUGAR TRANSPORT PROTEIN 13 mediates biotic and abiotic stress signaling.* Plant Signaling & Behavior, 2021. **16**(8): p. 1920759.
310. Oliva, R. and I.L. Quibod, *Immunity and starvation: new opportunities to elevate disease resistance in crops.* Current Opinion in Plant Biology, 2017. **38**: p. 84-91.
311. Gupta, P.K., *SWEET Genes for Disease Resistance in Plants.* Trends in Genetics, 2020. **36**(12): p. 901-904.
312. Gebauer, P., et al., *Sugar Accumulation in Leaves of Arabidopsis sweet11/sweet12 Double Mutants Enhances Priming of the Salicylic Acid-Mediated Defense Response.* Frontiers in Plant Science, 2017. **8**.
313. Avila, J.R., J.S. Lee, and K.U. Torii, *Co-Immunoprecipitation of Membrane-Bound Receptors.* The arabidopsis book, 2015. **13**: p. e0180-e0180.
314. Haughn, G. and C.R. Somerville, *Selection for Herbicide Resistance at the Whole-Plant Level*, in *Biotechnology in Agricultural Chemistry*. 1987, American Chemical Society. p. 98-107.